

**AN EXPERIMENTAL INVESTIGATION AND OPTIMIZATION
OF MICROWAVE HYBRID HEATING FOR JOINING OF
INCONEL-625 ALLOY**

Thesis

submitted in partial fulfillment of the requirements for the degree of

DOCTOR OF PHILOSOPHY

by

RAVINDRA ISHWAR BADIGER



DEPARTMENT OF MECHANICAL ENGINEERING

NATIONAL INSTITUTE OF TECHNOLOGY KARNATAKA,

SURATHKAL, MANGALORE -575025

MAY- 2019

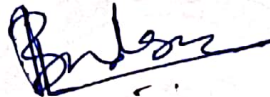
DECLARATION

I hereby declare that the Research Thesis entitled **AN EXPERIMENTAL INVESTIGATION AND OPTIMIZATION OF MICROWAVE HYBRID HEATING FOR JOINING OF INCONEL-625 ALLOY** which is being submitted to the **National Institute of Technology Karnataka, Surathkal** in partial fulfillment of the requirements for the award of the degree of **Doctor of Philosophy** in Mechanical Engineering is a *bonafide report of the research work carried out by me*. The material contained in this Research Thesis has not been submitted to any University or Institution for the award of any degree.

Register Number: **112008 ME11P06**

Name of the Research Scholar: **RAVINDRA ISHWAR BADIGER**

Signature of the Research Scholar:



Department of Mechanical Engineering

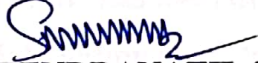
National Institute of Technology Karnataka, Surathkal

Place: NITK-Surathkal

Date: **29/05/2019**

CERTIFICATE

This is to *certify* that the Research Thesis entitled **An Experimental Investigation and Optimization of Microwave Hybrid Heating for Joining of Inconel-625 Alloy** submitted by **Mr. RAVINDRA ISHWAR BADIGER** (Register Number: 112008-ME11P06) as the record of the research work carried out by him, is *accepted as the Research Thesis submission* in partial fulfillment of the requirements for the award of degree of **Doctor of Philosophy**.



PROF. NARENDRANATH. S,

Research Guide



Chairman - DRPC

Date: **7/6/2019**



Department of Mechanical Engineering

National Institute of Technology Karnataka, Surathkal

ACKNOWLEDGEMENTS

I deem it a great privilege to have worked under the guidance of **Dr. Narendranath S**, Professor, Department of Mechanical Engineering, National Institute of Technology Karnataka, Surathkal, He has rendered excellent guidance and encouragement throughout the research work. His expertise knowledge, critical review, inspiring discussions and cooperation during the entire course are invaluable.

My heartfelt thanks are especially due to **Dr. Srinath M. S**, Professor, Department of Industrial and Production Engineering, Malnad College of Engineering, Hassan for mentoring me throughout the research work. He as motivated me with his in-depth knowledge and unconditional support right from the beginning of this work.

I am grateful to the members of the Research Program Assessment Committee including **Dr. G. C. Mohankumar**, Professor, Department of Mechanical Engineering, **Dr. G. S. Dwarakish**, Professor, Department of Applied Mechanics and Hydraulics and **Dr. K. Ram Chandar**, Associate Professor, Department of Mining Engineering for their unbiased and critical evaluation during the progress of my research.

My sincere thanks are due to **Dr. Shrikantha S. Rao**, Professor and Head, Department of Mechanical Engineering for extending the departmental facilities without which I could not have completed my research work satisfactorily.

I would be failing in my duty if I don't remember **Dr. Manjaiah M**, Asst. Professor, Department of Mechanical Engineering, Manipal Institute of Technology, Manipal, for his encouragement and timely support during every phase of my research work.

I express my sincere thanks to **Dr. Ajith M Hebbale**, Asst. Professor, Department of Mechanical Engineering, NMAM Institute of Technology, Nitte, and **Mr. Abhijeet A Patil**, Asst. Professor, Department of Mechanical Engineering, Dr. J. J. Magdum college

of Engineering, Jaysingpur, Maharashtra, for providing innovative ideas and extending support during the experimentation work.

I am indebted to all my research colleagues of Department of Mechanical Engineering, Dr. Hargovind Soni, Mr. Abhinaba Roy, Mr. Gajanan M Naik, Mr. Sachin B, Mr. Mahesh Davanageri, Mr. Sachinkumar Patil, Mr. Manoj I.V, and Mr. Prithvirajan Sekar and also the Teaching and Non-teaching staff members of the Department of Mechanical Engineering, NITK for their continuous help and support throughout the research work.

I do thank **Dr. Sathisha N**, Professor and Head, Department of Mechanical Engineering, Yenepoya Institute of Technology, Moodbidri and **Mr. Sadashiv M Bellubbi**, Asst. Professor, Department of Mechanical Engineering, Alva's Institute of Engineering and Technology, Moodbidri for their timely help and cooperation extended to me during composition of the thesis.

I am extremely grateful to my parents **Shri. Ishwar Badiger** and **Smt. Kamala Badiger** who have been a motivating force throughout my life. I am also grateful to my Father-in-law Shri. Kalappa Manuvacharya for his support rendered during the study. It is a pleasure to thank my sister Mrs. Kasturi, my wife Mrs. Vishalaxi and my children Prajwal and Pranati for their encouragement during the course of this research work.

Finally, I wish to thank all those who have helped me directly or indirectly during various phases of this research work.

Ravindra Ishwar Badiger

ABSTRACT

Inconel-625 is a nickel-chromium alloy strengthened by additions of carbon, chromium, molybdenum and niobium known for its high strength, excellent weldability, and outstanding corrosion resistance. The alloy finds widespread use in strategic industries due to its exceptional mechanical properties, excellent weldability and resistance to high temperature corrosion on extended exposure to harsh environments. These alloys are preferred for, high temperature as well as aqueous corrosion resistance, high strength at elevated temperatures, toughness and ductility at cryogenic temperatures, definite electrical properties and many other property dependent applications.

As present-day industries demand for a technology that is environment friendly and equally competent with the existing processes at reduced costs, the development of novel processes to weld Inconel-625 has to be addressed. Processing of metallic materials through microwave energy is a recently developed technology that is drawing the attention of manufacturing industries. Microwave processed components exhibit similar characteristics at reduced processing times and energy savings to those produced using conventional techniques.

In the present work, development of Inconel-625 welded joints using microwave hybrid heating technique (MHH) has been achieved successfully in a low cost 2.45GHz, 900W home microwave oven. Nickel based powder EWAC was employed as interface filler material. Microwave induced joints were examined by uniaxial tensile testing, 3-point bend test, microhardness test, XRD analysis and microstructural studies. Furthermore, an investigation on the effect of process parameters on tensile strength and flexural strength of Inconel-625 plates welded by MHH was conducted. Experiments were planned according to Taguchi L_{16} orthogonal array (OA) by considering three factors; separator, susceptor and filler powder particle size. Ultimate tensile strength (UTS) and flexural strength (FS) of the specimens welded at 600W and 900W were chosen as response characteristics.

The Taguchi method has been used to ascertain the individual effect of separator type, susceptor type and filler powder size on ultimate tensile strength and flexural strength of the welded joints was analyzed. In addition the combination of process parameters that yield the best UTS and FS were determined. Analysis of variance (ANOVA) was performed to determine the contribution of process parameters on the output responses using MINITAB statistical software. The fineness of the interface filler powder was found to be the most significant parameter influencing the tensile and flexural strength of the joints. The strengths of microwave induced joints increased when finer powder (APS 50 μ m) was used. Graphite separator exhibited better heating characteristics when compared to glasswool regardless of power used for processing.

Phase analysis through XRD revealed the formation of chromium carbide in the interface region which in turn contributed to increase the hardness of the joint in the interface region. In addition, the carbides of Niobium and molybdenum and other intermetallics were also observed in the joint region. EDS analysis showed that the amount of Nb, Ti and Mo content was considerably lower in secondary phase of joints developed at 600W which would consequently result in lower amount of Laves volume fraction compared to their counterparts produced at 900W. Further, the specimens produced at 600W also exhibited lower porosity values and higher joint hardness which is attributed to a fine grained structure. All the specimens fractured in the joint zone due to the presence of a hard carbide phase at the interface and fractography study revealed mixed mode fracture.

Multi response optimization of the microwave welding process showed that Experiment No. 9 yielded optimum combination of process parameters obtained through GRA which was observed to be separator with combination of graphite and flux followed by coal susceptor and 50 μ m (APS) filler powder. Confirmation experiment along with subsequent characterization of the microwave induced joints has been carried out to validate the experimental results.

Keywords: *Microwave hybrid heating, Inconel-625, Separator, Susceptor, Filler powder, Tensile strength, Flexural strength and Grey relational analysis*

CONTENTS

<i>Declaration</i>	
<i>Certificate</i>	
<i>Acknowledgements</i>	
<i>Abstract</i>	
<i>Contents</i>	<i>i</i>
<i>List of Figures</i>	<i>vi</i>
<i>List of Tables</i>	<i>xiv</i>
<i>List of Abbreviations</i>	<i>xvi</i>
CHAPTER 1 - INTRODUCTION	1
1.1 NICKEL BASED SUPERALLOYS	1
1.2 INCONEL-625 ALLOY AND ITS APPLICATIONS	3
1.3 WELDING OF INCONEL-625 SUPERALLOY	7
1.4 INTRODUCTION TO MICROWAVE PROCESSING OF MATERIALS	8
1.4.1 Dielectric properties	9
1.4.2 Penetration depth and power absorbed	10
1.4.3 Microwave-material interaction	11
1.4.4 Working principle of microwave oven	12
1.4.5 Magnetron	13
1.4.6 Principle of joining bulk metals through microwave hybrid heating (MHH)	14
1.4.7 Advantages of microwave processing	15
1.5 PROCESS PARAMETERS IN MICROWAVE WELDING	16
1.5.1 Susceptor	16
1.5.2 Separator	16
1.5.3 Filler powder size	17
1.5.4 Rated power of microwave oven	17

1.6	INTRODUCTION TO DESIGN OF EXPERIMENTS (DOE)	17
1.6.1	Taguchi method	18
1.7	OPTIMIZATION TECHNIQUES	18
1.7.1	Grey relational analysis (GRA)	18
1.8	THESIS OUTLINE	19
	CHAPTER 2 - LITERATURE REVIEW	22
2.1	INTRODUCTION	22
2.2	CONVENTIONAL WELDING OF INCONEL-625 ALLOY	22
2.3	HEATING TECHNIQUES IN MICROWAVE PROCESSING	25
2.3.1	Conventional and microwave heating	25
2.3.2	Direct microwave heating	26
2.3.3	Microwave hybrid heating (MHH)	26
2.3.3.1	Susceptor assisted microwave heating	27
2.4	PROCESSING OF METALLIC MATERIALS THROUGH MHH	28
2.4.1	Comparison of metallic material processing applications involving MHH	29
2.4.2	Sintering of metallic powders	31
2.4.3	Cladding of bulk metals with metallic powders	36
2.4.4	Joining of bulk metals with metallic powder interface	40
2.5	EFFECT OF PROCESS PARAMETERS ON OUTPUT RESPONSES	44
2.5.1	Effect of interface powder size on ultimate tensile strength (UTS) and flexural strength (FS)	44
2.5.2	Effect of susceptor/separator on UTS and FS	45
2.5.3	Effect input power on UTS and FS	46
2.5.4	Investigations on UTS and FS of MHH developed joints	47
2.5.5	Observation of fractured surfaces	49
2.5.6	Observations from microhardness studies	53
2.6	STUDIES ON METALLURGICAL CHARACTERIZATION OF MHH INDUCED JOINTS	57

2.6.1	Observations from XRD analysis	58
2.6.2	Observations from microstructure studies	62
2.6.3	Observations on porosity and grain size	68
2.7	STUDIES ON OPTIMIZATION OF WELDING PROCESS PARAMETERS	72
2.7.1	Optimization techniques employed during joining bulk metals through MHH	73
2.7.2	Optimization of process parameters in conventional welding using GRA	74
2.7.3	Concluding remarks	75
2.8	RESEARCH GAPS	76
2.9	PROBLEM DEFINITION	76
2.10	OBJECTIVES OF THE PRESENT WORK	77
	CHAPTER 3 - EXPERIMENTAL WORK	78
3.1	INTRODUCTION	78
3.2	RESEARCH METHODOLOGY	78
3.3	SELECTION OF MATERIALS	80
3.4	CHARACTERIZATION OF MATERIALS	81
3.4.1	Characterization of as-received Inconel-625 plate	81
3.4.2	Characterization of EWAC filler powder	83
3.5	MICROWAVE JOINING PROCESS	84
3.6	MECHANISM OF JOINT FORMATION	86
3.7	MECHANICAL CHARACTERIZATION OF MICROWAVE WELDED JOINTS	88
3.7.1	Specimen preparation for uniaxial tensile test and 3-point bend test	88
3.7.2	Uniaxial tensile test	94
3.7.3	3-point bend test	95
3.7.4	Microhardness test	95

3.8	METALLURGICAL CHARACTERIZATION OF MICROWAVE WELDED JOINTS	97
3.8.1	Specimen preparation	97
3.8.2	X-Ray Diffraction	97
3.8.3	Optical Microscope	97
3.8.4	Scanning Electron Microscope	98
3.9	DESIGN OF EXPERIMENTS	99
3.10	ANALYSIS OF VARIANCE (ANOVA)	101
3.11	GREY RELATIONAL ANALYSIS (GRA)	102
3.12	SUMMARY	103
	CHAPTER 4 - ANALYSIS OF RESULTS AND CHARACTERIZATION	104
4.1	INTRODUCTION	104
4.2	EXPERIMENTAL RESULTS	104
4.3	EFFECTS OF PROCESS PARAMETERS ON OUTPUT RESPONSES	104
4.3.1	Effect of separator on ultimate tensile strength (UTS) and flexural strength (FS)	105
4.3.2	Effect of susceptor on UTS and FS	107
4.3.3	Effect of interface powder size (APS) on UTS and FS	108
4.4	ESTIMATION OF OPTIMAL RESPONSE CHARACTERISTICS	110
4.5	ANOVA STUDY	112
4.6	CHARACTERIZATION OF THE DEVELOPED JOINTS	114
4.6.1	XRD observations	114
4.6.2	Microstructural observations	118
4.6.3	Grain size and porosity measurement	127
4.6.4	Observations on microhardness	130
4.6.5	Observations from tensile test	133
4.6.6	Observations from 3-point bend test	136
4.6.7	Fractography	138
4.7	SUMMARY	144

CHAPTER 5 - MULTI OBJECTIVE OPTIMIZATION USING GREY	147
RELATIONAL ANALYSIS	
5.1 INTRODUCTION	147
5.2 GREY RELATIONAL ANALYSIS	147
5.3 ANOVA STUDY	154
5.4 CONFIRMATION TEST	155
5.5 CHARACTERIZATION OF MICROWAVE WELDED JOINTS	155
5.5.1 XRD observations	155
5.5.2 SEM observations	158
5.5.3 Observations on microhardness	162
5.5.4 Grain size and porosity	164
5.5.5 Fractography	165
5.6 SUMMARY	166
CHAPTER 6 - CONCLUSIONS AND SCOPE FOR FUTURE WORK	168
6.1 CONCLUSIONS	168
6.2 SCOPE FOR FUTURE WORK	170
6.3 CHALLENGES IN MICROWAVE PROCESSING OF MATERIALS	171
REFERENCES	173
TECHNICAL PAPERS PUBLISHED	
BIO-DATA	

LIST OF FIGURES

Figure No.	Description	Page No.
Figure 1.1	Application of solid solution strengthened Ni-Cr alloys in industrial gas turbine (Haynes International)	5
Figure 1.2	Typical applications of Inconel-625 alloy (a) Exhaust for BMW Model: E92/3 M3 (b) Weld neck flanges for marine applications (c) Aerospace flow bodies (d) Alloy steel weld overlaid with Inconel-625 (Shoemaker, 2005)	6
Figure 1.3	Electromagnetic spectrum and frequencies used in microwave processing (Meredith,1998)	8
Figure 1.4	Relation between dielectric loss factor and power absorbed (Thostenson and Chou, 1999)	11
Figure 1.5	Schematic of microwave oven	13
Figure 1.6	Schematic of magnetron (Borrell and Salvador, 2018)	14
Figure 1.7	Schematic of joining bulk metals through microwave hybrid heating	15
Figure 2.1	SEM micrographs (a) Interfaces between the filler 310 SS weld metal and the 310 SS base metal and (b) between the filler 310 weld metal and the Inconel 617 base metal (Hosseini et al., 2011)	22
Figure 2.2	Heat distribution in a sample during (a) conventional heating (b) microwave heating (Gupta and Wong, 2007)	26
Figure 2.3	Microwave hybrid heating (Bhattacharya and Basak, 2016)	27
Figure 2.4	Principle of MHH illustrating (a) Sintering (b) Cladding	30

(c) Joining processes

Figure 2.5	Schematic of experimental setup used for sintering (Gupta and Wong, 2005)	33
Figure 2.6	SEM micrographs of (a) microwave sintered (b) conventionally sintered 92.5W-6.4Ni-1.1Fe alloy compacts (Upadhyaya et al., 2007)	33
Figure 2.7	Casket set-up used for sintering of Al-Cu-Mg-Si-Sn alloys (Padmavati et al., 2012)	35
Figure 2.8	Schematic of cladding process (Gupta and Sharma, 2011)	37
Figure 2.9	SEM micrographs of (a) morphology of EWAC powder (b) as-received SS-316 plate and (c) microwave developed clad (Gupta and Sharma, 2011)	37
Figure 2.10	SEM micrograph of EWAC+Cr ₂₃ C ₆ composite clad (Gupta et al.; 2012)	38
Figure 2.11	(a) Microwave induced EWAC clad samples (b) Clad samples prepared for metallurgical observations (Hebbale and Srinath, 2016)	39
Figure 2.12	SS-316 welded specimens developed through MHH (Srinath et al., 2011)	41
Figure 2.13	(a) schematic tooling used for joining copper plates (b) macrostructure of joint developed through MHH (Srinath et al., 2011)	42
Figure 2.14	a) Dimensions of tensile test specimen as per ASTM-E8 standard and (b) Photograph of microwave welded SS-316 tensile test specimen (Bansal et al., 2014).	47
Figure 2.15	Load-extension characteristics of the SS-316/MS welded specimen during 3-point bend test (Bansal et al., 2016)	48

Figure 2.16	Stress-strain characteristics of Inconel-718/SS-316 dissimilar joint (Bansal et al., 2016)	49
Figure 2.17	Schematic arrangement of 3-point bend test (Sharma and Gupta, 2012)	49
Figure 2.18	SEM micrograph of fractured copper joint (Srinath et al., 2011)	50
Figure 2.19	Photographs of fractured (a) and (b) tensile specimens and (c) and (d) 3-point bend test specimens (Bansal et al., 2016)	51
Figure 2.20	SEM micrograph of fractured SS-316 microwave induced joint showing ductile fracture (Bansal et al., 2014)	51
Figure 2.21	(a) and (b) Fractured surfaces of Inconel-718/SS-316 weld joint, (c) and (d) EDS analysis at locations 1 and 2 respectively (Bansal et al., 2016)	52
Figure 2.22	Variation in microhardness distribution of WC-10Co-2Ni clad (Gupta and Sharma, 2011)	53
Figure 2.23	SEM micrographs showing skeleton like carbide phases and microhardness indentations at different locations (a) across the section (b) clad surface (matrix phase) (Zafar and Sharma, 2014)	54
Figure 2.24	Vickers microhardness measurements at various locations in SS-316 microwave induced joint (Srinath et al., 2011)	55
Figure 2.25	SEM micrographs of microhardness indentations (a) base metal (b) joint zone (Bansal et al., 2014)	56
Figure 2.26	(a) SEM micrographs of indentations across the joint (b) microhardness profile (Bansal et al., 2016)	57
Figure 2.27	XRD spectrum of (a) SiC powder (b) Ni based powder (Kaushal et al., 2018)	58
Figure 2.28	XRD spectrum of EWAC clad on SS-304 substrate, (Hebbale and Srinath, 2016)	59
Figure 2.29	XRD spectrum of (a) Inconel-718 powder	61

	(b) microwave induced dissimilar Inconel-718/SS-316 joint (Bansal et al., 2016)	
Figure 2.30	Back scattered SEM micrographs of microwave induced EWAC + WC-10Co-2Ni composite clad (Sharma and Gupta, 2012)	62
Figure 2.31	EDS analysis at (a) matrix phase (b) white phase in Figure 2.30 (Sharma and Gupta, 2012)	63
Figure 2.32	SEM micrograph of WC-10Co-2Ni microwave induced clad showing skeleton like structure (Gupta and Sharma, 2011)	63
Figure 2.33	(a) SEM micrograph showing skeleton like structure (b) EDS spectra at point 1 (c) EDS spectra at point 2 (d) EDS spectra at point 3 (Zafar and Sharma, 2014)	64
Figure 2.34	SEM microstructure of EWAC clad showing (a) chromium carbide precipitation at grain boundaries (b) cellular structure of the developed clad (Gupta and Sharma, 2011)	65
Figure 2.35	SEM micrograph of SS-316 joint fusion zone (Srinath et al., 2011)	66
Figure 2.36	SEM microstructure showing the joint zone of welded CI plates (Singh et al., 2018)	66
Figure 2.37	(a) SEM microstructure of microwave induced SS-316/MS joint indicating the location of EDS (b) EDS inside the grain (c) EDS at the grain boundary (Bansal et al., 2014)	67
Figure 2.38	SEM micrographs of (a) MS plates (Bansal et al., 2013) and (b) MS pipes (Gamit et al., 2017) joined through MHH	68
Figure 2.39	SEM micrographs showing porosity in microwave induced joints of (a) Copper plates (b) SS-316/MS plates (Srinath et al., 2011)	70
Figure 2.40	SEM micrographs showing growth of reinforcement phase in (a) MM and (b) NM clads (Zafar and Sharma, 2015)	71

Figure 2.41	Optical images of microstructures of Al-Zn-Mg alloy in-situ casts developed through MHH (Mishra and Sharma, 2017)	72
Figure 2.42	Effect of process parameters on tensile strength (Dwivedi et al., 2014)	73
Figure 3.1	Research methodology flow diagram	79
Figure 3.2	(a) SEM microstructure of Inconel-625 sample (b) EDS showing the elemental composition (c) XRD spectrum of as-received Inconel-625 plate indicating the dominating peaks of Cr ₂ Ni ₃	82
Figure 3.3	SEM micrograph of nickel based powder with average particle size (a) 50µm and (b) 75µm	83
Figure 3.4	XRD spectrum of nickel based powder EWAC	84
Figure 3.5	Photograph of microwave oven (Make: LG Model: Solardom ML3483FRR) used in the present work	85
Figure 3.6	Sectional schematic of experimental setup	85
Figure 3.7	Schematic of mechanism of joint formation	87
Figure 3.8	As-welded Inconel-625 tensile specimens at (a) 900W (b) 600 power levels	89
Figure 3.9	Specimens processed at (a) 900W (b) 600W power after polishing	90
Figure 3.10	ASTM-E8 standard for tensile test specimen	91
Figure 3.11	Tensile test specimens machined according to ASTM-E8 standards processed at (a) 900W (b) 600W	91
Figure 3.12	Schematic arrangement for 3-point bend test and ASTM-E190-92 standard 3-point bend test specimen	92
Figure 3.13	Inconel-625 specimens 3-point bend test specimens in as-welded condition processed at (a) 900W (b) 600W	92, 93

Figure 3.14	3-point bend test specimens processed at (a) 900W (b) 600W and polished according to ASTM E190-92 standards.	93, 94
Figure 3.15	(a) Universal testing machine (b) Attachment for uniaxial tensile test	95
Figure 3.16	Attachment for 3-point bend test	96
Figure 3.17	Vickers microhardness tester	96
Figure 3.18	Optical microscope	98
Figure 3.19	Scanning electron microscope	98
Figure 4.1	Influence of separator on UTS and FS of welded joints processed at 600W and 900W	106
Figure 4.2	Influence of susceptor on UTS and FS of welded joints processed at 600W and 900W	108
Figure 4.3	Influence of interface powder size on UTS and FS of welded joints processed at 600W and 900W	109
Figure 4.4	XRD pattern of the joint developed in experiment No. 1	115
Figure 4.5	XRD pattern of the joint developed in experiment No. 3	116
Figure 4.6	XRD pattern of the joint developed in experiment No. 9	116
Figure 4.7	XRD pattern of the joint developed in experiment No. 11	117
Figure 4.8	Optical microscope images showing the welded joint and base metal obtained from experiment No. (a) 1 (b) 3 (c) 9 and (d) 11.	119
Figure 4.9	Typical SEM micrographs of microwave welded joints	120
Figure 4.10	SEM microstructure of specimen No.1 and EDS analysis at grain boundary (Point 1) and grain interior (Point 2)	121
Figure 4.11	SEM microstructure of specimen No.3 and EDS analysis at grain boundary (Point 1) and grain interior (Point 2)	122
Figure 4.12	SEM microstructure of specimen No.9 and EDS analysis at grain	123

	boundary (Point 1) and grain interior (Point 2)	
Figure 4.13	SEM microstructure of specimen No.11 and EDS analysis at grain boundary (Point 1) and at grain interior (Point 2)	124
Figure 4.14	SEM microstructure showing the segregation of alloying elements	125
Figure 4.15	Fusion zone microstructures of specimen processed at 600W in Expt. No. (a) 1 (b) 3 (c) 9 and (d) 11	128
Figure 4.16	Fusion zone microstructures of specimen processed at 900W in Expt. No. (a) 1 (b) 3 (c) 9 and (d) 11	129
Figure 4.17	Typical SEM micrographs showing microhardness indentations in (a) weld zone (b) base metal and joint interface (c) joint interface and weld zone	131
Figure 4.18	Microhardness profile obtained across the joints for the specimens developed at 600W power	132
Figure 4.19	Microhardness profile obtained across the joints for the specimens developed at 900W power	132
Figure 4.20	Stress-strain curves from uniaxial tensile test	134
Figure 4.21	(a) Stress-strain curves from 3-point bend test (b) Typical load-displacement characteristics during 3-point bend test	137
Figure 4.22	Fractured tensile specimens processed at 600W	139
Figure 4.23	Fractured tensile specimens processed at 900W	139
Figure 4.24	SEM micrographs showing tensile fractured surfaces of the specimens developed with 600W power	140
Figure 4.25	SEM micrographs showing tensile fractured surfaces of the specimens developed with 900W power	141
Figure 4.26	Fractured 3-point bend test specimens processed at 600W	142
Figure 4.27	Fractured 3-point bend test specimens processed at 900W	142

Figure 4.28	SEM micrographs showing fractured surfaces of the specimens developed with 600W power	143
Figure 4.29	SEM micrographs showing fractured surfaces of the specimens developed with 900W power	144
Figure 5.1	Influence of control factors	151
Figure 5.2	Surface plot of GRG versus separator and powder size	151
Figure 5.3	Surface plot of GRG versus susceptor and powder size	152
Figure 5.4	Surface plot of GRG versus susceptor and separator	153
Figure 5.5	XRD pattern of the welded joint developed at 600W	156
Figure 5.6	XRD pattern of the welded joint developed at 900W	156
Figure 5.7	SEM micrographs of Inconel-625 welded joints obtained after confirmation experiment processed at (a) 600W (b) 900W	159
Figure 5.8	SEM micrograph and EDS analysis of Inconel-625 specimen welded at 900W	160
Figure 5.9	SEM micrograph and EDS analysis of Inconel-625 specimen welded at 600W	161
Figure 5.10	Variation in hardness profile of specimens processed at 600W and 900W	163
Figure 5.11	Fusion zone optical microstructures of welded joints developed at (a) 600W (b) 900W	165
Figure 5.12	SEM micrographs of fractured specimens processed at (a) 600W (b) 900W	166

LIST OF TABLES

Table No.	Description	Page No.
Table 1.1	Most commonly used solid solution strengthened alloys (DuPont et al., 2009)	4
Table 2.1	Most commonly used susceptor materials (Bhattacharya and Basak 2016)	28
Table 2.2	Observed porosity during microwave joining of different metals (Sharma and Mishra, 2017)	69
Table 3.1	Mechanical properties of as-received Inconel-625 plate	81
Table 3.2	Chemical composition of various elements in Inconel-625	83
Table 3.3	Chemical composition of EWAC powder (wt. %)	84
Table 3.4	Control factors and their levels	99
Table 3.5	L ₁₆ orthogonal array	100
Table 4.1	Experimental results for UTS and FS using L ₁₆ orthogonal array	105
Table 4.2	Response Tables for UTS and FS	111
Table 4.3	Optimum combination of process parameters	112
Table 4.4	Results of ANOVA for response characteristics	113
Table 4.5	Elemental composition of microwave welded specimens in different experiments	127
Table 4.6	Grain size measurement and porosity	129
Table 4.7	Vickers microhardness values in different regions	133
Table 4.8	Tensile properties of MHH processed welded joints	135

Table 5.1	Pre-processing of data by normalizing S/N ratio	148
Table 5.2	Calculated grey relational coefficient, grey relational grade and rank	149
Table 5.3	Response table for grey relational grade	150
Table 5.4	ANOVA of grey relational grade	154
Table 5.5	Predicted and confirmation test results for optimal condition A3B1C1	155
Table 5.6	Relative phase intensities in the joint zone of the specimen processed at 600W	157
Table 5.7	Relative phase intensities in the joint zone of the specimen processed at 900W	158
Table 5.8	Elemental composition in the secondary phase	162
Table 5.9	Vickers microhardness values in different regions	164

LIST OF ABBREVIATIONS

ANOVA	:	Analysis of Variance
APS	:	Average Particle Size (μm)
ASTM	:	American Society for Testing and Materials
CCGTAW	:	Continuous Current GTAW
DF	:	Degrees of Freedom
DOE	:	Design of Experiments
EDS	:	Energy Dispersive X-Ray Spectroscopy
FS	:	Flexural Strength
GHz	:	Giga Hertz
GRA	:	Grey Relational Analysis
GRC	:	Grey Relational Coefficient
GRG	:	Grey Relational Grade
GTAW	:	Gas Tungsten Arc Welding
HAZ	:	Heat Affected Zone
HV	:	Vicker's Microhardness
MHH	:	Microwave Hybrid Heating
NIR	:	Normalised Intensity Ratio
OA	:	Orthogonal Array
PCGTAW	:	Pulsed Current GTAW
SEM	:	Scanning Electron Microscope
$\tan \delta$:	Loss Tangent
T_c	:	Critical Temperature
UNS	:	Unified Numbering System
UTS	:	Ultimate Tensile Strength
XRD	:	X-Ray Diffraction
δ	:	Skin depth (μm)

CHAPTER 1

INTRODUCTION

Welding provides a means of manufacturing complicated structures that cannot be made or are too expensive to be made in a single piece. Contemporary techniques to obtain permanent joints also include soldering and brazing which are widely practiced in industries. Each of these joining processes has its own limitations in terms of materials to be joined and strength of the joints. However, it must be noted that since 1950s only welding has been the core technique of assembly, as riveting was the mostly used those days. The differences in metallurgical characteristics, thermal expansion and melting temperatures of metals to be joined have created opportunities in developing the most suitable welding technique. Recent evolutions in welding technology have been emphasizing on the development of new processes to weld advanced materials so as to attain higher productivity, better quality and environment friendly process.

Nickel based alloys are a class of advanced materials that can be operated at cryogenic temperatures and elevated temperatures up to 1200°C. Welding of these alloys is considered to be the most critical fabrication techniques. Considerable efforts are being conducted for the last few decades in order to better understand and control the weldability of nickel based alloys and also to develop the appropriate welding consumables (DuPont et al., 2009).

1.1 NICKEL BASED SUPERALLOYS

Superalloys are multifaceted materials capable of retaining certain of their room temperature mechanical and physical properties at higher temperatures. Due to its high melting point (1453°C), adequate corrosion resistance, capability to dissolve many metals to some extent which strengthen and improve its corrosion resistance, Nickel is considered as ideal base for superalloys. The present day Nickel based superalloy signifies a composite material comprising a number of intermetallic phases bound in a

metallic matrix. The most predominant phases are the matrix phase γ , the intermetallic precipitate γ' and the carbides MC and $M_{23}C_6$ types, where M symbolizes a metal. Under certain conditions of composition and heat treatment, another stable carbide phase, M_6C , can also precipitate. However, constituents such as σ , μ and Laves phases are also formed in Ni-based superalloys depending upon the operating conditions (Sabol and Stickler, 1969). Nickel based superalloys are classified depending upon their composition as (i) commercially pure nickel based, (ii) precipitation strengthened, (iii) specialty and (iv) solid solution strengthened alloys.

Commercially pure Nickel alloys primarily contain Nickel exceeding 99wt% (alloys 200 and 201). These materials possess low hardness and strength, and are used mainly for their corrosion resistance in caustic surroundings. Some of the commercially pure nickel alloys are also widely used in magnetostrictive or electrical applications. These alloys have excellent weldability however, are vulnerable to porosity when cast or welded.

The precipitation strengthened Nickel based alloys consist of additions of aluminum, titanium and/or niobium to produce a strengthening precipitate with nickel after a suitable heat treatment procedure. In most of the situations, these precipitates are consistent with austenite matrix, and thus deform the matrix such that strength of the alloy is enhanced significantly. The popular alloy of this category is Alloy 718. In general the alloy has a very good resistance to strain age cracking during post-weld heat treatment. Alloy 718 is mostly used for aerospace gas turbine shafting and pressure containment (DuPont et al., 2009).

Specialty alloys are the class of Nickel based alloys that display an outstanding creep resistance via both, precipitation hardening and dispersion hardening produced by a fine dispersed particles that are stable at high temperatures. MA6000 and MA754 are the examples of this category which possess very good oxidation resistance at high temperatures. However, they lose their high strength when welded through fusion processes. Nickel-aluminides, Ni-Cr-B and Ni-Mo-Si are also some of the alloys that are

considered under specialty alloys. These alloys are designed for excellent wear and corrosion resistance and high strength at elevated temperatures (DuPont et al., 2009).

Solid solution strengthened alloys are primarily strengthened by the alloying additions of substitutional elements Cr, Mo and Fe that provide solid solution strengthening of austenitic matrix. These alloys are extensively used in the chemical processing, power generation (industrial gas turbines), petrochemical industries and a number of other industries like cryogenic liquid handling, paper and pulp and composite tooling. These alloys normally contain carbides, the nature of which is determined by a combination of composition and heat treatment. The additions of alloying with Nb, Ti, W, Mo, and Ta forms MC type carbides while, $M_{23}C_6$ carbides are formed by Cr, Mo, and W. In many processing conditions, the $M_{23}C_6$ and MC carbides are usually found in these alloys (Sabol and Stickler, 1969; Shankar et al., 2001). Table 1.1 presents the most commonly used solid solution strengthened Ni-Cr alloys and their compositions. These alloys are susceptible to solidification cracking, however Alloy 625 among most of solid solution strengthened alloys exhibits excellent resistance to weld solidification cracking and is often selected to avoid problems with cracking, particularly when welding dissimilar materials. Figure 1.1 illustrates typical application of solid solution strengthened alloys in industrial gas turbine (DuPont et al., 2009).

1.2 INCONEL-625 ALLOY AND ITS APPLICATIONS

Inconel-625 is a solid solution nickel based alloy, strengthened by additions of molybdenum and niobium in its nickel-chromium matrix and is known for its high strength, excellent weldability and outstanding corrosion resistance. High tensile, creep and rupture strength, outstanding fatigue and thermal-fatigue strength and oxidation resistance are the properties of Inconel-625 that make the alloy suitable for its increased use in industrial gas turbines (Rai et al., 2004; Song and Nakata, 2010).

Table 1.1 Most commonly used solid solution strengthened alloys (DuPont et al., 2009)

Alloy	UNS	C	Cr	Fe	Mn	Ni	Mo	Si	Al	Other
600	N06600	0.15	14-17	6-10	1	72 min.	—	0.5	—	
601	N06601	0.1	21-25	Bal.	1	58-63	—	0.5	1-1.7	
617	N06617	0.15	20-24	3	1	Bal.	8-10	1	0.8-1.5	Co 10-15
625	N06625	0.1	20-23	5	0.5	Bal.	8-10	0.5	0.4	Nb 3.15-4.15
690	N06690	0.05	27-31	7-11	0.5	58 min.	—	0.5	—	
693	N06693	0.15	27-31	2.5-6	1	Bal.	—	0.5	2.5-4	Ti 1, Nb 0.5-2.5
C-4	N06455	0.015	14-18	3	1	Bal.	14-17	0.08	—	
C-22	N06022	0.01	20-24	3	0.5	Bal.	12-14	0.08	—	Co 2.5, W 3
C-276	N10276	0.02	14.5-16.5	4-7	1	Bal.	15-17	0.08	—	Co 2.5
C-2000	N06200	0.1	22-24	3	0.5	Bal.	15-17	0.08	0.5	
59	N06059	0.1	22-24	1.5	0.5	Bal.	15-16.5	0.1	0.4	
230	N06230	0.05-0.15	20-24	3	0.3-1	Bal.	1-3	0.25-0.75	0.2-0.5	
RA333	N06333	0.08	24-27	Bal.	2	44-47	2.5-4	0.75-1.5	—	
G3	N06985	0.015	21-23.5	18-21	1	Bal.	6-8	—	—	Cu 1.5-2.5
HX	N06006	0.05-0.15	20.5-23	17-20	1	Bal.	8-10	—	—	W 0.2-1
S	N06635	0.02	14.5-17	3	0.3-1	Bal.	14-16.5	0.2-0.75	0.1-0.5	
X	N06002	0.05-0.15	20.5-23	17-20	1	Bal.	8-10	—	0.5	Co 0.5-2.5, W 0.2-1
686	N06686	0.01	19-23	2	0.75	Bal.	15-17	0.08	—	W 3-4.4

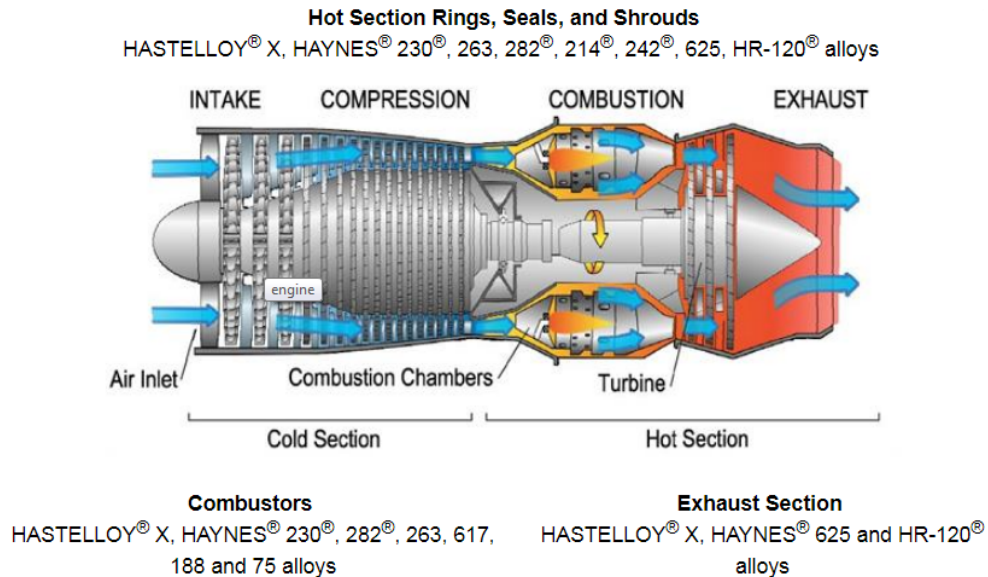


Figure 1.1 Application of solid solution strengthened Ni-Cr alloys in industrial gas turbine (Haynes International, 2015)

Inconel-625 derives its excellent corrosion resistance from the alloying elements that make the alloy as an attractive choice for marine, petroleum refineries, hydrotreating and hydrocracking units, and WTE boiler tubings. For instance, in mild environments, sea and fresh water, alkaline media and neutral salts alloy 625 is almost corrosion free. In more severe corrosive atmosphere, chromium offers resistance to oxidizing elements, whereas the combination of nickel and molybdenum makes the alloy impervious to non-oxidizing environments. High molybdenum content in alloy 625 makes it resistant to pitting and crevice corrosion while, niobium content stabilizes the alloy against sensitization during welding, so as to prevent intergranular attacks. The alloy being Nickel based develops freedom from chloride-ion stress corrosion attack due to its high nickel content (Smith et al., 2001). It is used as wire rope for mooring cables, propeller blades for motor patrol gun-boats, submarine auxiliary propulsion motors, submarine quick disconnect fittings, sheathing for under-sea communication cables, submarine transducer controls, and steam-line bellows (Korrapati et al., 2014). As evident from the literatures, Inconel-625 is considered to be the most appropriate material for the

components in nuclear water reactors because of its high allowable design strength at elevated temperatures between 649-760°C (Shankar et al., 2001). Automotive applications of Inconel-625 include the major portion of exhaust system bellows of flexible couplings and exhaust gas recirculation tubing. It is also suitable for combustion system transition liners, turbine seals, compressor vanes, and thrust-chamber tubing for rockets.

Some of the aerospace applications of Inconel-625 alloy include aircraft ducting systems, engine exhaust systems, resistance welded honeycomb structures for housing engine controls, fuel and hydraulic line tubing, turbine shroud rings, and heat-exchanger tubing in environmental control systems (Shankar et al., 2001). Figure 1.2 shows some of the real-time applications of Inconel-625 alloy.

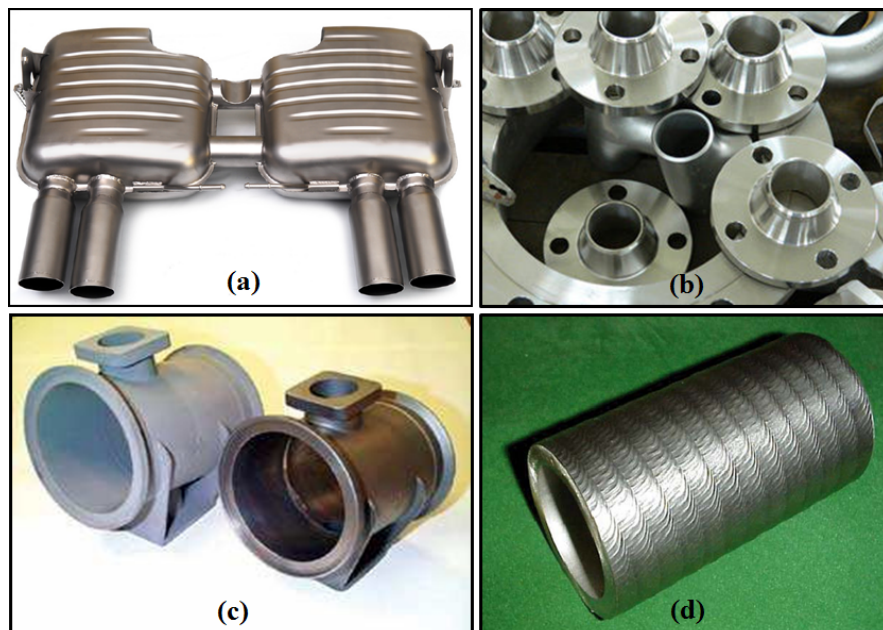


Figure 1.2 Typical applications of Inconel-625 alloy (a) Exhaust for BMW Model: E92/3 M3 (Precision sport industries, 2019) (b) Weld neck flanges for marine applications (Ganpat Industrial corporation, 2016) (c) Aerospace flow bodies (d) Alloy steel weld overlaid with Inconel-625 (Shoemaker, 2005)

Superalloy Inconel-625 has become an attractive alloy in development of strategic industries and cannot be substituted by any other alloy for typical applications due to its combination of mechanical and physical properties and easy fabricability. Therefore, current research work focuses on the welding of superalloy Inconel-625.

1.3 WELDING OF INCONEL-625 SUPERALLOY

Inconel-625 alloy is primarily used for the parts manufactured by solidification processes like casting and fusion welding. Previous reports have shown that a slight variation in composition of Nb, Si and C strongly influence the type and amount of secondary phases (γ +NbC/Laves) that form during the termination of solidification process. However, the alloy is susceptible to hot cracking in the fusion zone which is attributed to the formation of these secondary phases (DuPont et al., 1998). For decades fusion welding is used as one of the most reliable method to join Inconel-625 components with similar and dissimilar alloys. For any specific combination of metals to be welded several choices exist among the fusion welding techniques such as most commonly used shielded metal arc, gas metal arc, gas tungsten arc and submerged arc welding. More advanced fusion welding techniques are characterized by process involving high energy density like plasma arc, electron beam and laser beam welding. In addition to fusion welding, friction welding techniques are also available which offer advantages over the fusion welding techniques in that the substrate metals remain in solid state during joining. However, friction welding cannot be employed for all types of joint geometries. Therefore, today's industry still relies on high energy density processes like electron beam welding and laser welding for producing joints of Inconel-625 (Sun and Karppi., 1996).

The efficiency of these joining techniques to produce a defect free joint for a typical application depends on the variants of the processes such as thickness of the base metal to be welded, form and composition of parent metal and filler metal to be used, joint design and welding skill (Henderson et al., 2004). Further, environmental hazards and ease of processing are some of the key concerns that need to be addressed. Thus a more versatile, faster and cleaner process can ensure a huge impact on production. Studies in the past

reveal that application of microwave energy for materials processing is not only a green manufacturing process, but also significantly faster process and economical.

Microwave materials processing offers a substitute to high energy consumption heating techniques that are commonly used in industries. Processing materials with microwaves is emerging as one of the advanced processing techniques in the recent years. Microwave processing of materials fundamentally differs from traditional thermal processing techniques in a manner that microwave heating occurs at molecular level which results in volumetric heating. Microwave processing of materials is one of the pragmatic processes that has potential to produce parts with superior mechanical properties and improved microstructures.

1.4 INTRODUCTION TO MICROWAVE PROCESSING OF MATERIALS

Microwaves are electromagnetic waves in the frequency band from 300 MHz (3×10^8 cycles/second) to 300 GHz (3×10^{11} cycles/second).

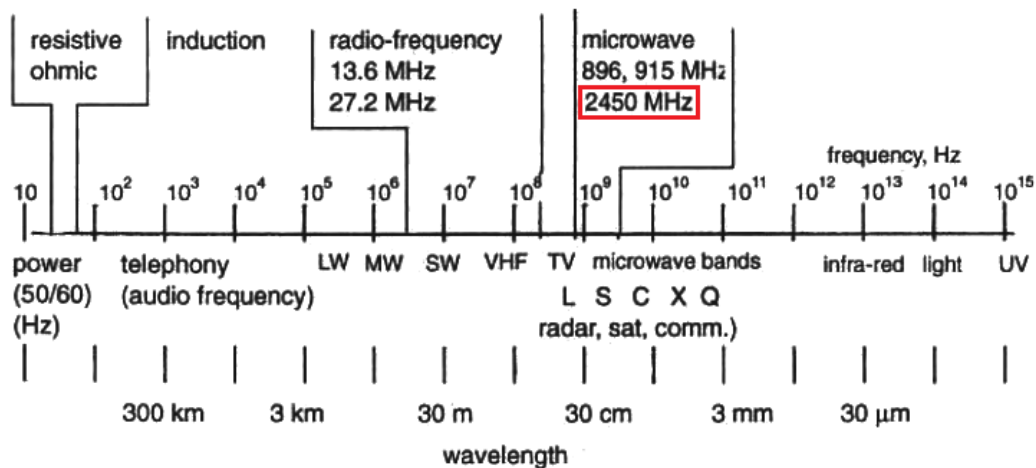


Figure 1.3 Electromagnetic spectrum and frequencies used in microwave processing (Meredith,1998)

As recommended by Federal Communications Commission (FCC), industrial microwave processing is usually accomplished at the frequencies reserved for industrial use 915 MHz, 2.45 GHz, 5.8 GHz, and 24.124 GHz. Microwaves belong to the portion of the electromagnetic spectrum with wavelengths from 1mm to 1m between these frequencies as shown in Figure 1.3. Depending upon the dielectric and magnetic properties microwaves can be reflected, absorbed and/or transmitted by the materials as the electric and magnetic fields interact with material during irradiation. During interaction, energy in the form of heat is generated in the material primarily through absorption (Thostenson and Chou, 1999; Osepchuk, 2002).

Microwaves find widespread application in many sectors as cooking, communication and information transfer, synthesis of materials, diagnostics and analysis, medical treatment, and manufacturing or material processing (Clark and Sutton, 1996). Microwave processing of materials till recent past was mostly restricted to semiconductors, ceramics, polymeric and inorganic materials. However, it has been revealed that the microwave energy can be efficiently employed to process essentially all metal powders as effectively as ceramic parts through hybrid heating techniques. This has provided an entirely new platform to explore the advantages of microwaves to process metallic materials so as to meet the ever-growing requirements of manufacturing industries.

1.4.1 Dielectric properties

Materials during microwave processing undergo physical and structural changes that affect dielectric properties and hence capacity of microwaves to generate heat does not remain same during the process. Microwave processing of materials is due to the combined effect of electromagnetic field properties, chemical composition of the material being processed, structural changes in the material during processing, dimensions of the specimen being heated and the physics of microwave-material interaction (Thostenson and Chou, 1999).

The ability of a dielectric material to absorb microwaves and store energy is given by the complex permittivity ϵ^*

$$\epsilon^* = \epsilon' - j\epsilon'' \quad \text{Eq. 1.1}$$

where ϵ^* is the complex permittivity (F/m) and j is the imaginary unit. ϵ' is dielectric constant which is the ability of the material to store energy, ϵ'' is the dielectric loss represents the ability of the material to convert absorbed energy into heat.

The ratio of the dielectric loss to the dielectric constant is known as the loss tangent ($\tan \delta$) which is given as;

$$\tan \delta = \frac{k''}{k'} = \frac{\epsilon''}{\epsilon'} \quad \text{Eq. 1.2}$$

where, k' and k'' are relative dielectric constant and relative dielectric loss respectively, which are given as $k' = \epsilon'/\epsilon_0$ and $k'' = \epsilon''/\epsilon_0$, ϵ_0 being the permittivity of free space. Hence, with small values of dielectric constant and large values of loss tangent or dielectric loss, materials couple with microwave with great efficiency (Chandrasekaran et al., 2012).

1.4.2 Penetration depth and power absorbed

The penetration depth D_p is an important parameter that determines the depth of penetration (meter) at which the incident power is reduced by one half exhibiting the uniformity of heating throughout the material. The extent of penetration depth determines whether the materials will absorb, transmit or reflect microwaves. The penetration depth can be expressed as,

$$D_p = \frac{c}{\left[\left(\left(1 + \left(\frac{k''}{k'} \right)^2 \right)^{1/2} - 1 \right) k' \right] \pi f \sqrt{2}} \quad \text{Eq. 1.3}$$

where, α is the attenuation factor, c is the velocity of light, f is the frequency (Chandrasekaran et al., 2012).

The type of heating achieved during microwave processing; whether volumetric or skin is dependent upon the dielectric and electrical properties of the materials. Since these properties depend on temperature, the penetration depth increases with the increasing

temperature. The penetration depth in case of metals is termed as skin depth ‘ δ ’ which is defined as the depth into the conductor from the surface at which the current density is $1/e$ (36.8% drop in the incident power) of its value at the surface. The unit of skin depth is micrometer and is expressed as,

$$\delta = (\rho / \pi f \mu)^{1/2} \quad \text{Eq. 1.4}$$

where, δ is the skin depth (microns), ρ is the resistivity ($10^{-6} \Omega \cdot \text{cm}$), f the operating frequency (GHz), μ is the magnetic permeability $\mu = \mu_r \mu_0$ (H/m), μ_0 is the absolute permeability = $4 \times \pi \times 10^{-7}$ (H/m) and μ_r is the relative permeability. Most metals generally have a penetration depth of the micrometer order, so the direct heating tends to remain superficial, but using the metallic materials with particle size less than that of the penetration depth it is possible to heat them directly (Oghbaei and Mirzaee, 2010; Mondal et al., 2010).

1.4.3 Microwave - material interaction

The microwave energy absorbed per unit volume of material depends on dielectric loss factor ϵ'' , material properties and its electric field. Figure 1.4 illustrates the relation between dielectric loss factor and power absorbed per unit volume of material.

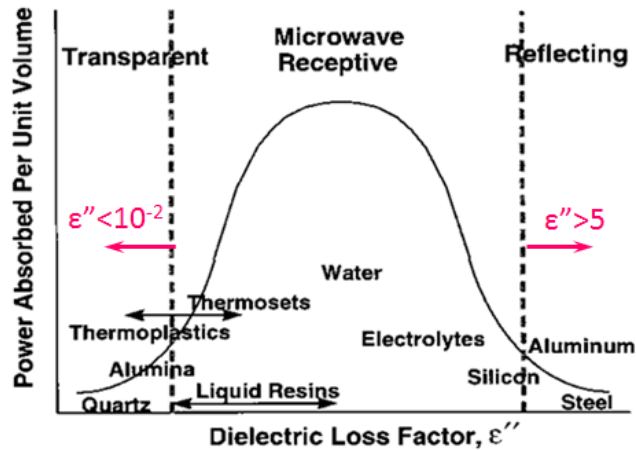


Figure 1.4 Relation between dielectric loss factor and power absorbed (Thostenson and Chou, 1999)

Materials with loss factors between 10^{-2} and 5 are called as absorbers and are considered as good candidates for microwave heating (Ex: SiC, graphite, water). Materials with dielectric loss factor less than 10^{-2} known as transparent, have no interaction with microwaves (Ex: teflon, quartz) while the materials with $\epsilon'' > 5$ called as opaque (Ex: metallic materials), the interaction of microwaves is restricted only to the surface (Clark and Folz, 2005). Processing of metallic materials through microwaves is extremely difficult, since metals do not couple with microwaves at room temperature due to very low skin depth. However, metallic materials can be heated efficiently through microwaves via the use of a microwave absorbing material (carbonaceous material, SiC, etc.) known as *susceptor*. This mode of heating is called as susceptor assisted heating or microwave hybrid heating (MHH).

1.4.4 Working principle of microwave oven

The microwave processing facility is used to convert the electrical energy into electromagnetic energy. Microwave oven is the equipment employed for microwave heating. It consists of three key components:

- (i) Microwave source/generator: This produces the electromagnetic energy by accelerating charges through vacuum tubes. The commonly used vacuum tubes are magnetrons, traveling wave tube (TWT) and klystron.
- (ii) Transmission line: This guides and couples the microwaves from the source to the applicator. For low frequency transmission co-axial cables are used while waveguides are used for high frequency transmission due to losses in co-axial cables. The transmission line is equipped with a circulator that safeguards the magnetron from reflected power.
- (iii) Microwave applicator: This is an open cavity where the target materials absorb electromagnetic energy and get heated up. Some of the microwave applicators are traveling wave applicator, waveguide, single mode cavity and multimode cavity. In general, the type of applicator used depends on the materials to be processed (Thostenson and Chou, 1999).

The schematic of domestic multimode microwave oven setup is shown in Figure 1.5. Microwave oven is equipped with a safety control unit which consists of thermal protectors and numbers of fuses, designed to disable the oven during electric short circuit or in case of overheating condition. The electrical path establishes automatically by a sequence of safety interlock switches, when the system door closes.

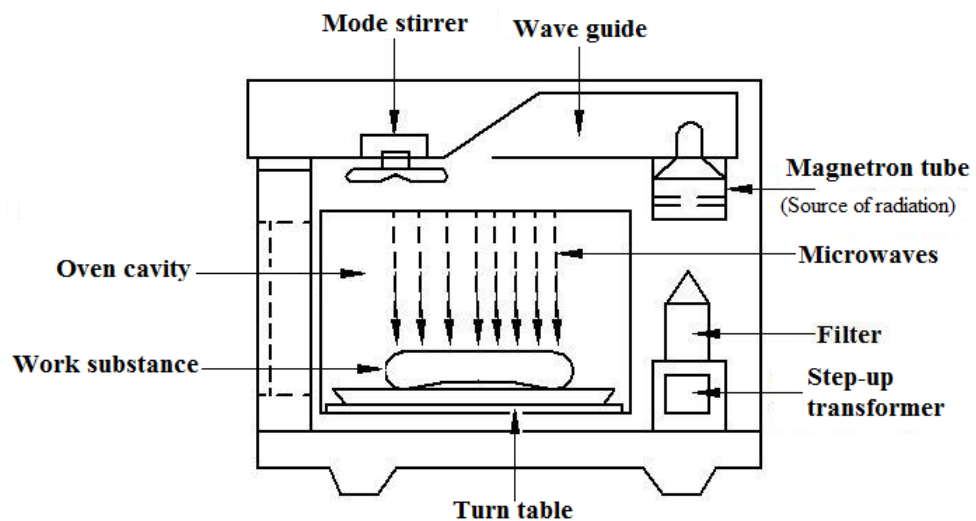


Figure 1.5 Schematic of microwave oven

The high voltage transformer along with capacitor and special diode arrangement increases the usual domestic voltage up to ~3000 volts. Microwaves are generated in the magnetron; pass through the wave guide and are directed to the work substance located on turn table. The work substance depending upon its dielectric properties absorbs the incident microwaves and gets heated up. To facilitate uniform heating, these ovens are provided with turn table and mode stirrer. The domestic microwave oven is designed to produce microwaves at an operating frequency of 2.45GHz with a provision to vary the microwave power in discrete steps between minimum and maximum limits.

1.4.5 Magnetron

Since magnetrons are compact in size and mass produced, these are generally used as microwave sources in domestic ovens. In magnetrons, the anode is at elevated potential in comparison to the cathode. This variation in potential generates a strong electric field, and the heated cathode eliminates the slackly bound valence electrons. Once the electrons are eliminated from the cathode, they are all accelerated towards the anode by the electric field. In a magnetron (Figure 1.6), a magnet is used externally to produce a magnetic field orthogonal to the electric field, and the applied magnetic field creates a circumferential force on the electron as it is accelerated to the anode. The circumferential force causes the electrons to travel spirally, and creates a swirling cloud of electrons. As electrons pass through corresponding cavities, the cavities set up oscillations in the electron cloud, and the frequency of the oscillations depends on the volume of the cavities. The electromagnetic energy is coupled with one of the resonant cavities of the transmission lines through a coaxial line or waveguide launcher (Thostenson and Chou, 1999).

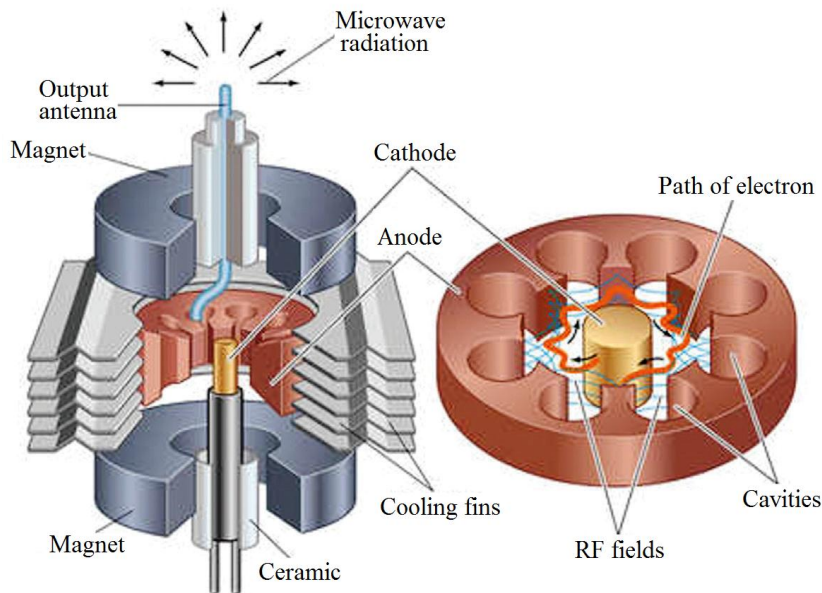


Figure 1.6 Schematic of magnetron (Borrell and Salvador, 2018)

1.4.6 Principle of joining bulk metals through microwave hybrid heating

Figure 1.7 shows a schematic of joining metallic plates through MHH technique. The surfaces of plates to be joined are cleaned with acetone and air dried prior to joining. A suitable interface filler powder is mixed with an epoxy resin to form thick slurry and applied as sandwich layer between the surfaces to be joined. The bulk pieces are covered with insulating material so that they are not directly exposed to microwaves. As metals reflect microwaves at room temperature, they do not get heated on direct exposure to microwaves and result in sparking. To overcome this problem a microwave absorbing material called as susceptor is employed around the joint interface.

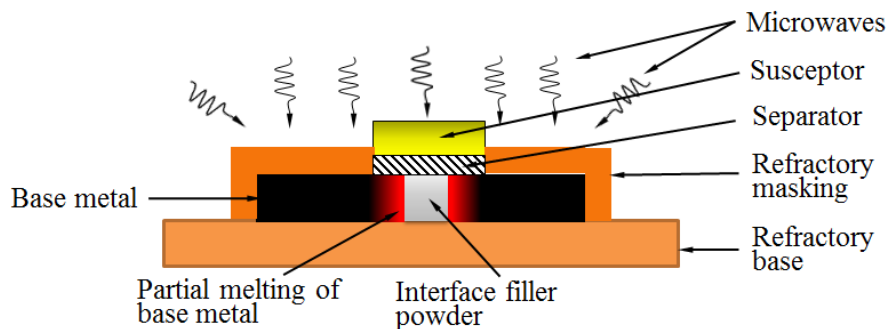


Figure 1.7 Schematic of joining bulk metals through microwave hybrid heating

As the exposure starts, susceptor couples with microwaves and gets heated to high temperature. The heat from susceptor is absorbed by the filler powder via a separator plate, which is used between the base metal and susceptor. The separator prevents intermixing of susceptor and interface filler powder. When the interface temperature reaches a critical temperature T_C , interface powder particles couple with microwaves and start absorbing microwaves directly. As the heating of the sample occurs in two modes; conventional mode during initial phase and microwave heating in the second phase, the process is called mixed mode heating or **hybrid heating**. Thus the temperature of the joint interface rises to its melting point and a narrow pool of molten metal forms between the interfacing surfaces and gets diffused through a thin dilution band in the joint zone. On cooling, a homogenous and dense joint is obtained through metallurgical bonding with the substrate.

1.4.7 Advantages of microwave processing

Since microwaves can penetrate materials and deposit energy, heat can be generated throughout the volume of the material (volumetric heating). As the transfer of energy does not rely on diffusion of heat from the surfaces, it is possible to achieve rapid and uniform heating of thick materials (Oghbaei and Mirzaee, 2010). Further, susceptor assisted heating combined with microwave heating results in uniform microstructure from surface to the center and also facilitates selective heating. In the present day, processing materials with microwaves has emerged as one of such candidate processing method which can satisfy industrial needs in near future as the most appropriate alternate process for energy efficient and eco-friendly material processing.

1.5 PROCESS PARAMETERS IN MICROWAVE WELDING

Process parameters in welding of bulk metals through MHH play important role in determining the quality characteristics such as tensile strength and flexural strength of the joints produced. The most important process parameters selected in the present study are as follows:

1.5.1 Susceptor

Metallic materials can be made to absorb microwaves efficiently at room temperature by raising their initial temperature through susceptor assisted heating. Susceptors are the materials that possess high dielectric loss factor and readily absorb microwaves at room temperature. As shown in Figure 1.7 the susceptor gets heated up by absorbing energy from the incident microwaves and further transfers this heat to the target material through conventional mode. Most commonly used susceptor materials include coal, graphite, carbon nanotubes, SiC, etc., (Bhattacharya and Basak, 2016).

1.5.2 Separator

Separator is a refractory layer used between the joint interface and susceptor as illustrated in Figure 1.7. The separator not only prevents intermixing of susceptor and interface filler

materials, but also plays an important role in transmitting the heat energy from susceptor to the joint interface. A refractory or carbonaceous material can be used as separator material.

1.5.3 Filler powder size

Interface filler powder is applied between the surfaces of the base metal plates to be joined as presented in Figure 1.7. It is one of the important parameters since the properties of an efficient joint largely depend on the chemical composition of interfacing (filler) material due to the fact that filler materials used must have good solubility between the base materials to be joined. Further, the studies carried out in the past (Yoshikawa et al., 2006; Ma et al., 2007; Mondal et al., 2008; Zafar and Sharma, 2015; Bagha et al., 2017; Soni et al., 2018) reveal that, mechanical properties of the microwave welded joint are largely influenced by average particle size of the interface filler powder.

1.5.4 Rated power of microwave oven

The rated power of the oven governs the heat input to the process which in turn determines heating rate. Further the rate of cooling also depends on heat input such that, higher heat input to the process results in slow cooling and vice-versa. Investigations in the past have shown that, heating rate to a great extent influences grain growth and thereby mechanical properties of the microwave processed components and overall processing time (Rodiger et al., 1998; Upadhyaya et al., 2007; Mondal et al., 2011; Chandrasekaran et al., 2011; Dwivedi et al., 2014).

1.6 INTRODUCTION TO DESIGN OF EXPERIMENTS (DOE)

In any experimentation process, a plan or strategy is necessary so as to minimize the number of experiments since the procedures are laborious and expensive. Therefore, it is desirable to attain the expected objectives be fulfilled with the least number of experiments. In this context, Design of Experiments (DOE) is a very effective statistical tool which was first introduced by Fisher R A (Roy, 2001). Later in 1940's considerable

amount of research was carried out by Dr. Genechi Taguchi using DOE technique to improve the quality of the manufactured products. Taguchi method facilitates the designer with a systematic and efficient approach for performing experiments to determine near optimum settings of design parameters in terms of performance and cost (Roy, 2001; Montgomery; 2013). Some other DOE techniques are full factorial design and response surface design methods. In the present study Taguchi approach is used.

1.6.1 Taguchi method

Taguchi developed a technique based on “Orthogonal array” of experiments which gives much reduced “variance” for the experiment with optimum settings of process parameters. Orthogonal array is a statistical method of defining parameters that converts test areas into factors and levels. The purpose of orthogonal array is to provide for selection of optimum level for each factor using analysis of means and to determine the relative significance of individual factor using analysis of variance (ANOVA). Test design using orthogonal array creates an efficient and concise test suite with fewer test cases without compromising test coverage. Taguchi method classifies the objective functions into three categories as, ‘smaller the better’, ‘larger the better’ and ‘nominal the best’. In the Taguchi method, analysis of the experimental results is made; to establish the best condition for a process; to estimate the percentage contribution of individual parameter; to predict optimal response at the best setting of factors (Ross, 1996).

1.7 OPTIMIZATION TECHNIQUES

Optimization technique is a key step to achieve a combination of process parameters for the desired output characteristics. There are two types of optimization techniques (i) single objective optimization and (ii) multi objective optimization. Single objective optimization is performed using desirability function while, grey relational analysis (GRA), entropy measurement, response surface method, artificial neural network techniques etc. are the examples of multi objective optimization technique. In the present

work, optimization of process parameters is carried out using Taguchi based GRA technique.

1.7.1 Grey relational analysis (GRA)

A grey system is defined as a system comprising of unknown information offered by grey numbers and grey variables. In Grey theory, black represents a system lacking information, while white represents complete data. Thus, the information that is either insufficient or uncertain is called grey (Moran et al., 2006). GRA was initiated by Deng Ju-Long in the year 1982 and has proved to be beneficial in handling poor, uncertain and incomplete information. GRA based on the theory of grey system can be used to solve the complex interrelationships between the multiple performance characteristics effectually. A grey relational grade is obtained through GRA, to assess the multiple response characteristics. Consequently, optimization of the intricate multiple response characteristics are converted into optimization of a single grey relational grade (GRG) (Lin and Lin, 2002). For the data pre-processing, there are three conditions of normalization namely higher the best, lower the best and nominal the best. In the present work, higher the best condition is used for normalization of tensile strength and flexural strength.

1.8 THESIS OUTLINE

The thesis comprises of six chapters to address the various aspects discussed in the above sections.

CHAPTER 1

In this chapter, the applications of Inconel-625 alloy in various fields, different techniques used to weld nickel based alloys and the limitations of these processes, processing of materials through microwave energy and its advantages have been discussed. The chapter also briefs about process parameters, optimization techniques and thesis outline.

CHAPTER 2

This chapter presents an exhaustive literature survey pertaining to the works reported on welding of Inconel-625 alloy using existing techniques, fundamentals of microwave processing and recent developments in microwave processing of metallic materials. In addition, parametric optimization techniques applied to welding of nickel based alloys are presented.

CHAPTER 3

The chapter describes the methodology adopted in experimentation process in detail. The selection of materials (base metal and filler), specimen preparation for mechanical and metallurgical characterization have been discussed. The chapter also illustrates the experimental setup used and various facilities employed to evaluate different performance characteristics of the microwave induced joints. Identification of the process parameters and their levels and selection of orthogonal array of experiments using Taguchi method are also elucidated.

CHAPTER 4

Investigation on the effects of process parameters on the responses such as ultimate tensile strength and flexural strength of the welded joints developed through microwave hybrid heating technique are presented in this chapter. Optimum combination of the process parameters that produce the best quality characteristics of the welded joint has been determined based on main effect plots and ANOVA tables. The Taguchi parametric design approach has been used to achieve the aforementioned aspects. Further, the metallurgical as well as mechanical characterization of the welded joints that exhibited best quality characteristics also has been carried out to verify the obtained results.

CHAPTER 5

Taguchi method of optimization is extended for the complete evaluation of multiple quality characteristics in joining of Inconel-625 alloy using MHH technique through

GRA. Multi objective optimization using grey relational analysis has been adopted to solve the problem of multiple quality characteristics to correlate the ultimate tensile strengths and flexural strengths mutually. Confirmation experimental verification supported by mechanical and metallurgical characterization has been performed with the optimized combination of process parameters.

CHAPTER 6

The chapter deals with the summary of the conclusions on the investigations carried out through this research work which further includes the recommendations addressing the scope for future research.

CHAPTER 2

LITERATURE REVIEW

2.1 INTRODUCTION

The literature review mainly focuses on works reported on welding of Inconel-625 alloy using existing techniques, microwave absorption in metallic materials, recent developments and effect of process parameters in microwave processing of metallic materials. In addition parametric optimization techniques applied to welding of nickel based alloys is also discussed.

2.2 CONVENTIONAL WELDING OF INCONEL-625 ALLOY

Several studies have been carried out in the past to investigate weldability of Ni-Cr alloys with stainless steels through GTAW using different filler metals (Lee et al., 2004; Naffakh et al., 2009; Hosseini et al., 2011). However, it has been found that the quality of the dissimilar joints obtained depends upon proper selection of filler wire and amount of heat input provided to the process which otherwise would lead to solidification cracking, heat affected zone liquation cracking and formation of unmixed zones as shown in Figure 2.1.

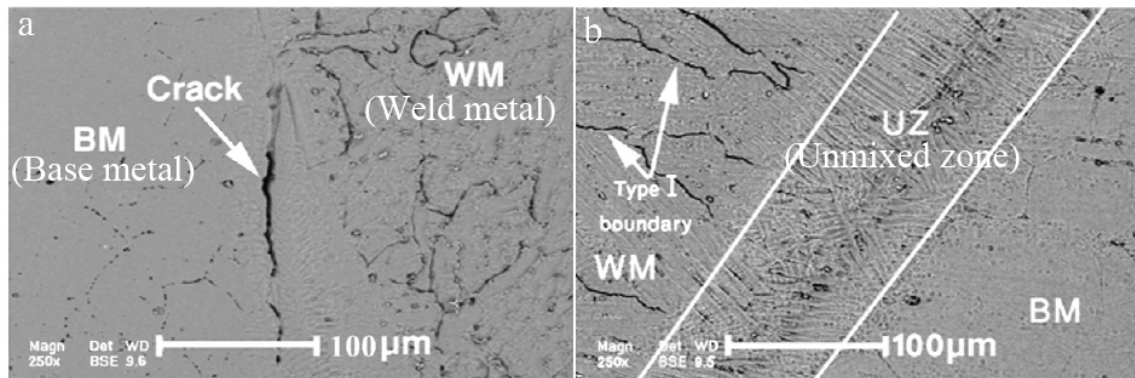


Figure 2.1 SEM micrographs (a) Interfaces between the filler 310 SS weld metal and the 310 SS base metal and (b) between the filler 310 weld metal and the Inconel 617 base metal (Hosseini et al., 2011)

Many researchers (Patterson and Milewski, 1985; Sridhar et al., 2014) investigated the characteristics of dissimilar welded joints between Inconel-625 with different stainless steels through GTAW using several grades of ERNiCrMo filler wires. The studies revealed the formation of hot cracked surfaces along with precipitation of secondary eutectic Laves phase in microstructures. Formation of Laves phases is detrimental to the strength of the welded joint as it consumes useful elements such as Nb and Mo from the alloy and precipitates as a hard secondary eutectic phase along the interdendritic regions. However, it was observed that, welded joints produced using filler ERNiCrMo-3 exhibited improved mechanical properties in comparison with other grades. Furthermore, Wilson et al. (1991) and Caiazzo et al. (2017) reported that, amount of Laves phases developed during the solidification of weld depends upon the process employed for welding as well as the amount of heat input supplied to the process. Several researchers (Ramkumar et al., 2014; Kumar et al., 2015; Ramkumar et al., 2017) successfully demonstrated this fact by employing CCGTAW and PCGTAW techniques to vary the heat input during welding of Inconel-625. The results were surprising and amount of the secondary phases reduced for the PCGTA welded joints in turn resulted in better mechanical properties.

Many successful attempts have been made in the past to weld Inconel-625 alloy with variety of stainless steels using EBW and Laser welding to obtain sufficiently strong dissimilar joints (Zapirain et al., 2011; Shakil et al., 2014; Ramezani et al., 2014; Li et al., 2015; Ramkumar et al., 2015). Shakil et al. (2014) noticed the occurrence of micro cracks at few places in fusion zone which is attributed to the segregation of sulphur, niobium and molybdenum. Further, it was reported that, Nb and Mo rich Laves phases in the fusion zone reduced the tensile strength and impact strength drastically. Duan et al. (2014) employed explosion welding to develop a hollow structure consisting of sealed pathways used in vacuum chamber of thermonuclear reactors. The effects of stand-off distance and explosive loading on the bonding strength were investigated and the joints obtained possessed higher tensile shear strength than that of the base metal. In addition to fusion welding techniques, friction stir welding is also used to join Inconel-625 alloy

since it is possible to attain exceptional mechanical properties as the material remains in solid state due to low heat input. Song and Nakata (2009) investigated the mechanical properties of friction stir welded Inconel-625 alloy and reported that the UTS of friction stir welded samples was 20% higher than that of base metal.

Most of the conventional techniques are well developed in terms of technological developments and academic research. However, the large heat input through these conventional processes results in substantial change in base metal and fusion zone microstructure, which leads to diminish the mechanical properties. Moreover while welding thick parts, multiple passes are required to obtain sufficient joint strength due to which the components are subjected to thermal cycling effect leading to the formation of carbides. This results in significant change in the base metal and fusion zone microstructures (Henderson et al., 2004; Song et al., 2012; Rajani and Mousavi, 2012; Shakil et al., 2014). In addition, high operating and maintenance costs associated with conventional welding processes also need to be considered (Ex: laser beam and electron beam welding are costlier to operate). On the other hand, EBW requires a very high vacuum to be maintained which is very difficult and at the same time uneconomical. Further, the higher power requirements associated with conventional welding processes also need to be addressed. These processing limitations of conventional joining techniques pave the way for exploring modern cost and energy effective processes involving low heat input. Innovative processes however are accepted by the manufacturing industries once they are economical with higher speed of processing.

In recent years application of microwave energy has been explored successfully for joining of metallic materials. The use of microwave energy for joining bulk metals has the potential to offer similar advantages as the conventional techniques of joining in reduced processing times and energy savings. In conventional thermal processing, energy is transferred to the material through convection, conduction and radiation of heat from the surfaces of the material. In contrast, microwave energy is delivered directly to materials through molecular interaction with the electromagnetic field. Because

microwaves can penetrate materials and deposit energy, heat can be generated throughout the volume of the material. The transfer of energy does not rely on diffusion of heat from the surfaces, and it is possible to achieve rapid and uniform heating of thick materials (Oghbaei and Mirzaee, 2010). Processing of metallic materials is difficult owing to the fact that metallic materials (powder as well as bulk) reflect microwaves at room temperature as dielectric loss factor of these materials is very high and thus the heating is restricted to surface only. However, metallic materials can be processed efficiently through the use of hybrid heating technique (Annamalai et al., 2013).

2.3 HEATING TECHNIQUES IN MICROWAVE PROCESSING

Microwave heating differs fundamentally with the conventional heating wherein heat transfer between materials takes place through conduction, convection and radiation. However, in microwave heating electromagnetic energy is directly converted into heat energy rather transfer of heat due to thermal gradients and therefore it is possible to achieve rapid volumetric heating (Oghbaei and Mirzaee, 2010).

2.3.1 Conventional and microwave heating

In conventional heating, thermal energy radiated by the heat source is restricted to the outer surface of the sample and heat transfer to the interior of the material takes place through conduction from hotter to colder region. Figure 2.2(a) illustrates the mechanism in conventional heating where the temperature of the material is usually hotter at the surface than at the core. As microwaves have the ability to penetrate inside the material, heat in microwave processing is generated from within the material since the material absorbs electromagnetic energy directly and does not rely on heat transfer from the walls of furnace. In Figure 2.2(b) the heat is generated inside the material and is radiated towards the surface of specimen. Outer surface of the specimen is usually at lesser temperature compared to core since the surface dissipates heat to the surroundings and an inverse temperature profile exists (Gupta and Wong, 2008).

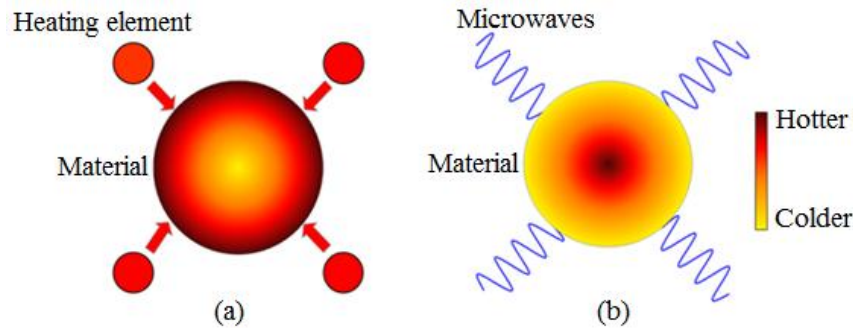


Figure 2.2 Heat distribution in a sample during (a) conventional heating (b) microwave heating (Gupta and Wong, 2008)

2.3.2 Direct microwave heating

Direct microwave heating is found suitable to heat water, food products, ceramics and very fine metallic powders. In this method the sample to be heated is directly exposed to microwave irradiation. Heat flows from center to the outside of material and an inverse temperature profile to that of conventional heating is observed. However, direct microwave heating leads to thermal gradients and hotspots as is observed during sintering some type of ceramics; alumina, zirconium oxide etc., (Lewis et al., 1997; Brosnan et al., 2003). Direct microwave heating often leads to a temperature rise (thermal runaway) due to continuous escalation of microwave absorption which is beyond control. Thermal runaway produces inferior qualities in the product and makes the reproducibility difficult (Menezes and Kiminami, 2008). These difficulties associated with direct heating can be overcome by means of MHH.

2.3.3 Microwave hybrid heating (MHH)

Many ceramics and polymers at room temperature when processing with 2.45 GHz frequency are transparent to microwaves and a long warm-up period is required to reach microwave processing temperature. However, these materials can be made to absorb microwaves at room temperature by adding microwave absorbing materials (doping) or by the use of susceptors. Doping alters the chemical composition of the part to be microwave processed and therefore not used frequently. On the other hand, external

susceptors provide the necessary heat without changing the chemical composition and therefore have been widely used by many researchers (Goldstein et al., 1998; Aravindan and Krishnamurthy, 1999; Ramesh et al., 1999; Rajkumar and Aravindan, 2009; Charmond et al., 2010) in the past for several applications involving MHH.

2.3.3.1 Susceptor assisted microwave heating

Susceptors are materials with a high dielectric loss factor that readily absorb microwaves at room temperature. The susceptor is heated by direct exposure to microwaves and transfers this heat to the target material (sample) through conventional mode. Thus the sample absorbs energy from the susceptor until its temperature increases to a critical value T_c . At this stage the sample gains the ability to absorb microwave energy and the next part of the heating continues by direct coupling of the sample with microwaves.

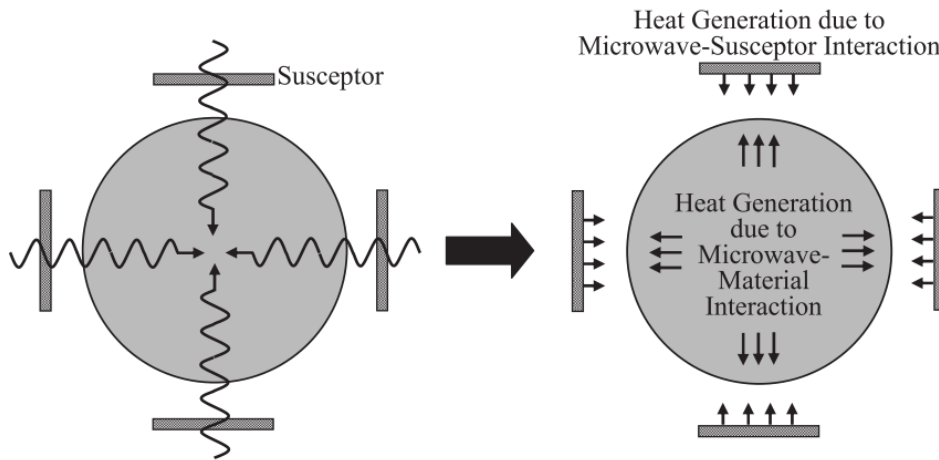


Figure 2.3 Microwave hybrid heating (Bhattacharya and Basak, 2016)

In this case heating of the sample occurs in two directions; susceptor heats the sample from outside towards center and microwaves heat the sample from center towards the core (Figure 2.3). Thus compared to direct microwave heating a uniform temperature distribution throughout the sample is observed since in direct heating, center is hotter than outer surface that loses heat to the surroundings continuously (Bhattacharya and Basak, 2016). Processing of metallic materials through microwaves is extremely difficult since metals do not couple with microwaves at room temperature due to very low skin

depth. Nevertheless, metallic materials can be made to absorb microwaves efficiently at room temperature by raising their initial temperature through susceptor assisted heating.

Table 2.1 Most commonly used susceptor materials (Bhattacharya and Basak, 2016)

Material	Frequency (GHz)	$\tan \delta$	Penetration depth (cm)
SiC	2.45-2.5	0.37	1.93
Water	2.45-2.5	0.15	3
Carbon Black	2.45	0.23	5.75
Graphite Powder	2.45	0.36-0.67	1.34-2.09
Activated Carbon	2.45	0.31-0.9	0.7-3.43
Coal	2.45	0.14-0.38	6-11
Carbon Fibers	8.2	0.45-0.5	0.5-0.7
Carbon Nanotube	8	1.11	0.2

In the present work, susceptor assisted heating or microwave hybrid heating technique is adapted to develop Inconel-625 welded joints. Table 2.1 presents the most commonly used susceptor materials along with their loss tangent and penetration depth values. The indicated properties in Table 2.1 are valid for the corresponding operating frequencies at room temperature.

2.4 PROCESSING OF METALLIC MATERIALS THROUGH MHH

Based on the published research, processing metallic materials through MHH can be broadly categorized into three groups; (i) powdered metal (ii) bulk metal-powdered metal and (iii) bulk metal. Prior to 1988 there was a misconception that metallic materials cannot be processed through microwave energy, since the exposure of metals to microwaves cause plasma formation resulting in sparking. However, this misconception was valid only for powdered metal compacts and bulk metals at room temperature. It was demonstrated for the first time by Walkiewicz et al. in 1988 that metals in fine powdered form can be heated efficiently in a commercial microwave oven (Gupta and Wong, 2008). In later years remarkable works in terms of theoretical and experimental

investigations were reported on processing of powdered metals in the form of sintering through MHH. Sintering of metallic powders through MHH is well matured in terms of academic research; however in recent years, hybrid heating technique which was used earlier for sintering metallic powders has been effectively extended for processing of bulk metal-powdered metal system and bulk metal system in the form of joining, brazing, cladding and melting.

2.4.1 Comparison of metallic material processing applications involving MHH

Processing of metallic materials through MHH differs in the way the target material is exposed to the microwaves in each application as for sintering, cladding and joining. However, since the principle of MHH makes use of susceptor aided heating applied to sintering (powder metal system) and cladding and joining (bulk metal-powder metal system) in common, these processes are combined in one figure as illustrated in Figure. 2.4. The key components of the hybrid heating system in each case have been isolated from the main figure and are depicted in separate Figures 2.4 (a), (b) and (c) for better clarity to demonstrate sintering, cladding and joining.

Microwave sintering is carried out by exposing the isostatic pressed metallic powder compacts to the microwave irradiation for prolonged periods at predetermined temperature which results in densification of the metallic powders. As shown in Figure. 2.4 (a), 1-2-3-4-5-6-7-8 represents a powder compact. The susceptor is heated by absorbing the microwave energy and transfers this heat to the powder compact by conventional mode until the powder compact attains a critical temperature T_c . Thereafter the powder compact absorbs microwave energy by direct coupling with microwaves and a bidirectional heating phenomena is observed i.e. susceptor heats the compact from outside towards the center and the microwaves produce heat from center of the compact towards the surface.

Cladding of metallic surfaces is carried out to improve the surface properties of soft metallic materials by depositing a coating of hard metallic powder on metallic substrate.

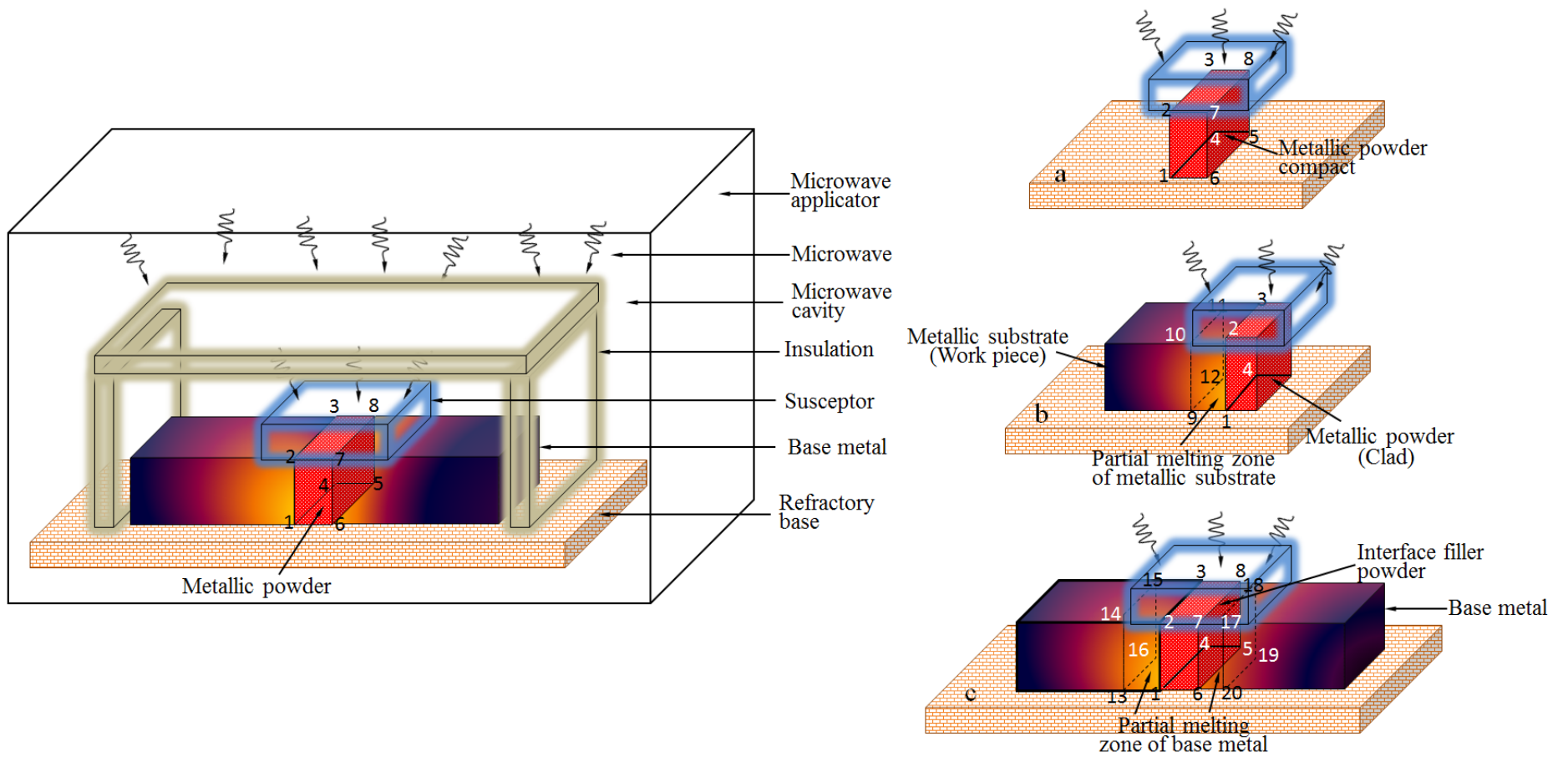


Figure 2.4 Principle of MHC illustrating (a) Sintering (b) Cladding (c) Joining processes

In cladding through MHH, metallic / cermet powder is placed in contact with the substrate surface requiring cladding as depicted in Figure 2.4 (b). The susceptor couples with microwaves and heats the clad powder through conventional mode of heat transfer until the temperature of clad powder reaches a critical value T_c . This initiates the coupling of microwaves with the metallic / cermet powder so as to cause complete fusion of clad powder and partial melting of substrate surface along a narrow band between planes 1-2-3-4 and 9-10-11-12 resulting in a strong metallurgical bond between the substrate (sample) and clad.

Joining of metallic materials through MHH is a distinct application of susceptor to selectively heat a localized area without affecting the remaining part of the metal. As illustrated in Figure 2.4 (c), exposure of microwaves is focused on the interface area through susceptor. Similar to sintering and cladding processes the fusion of interface powder represented by 1-2-3-4-5-6-7-8 occurs so as to form a solid joint with the base metal. The joint is obtained by complete melting of filler powder in the interface and partial melting of base metal surface near the joint region along the thin bands between planes (i) 1-2-3-4 and 13-14-15-16 and (ii) 5-6-7-8 and 17-18-19-20.

The MHH principle described in Figure 2.4 is only to illustrate the similarities between sintering, cladding and joining processes. However, in actual practice these processes require special tooling and appropriate arrangement of materials being processed. In the following sections contributions of several researchers in the area of sintering, cladding and joining of metallic materials through MHH have been discussed.

2.4.2 Sintering of metallic powders

Conventional sintering processes consume significant energy due to longer soaking periods to facilitate inter-grain diffusion and also due to longer heating and cooling periods required to minimize thermal gradients in the sample. In addition as the heating takes place from the outer surface towards the core, often the center of the samples in conventional sintering remains under-processed.

This leads to non-uniform microstructure and development of undesirable phases in the microstructure of the samples (Anklekar et al., 2005; Gupta and Wong, 2005). These problems can be overcome by employing microwave energy for sintering that result in rapid and volumetric heating.

Roy et al. (1999) for the first time successfully demonstrated full sintering of wide range of porous metal powder compacts including iron and steel, copper, molybdenum, aluminum, cobalt, nickel, tungsten, tungsten carbide, tin and their alloys using microwave energy in a 6kW, 2.45GHz multimode oven. The green compacts were placed inside an alumina tube surrounded by mullite fibers for insulation purpose. Principles of MHH were applied for heating by placing SiC rod susceptors around the compacts. Sintered compacts exhibited dense structure with better mechanical properties than their conventionally sintered counterparts. In later years many works were successfully reported on microwave sintering of tungsten and its alloys, ferrous alloys, copper and its alloys etc. Anklekar et al. (2005) reported on a comparative study of sintering of FC-0208 and FN-0208 composition steel powder compacts processed through conventional as well as microwave energy. Microwave sintering was carried out in a 2kW multimode oven at 2.45GHz frequency. SiC rods were used as susceptor for raising the initial temperature of the compacts. Microwave sintered compacts exhibited a higher crushing strength and microstructure consisting of uniformly distributed alloying elements. Gupta and Wong (2005) carried out SiC aided sintering of different metallic powders including aluminium, magnesium and Viomet solder alloy using 900W-2.45GHz microwave facility. Figure 2.5 shows the schematic of the set-up used for sintering. Saitou (2006) reported on microwave hybrid sintering of iron, cobalt, nickel, copper and stainless steel powders in the presence of a 5mm thick SiC tube as the susceptor. A boronitride tube was used to house the green compacts and this boronitride tube was inserted in SiC tube to perform sintering under a controlled atmosphere in a single mode applicator. Microwave sintered compacts exhibited higher density with 80K/min heating rate compared to that of 10K/min in conventional sintered samples.

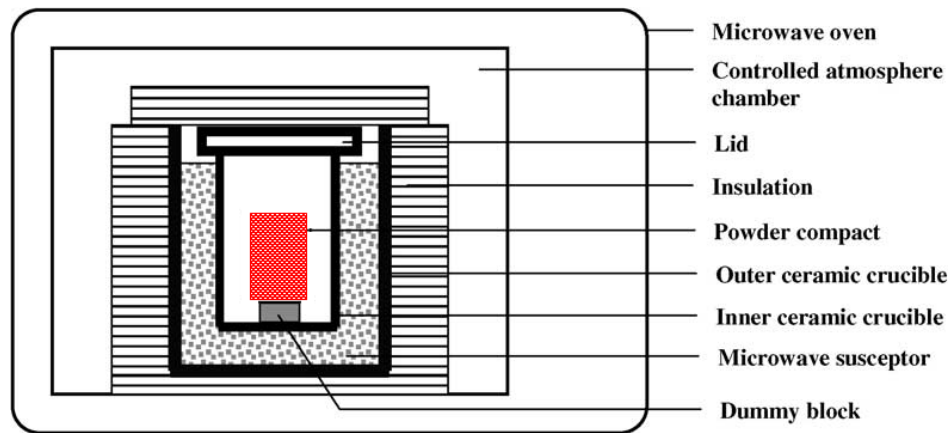


Figure 2.5 Schematic of experimental setup used for sintering (Gupta and Wong, 2005)

Upadhyaya et al. (2007) in their study compared the mechanical properties and microstructure of 92.5W-6.4Ni-1.1Fe compacts sintered at 1500°C through conventional as well as microwave modes. Microwave sintering was performed in a 2kW, 2.45GHz commercial oven.

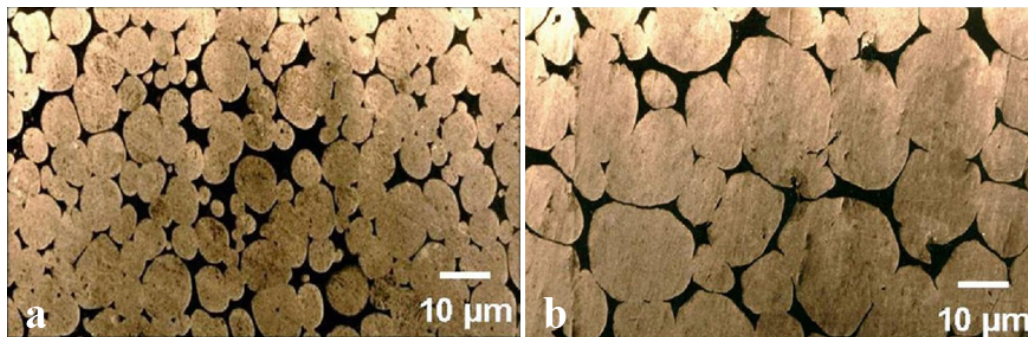


Figure 2.6 SEM micrographs of (a) microwave sintered (b) conventionally sintered 92.5W-6.4Ni-1.1Fe alloy compacts (Upadhyaya et al., 2007)

Heating rates observed with microwave and conventional sintering were 20°C/min and 5°C/min respectively. 75% reduction in processing time was observed with microwave sintering process despite low power consumption. Microstructure examination of the microwave sintered compacts showed fine grain structure in comparison with their

conventionally sintered counterparts as shown in Figure 2.6 which is attributed to the volumetric heating associated with microwave processing. Sunil et al. (2010) studied the microwave sintering of nano-crystalline WC-12Co compacts in a 6kW furnace at different temperatures ranging between 1100°C and 1550°C. The green compacts were housed in an alumina fiber board casket and sliced SiC cylinders were used as susceptor surrounding the compacts. Microwave sintered compacts displayed better mechanical properties compared to the conventional sintered ones. Rajkumar and Aravindan (2009) carried out microwave hybrid sintering of copper-graphite MMC in a 3.2kW-2.45GHz industrial oven with copper volume fraction varying between 70% and 95%. The compacted specimens were placed inside an alumina fiber casket and surrounded by SiC fence for uniform heating. Microwave sintered compacts exhibited fine microstructures with rounded pores. Mahmoud et al. (2015) investigated on the effect of oxide shell formation on microwave absorption behavior of copper powder. Copper powder was microwave sintered in presence of argon, nitrogen and hydrogen gases with a heating rate of 10°C/min at 1000°C with different holding times. Formation of oxide layer on the copper powder promoted the microwave absorption which signifies volumetric heating associated with microwave processing.

Aluminium alloys due to their light weight, higher specific strength, high malleability and low cost are extensively used in automotive industries. Peng and Binner, 2002 performed microwave hybrid sintering of Al powder by employing carbon powder as susceptor, that was packed inside an alumina tube placed around the sample in nitrogen atmosphere. Hybrid heating resulted in higher heating rates (70-140°C/min) and the complete synthesis was accomplished in approximately 15min. Padmavati et al., 2012 reported on microwave assisted sintering of Al-3.8Cu-1Mg-0.8Si-0.3Sn (105µm) in vacuum, nitrogen, argon and hydrogen atmospheres at temperatures ranging between 570°C to 630°C. The experiments were performed in 6kW-2.45GHz multimode applicator and the compacts were placed in a mullite casket fitted with graphite coated SiC rods.

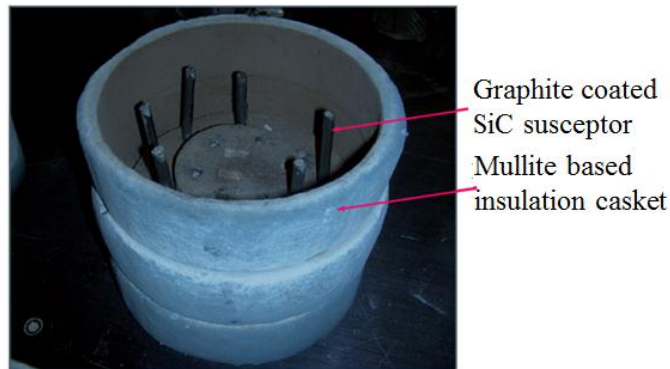


Figure 2.7 Casket set-up used for sintering of Al-Cu-Mg-Si-Sn alloys (Padmavati et al., 2012)

Figure 2.7 presents a photograph of the arrangement used for placement of green compacts during sintering. The compacts sintered in nitrogen atmosphere exhibited higher densities and better corrosion resistance while, the compacts sintered in argon and hydrogen atmosphere suffered with increased porosity. Xu et al. (2015) reported on effect of pore size on microstructure and properties of porous nitinol alloys processed using microwave energy. Powders of Ni-Ti were blended with varying proportions of ammonium hydrogen carbonate (NH_4HCO_3). The green compacts were sintered by placing them in an alumina crucible by covering the compacts with SiC particles. Kutty et al. (2004) applied SiC assisted microwave heating to develop dental implants of titanium with the porous surface and dense core. Sintering was carried out by placing Ti powder compact between two SiC susceptors in an alumina based fiberboard thermal insulator box. Ti powders were heated to 1300°C in approximately 11 min with 1.5kW input power and additional sintering for 30 min lead to desired densification of the compacts. Luo et al. (2010) successfully investigated the microwave sintering of pure titanium (Ti) powders by employing susceptor. The authors reported that direct microwave heating Ti powders exhibited very low heating rates for the powder size ranging between $20\text{-}63\mu\text{m}$. On the other hand, susceptor based microwave heating employing SiC or MoSi_2 rapidly heated the Ti powders to 1200°C within 90 minute at 0.3-0.8 kW input power and revealed a density up to 92-96% TD. Tang et al. (2013)

performed bidirectional SiC assisted microwave sintering of compacts of Ti_6Al_4V in association with carbon nanotubes to produce porous compacts of Ti alloy/TiC composite for orthopedic applications.

2.4.3 Cladding of bulk metals with metallic powders

Surface of the components may be subjected to different type of loadings (independent or combined) including mechanical, chemical, thermal, etc. Under such circumstances damage of the component occurs by degradation of the exposed surface. However, the surface properties can be improved by suitable modifications in the structure and chemistry of the surface or by cladding on the exposed surfaces resulting in improved life of the component (Sharma and Krishnamurthy, 2002). In microwave cladding process sound metallurgical bonding results between completely fused clad powder and partially fused substrate surface. Earlier works by Sharma et al. (2001) report on processing of plasma sprayed ceramic composite coatings through microwave irradiation. Alumina-titania composite coatings 0.9mm thick were developed on mild steel substrate with Ni-Al interfacial bond coating of 0.1mm thickness using atmospheric plasma spraying facility. These as-sprayed specimens were later exposed to microwave irradiation in a charcoal environment for 30 minutes. It was reported that volumetric heating associated with microwave processing, refined the grain structure of as-sprayed coatings and healed the cracks present on the surface prior to the treatment which resulted in enhanced surface properties.

Most of the available literature on susceptor assisted cladding reports on development of clads on stainless steel substrates. Gupta and Sharma (2011) reported on development and characterization of WC-10Co-2Ni clad developed on austenitic stainless steel (SS-316) substrate in a 900W-2.45GHz multimode oven. A 2mm thick clad of WC-10Co-2Ni was developed by depositing coal powder (susceptor) on a thin graphite separator placed between clad powder (APS 40 μ m) and susceptor as shown in Figure 2.8. Average microhardness of the developed clad was observed to be 1064 \pm 99 HV with approximately 0.89% porosity. Gupta and Sharma (2011) later demonstrated the

microwave cladding of nickel based powder EWAC (APS 40 μ m) on austenitic SS-316 substrate in a coal environment (susceptor). A 900W, 2.45GHz domestic microwave oven (LG Solardom) was employed to conduct the experiments.

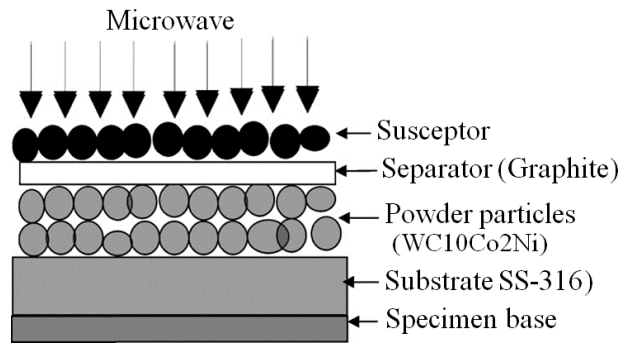


Figure 2.8 Schematic of cladding process (Gupta and Sharma, 2011)

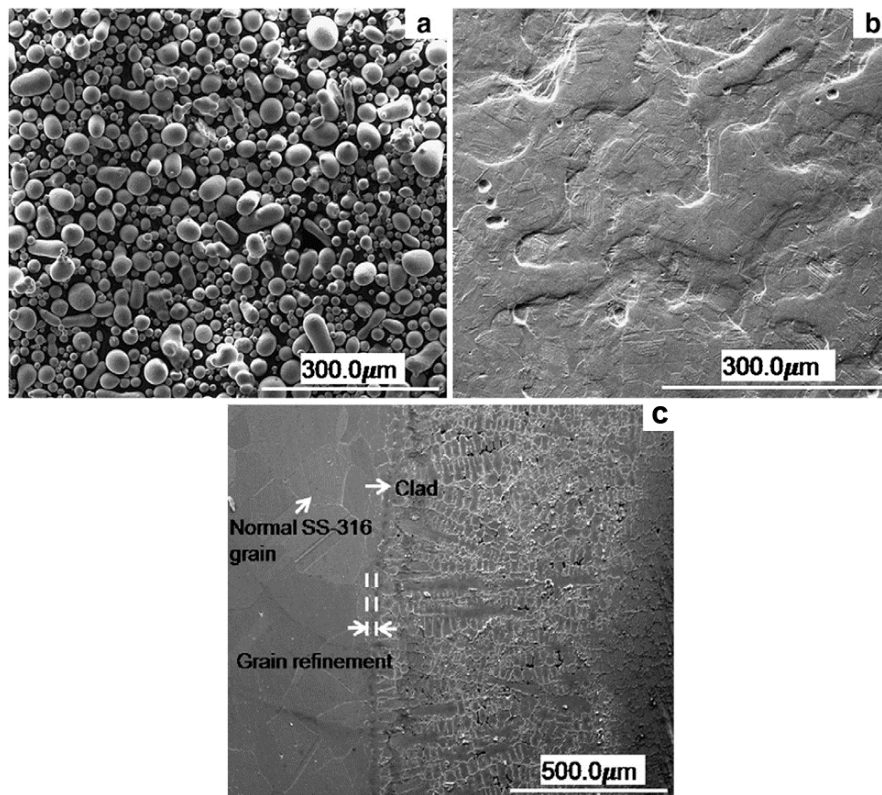


Figure 2.9 SEM micrographs of (a) morphology of EWAC powder (b) as-received SS-316 plate and (c) microwave developed clad (Gupta and Sharma, 2011)

Microstructure of the clad exhibited a cellular structure without any visible pores and cracks. Elemental analysis indicated the segregation of chromium at the grain boundaries to react with carbon and form chromium carbide. Average microhardness of the clad surface was observed approximately double that of the substrate material. Figure 2.9 presents the SEM micrographs of EWAC powder, base metal and the developed clad. In a similar investigation Gupta et al. (2012) developed and characterized the microwave irradiated composite clad consisting of EWAC and Cr_{23}C_6 chromium carbide powders (APS $40\mu\text{m}$) in proportions of 80% and 20% respectively on austenitic steel SS-316 substrate. Cladding was carried out with the help of coal susceptor and graphite separator in a 900W, 2.45GHz domestic oven. Figure 2.10 depicts the SEM micrograph of the developed clad with 0.5mm thickness which exhibited uniform distribution of hard Cr_{23}C_6 particles, embedded in a soft and tough nickel matrix.

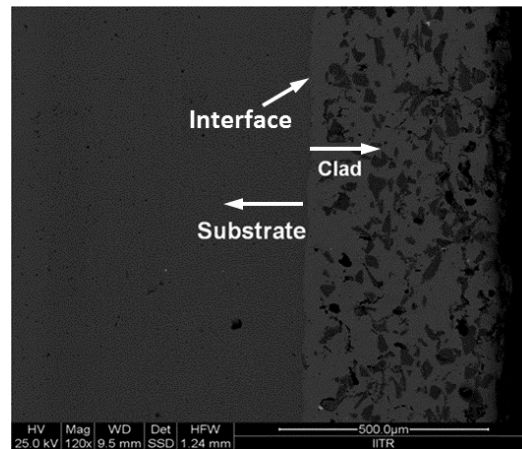


Figure 2.10 SEM micrograph of EWAC+ Cr_{23}C_6 composite clad (Gupta et al., 2012)

Sharma and Gupta (2012) deposited a microwave composite cladding of nickel based powder EWAC and $\text{WC}_{10}\text{Co}_2\text{Ni}$ (APS $40\mu\text{m}$) in proportions of 80% and 20% respectively on austenitic stainless steel SS-316 substrate. Cladding was carried out with the help of coal susceptor and graphite separator in a 900W, 2.45GHz domestic oven. Presence of WC, W_2C , $\text{Co}_3\text{W}_3\text{C}$, NiSi and NiW phases was identified in the tough Ni based matrix through XRD study. Microstructure of the clad samples exhibited cellular

structure with precipitation of free carbon at the grain boundaries. Developed clads showed an average hardness almost twice as that of the substrate material.

Bansal et al. (2015) developed a clad of Ni-WC on mild steel substrate in a 1.1kW, 2.45GHz industrial microwave oven. Susceptor assisted cladding was performed in coal environment with alumina sheet separator. The average particle size of the clad powder was measured to be 30-40 μ m. The authors reported the formation of planner structure near the interface region followed by interlocked white phase of tungsten carbide reinforcement in tough nickel matrix. The average microhardness of the clad was observed to be approximately three times that of the MS substrate. In a similar work, Pathania et al. (2015) carried out susceptor assisted cladding of MS by using composite EWAC + 20%WC10Co2Ni powder. A 900W, 2.45GHz LG (Model: Light wave convection) microwave oven was used for processing with coal powder susceptor and graphite separator. The developed clad exhibited significantly higher hardness (980HV) compared to the base metal (140HV) which was attributed to the formation of tungsten carbide phase in soft nickel matrix. Hebbale and Srinath (2016) developed microwave cladding of Ni based powder EWAC on SS-304 substrate via the use of coal susceptor and graphite separator in a 900W, 2.45GHz domestic oven. FeNi₃, NiSi, Cr₂₃C₆ and Cr₃C₂ phases were detected during the phase analysis. Figure 2.11 shows the clad samples developed through MHH.



Figure 2.11 (a) Microwave induced EWAC clad samples (b) Clad samples prepared for metallurgical observations (Hebbale and Srinath, 2016)

Kaushal et al. (2018) deposited a composite clad of Ni based powder and 10% SiC powder on martensitic stainless steel SS-420 substrate through MHH technique in a 900W, 2.45GHz oven via coal susceptor and graphite separator. It was reported that microstructure of the clad exhibited uniform distribution of SiC particles in tough Ni matrix and average microhardness in the clad section was observed to be $652\pm 90\text{HV}$. Kaushal et al. (2018) in a similar study developed a composite clad of EWAC and alumina powder on SS-304 substrate using charcoal susceptor and alumina sheet separator. The clad exhibited a hardness which was 40% higher than that of base metal.

2.4.4 Joining of bulk metals with metallic powder interface

Initial attempts to weld metallic materials using microwave energy were demonstrated by Soares and Rego (1995). Thin steel strips in the range of 0.1-0.3mm were exposed directly to microwave radiation in a 2kW multimode oven. Joining of the strips occurred due to arcing at the joint interface. However, joining of thick bulk metals is very difficult owing to the reflection of microwaves. Early contributions by researchers to braze bulk metals under specific conditions through microwave energy provide the potential to join bulk metals in a low-cost microwave oven. Barmatz et al. (2000) proposed a new method to braze polycrystalline diamond tip to a tungsten carbide support of a drill bit head used in petroleum industries through selective heating of substrate materials by melting the interface braze powder using microwave energy. The experiments were carried out using a single mode microwave oven with variable frequency in vacuum.

Susceptor aided microwave joining of metallic materials is a distinctive application of suscepting material to selectively heat a localized area without affecting the remaining part of the metal. This characteristic has been successfully explored by many researchers to join variety of similar and dissimilar metallic materials. Budinger (2008) in the form of patent reported microwave brazing of nickel-based super alloys using fine metallic interface powder of similar composition as that of substrates. A 1kW, 2.45GHZ multimode microwave oven was used and the brazing was carried out in a SiC enclosure. Microwave joining of austenitic SS-316 (25mm×12mm×6mm) through MHH and its

characterization was carried out by Srinath et al. (2011) in a 900W domestic microwave oven using charcoal susceptor and nickel based powder EWAC (APS 40 μ m) as the interface filler. A thin graphite sheet was used as separator between the interface filler and coal powder. Figure 2.12 presents the photograph of the SS-316 welded specimens. Complete fusion of the interface powder occurred and the joints were free from any interfacial cracks. Formation of carbides of nickel, iron and chromium in the joint zone during the exposure of joints to microwaves was reported. The hardness of the fusion zone was noticed to be approximately same as that of base metal.

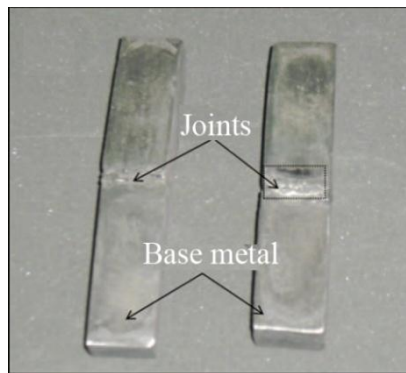


Figure 2.12 SS-316 welded specimens developed through MHH (Srinath et al., 2011)

SS-316 joints exhibited significant strength with 11.6% elongation which indicates the efficacy of the microwave joining process. Srinath et al. (2011) in a later study investigated on characterization of welded joints of copper developed through MHH. Copper powder of particle size $\sim 5\mu$ m and 99.5% purity was used as an interface filler powder. The microwave induced joints exhibited reasonably good tensile strength with 29% elongation which was attributed to the complete fusion of copper powder particles with good metallurgical bonding with the base metal. Figure 2.13 shows the schematic of the process and macrostructure of the developed copper joint. Subsequently, Srinath et al. (2011) reported on microstructure and mechanical properties of dissimilar joints obtained by welding SS-316 and MS through microwave hybrid heating. Nickel based powder

EWAC of 40 μm particle size was used as interface filler material along with coal susceptor.

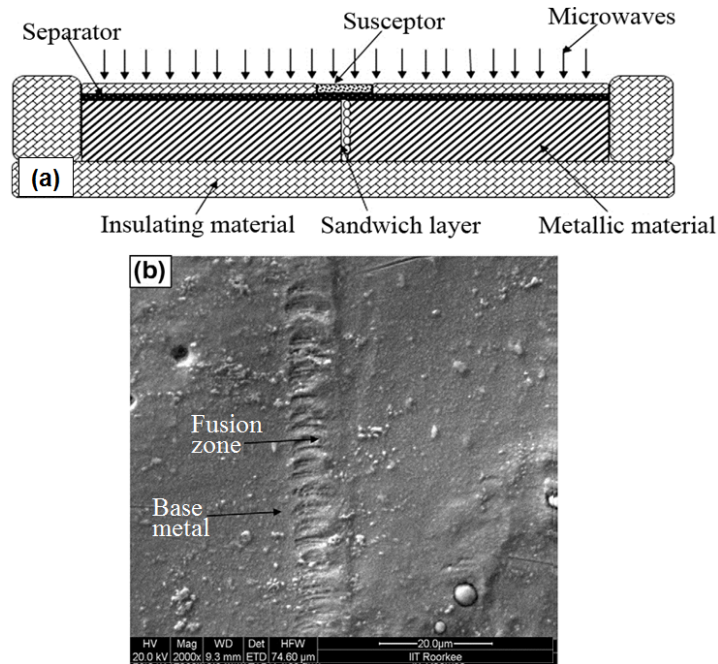


Figure 2.13 (a) schematic tooling used for joining copper plates (b) macrostructure of joint developed through MHH (Srinath et al., 2011)

Bansal et al. (2013) in their preliminary work, joined MS plates through MHH technique using Ni based powder as interface filler and charcoal powder as susceptor. EDS analysis of the joint indicated the presence of elements Fe and Mn in addition to Ni and Cr which is attributed to the dilution of Fe and Mn from the base metal into the joint zone at elevated temperature. UTS of the joint was found to be 50% of the parent metal strength. Bansal et al. (2014) in a later investigation reported on joining of SS-316 plates using SS-316 interface powder (APS 50 μm). Silicon carbide block was used as susceptor along with a thin alumina sheet as separator. Joints fractured in a ductile mode and UTS of the joint was ~85% of base metal strength with an elongation of 9.44%. Singh et al. (2015) developed the welded joints between Aluminium plates through MHH using Aluminium powder as interface filler material. Characterization of the joints was carried out through XRD, SEM and microhardness tester. Developed joints exhibited completely fused

interface with a good metallurgical bonding. XRD study revealed the dominant peaks of Aluminium and small peaks of Aluminium oxide.

Bansal et al. (2015) investigated the metallurgical and mechanical characteristics of post weld heat treated Inconel-718 welded joints produced through microwave hybrid heating. Microstructural investigation revealed that, compared to as-weld condition no significant changes in the mechanical properties were observed after direct aging treatment. Microwave induced specimens treated at 981 solution treated and aged significantly dissolved large amount of Laves phase and complete dissolution of Laves phase occurred with 1080 solution treated and aged specimens. In a similar study, Bansal et al. (2016) attempted joining of dissimilar metals SS-316 and MS using microwave hybrid heating in 1.2kW applicator. They reported that, microhardness in the joint zone was significantly higher as of base metals. The measured strength values were in the range of 70 to 80% of the strengths of base metals. In a subsequent work, Bansal et al. (2016) carried out joining of dissimilar metals Inconel-718 and SS-316 using Inconel-718 powder as interface filler between the base metals. Charcoal was used as a susceptor material and a flux UV420TT in agglomerated form was employed as separator. Average ultimate tensile strength of the joint was estimated to be 99.5% and 60.8% for SS-316 and Inconel-718 plates respectively.

Bagha et al. (2017) studied the effect of Ni based interface filler powder size on mechanical properties of SS-304 joints. Microhardness test results indicated higher hardness values in joint zone as well as at the interface of specimens welded with finer powder compared to other combinations. A more homogeneous structure was obtained with finer size powder (20 μ m) and resulted in higher ultimate tensile strength of the joint. However, the ductility of the joint was affected as the powder size decreased from 50 μ m to 20 μ m. Recently, Gamit et al. (2017) explored the theoretical aspects of microwave welding of MS tubes and successfully carried out the joining of MS tubes using a domestic 900W oven.

Though, joining of bulk metals through MHH is a recent technological development, it has a potential to join many advanced materials; however, the process is presently limited to laboratory level and needs to be industrialized.

2.5 EFFECT OF PROCESS PARAMETERS ON OUTPUT RESPONSES

The effect of influencing parameters in microwave welding largely depends on many factors and has to be investigated individually for each new material to be welded. Several processing conditions employed for joining bulk metals through MHH has been well documented in literature. Consequently, it is essential to realize the importance of these parameters during processing of metallic materials through microwaves. In the present work the effect of process parameters; interface powder size, susceptor material, separator material and rated power on quality of microwave welded Inconel-625 alloy has been investigated.

2.5.1 Effect of interface powder size on ultimate tensile strength (UTS) and flexural strength (FS)

The size of the metallic powder employed for processing is one of the crucial parameters that affects product characteristics and absorption of microwaves in the candidate metallic materials. The skin depth of the metallic material depends upon the resistivity i.e. lesser the resistivity lower is the skin depth. It has been observed that very fine metallic powders couple well with microwaves and exhibit higher heating rates (Ma et al., 2007; Prabhu et al., 2009; Mondal et al., 2008; Oghbaei and Mirzaee, 2010).

Ertugrul et al. (2014) sintered compacts of SS-316L powders with varying particle size in a 2.45GHz microwave applicator. The authors reported that, compacts prepared from 45 μ m particle size displayed higher yield strength, when compared to the compacts of 56 μ m particle size. Srinath et al. (2011) in different works joined Cu\Cu, SS-316\SS-316 and SS-316\MS through MHH (Sharma and Mishra, 2017). The copper plates were joined using copper powder (5 and 40 μ m size) while, SS-316\SS-316 and SS-316\MS joints were obtained by employing nickel based powder EWAC (5 and 40 μ m size). Due

to the fact that, powder with smaller particle size exhibit better heating rates compared to coarser powder consequently, processing with fine powders results in uniform and volumetric heating so as to produce improved mechanical properties. The investigations revealed that the use of finer interfacing powders dramatically improved tensile strength of the developed joints. Furthermore, it was observed that, reduced particle size of interfacial powder resulted in reduced porosity, improved tensile strength and micro hardness of the developed joints. Bagha et al. (2017) during joining of SS-304 noticed that, homogeneity of the joints and tensile strength of SS-304 joints improved significantly with interfacial decreased Ni powder size. Nickel based interface powder with particle size 20, 30, 40, and 50 μ m were considered for their study. The joints developed with 20 μ m displayed a highest UTS of 337MPa while the UTS reduced dramatically (240MPa) with 50 μ m interface powder. However, on the other hand it was noticed that, the ductility of the joints reduced with increasing UTS. Soni et al. (2018) employed nickel nano size powder as interface filler to join SS-316 plates through MHH in a 800W-2.45GHz oven. The developed joints exhibited improved tensile strength compared to those in earlier works carried out using micro size powders. It was reported that tensile strength and hardness of the joints improved by ~24% with nano Nickel powder interface.

2.5.2 Effect of susceptor/separator on UTS and FS

Both the susceptor and separator are important components in joining of bulk metals through MHH since they have a crucial role in mechanism of heat transfer to the joint interface followed by melting of the interface filler powder and partial fusion of adjacent base metal (Vaidhyanathan and Rao, 1997; Saxena et al., 2014; Gamit, 2017; Mishra and Sharma, 2017). Anklekar et al. (2001) carried out the susceptor assisted microwave hybrid sintering of Cu-steel 97Fe-2 Cu using SiC rods and local carbon coating as susceptors. The powder metal compacts were located in an alumina dish, which was placed in a mullite tube inside a fiberfrax insulator. The authors (Anklekar et al., 2001) reported that the hybrid heating with carbon coated dish exhibited highest heating rate to

that with SiC rods. Further, the compacts sintered using carbon based coating susceptor yielded a FS of 1077MPa which was significantly higher than those sintered using SiC. Saxena et al. (2014) in a successful attempt joined Cu pipes through MHH via three types of susceptors charcoal, coal and graphite. The authors (Saxena et al., 2014) claimed that, the joint developed with graphite susceptor, exhibited higher strength compared to other susceptors. In a similar work Gamit (2017) joined MS pipes by employing charcoal, SiC and graphite susceptors. Charcoal exhibited better heating characteristics compared to the other two susceptor materials and resulted in good metallurgical bonding between the pipes. The joints developed with charcoal susceptor witnessed a UTS of 397MPa which accounted to 65% of base metal strength. However, no other facts regarding the characterization of the joints were reported.

2.5.3 Effect of input power on UTS and FS

The microwave power is another parameter that considerably influences the heating rate of the candidate material being processed. Microwave power absorbed by a material is the power dissipated due to the electromagnetic field which can be represented as energy converted within the heated material. Thus the power absorbed by a material is determined by skin depth of the material. Due to variation in the dielectric properties of material with varying temperature and time, real time measurement of power absorbed by a material in a microwave applicator becomes very difficult. However, energy balance can be applied to estimate the power term using an empirical approach (Mishra and Sharma, 2016). Researchers in the past (Upadhyaya et al., 2007; Mondal et al., 2011; Chandrasekaran et al., 2011) have demonstrated the fact that increasing the input microwave power considerably enhances the heating rate thereby, reducing the cycle time. Dwivedi et al. (2014) investigated the effect of rated power on tensile strength of mild steel welded joints by considering three power levels; 800W, 850W and 900W. Microwave induced joints developed at 800W exhibited higher UTS. This is due to the fact that, though higher power levels improved the heating rate, the large amount of heat

in the vicinity of the joint area promoted the formation of porosity and temperature gradients.

2.5.4 Investigations on UTS and FS of MHH developed joints

Srinath et al. (2011) carried out joining of SS-316/SS-316 using nickel based powder EWAC as interface filler. The developed joints exhibited UTS of 309MPa (~60% of the base metal strength) with 12% elongation. In a similar investigation, Soni et al. (2018) employed nickel nano size powder as interface filler to join SS-316 plates through MHH in a 800W-2.45GHz oven. The welded joints displayed UTS of 74% of the base metal strength. Bansal et al. (2014) on the other hand employed SS-316 interface powder for joining SS-316 plates and noticed that MHH developed joints exhibited a UTS of 85% of base metal strength with an elongation of 9.4%. Figure 2.14 depicts the tensile specimen developed for carrying out uniaxial tensile tests.

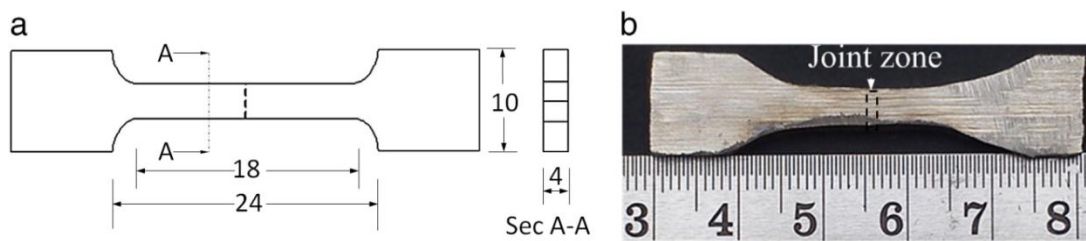


Figure 2.14 (a) Dimensions of tensile test specimen as per ASTM-E8 standard and (b) Photograph of microwave welded SS-316 tensile test specimen (Bansal et al., 2014).

Srinath et al. (2011) in a different work joined copper plates using copper interface powder of 5 μ m average particle size (APS). The microwave induced copper joints exhibited UTS of 164MPa and 29% elongation. Subsequently, Srinath et al. (2011) investigated on UTS of dissimilar joints obtained by welding SS-316 and MS through MHH. The UTS of 346MPa with 13% elongation was achieved for the joints developed using 40 μ m interface powder. Bansal et al. (2016) in a similar investigation with SS-316 interface powder observed that microwave induced dissimilar joints of SS-316/MS demonstrated UTS of 420MPa with 6% elongation. Furthermore the dissimilar joints exhibited a FS of 787MPa (73% of base metal strength) with an elongation of 5%. Figure

2.15 shows a typical load-elongation curve obtained during flexural 3-point bend test. Bansal et al. (2016) carried out joining of dissimilar metals Inconel-718 and SS-316 using Inconel-718 powder as interface filler between the base metals. Average ultimate tensile strength of the joint was estimated to be 517MPa, (~99.5% and 60.8% of the SS-316 and Inconel-718 plates respectively) with 18% elongation.

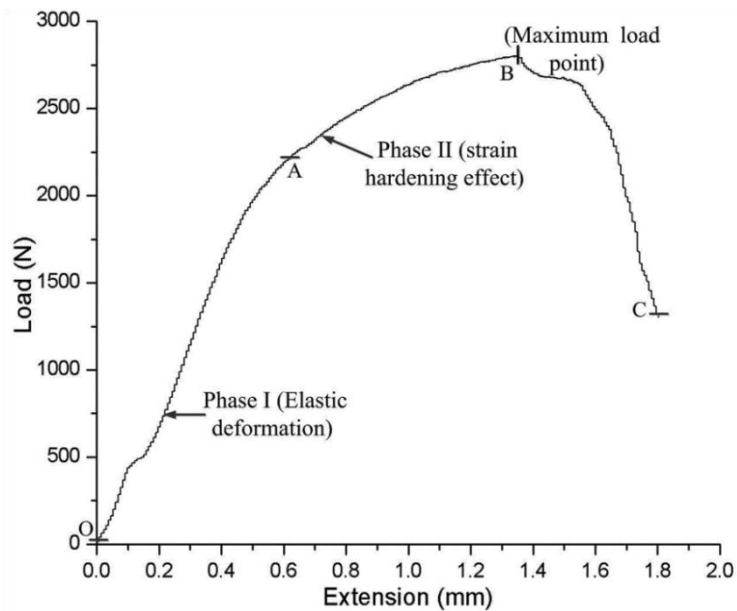


Figure 2.15 Load–extension characteristics of the SS-316/MS welded specimen during 3-point bend test (Bansal et al., 2016)

Figure 2.16 shows the stress-strain characteristics of Inconel-718 and SS-316 microwave induced joints. Sharma and Gupta (2012) deposited a microwave composite cladding of nickel based powder EWAC and WC10Co2Ni (APS 40 μ m) in proportions of 80% and 20% respectively on austenitic stainless steel SS-316 substrate. Cladding was carried out with the help of coal susceptor and graphite separator in a 900W, 2.45GHz domestic oven. In order to evaluate the clad peel-off strength, 3-point flexural test was conducted as per the schematic arrangement shown in Figure 2.17 The clad exhibited good adherence with the substrate material even after the fracture till the end of test which is attributed to presence of soft Ni phase.

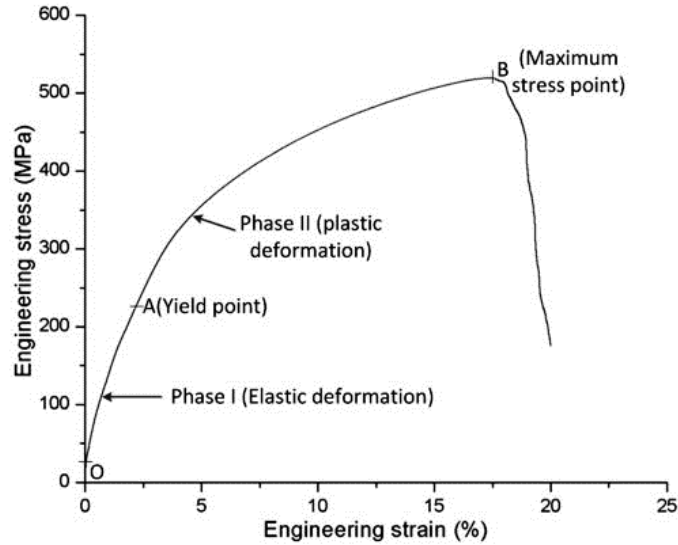


Figure 2.16 Stress-strain characteristics of Inconel-718/SS-316 dissimilar joint (Bansal et al., 2016).

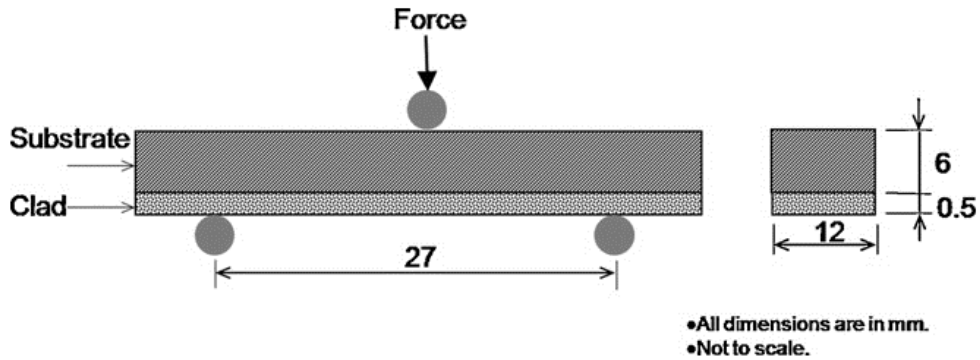


Figure 2.17 Schematic arrangement of 3-point bend test (Sharma and Gupta, 2012)

2.5.5 Observation of fractured surfaces

Srinath et al. (2011) investigated on failure mode in fractured surfaces of the microwave welded copper plates subjected to uniaxial tensile test. The fractography studies were

carried out with the aid of scanning electron microscope. As can be seen from Figure 2.18 the micrograph consists of sharp honey-comb like structure which signifies a brittle fracture.



Figure 2.18 SEM micrograph of fractured copper joint (Srinath et al., 2011)

The formation of honey-comb structure was observed in the regions where complete melting and resolidification of powder particles occurred. Consequently these resolidified particles lost their ductility resulting in brittle fracture. On the other hand the morphology also shows partially melted copper particles which contributed to enhance the tensile strength of the joint. Further, the presence of dimples or concave depressions was also witnessed which indicated a ductile fracture. Thus from the micrograph of fractured surfaces it was observed that the failure of microwave induced copper joint took place in mixed mode.

Bansal et al. (2013) carried out joining of MS plates by employing Ni based interface filler powder through microwave energy. The welded specimens were tested under tensile loading and the fractured specimens were subjected to fractography analysis through SEM. The examination of fractured surfaces indicated failure of the joints in both ductile as well as brittle manner. It was reported that the ductile fracture occurred due to plastic deformation of matrix phase consisting of solidified nickel powder particles. On the other hand, carbides present in the matrix could not deform plastically; however when the applied load reached a critical value, these carbide phases fractured in brittle manner.

Similar observations were made by the authors (Bansal et al., 2016) during joining SS-316/MS with SS-316 interface powder through MHH. The developed joints were subjected to uniaxial tensile test as well as 3-point bend test up to the fracture. Figure 2.19 shows the photographs of fractured tensile and 3-point bend test specimens. Investigation of the fractured surfaces revealed that the failure of the joints occurred in mixed mode.

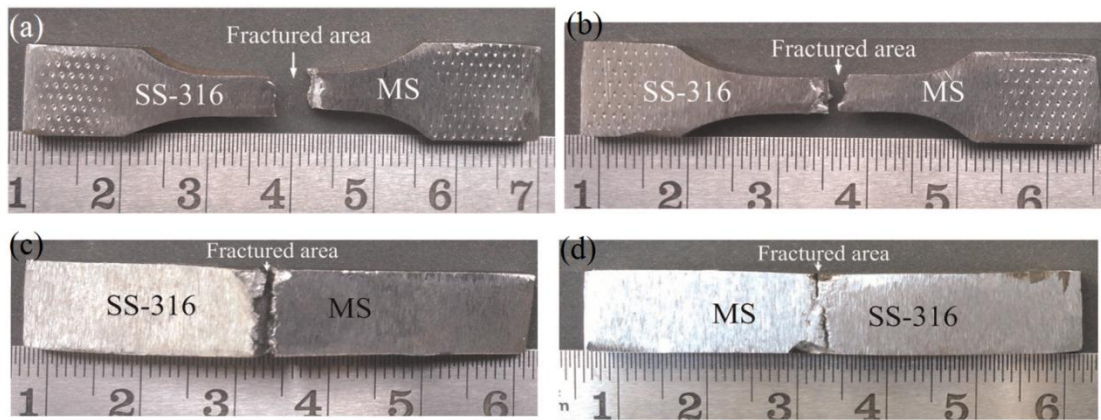


Figure 2.19 Photographs of fractured (a) and (b) tensile specimens and (c) and (d) 3-point bend test specimens (Bansal et al., 2016)

Bansal et al. (2014) developed the microwave induced welded joints between SS-316 plates using SS-316 interface powder. The mechanical characterization of the welded specimens was carried out by conducting uniaxial tensile test.

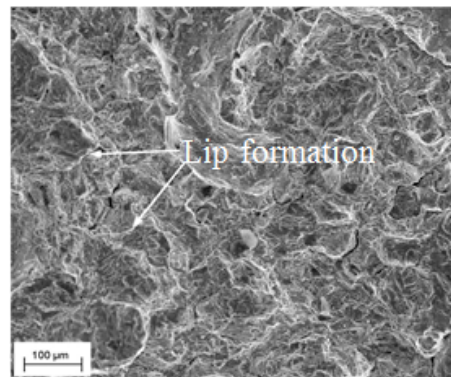


Figure 2.20 SEM micrograph of fractured SS-316 microwave induced joint showing ductile fracture (Bansal et al., 2014)

It was reported that all the specimens fractured in the joint zone; however, a ductile mode of fracture was exhibited by the fractured surfaces as shown in Figure 2.20. The micrograph clearly shows the formation of lips at several places which signifies a ductile fracture. Bansal et al. (2016) in their continued research, carried out joining of dissimilar metals Inconel-718 and SS-316 using Inconel-718 powder as interface filler.

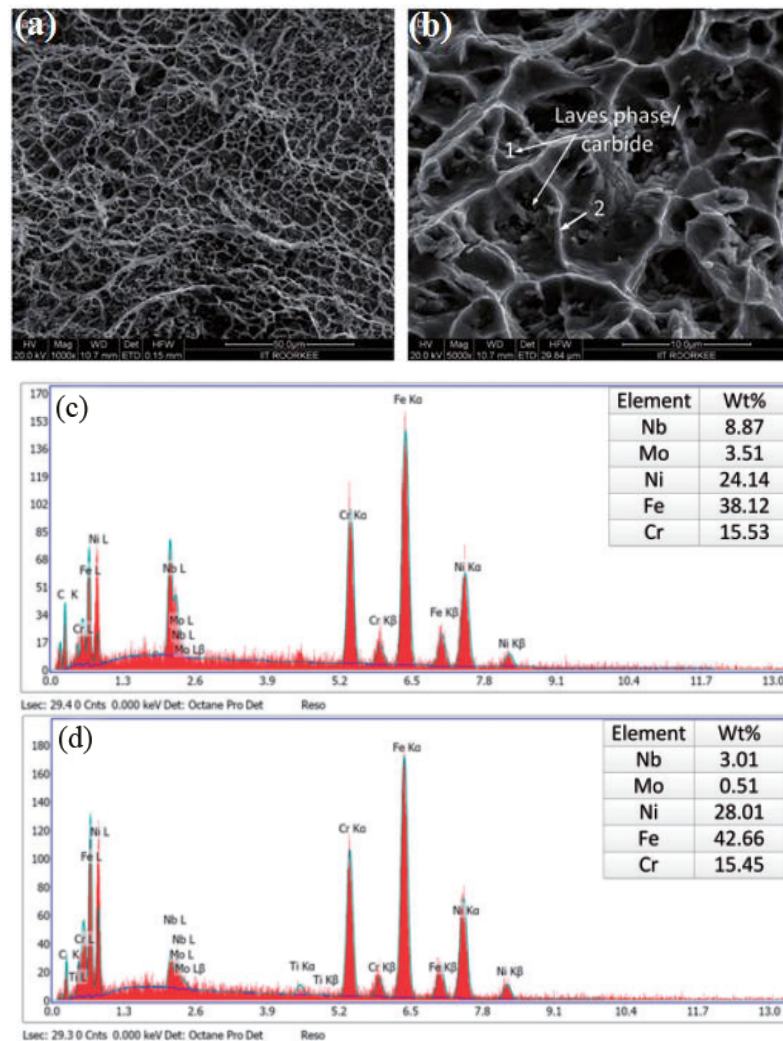


Figure 2.21 (a) and (b) Fractured surfaces of Inconel-718/SS-316 weld joint, (c) and (d) EDS analysis at locations 1 and 2 respectively (Bansal et al., 2016)

Uniaxial tensile test was conducted to ascertain the relevant characteristics of the microwave induced joints. Fractured specimens were further analysed through SEM.

Fractography study revealed the formation of dimples in the fractured zone which signifies a ductile fracture. Further, the presence of Laves phase particles was also seen in the interior of the dimples as shown in Figure 2.21. Laves phase provide favorable sites for the formation of microvoids during plastic deformation and subsequent growth of microcracks.

2.5.6 Observations from microhardness studies

Prabhu et al. (2009) investigated the microwave sintering behavior of as-received tungsten powder 99.95% purity and particle size $5\mu\text{m}$ to $7\mu\text{m}$ with that of the same powder ball milled (activated tungsten powder) with further reduced particle size. The sintering was performed under nitrogen atmosphere in a 3kW-2.45GHz industrial microwave furnace. Microwave sintered activated powder compacts exhibited increased hardness (303HV) as compared to that of as-received tungsten compacts (265HV). Gupta and Sharma (2011) developed WC-10Co-2Ni clad on austenitic stainless steel (SS-316) substrate.

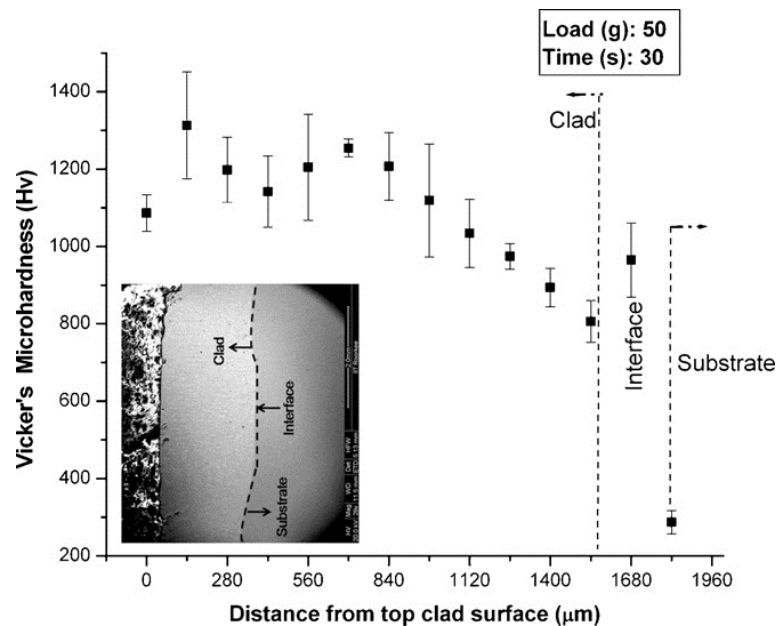


Figure 2.22 Variation in microhardness distribution of WC-10Co-2Ni clad (Gupta and Sharma, 2011)

A uniform hardness of 1100HV was recorded up to the center of the clad attributed to the presence of hard tungsten carbide phase; however, the hardness reduced as the clad interface approached. The hardness at the clad substrate interface reduced to 800HV which is due to the dilution of metallic elements. Figure 2.22 shows the variation of the microhardness profile obtained for WC-10Co-2Ni clad. Gupta and coworkers (2011, 2012) in different works developed the clad of EWAC (2011) and a composite clad of EWAC+ Cr₂₃C₆ (2012) powders on SS-316 substrate. Average microhardness of the EWAC clad surface was observed to be 304±48HV, approximately twice as that of the substrate material, while the composite clad of EWAC+Cr₂₃C₆ exhibited an average microhardness of 425±140HV. Zafar and Sharma (2014) developed a cermet clad of WC-12Co (APS 45µm) on SS-304 to obtain a wear resistant surface. Experiments were performed in 1.445kW, 2.45GHz industrial microwave furnace. During the process coal powder and a thin alumina sheet were used as susceptor and separator respectively. The microhardness test results indicated the average hardness of clad surface approximately 3.5 times higher than that of substrate material which is attributed to the formation of Fe₆W₆C known for its superior hardness properties. Micrographs of scanning electron microscope revealed the skeleton like structure of hard carbide phases reinforced in parent matrix.

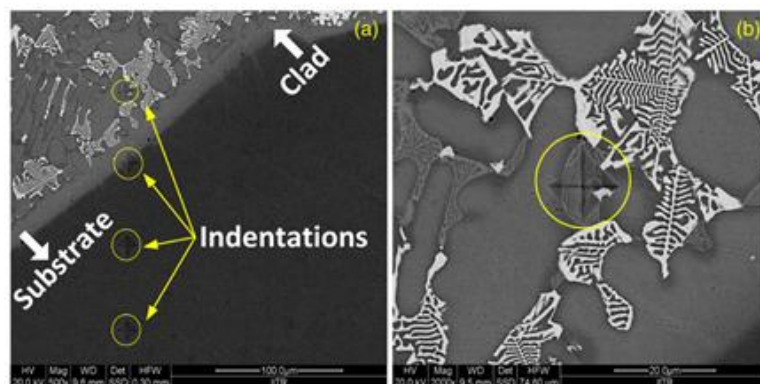


Figure 2.23 SEM micrographs showing skeleton like carbide phases and microhardness indentations at different locations (a) across the section (b) clad surface (matrix phase) (Zafar and Sharma, 2014)

Figure 2.23 indicates the SEM micrographs of skeleton like carbide phases along with microhardness indentations.

Srinath et al. (2011) in different works carried out joining of copper plates using copper interface powder and SS-316/MS and SS-316/SS-316 employing EWAC powder. It was reported that the joints developed with finer interface powder ($5\mu\text{m}$) exhibited higher hardness compared to those developed with $40\mu\text{m}$ powder (Sharma and Mishra, 2017). Further it was also observed that, microwave induced joints displayed higher hardness values at the joint interface which is attributed to the development of hard carbide phases in the interface region. Figure 2.24 shows the variation in microhardness profile across the microwave induced SS-316 joints.

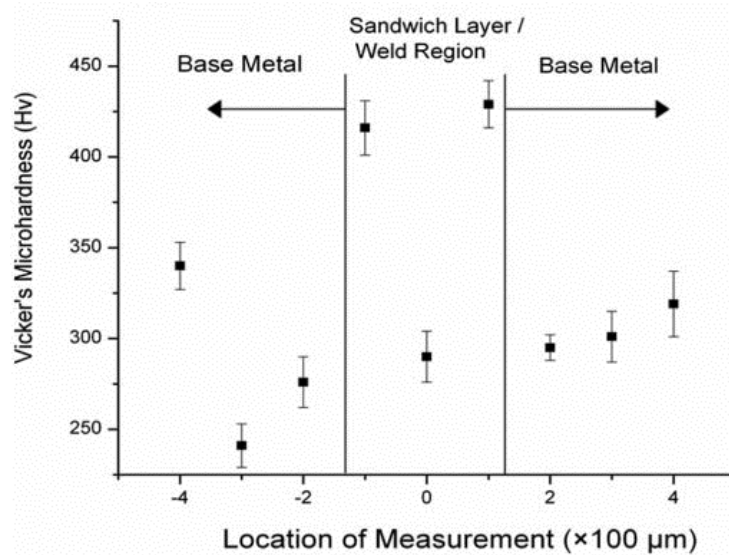


Figure 2.24 Vickers microhardness measurements at various locations in SS-316 microwave induced joint (Srinath et al., 2011)

Similar findings were reported by Bagha et al. (2017) while welding of SS-304 plates using nickel based powder. The authors used different sizes of interface powder ranging between $20\mu\text{m}$ to $50\mu\text{m}$. It was noticed that hardness of the weld decreased with increase in the interface powder size. The joints developed with $20\mu\text{m}$ exhibited highest hardness (356HV) in the joint region while, those developed with $50\mu\text{m}$ observed the lowest

hardness (180HV). Gamit et al. (2017) explored joining of MS pipes through MHH using nickel based powder. The microhardness indentations were obtained at various locations in the vicinity of the joint zone with weld center as reference. Highest microhardness (572HV) was recorded at the center of the joint and microhardness near the joint interface was observed to be 519HV. The lowest hardness value was noticed at the base metal (397HV). The authors reported that increase in hardness at the joint zone and its interface was due to the formation of nickel based intermetallic compounds and carbides during the microwave irradiation.

Bansal et al. (2014) during joining of SS-316 plates using SS-316 interface powder observed average microhardness in the interior of grain in joint zone was observed to be 275 ± 20 HV whereas microhardness at the grain boundaries was significantly higher (650 ± 40 HV). This higher hardness was attributed to the formation of chromium carbide phases in the grain boundaries and joint interface. Figure 2.25 illustrates the SEM micrograph of microhardness indentations in the joint zone and on base metal. In a similar work, Bansal et al. (2016) investigated on joining of Inconel-718 and SS-316 using Inconel-718 as interface powder. The microhardness measurements revealed that there was a large amount of deviation in the hardness values in the Inconel-718 region due to the formation of Laves phase.

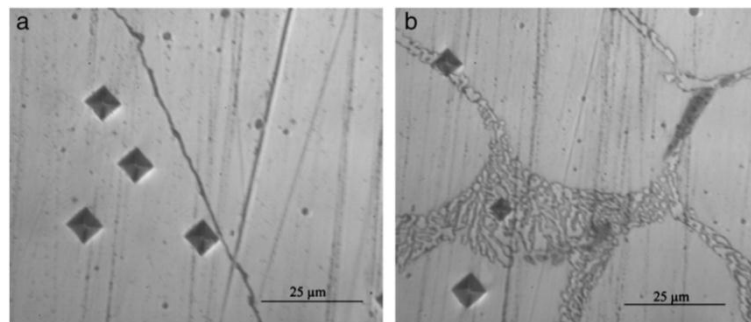


Figure 2.25 SEM micrographs of microhardness indentations (a) base metal (b) joint zone (Bansal et al., 2014)

Average microhardness was observed to be 230HV and maximum hardness measured on the carbide phase was 600HV while, in the matrix phase the hardness was 300HV.

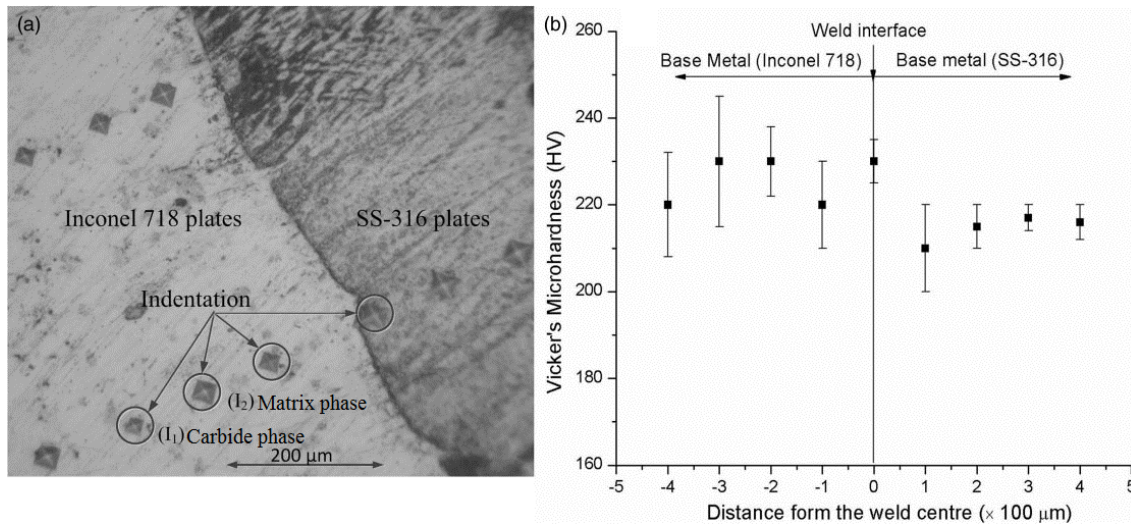


Figure 2.26 (a) SEM micrographs of indentations across the joint (b) microhardness profile (Bansal et al., 2016)

Figure 2.26 depicts the micrograph of the microhardness indentations and variation in the microhardness profile.

2.6 STUDIES ON METALLURGICAL CHARACTERIZATION OF MHH INDUCED JOINTS

Recent technological advancement has provided qualitative assessment of the microstructure and composition of materials. Metallurgical characterization offers a means to ascertain the probable reason for particular behavior of a component under specified conditions. Accordingly most of the reported works in cladding and joining have emphasized on characterization of the microwave induced clads/joints through microstructure and phase analysis. The following sections highlight the characterization techniques such as X-ray diffraction analysis, optical and scanning electron microscopy and energy dispersive spectroscopy employed in several investigations in the past pertaining to microwave cladding and joining.

2.6.1 Observations from XRD analysis

Kaushal et al. (2018) deposited a composite clad of Ni based powder and 10% SiC powder on martensitic stainless steel SS-420 substrate through MHH technique in a 900W, 2.45GHz oven via coal susceptor and graphite separator.

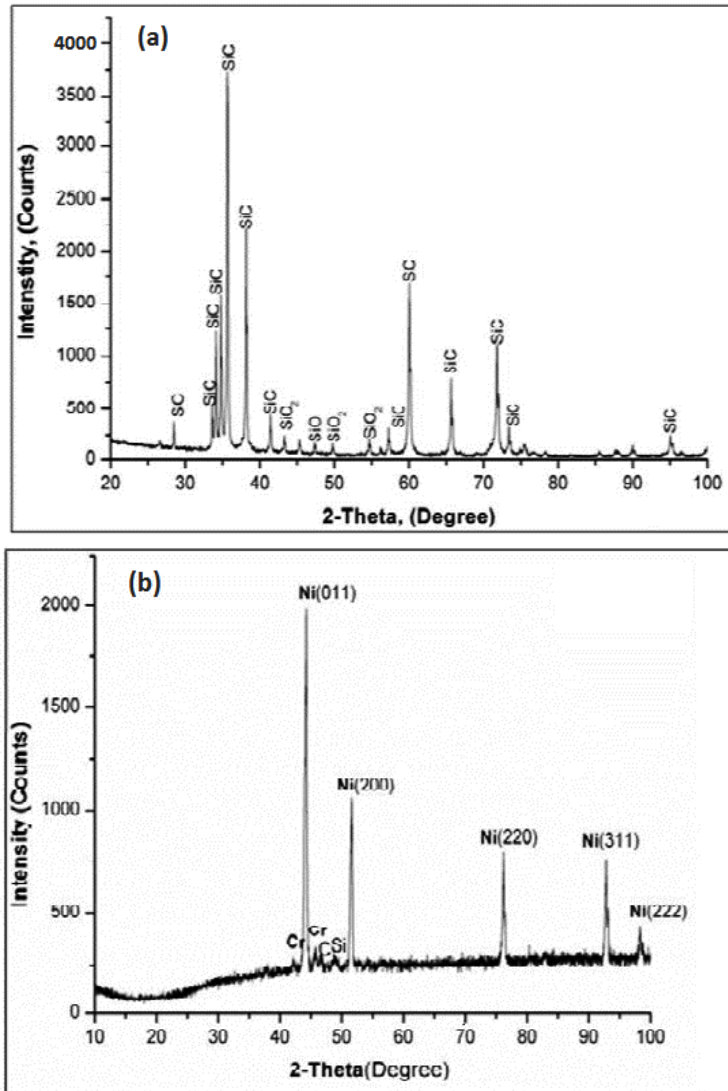


Figure 2.27 XRD spectrum of (a) SiC powder (b) Ni based powder (Kaushal et al. 2018)

Figure 2.27 shows XRD spectrum of starting Ni based powder and SiC powder used for development of clad. It is evident that both Ni and SiC were dominant in the starting

powders and it was reported that, XRD analysis of the microwave induced composite clad revealed the formation of chromium carbide and intermetallic phases. Formation of chromium carbide is attributed to the decomposition of SiC powder into Si+C and subsequent reaction of this free carbon with chromium at elevated temperature. Further, the presence of free silicon contributed to the formation of nickel silicide. Sharma and Gupta (2012) deposited a microwave composite cladding of nickel based powder EWAC and WC10Co2Ni (APS 40 μ m) in proportions of 80% and 20% respectively on austenitic stainless steel SS-316 substrate. At critical temperature, decomposition of WC10Co2Ni resulted in the formation of complex carbide Co₃W₃C. On the other hand Ni and Si in EWAC powder in free form at elevated temperature combined to form intermetallic NiSi. It was reported that, the presence of WC and Co₃W₃C acted as reinforcement in Ni and Co matrix and contributed in improving the hardness of the microwave induced clad. Hebbale and Srinath (2016) developed microwave cladding of Ni based powder EWAC on SS-304 substrate. XRD analysis of the developed clad was carried out at a scan rate of 1°/min and a scan range of 20° to 100°. XRD pattern exhibited the formation of hard chromium carbide phase, nickel silicide and dominant intermetallic FeNi₃ as depicted in Figure 2.28.

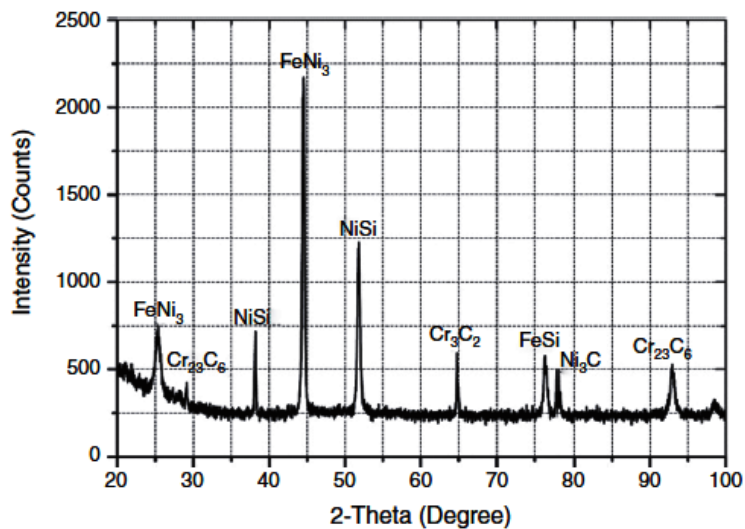


Figure 2.28 XRD spectrum of EWAC clad on SS-304 substrate, (Hebbale and Srinath, 2016)

Furthermore, the amount of different phases developed in the clad was determined using normalized intensity ratio (NIR) technique. NIR calculations revealed the formation of 14% chromium carbide, 24% nickel silicide and 47% FeNi₃ intermetallic phases. In a similar investigation Gupta and Sharma (2011) developed a clad of EWAC powder on SS-316 substrate. The amounts of phases developed were calculated using NIR method. The calculations revealed that after the microwave processing starting EWAC powder was transformed into 22.2% chromium carbide, 13.7% nickel silicide and 64.1% FeNi₃ phases. Gupta et al. (2012) developed and characterized the microwave irradiated composite clad consisting of EWAC and Cr₂₃C₆ chromium carbide powders (APS 40µm) in proportions of 80% and 20% respectively on austenitic steel SS-316 substrate. XRD study showed the formation of chromium carbide Cr₂₃C₆ and intermetallic phases NiSi and FeNi₃. Formation of intermetallic phases was attributed to the dilution of the elements from the substrate into the clad powder melt at elevated temperatures.

Bansal et al. (2014) carried out joining of SS-316 plates using SS-316 interface powder through MHH. XRD analysis of the microwave induced joints was obtained using Bruker AXS diffractometer with Cu-Kα radiation at a scan rate of 0.5°/min between the range 10° to 120°. XRD analysis showed the presence of chromium carbides (Cr₇C₃, Cr₂₃C₆) and dominant FeNi peaks in austenitic matrix. In a succeeding work, Bansal et al. (2016) accomplished joining of dissimilar metals Inconel-718 and SS-316 using Inconel-718 powder as interface filler. The XRD spectrum of starting Inconel-718 powder and microwave induced dissimilar joint are shown in Figure 2.29. XRD spectrum of Inconel-718 powder showed the presence of dominating Ni-Cr (FCC) peaks. On the other hand XRD pattern obtained after the formation of welded joint revealed the formation of chromium carbide, niobium carbide, titanium carbide and intermetallic Ni₃Nb in Ni-Cr matrix. The amount of different phases developed was determined using NIR method which indicated that approximately 54% of starting Inconel-718 powder got transformed into carbides and intermetallic phases. Similar observations were made by Srinath et al. (2011) during joining of bulk copper using high purity copper powder through microwave energy. XRD pattern of the copper joint revealed the presence of dominating

peaks of copper and copper oxide. Relative phase intensities in the joint were calculated using NIR method. The authors reported that 26% of starting copper powder was transformed into copper oxide.

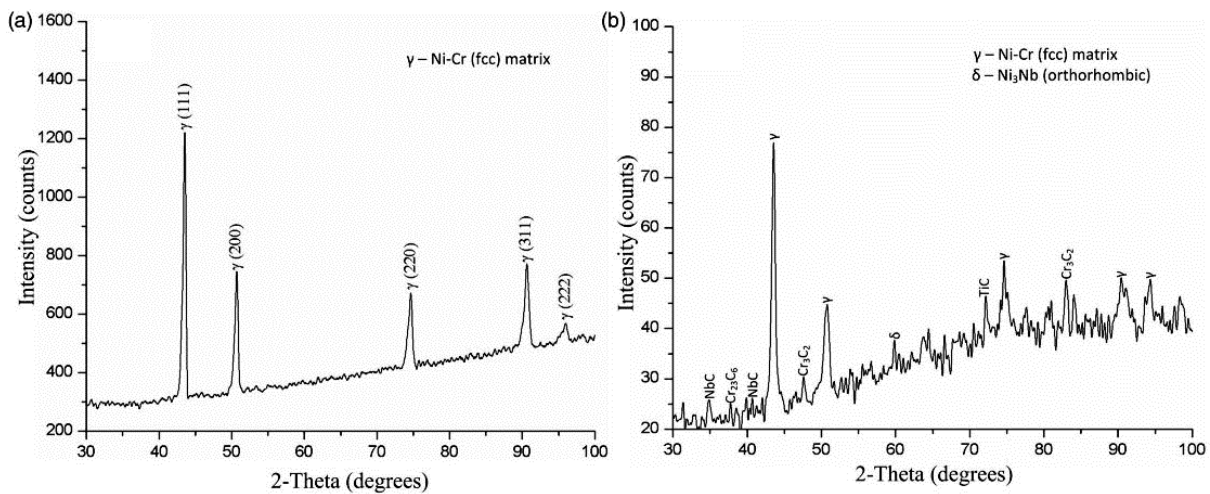


Figure 2.29 XRD spectrum of (a) Inconel-718 powder (b) microwave induced dissimilar Inconel-718/SS-316 joint (Bansal et al., 2016)

Singh et al. (2015) developed the welded joints between Aluminium plates through MHH using Aluminium powder as interface filler. XRD pattern obtained after joining aluminium plates showed the dominating peaks of Al and Al_2O_3 . The formation of Al_2O_3 was due to slow cooling rate and the entire process being carried out in atmospheric conditions. Further, the authors reported that the formation of oxides enhances the coupling of microwaves in the joint interface. Gamit et al. (2017) explored the possibility of microwave welding of MS tubes and successfully carried out the joining of MS tubes using a domestic 900W oven. Nickel based powder was used as interface material and charcoal was used as susceptor to elevate the initial joint temperature. XRD analysis indicated the formation of FeNi phase in Fe matrix along with small traces of NiC_x . Srinath et al. (2011) investigated the joining of SS-316 plates through MHH using nickel based powder. XRD pattern indicated the dominating peaks of FeSi, NiC_x , $(FeNi)_{23}C_6$ and chromium carbide. The presence of these phases was attributed to fast heating of the

nickel-based interface layer and abrupt cooling of the molten pool to room temperature associated with the end of the microwave radiation cycle.

2.6.2 Observations from microstructure studies

Sharma and Gupta (2012) developed a composite clad of 80% EWAC+20% WC10Co2Ni powders on SS-316 substrate through MHH. The developed clad displayed a cellular structure with good metallurgical bonding with the substrate and appeared defect free without the presence of any pores or interfacial cracks as shown in Figure 2.30. Since the melting point of carbide particles is relatively higher than EWAC powder, the tungsten carbide and other metallic carbide particles remain undissolved and are dispersed throughout this melt in agglomerated form. EDS spectrum at the clad matrix (Figure 2.31(a)) showed the dominating nickel and cobalt while, EDS at white phase (Figure 2.31(b)) indicated the formation of tungsten and nickel carbide along with free carbon phase. The authors reported that these white phases serve as reinforcement by providing strength to the soft matrix. Similar findings were reported earlier by Gupta and Sharma (2011) on development and characterization of WC-10Co-2Ni clad developed on austenitic stainless steel (SS-316). The microstructure of the clad (Figure 2.32) showed white skeleton like phase in soft matrix.

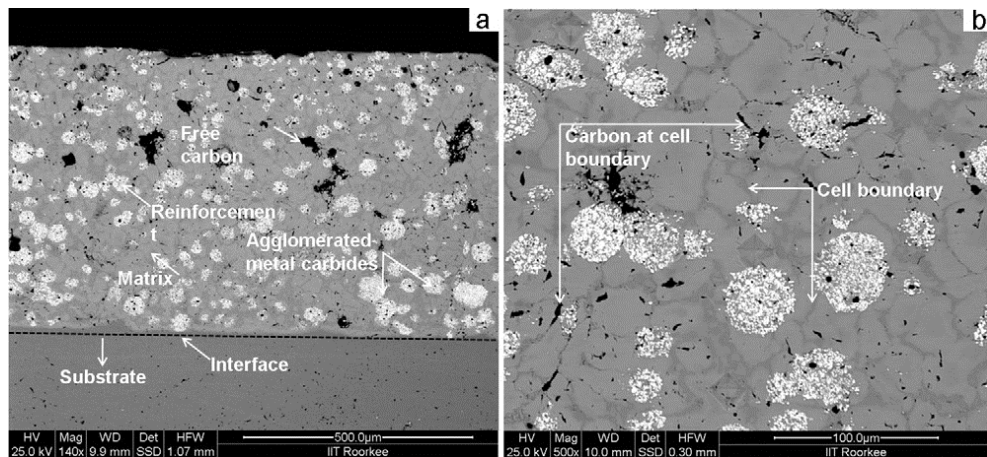


Figure 2.30 Back scattered SEM micrographs of microwave induced EWAC+WC-10Co-2Ni composite clad (Sharma and Gupta, 2012)

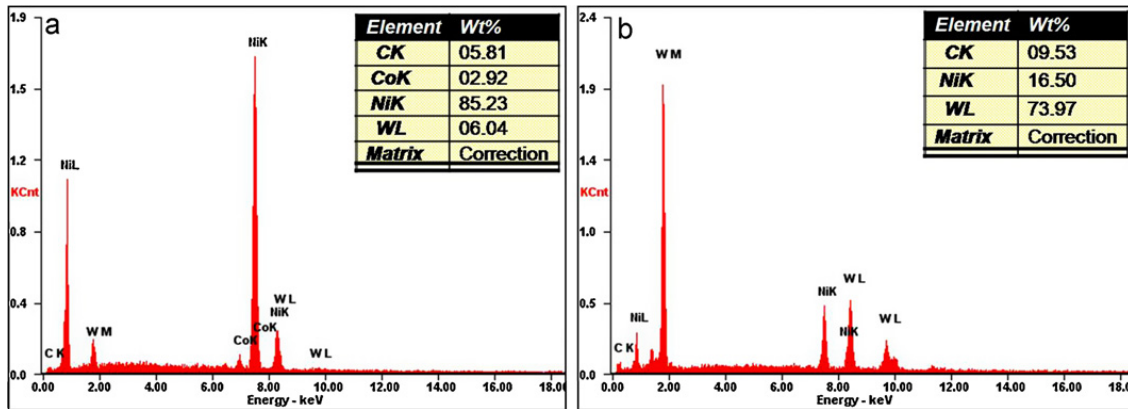


Figure 2.31 EDS analysis at (a) matrix phase (b) white phase in Figure 2.30 (Sharma and Gupta, 2012)

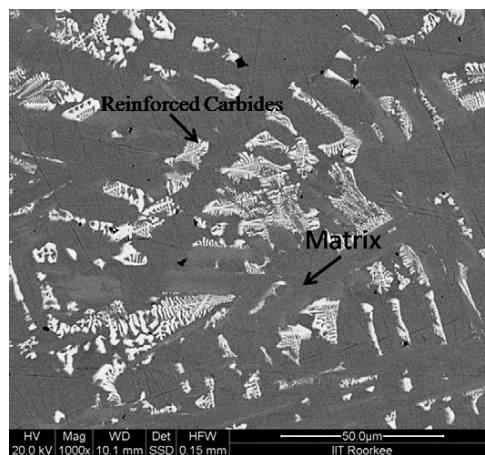


Figure 2.32 SEM micrograph of WC-10Co-2Ni microwave induced clad showing skeleton like structure (Gupta and Sharma, 2011)

It was observed that matrix phase consisted of Ni and Co existing in starting powder and Fe and Cr diluted from the substrate during processing. The skeleton like phase on the other hand consisted of carbides of W and Fe which provided reinforcement to the soft matrix and further improved the wear resistance of the substrate. Subsequent studies by Zafar and Sharma (2014) confirmed the formation of skeleton like carbide phase in clad of WC-12Co (APS 45 μ m) developed on SS-304 to obtain a wear resistant surface. Figure 2.33 illustrates the clad microstructure and EDS analysis carried out to determine the

elemental composition at different phases. EDS analysis at point 1 in skeleton phase indicated the presence of dominating W and C peaks. This further confirmed the formation of hard metallic carbide phase which acts as reinforcement in tough metallic matrix consisting of Fe, W and Cr at point 2 and Fe, Cr, Ni and Co at point 3.

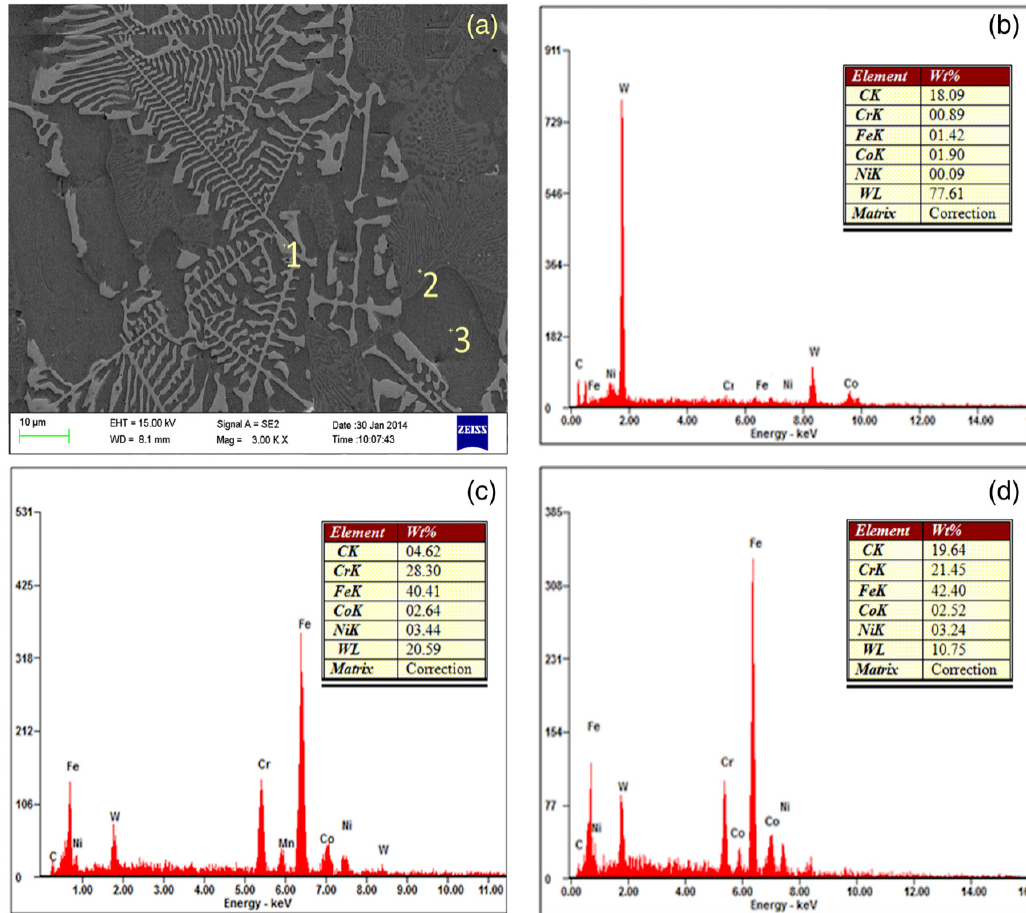


Figure 2.33 (a) SEM micrograph showing skeleton like structure (b) EDS spectra at point 1 (c) EDS spectra at point 2 (d) EDS spectra at point 3 (Zafar and Sharma, 2014)

Later identical investigations were carried out by Gupta and Sharma (2011) and Hebbale and Srinath (2016) wherein, nickel based powder EWAC was deposited on SS-316 and SS-304 substrates respectively. The microwave induced EWAC clads exhibited a cellular structure through good metallurgical bonding without any interfacial cracks. As reported

by Gupta and Sharma (2011), the clad microstructure (Figure 2.34) a thin planner zone was visible at the interface which contained refined grains as a result of resolidification during the microwave irradiation. Further it was mentioned through EDS analysis that, the microstructure consisted of Fe-Ni rich matrix and segregation of chromium carbide along the grain boundaries in the form of Cr_3C_2 and Cr_{23}C_6 .

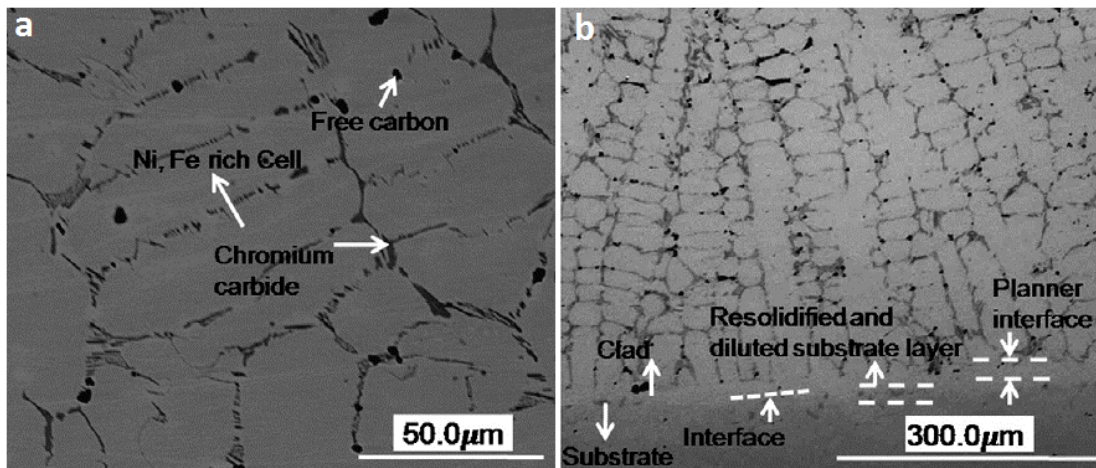


Figure 2.34 SEM microstructure of EWAC clad showing (a) chromium carbide precipitation at grain boundaries (b) cellular structure of the developed clad (Gupta and Sharma, 2011)

The formation of chromium carbide is due to the fact that the partition coefficient of chromium being less than unity it segregates at the grain boundaries and at elevated temperature reacts with carbon to form chromium carbide. Srinath et al. (2011) during joining of SS-316 plates using EWAC powder observed columnar structure in the interface region while, fusion zone exhibited equiaxed structure (Figure 2.35). The authors confirmed the formation of chromium carbide along the grain boundaries through XRD and EDS analysis. Bansal et al. (2014) observed the formation of chromium carbide phase in the grain boundaries and identical results were obtained with marginal variations in elemental compositions after joining SS-316 plates through MHH.

Singh et al. (2018) developed welded joints of CI plates through the use of nickel based filler powder in a 900W-2.5GHz microwave oven. Charcoal powder and thin graphite

sheet were used as susceptor and separator materials. Microstructure of the joint zone in Figure 2.36 consisted of cellular structure accompanied by the precipitation of carbide phase along the grain boundaries. The elemental composition through EDS was analyzed at the grain boundaries as well as interior of the grain. It was reported that EDS at grain boundaries consisted of C, Cr and Fe peaks while grain interior was rich in Ni and Fe with small amount of C.

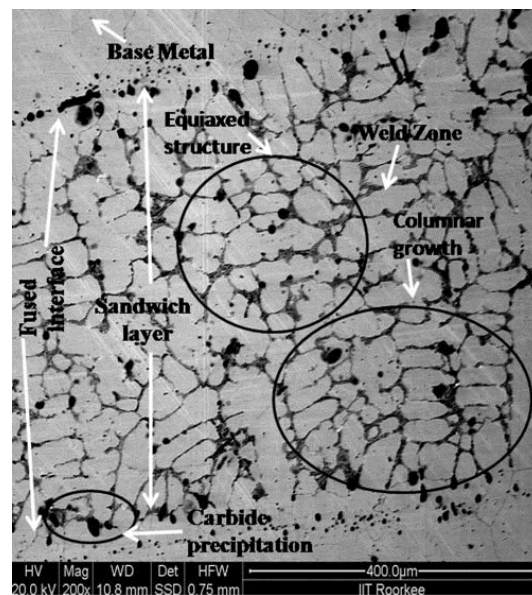


Figure 2.35 SEM micrograph of SS-316 joint fusion zone (Srinath et al.; 2011)

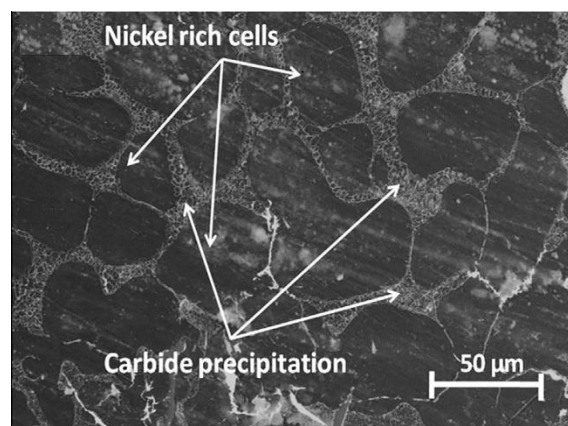


Figure 2.36 SEM microstructure showing the joint zone of welded CI plates (Singh et al., 2018)

Srinath et al. (2011) and Bansal et al. (2014) in different studies on dissimilar joints of SS-316/MS formed through MHH reported the precipitation of chromium carbide in the grain boundaries. However, Bansal et al. (2014) in addition noticed the higher percentage of Cr, Mo and V (Figure 2.37) at the grain boundaries compared to the interior of the grain. As these elements have a greater affinity with carbon at elevated temperature, result in formation of metallic carbides.

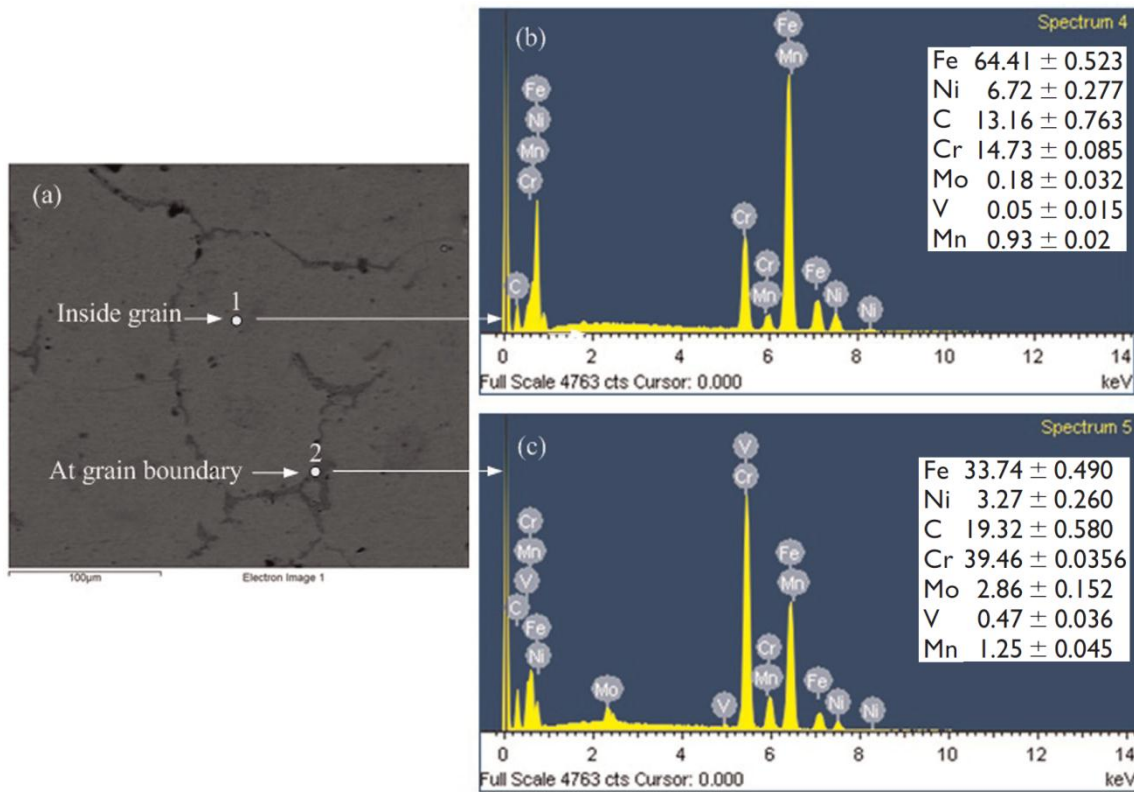


Figure 2.37 (a) SEM microstructure of microwave induced SS-316/MS joint indicating the location of EDS (b) EDS inside the grain (c) EDS at the grain boundary (Bansal et al., 2014)

Bansal et al. (2013) and Gamit et al. (2017) in different works performed joining of MS plates and MS pipes respectively using microwave energy as depicted in Figure 2.38. Nickel based powder was employed as the filler at the joint interface. The microstructures of joints in both the cases showed complete melting of nickel based powder and good metallurgical bond with the base metal.

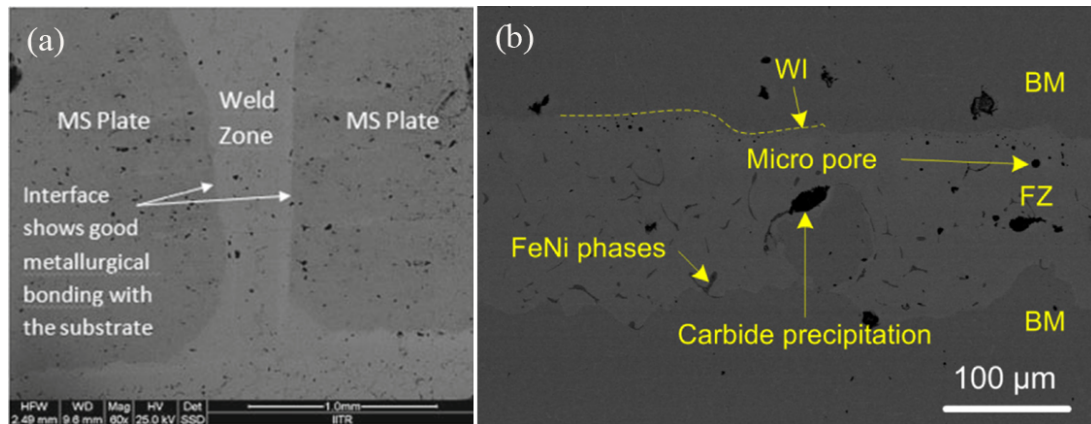


Figure 2.38 SEM micrographs of (a) MS plates (Bansal et al., 2013) and (b) MS pipes (Gamit et al., 2017) joined through MHH

EDS analysis of the joint zone revealed the presence of Ni and Fe peaks with small traces of Si. This is attributed to the diffusion of metallic elements.

2.6.3 Observations on porosity and grain size

Porosity to a great extent depends on heating rate employed for processing (Mondal et al., 2008); as the heating rate increases, it is accompanied by increase in porosity. Gupta and Sharma (2011) reported on development and characterization of WC-10Co-2Ni clad developed on austenitic stainless steel (SS-316) substrate. The porosity of the clad was measured using linear point count method. The observed results showed significantly lower porosity of 0.89% which is attributed to the volumetric heating associated with microwave processing. Gupta and Sharma (2011) later demonstrated the microwave cladding of nickel based powder EWAC (APS 40 μ m) on austenitic SS-316 steel substrate. The microwave induced clads were free from any interfacial cracks and exhibited much lower porosity of the order of 1.09%. The authors (Gupta and Sharma, 2011) claimed that the microwave induced clad displayed a significantly lower porosity when compared to that of conventional processes. Similarly Kaushal et al. (2018) used linear count method to evaluate the porosity of the microwave induced composite clads of EWAC powder+20% alumina powder on SS-304 substrate. The porosity of the developed clad was measured to be 0.97% which is attributed to the rapid escapement of

gases from the melted clad prior to termination of solidification process. Zafar and Sharma (2014) developed a cermet clad of WC-12Co (APS 45 μ m) on SS-304 using microwave energy. The clad characterization for assessment of porosity was carried out with the aid of optical microscope equipped with an image analysis software Dewinter Material Plus. The average porosity of the microwave induced clad was estimated to be 0.98%. Kaushal et al. (2018) in another study deposited a composite clad of EWAC+10% SiC powders on SS-420 substrate and the observed porosity of the clad based on linear count method was found to be 1.1%. Gupta et al. (2012) in a similar study developed and characterized the microwave irradiated composite clad consisting of EWAC and Cr₂₃C₆ chromium carbide powders. The porosity of the microwave induced clads was evaluated through linear point count method and observed to be 0.9%.

Gamit et al. (2017) during joining of MS pipes using nickel based interface powder through MHH observed that porosity of the joint at the outer surface (7%) was significantly higher than that at inner surface (3%). The authors reported the formation of round pores in the fusion zone which signifies the ductility of the joint (Figure 2.38(b)). The amount of porosity was estimated with the aid of optical microscope and Dewinter Material Plus software. The higher porosity at the outer surface of pipe was attributed to the direct contact of surface with the burning charcoal and escapement of gases through outer surface. Srinath et al. (2011) in different experiments carried out joining of ferrous and non-ferrous plates using 5 μ m and 40 μ m interface powders (Sharma and Mishra, 2017). The assessment of porosity was carried out by linear count method.

Table 2.2 Observed porosity during microwave joining of different metals (Sharma and Mishra, 2017)

Base metal	Interface filler powder	Powder size (μ m)	Porosity (%)
Copper	Copper	5	1.26
		40	1.27
SS-316	EWAC	5	0.85
		40	1.2
SS-316/MS	EWAC	5	0.8
		40	1.1

The details of the results obtained are tabulated in Table 2.2. It was observed that, porosity in the microwave induced joints reduced with decrease in the interface powder size.

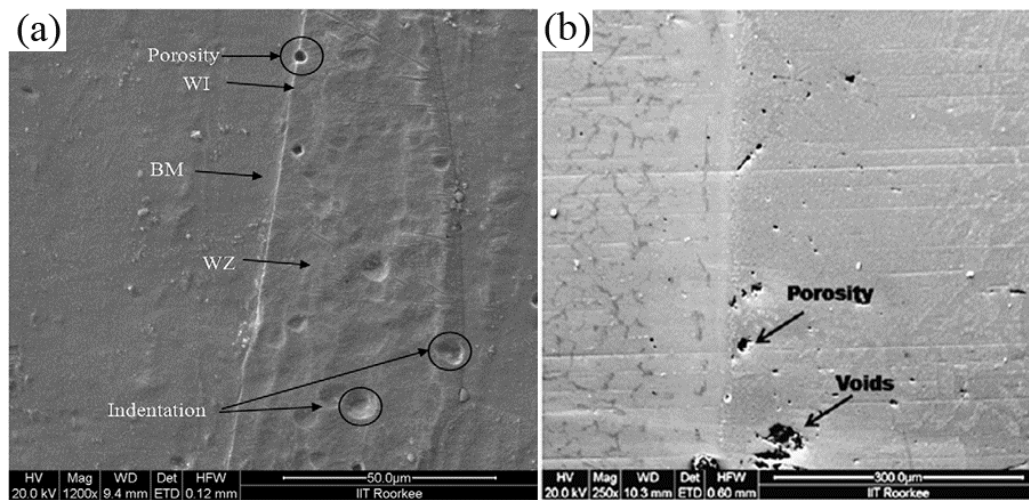


Figure 2.39 SEM micrographs showing porosity in microwave induced joints of (a) Copper plates (b) SS-316/MS plates (Srinath et al., 2011)

Figure 2.39 shows typical SEM micrographs of microwave welded joints indicating the formation of pores in the weld region. The authors further mentioned that formation of round pores in case of copper joints is an indication of ductility of the joint and observed lower porosity values signify the volumetric heating associated with MHH process. In a subsequent work, Bansal et al. (2014) reported on joining of SS-316 plates in which the porosity of microwave welded joints was assessed through Dewinter Material Plus software. Porosity of the joint was found to be 0.94% which was lesser than that observed with the weldments developed through other welding processes.

Grain size has a significant influence on mechanical properties of the welded joints. Finer grain size promotes strength and toughness of the joints while coarser grain improves high-temperature creep resistance (Min et al., 2016). Furthermore, it has been reported that the heating and cooling rates govern the type and size of the final grain structure of the component (Lee and Lee, 2008; Mishra and Sharma, 2017). Prabhu et al. (2009) investigated the microwave sintering behavior of as-received tungsten powder 99.95%

purity and particle size $5\mu\text{m}$ to $7\mu\text{m}$ with that of the same powder ball milled (activated tungsten powder) with further reduced particle size. The sintering was performed under nitrogen atmosphere in a 3kW 2.5GHz industrial microwave furnace. Microwave sintered activated powder compacts exhibited fine grain structure with increased hardness compared to the compacts of as-received powder. Zafar and Sharma (2015) investigated the wear characteristics of cermet clad of two different sized WC-12Co powders micrometer (MM) and nanometer (NM) developed on austenitic SS-304 substrate through microwave hybrid heating. As shown in Figure 2.40 microstructure of MM clad revealed the formation of skeleton like structure of carbides randomly distributed in clad matrix. Conversely, uniformly distributed clusters were observed in the micrographs of NM clad and the region neighboring the clusters was depleted with carbide. It was reported that due to the uniform distribution of carbide clusters, NM clads exhibited a significantly higher hardness as compared to MM clad.

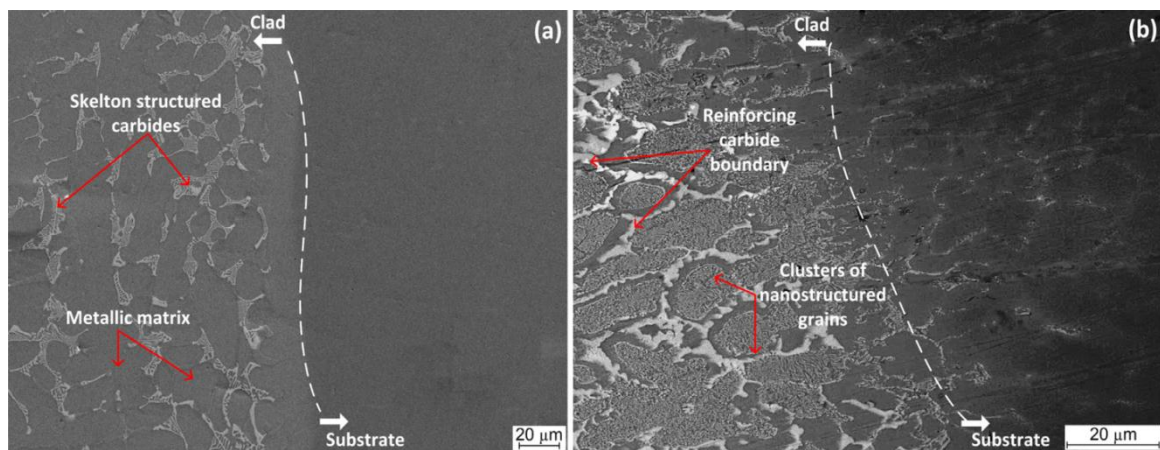


Figure 2.40 SEM micrographs showing growth of reinforcement phase in (a) MM and (b) NM clads (Zafar and Sharma, 2015)

Mishra and Sharma (2017) developed in-situ melting and casting of Al-Zn-Mg alloy using a 1.4kW-2.45GHz industrial oven under different processing conditions through MHH. Melting of charge was performed by employing two crucibles (susceptor) made out of SiC and ceramic material (CC) while; the molten alloy was poured in two different molds prepared with alumina and graphite. Figure 2.41 depicts the microstructures of the

Al-Zn-Mg alloy in-situ casts developed. The in-situ casting developed via the combination of CC susceptor and Alumina mold (AMC I) resulted in coarse grain structure whereas, in contrast the combination of SiC susceptor and Alumina mold (AMC II) resulted in fine microstructure. Similarly with GMC I (graphite mold employed with CC susceptor), resulted in coarse grain structure. In contrast, GMC II (graphite mold employed with SiC susceptor) resulted in formation of fine grains. This difference in the microstructure of in-situ casts is attributed to different heating and cooling rates associated with the susceptor and mold materials which in turn depended on their dielectric properties. As graphite has a very good thermal conductivity in comparison with alumina, heat dissipation from the mold took place at faster rate resulting in fine equiaxed grain structure in case of GMC I and GMC II.

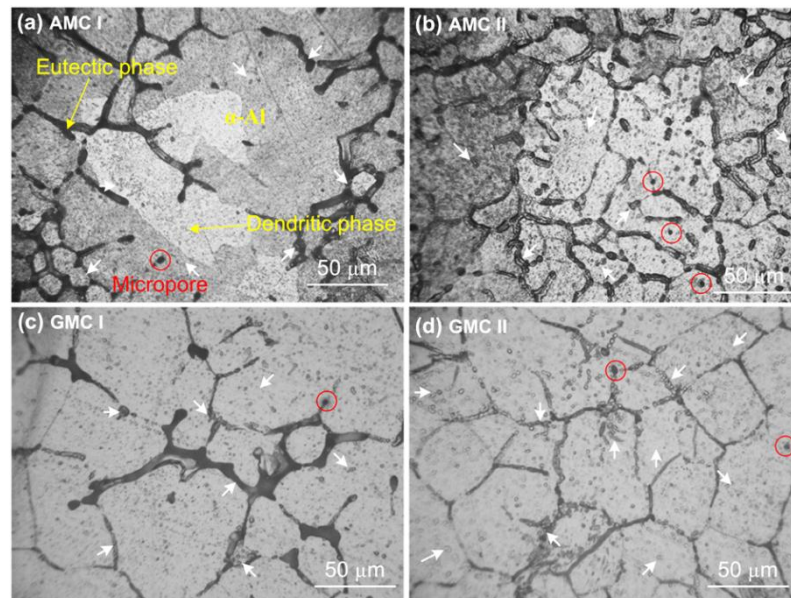


Figure 2.41 Optical images of microstructures of Al-Zn-Mg alloy in-situ casts developed through MHH (Mishra and Sharma, 2017)

2.7 STUDIES ON OPTIMIZATION OF WELDING PROCESS PARAMETERS

In any welding process, the process parameters directly or indirectly influence metallurgical and mechanical properties of the welded joints. Various optimization techniques such as grey relational analysis, response surface method, artificial neural

network etc., have been proposed to establish mathematical relationship between input parameters and performance characteristics in a welding process so as to produce the joint of desired quality.

2.7.1 Optimization techniques employed during joining bulk metals through MHH

Kumar (2010) during joining of copper plates through MHH optimized the process parameters namely, interface powder size, interface width and exposure time using response surface method. Porosity, microhardness and UTS were the response characteristics considered for the study. Optimum setting of parameters was observed to be 5 μ m powder size, 0.25mm interface width and 330s exposure time.

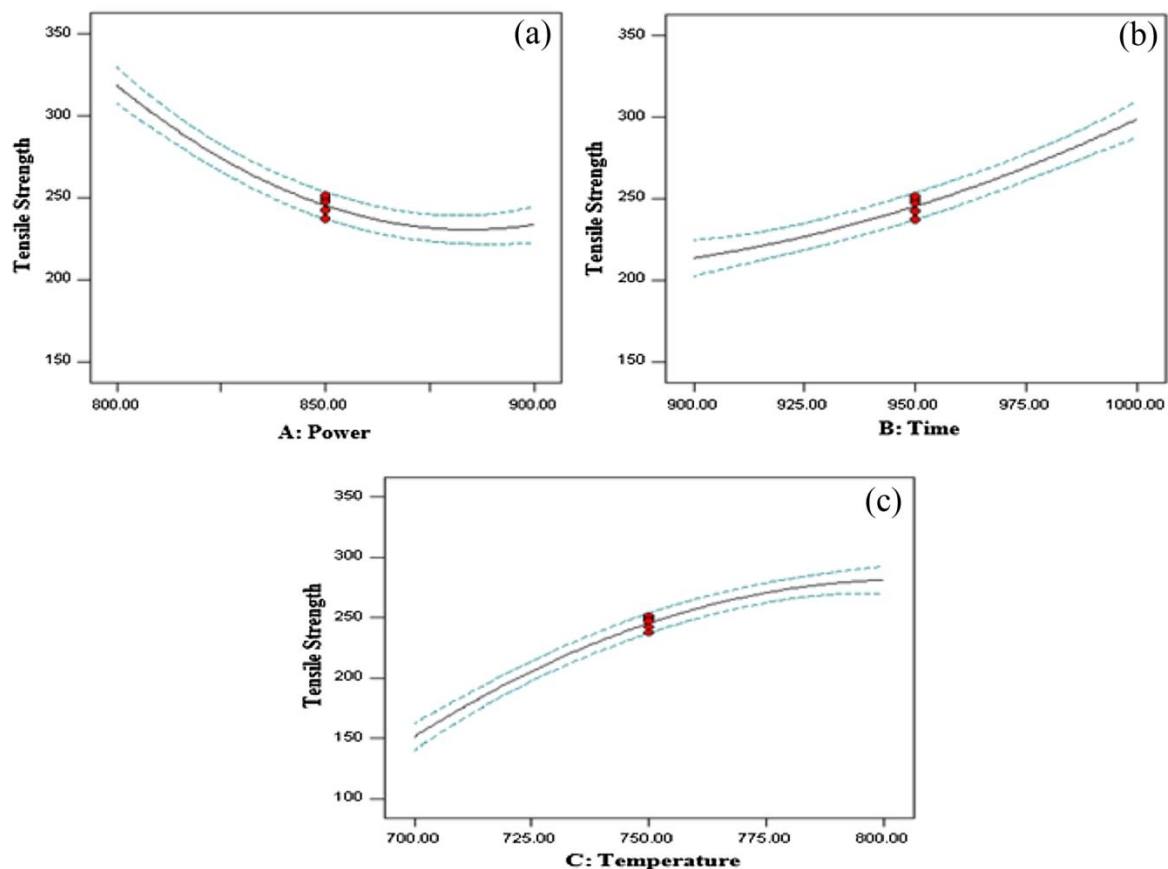


Figure 2.42 Effect of process parameters on tensile strength (Dwivedi et al., 2014)

Gupta and Kumar (2014) investigated the effect of process parameters on UTS of the joint using Taguchi method during joining SS-316 plates through MHH. Exposure time and composition of nickel based interface powder were the parameters considered for study. Dwivedi et al. (2014) studied the effect of rated power, exposure time and temperature on tensile strength of 1018 mild steel welded joints developed through MHH in a charcoal environment. Optimization of process parameters; input power, exposure time and temperature was performed through RSM. Optimum combination of parameters that produced a highest tensile strength was found to be 800W power, 1000s exposure time and 800°C temperature (Figure 2.42). Welding temperature was the most significant factor followed by exposure time and rated power.

2.7.2 Optimization of process parameters in conventional welding using GRA

Taguchi-based grey relational analysis (GRA) is one of the popular techniques used by most of the researchers to optimize multiple responses in a process. The use of orthogonal array with GRA to a large extent reduces the complexity in optimization procedure for computing the optimal process parameters with the multiple response characteristics. Through GRA, a grey relational grade is generated to evaluate the multiple response characteristics. Consequently, optimization of complex multiple quality characteristics can be transformed into optimization of a single grey relational grade. Several researchers in recent past have used this technique to extend a skillful control over the uncertainty, partial information and multiple inputs. Lin (2013) optimized the process parameters namely arc length, welding current, welding speed, argon flow rate and flux type in GTA welding of Inconel-718 to obtain the optimum depth to width ratio and penetration of weld bead using Taguchi, GRA and neural network techniques. Prasad et al. (2016) reported on influence of input process parameters; peak current, back current, pulse width and pulse frequency on fusion zone grain size, hardness and ultimate tensile strength of Inconel-625 welded joints produced using pulsed current micro plasma arc welding. Process optimization was carried out using with an objective to minimize grain size and maximize hardness and ultimate tensile strength. In subsequent study,

Prasad et al. (2015) optimized the parameters of weld bead geometry of Inconel-625 welded joints produced using pulsed current micro plasma arc welding. Sahu and Pal (2015) optimized the process parameters in friction stir welding of AM20 magnesium alloy. L_{18} orthogonal array with mixed level consisting of four input parameters plunge depth (2 levels), tool rpm, welding speed and shoulder diameter (3 levels each) were selected. Eight response characteristics including UTS, yield strength, percentage elongation etc., were selected for the experimentation. Padmanaban and Balasubramanian (2011) optimized the process parameters; peak current, back current, pulse on time and pulse frequency in TIG welding of magnesium alloy AZ31B with an objective of maximum tensile strength of the joint. Srirangan and Paulraj (2016) performed optimization of process parameters; welding current, voltage and welding speed in TIG welding of alloy Incoloy-800 HT by GRA method. UTS and yield strength at room temperature and at 750°C and impact toughness were considered as response parameters. Shanmugarajan et al. (2016) carried out the optimization of laser welded P92 steel using Taguchi GRA to arrive at optimum set of parameters consisting of welding power, welding speed and focus plane position. Multiple quality responses measured were weld bead width, depth of penetration and HAZ. Welding speed was the most significant parameter followed by laser power and focal length in determining the quality joint.

2.7.3 Concluding remarks

Through this literature review an attempt is made to record the earlier work reported on optimization of process parameters in welding of bulk metals using MHH. However, it was observed that very limited works have been published in this area as discussed in section 2.7.1. Therefore, there is a scope to optimize the process parameters in joining Inconel-625 through MHH. Furthermore, the works reported in section 2.7.2 though not related to microwave processing, prove the usefulness of GRA technique for optimizing the welding parameters. GRA is one of the popular techniques used by most of the engineers to optimize the multiple responses involved in a process. In the present work GRA technique has been employed to optimize microwave welding process parameters

(separator material, susceptor material and particle size of interface filler powder). Tensile strength and flexural strength were selected as the output response characteristics.

2.8 RESEARCH GAPS

After the comprehensive study of available literature, the following gaps have been identified in welding of Inconel-625 alloy.

- Most of the conventional fusion welding techniques employed for welding of nickel based alloys are expensive in terms of equipment and operating costs.
- Conventional fusion welding processes provide high heat input leading to the formation of secondary phases and solidification cracking that subsequently results in inferior mechanical properties of the welded joints.
- Sintering of metallic powders through microwave energy is well matured in terms of academic research; however processing of bulk metals using MHH is a recent technological development that needs to be explored.
- Researchers have successfully joined various ferrous and nonferrous alloys using MHH; however joining of Inconel-625 alloy has not been explored hitherto.
- Limited works have been published so far to optimize the multiple quality characteristics in microwave induced welding of bulk metals.

2.9 PROBLEM DEFINITION

Literature study reveals that, mechanical and metallurgical properties of bulk metallic materials processed through MHH are comparable to that produced using conventional welding techniques. However, it is also noticed that no works have been reported with welding of Nickel based alloys through MHH. Therefore it was decided to carry out the welding of Inconel-625 alloy using MHH and subsequent characterization of the developed joints through several techniques.

2.10 OBJECTIVES OF THE PRESENT WORK

Contemporary industrial applications with rapidly changing technology focus on energy efficient and inexpensive methods for processing wide variety of materials with minimum time. Microwave processing of materials is one of the latest developments that could be considered as an alternative to conventional welding technologies aiming to give grounds to industrial developments. In the recent past, researchers have successfully attempted the joining of various ferrous and non-ferrous alloys using MHH. However there is a wide scope to develop joints of Ni based alloys using microwave hybrid heating technique, as very limited work has been reported in this area.

The current research work broadly aims to investigate the following objectives:

1. To develop Inconel-625 alloy joint using microwave hybrid heating technique (MHH) using a low cost domestic microwave oven at two power levels.
2. To characterize the microwave induced joints through mechanical and metallurgical characterization techniques.
3. To investigate the influence of welding process parameters on the response characteristics such as ultimate tensile strength (UTS) and flexural strength (FS) of the developed joints.
4. Optimization of the microwave welding process parameters using Taguchi based GRA and validation.

CHAPTER 3

EXPERIMENTAL WORK

3.1 INTRODUCTION

The chapter illustrates the composition and properties of the materials used, description of the equipments used during experimentation, method of specimen preparation and experimental procedure adopted.

3.2 RESEARCH METHODOLOGY

In the present work, joining of Inconel-625 plates has been accomplished using nickel based powder EWAC as an interface filler material in a low-cost domestic microwave oven. In order to study the effect of heat input on the joint characteristics, two similar set of experiments were carried out using two power levels at 600W and 900W. The experiments were planned according to L_{16} orthogonal array designed using Minitab-16 software. The objective of present study was to investigate the influence of the various process parameters during welding of Inconel-625 alloy through MHH on tensile and flexural strength to obtain the best possible combination of process parameters so that the strength of the developed joints could be optimized.

Taguchi technique was employed to study the effect of individual parameters and consequently to predict sets of control factors for the best quality characteristics. Using Taguchi's method, the influence of three process parameters namely separator (4 levels), susceptor (2 levels) and average particle size (APS) of interface filler powder (2 levels) on two quality characteristics, ultimate tensile strength (UTS) and flexural strength (FS) of the welded joint have been investigated. Further, multi-response optimization using Taguchi based GRA is performed wherein, two response characteristics are converted into a single response characteristic and a single optimal setting has been attained for the Inconel-625 welded joints and the optimal combination of parameters has been determined.

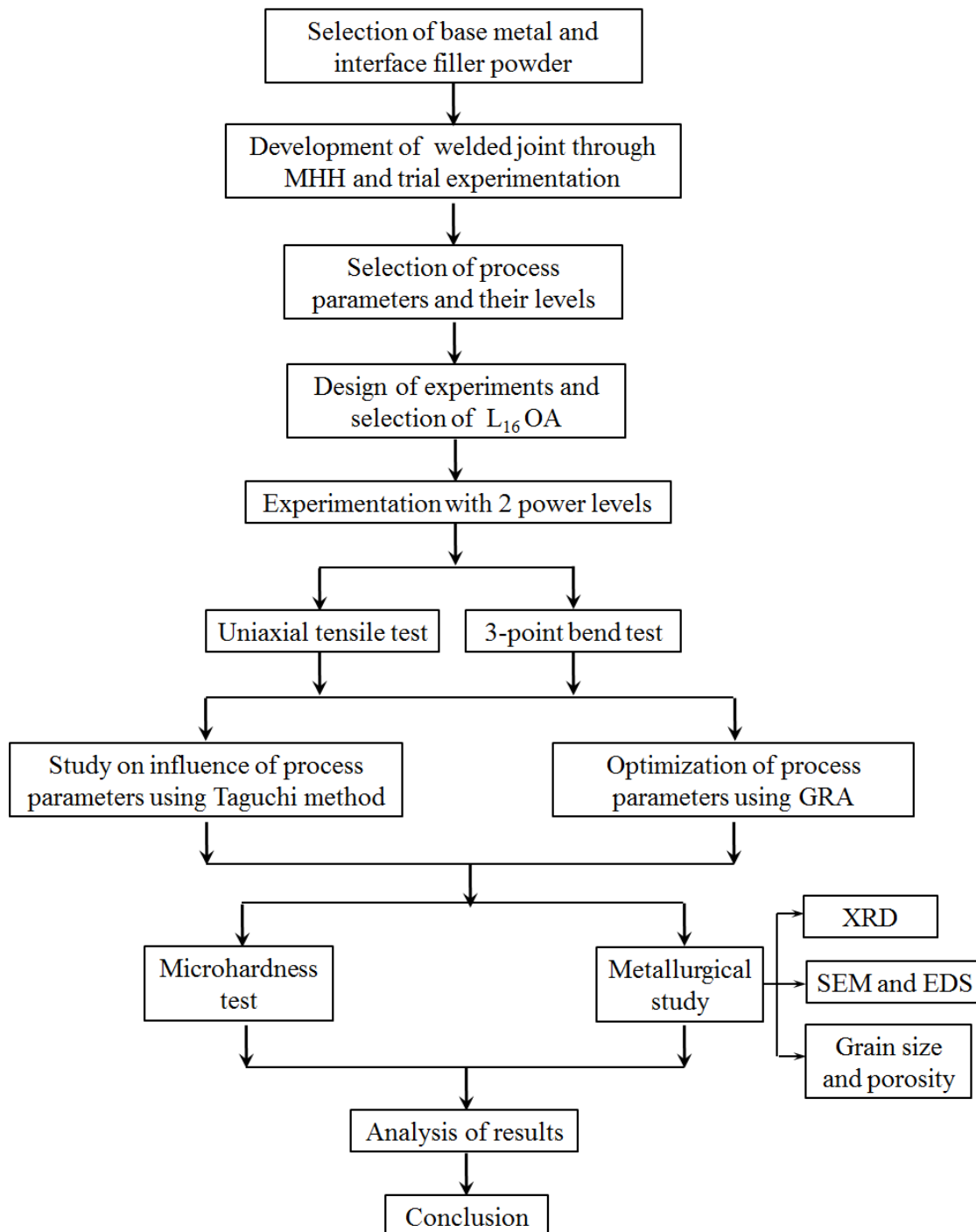


Figure 3.1 Research methodology flow diagram

Post weld characterization of the microwave welded joints was carried out through X-ray diffraction (XRD), scanning electron microscope (SEM), Vickers microhardness test, uniaxial tensile test and 3-point bend test. It is interesting to note that in contrast to most of the conventional techniques, welding in this work was achieved without the aid of any special fixtures and shielding gas. Figure 3.1 depicts the proposed plan and detailed steps involved in the present work in the form of a flow chart.

3.3 SELECTION OF MATERIALS

Inconel-625 alloy because of its superior properties plays a crucial role in development of strategic industries where the use of super alloys is obligatory. The alloy is widely used in marine, aerospace, nuclear power plant, petrochemical and automobile applications due to the combination of its excellent mechanical, physical and chemical properties. Therefore Inconel-625 alloy was selected as the candidate base material in the present work to explore the new processing possibilities.

The properties of an efficient joint largely depend on the chemical composition of interfacing (filler) material. Considering the fact that filler materials used must have good solubility between the base materials to be joined and nickel being the major element of Inconel-625 alloy, a nickel based powder EWAC was selected.

A susceptor is used to elevate the initial temperature of the joint interface to a critical temperature. In the present work, two variants of susceptor materials were used namely, SiC and coal as these materials are very good microwave absorbers at room temperature. In order to prevent the intermixing of susceptor with the interface filler, a thin sheet of microwave conducting material called as separator is placed on the joint interface. Two types of separator materials graphite and glasswool were employed in the present study. The objective behind selecting graphite and glasswool was to vary the microwave absorption characteristics at the joint interface as one of the materials being a very good microwave absorber (graphite) and the other transparent to microwaves (glasswool). In addition, a flux UV420TT available in agglomerated form was also used in combination

with separator materials. The entire welding process was carried out in an insulator box prepared from alumina fiber boards so as to minimize the heat loss.

3.4 CHARACTERIZATION OF MATERIALS

The detailed procedure for characterization of as received base metal and interface filler powders is elucidated in this section.

3.4.1 Characterization of as-received Inconel-625 plate

Commercially available Inconel-625 plates were purchased from M/s Special Metals Ltd., Mumbai with dimensions $1000 \times 25 \times 6.5 \text{mm}^3$ for the convenience during transportation. The average tensile strength, flexural strength and microhardness values of the as-received plate were evaluated as per the standard test procedure. In order to determine tensile strength, two ASTM-E8 standard tensile specimens were cut from the as-received plate and tested on UTM.

Similarly, flexural strength of the Inconel-625 plate was determined by machining two test pieces according to ASTM E190-92 standards (Lakshminarayanan and Balasubramanian, 2010) and tested on UTM. Hardness value of the as-received plate was evaluated through Vicker's microhardness tester. Table 3.1 presents the mechanical properties of the as received Inconel-625 plate.

Table 3.1 Mechanical properties of as-received Inconel-625 plate

Yield strength (MPa)	Ultimate tensile strength (MPa)	Flexural strength (MPa)	Hardness HV
699	945	1760	260

Further characterization of as-received Inconel-625 was carried out through SEM and XRD to evaluate the chemical composition. Figure 3.2(a) illustrates the SEM microstructure of as-received base metal showing a cellular structure. EDS analysis of Inconel-625 sample was carried out through SEM as shown in Figure 3.2(b) to determine the composition of various elements. Chemical compositions of some major elements in

Inconel-625 are presented in Table 3.2. XRD analysis of Inconel-625 sample was carried out at a scan rate of 1°m^{-1} with a scan range from 30° to 100° . Obtained XRD pattern was examined using JCPDS database (PDF Number 656291) which confirms the presence of major peaks corresponding to nickel and chromium Cr_2Ni_3 in FCC form as shown in Figure 3.2(c).

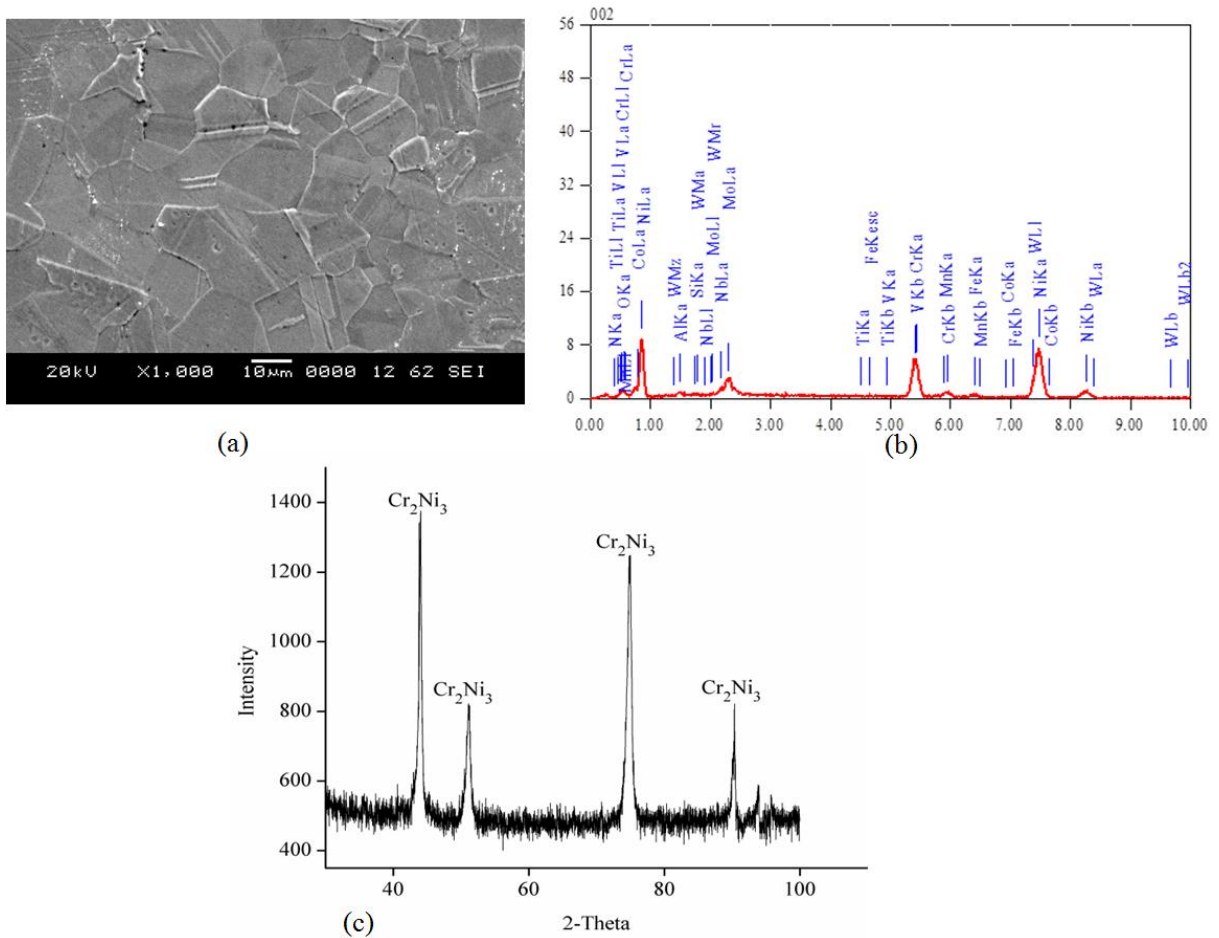


Figure 3.2 (a) SEM microstructure of Inconel-625 sample (b) EDS showing the elemental composition (c) XRD spectrum of as-received Inconel-625 plate indicating the dominating peaks of Cr_2Ni_3

Table 3.2 Chemical composition of various elements in Inconel-625

Element (Wt.%)	Ni	Cr	Mo	Fe	Nb	Ti	Co
	60.55	21.39	9.34	3.08	3.12	0.32	0.52

3.4.2 Characterization of EWAC filler powder

EWAC (Empowering Welding And Cutting) is a subsidiary product of L and T Ltd. based at Ankleshwar, Gujarat, involved in manufacturing of various grades of metallic thermal spray powders for coating and welding applications. EWAC is a nickel based powder available in 500g cartridges used as a filler interface in the present study. As-received EWAC powder was sieved to obtain two grades with average particle sizes (APS) 50 μ m and 75 μ m.

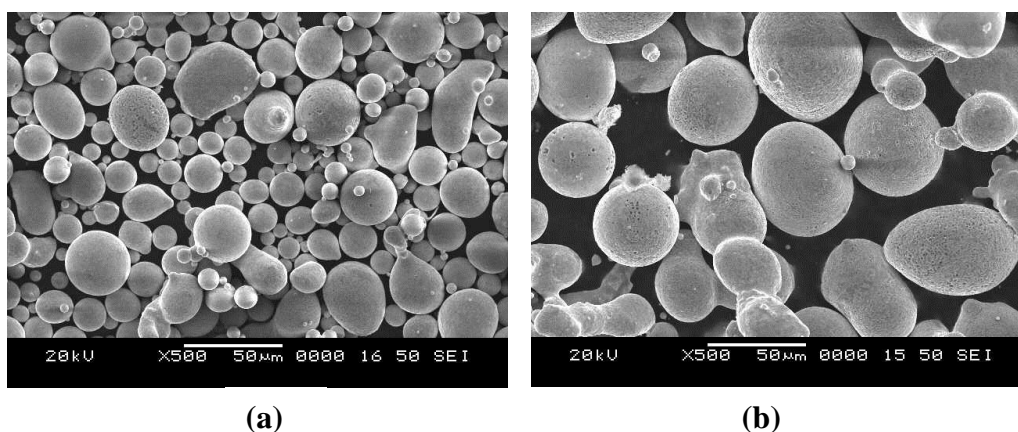


Figure 3.3 SEM micrograph of nickel based powder with average particle size (a) 50 μ m and (b) 75 μ m

SEM morphology of two grades of nickel based powder is illustrated in Figure 3.3. The chemical composition of EWAC powder was determined through SEM equipped with EDS as shown in Table 3.3. Further, XRD analysis of the nickel based powder was carried out to determine the elemental composition. Figure 3.4 illustrates the XRD spectrum of nickel based powder which shows the dominating high intensity peaks of nickel with small traces of chromium and silicon corresponding to low intensity peaks.

Table 3.3 Chemical composition of EWAC powder (wt. %)

Carbon	Silicon	Chromium	Nickel
0.2	2.8	0.17	Bal.

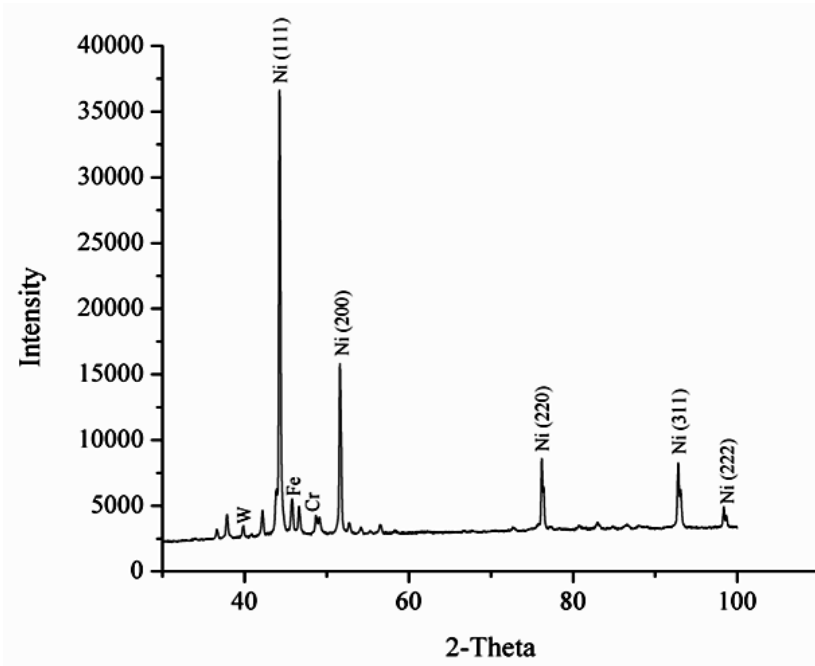


Figure 3.4 XRD spectrum of nickel based powder EWAC

3.5 MICROWAVE JOINING PROCESS

Experiments were conducted in a low-cost 34 liter, 900W multimode domestic microwave oven at 2.45GHz frequency in a non-inert atmosphere. Figure 3.5 shows the photograph of the microwave oven used in the present work. Figure 3.6 presents the schematic of experimental setup used in this study. Following are the steps involved in the microwave joining process.

- i. Preparation of specimens by cleaning the flat surfaces of base metal to be joined with SiC abrasive paper and washing with acetone.
- ii. Preparation of filler material paste by mixing EWAC powder with epoxy resin Bisphenol-A. Epoxy resin is used to bind the loose powder particles.

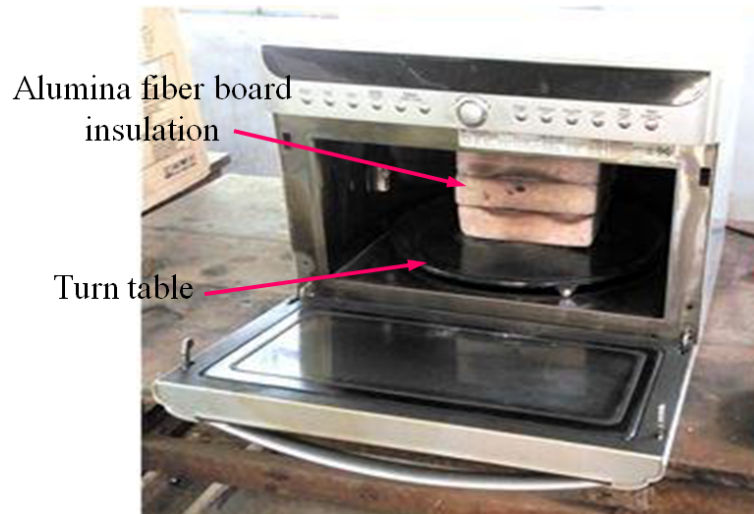
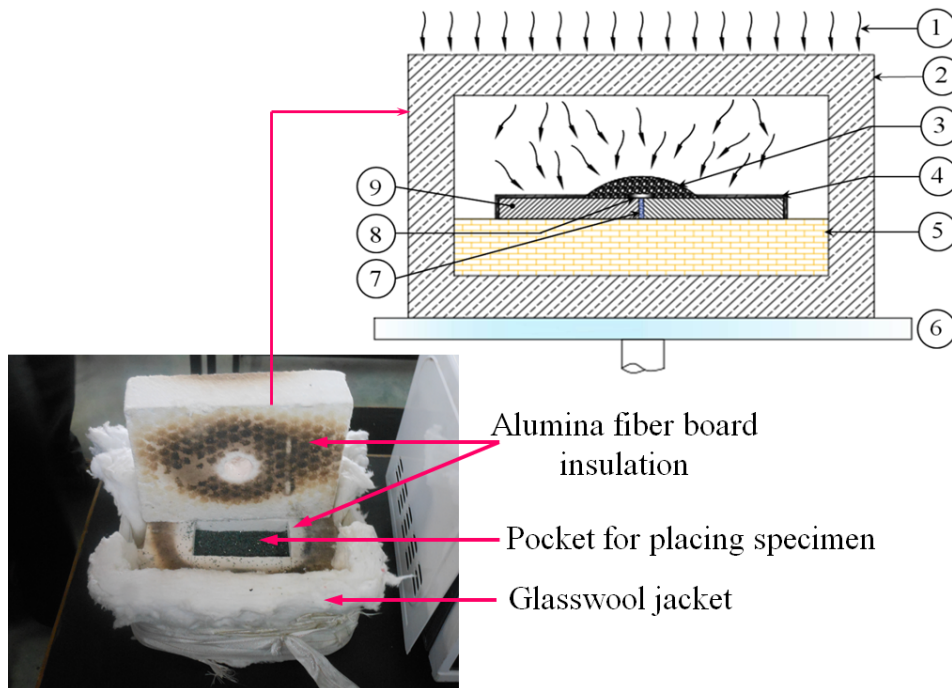


Figure 3.5 Photograph of microwave oven (Make: LG Model: Solardom ML3483FRR) used in the present work



(1) Incident microwaves; (2) Alumina insulation; (3) Susceptor; (4) Refractory masking; (5) Refractory brick; (6) Turn table; (7) Interface powder; (8) Separator; (9) Base metal

Figure 3.6 Sectional schematic of experimental setup

- iii. Applying filler material paste on the faying surfaces to be joined and arranging the specimens in proper alignment on a refractory base.
- iv. Masking the bulk metals with a refractory material except the joint interface.
- v. Placing a thin separator on the joint region and pouring the susceptor material on the top of separator.
- vi. Transfer the entire assembly in the insulator box made up of alumina fiber boards and shifting the insulator box on to the turntable of microwave oven.
- vii. Selecting the power level followed by heating up to the predetermined time.

3.6 MECHANISM OF JOINT FORMATION

The steps involved in joint formation are schematically illustrated in Figure 3.7. At 2.45 GHz frequency, interaction of bulk metal with microwaves at room temperature is restricted only to its surface due to very small penetration depth in metals also known as skin depth. The skin depth of a material is defined as a distance into the material at which the incident power reduces to $1/e$ (36.8%) of the surface value (Mondal et al., 2008). Mathematically skin depth is expressed by Eq. 3.1 as,

$$\delta = \sqrt{\frac{\rho}{\pi f \mu}} \quad \text{————— Eq. 3.1}$$

where, $\delta \Rightarrow$ skin depth (microns); $\rho \Rightarrow$ resistivity ($\mu\Omega.cm$); $f \Rightarrow$ operating frequency (GHz); $\mu \Rightarrow$ magnetic permeability = $\mu_r \mu_o$ (H/m); $\mu_o \Rightarrow$ absolute permeability = $4 \times \pi \times 10^{-7}$ (H/m)
 $\mu_r \Rightarrow$ relative permeability

The skin depth of any material depends on its resistivity, operating frequency and magnetic permeability. At an operating frequency of 2.45 GHz, it is possible to increase the skin depth of a material by changing the resistivity and magnetic permeability that are temperature dependent variables. At room temperature, skin depth for nickel, is calculated as 0.12 microns by substituting $\rho=8.707 \times 10^{-8} \Omega.m$, $f=2.45 \times 10^9 \text{Hz}$, $\mu_r=600$ in Eq. 3.1 (Gupta and Sharma, 2011). The calculated skin depth is very small compared to the size of nickel powder particles used in the present study and hence direct exposure of nickel powder particles to microwave radiation results in surface heating and reflection of

the incident microwaves takes place as shown in Figure 3.7(a). However, microwave hybrid heating is used to overcome this problem.

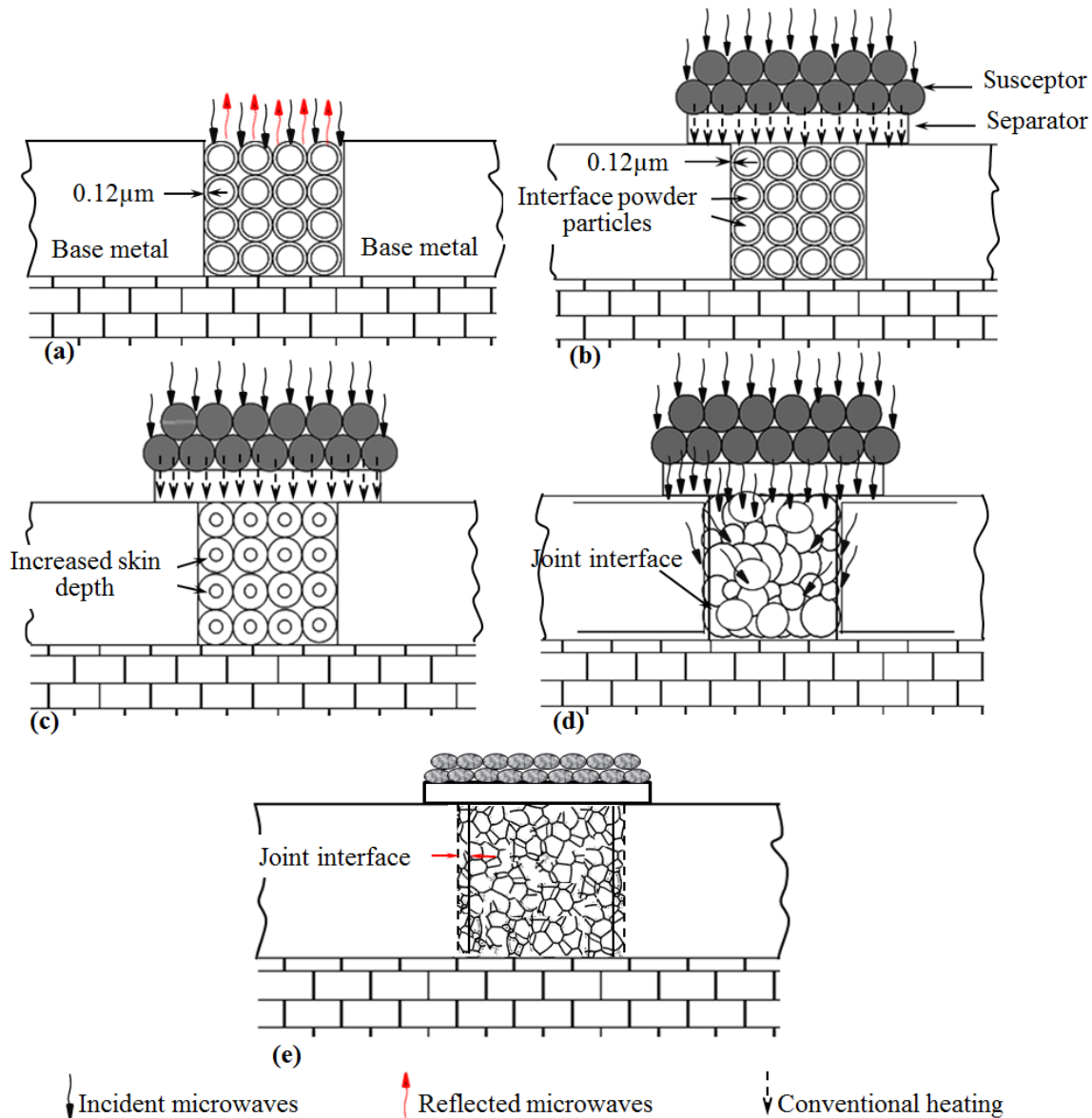


Figure 3.7 Schematic of mechanism of joint formation (a) powder particles in the interface region subjected to direct exposure of microwaves; (b) principle of microwave hybrid heating; (c) increased skin depth of Inconel-625 particles after attaining critical temperature T_c ; (d) direct interaction of Inconel-625 particles with microwaves and fusion of powder particles; (e) solidified joint.

In Figure 3.7(b) the powder particles in the interface region are shown with 0.12 μm skin depth at room temperature. The microwaves initially couple with susceptor that readily interacts and gets heated up. This heat from susceptor is transferred to the powder particles via separator which is in direct contact with susceptor through conventional mode till the powder particles attain a critical temperature T_c . At this temperature the skin depth of powder particles increases so as to facilitate direct interaction with microwaves as shown in Figure 3.7(c). The powder particles in the interface region couple with microwaves and fusion of particles takes place (Figure 3.7(d)); at the same time wetting of the joint interface occurs. Further heating results in diffusion of atoms from joint to base metal and vice versa. After the removal of microwave power, the diffusion process stops and the specimen cools down to room temperature resulting in solidified joint as shown in Figure 3.7(e).

3.7 MECHANICAL CHARACTERIZATION OF MICROWAVE WELDED JOINTS

Mechanical characterization of the microwave induced joints was carried out with universal testing machine and Vicker's microhardness tester.

3.7.1 Specimen preparation for uniaxial tensile test and 3-point bend test

Figure 3.8 (a) and (b) show the photographs of Inconel-625 specimens with square butt configuration welded through MHH for preparation of tensile test specimens. The size of the specimens shown in Figure 3.8 was maintained $110 \times 12 \times 6 \text{mm}^3$. As-welded specimens shown in Figure 3.8 were polished as represented in Figure 3.9 (a) and (b).

The polished specimens were machined using a WEDM according to ASTM E-8 (Figure 3.10) standards with 25mm gauge length to produce tensile test specimens. Figure 3.11 shows the photograph of welded tensile test specimens machined on WEDM from polished specimens shown in Figure 3.9.

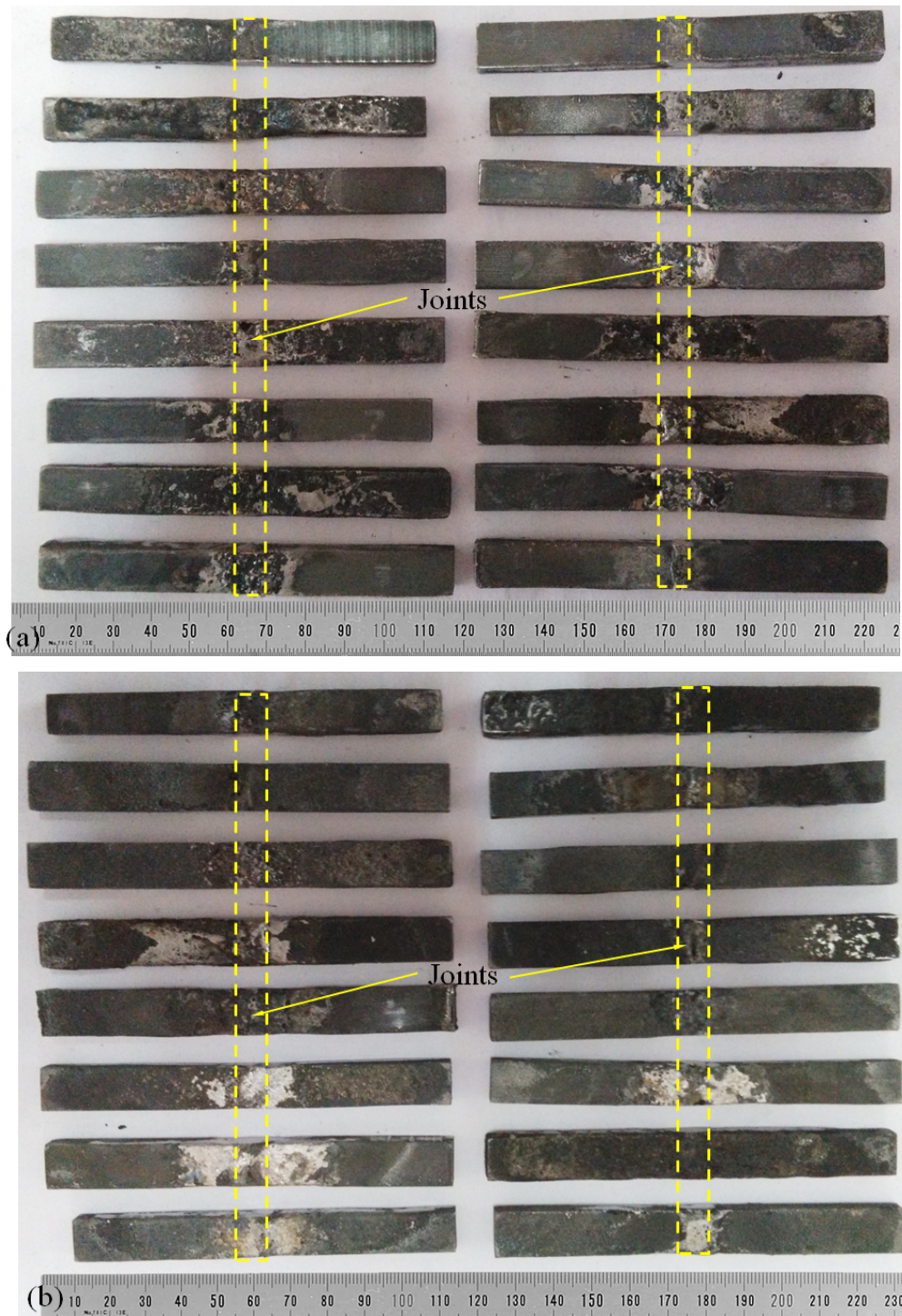


Figure 3.8 As-welded Inconel-625 tensile specimens at (a) 900W (b) 600W power levels



Figure 3.9 Specimens processed at (a) 900W (b) 600W power after polishing

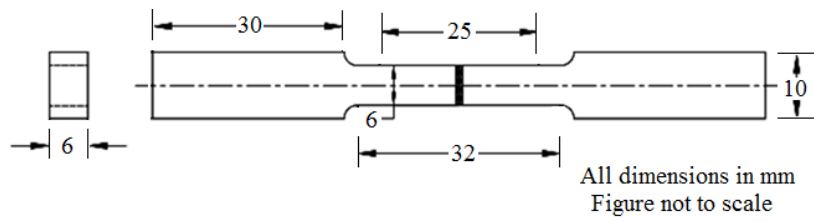


Figure 3.10 ASTM-E8 standard for tensile test specimen



Figure 3.11 Tensile test specimens machined according to ASTM-E8 standards processed at (a) 900W (b) 600W

Figure 3.12 depicts the proportions of 3-point bend test specimens and schematic arrangement for flexural test. Figure 3.13 shows the photograph of Inconel-625 specimens with square butt configuration welded through MHH for preparation of 3-point bend test specimens.

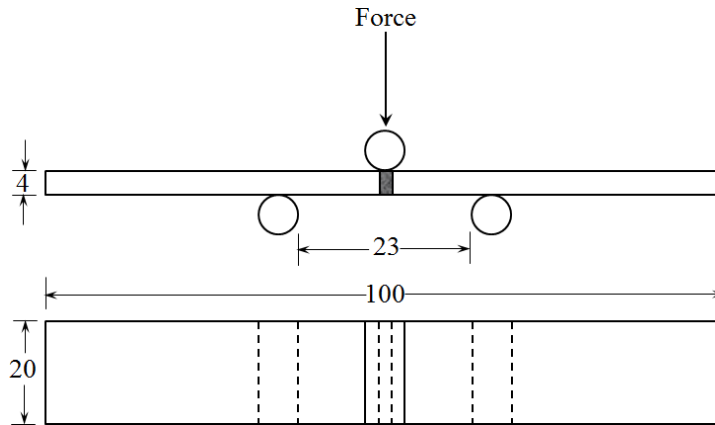
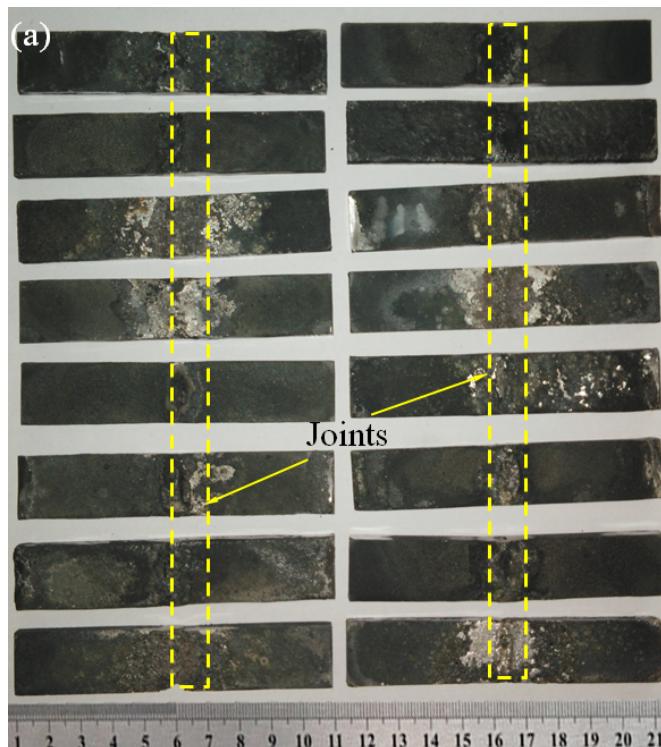


Figure 3.12 Schematic arrangement for 3-point bend test and ASTM-E190-92 standard 3-point bend test specimen



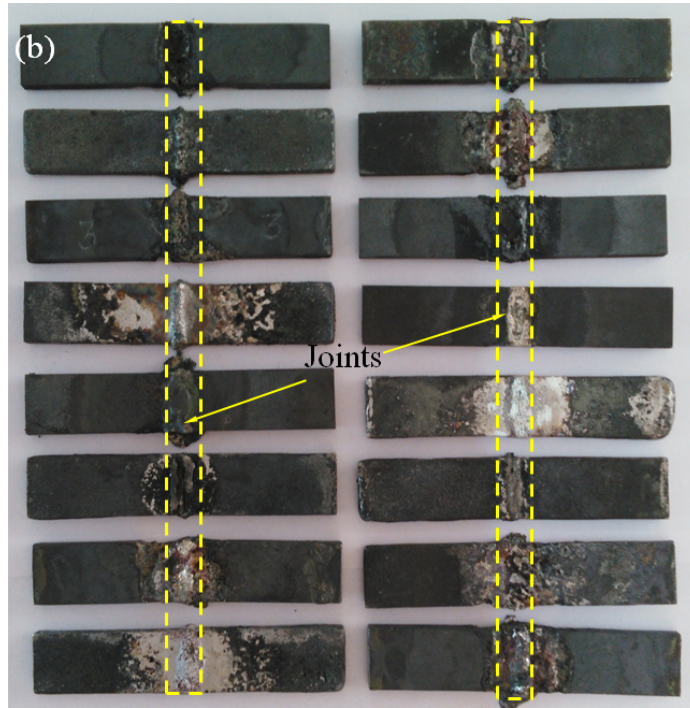
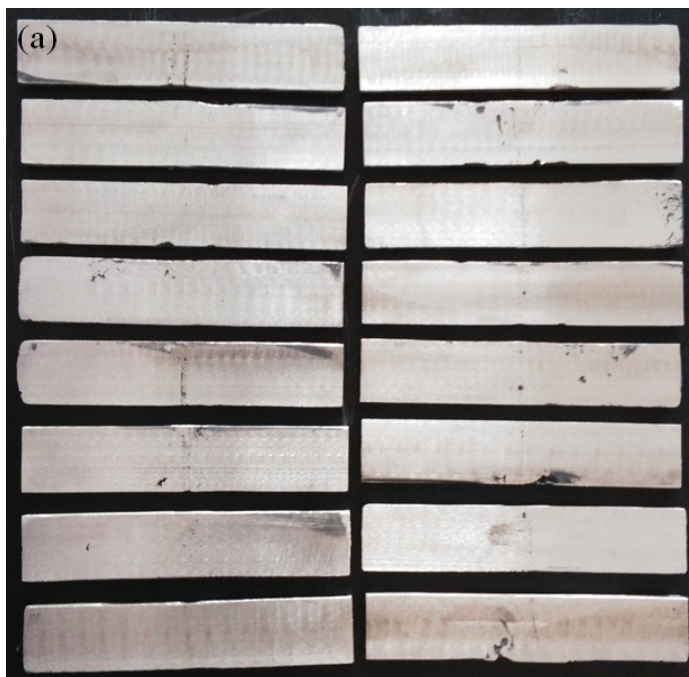


Figure 3.13 Inconel-625 specimens 3-point bend test specimens in as-welded condition processed at (a) 900W (b) 600W



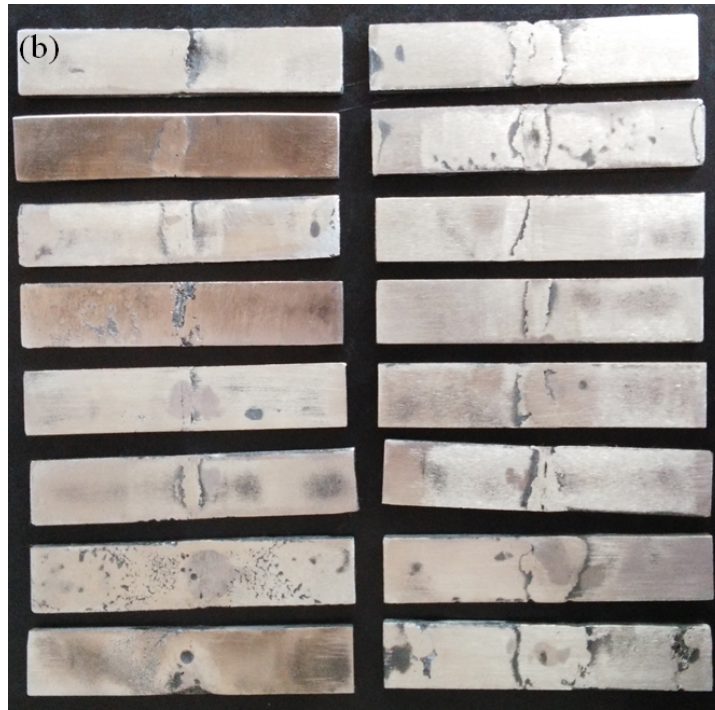


Figure 3.14 3-point bend test specimens processed at (a) 900W (b) 600W and polished according to ASTM E190-92 standards.

Figure 3.14 (a) and (b) shows the photographs of Inconel-625 final 3-point bend test specimens with ASTM E190-92 dimensions.

3.7.2 Uniaxial tensile test

Uniaxial tensile and 3-point bending tests were conducted on a universal testing machine Make: Tinius Olsen, UK. Model: H75KS-EL033 to estimate the tensile properties and flexural strength of the welded joints. The machine is equipped with load cells of max 50kN capacity. The output is obtained with the help of a computer interface which employs Horizon software for analysis of the results. The tensile strength of the joints was evaluated with a uniform strain rate of 0.008mm/s at room temperature. A photograph of the UTM employed in the present work is shown in Figure 3.15 (a). Figure 3.14(b) shows the set-up used to clamp the specimens for uniaxial tensile test.

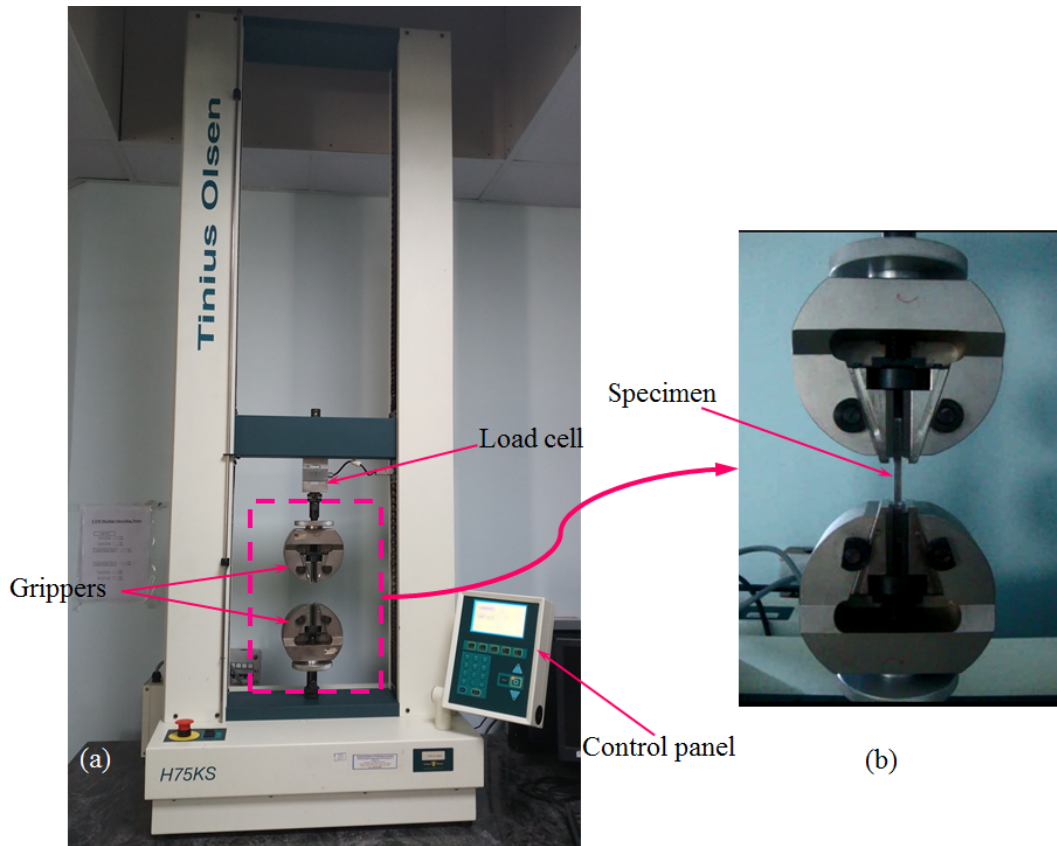


Figure 3.15 (a) Universal testing machine (b) Attachment for uniaxial tensile test

3.7.3 3-point bend test

The 3-point bend tests were conducted with a strain rate 0.01mms^{-1} using the set-up shown in Figure 3.16. Distance between the bottom rollers was calculated as $L=d+3t$, where d is the diameter of the rollers and t , the thickness of specimen.

3.7.4 Microhardness test

Microhardness of the microwave welded specimens was evaluated across the joint using micro Vickers hardness tester (Make: OMNI TECH, Pune, India. Model: MVH-S-AUTO) shown in Figure 3.17. For the micro-indentations, 50g load was applied for dwell time of 10 sec. and the microhardness value is calculated using Eq. 3.2.

$$HV=1.854 \times F/d^2 \quad \text{————— Eq. 3.2.}$$

where,

HV = Vickers hardness of the specimen, d = Mean of diagonals length of a square pyramid and F = Applied load.

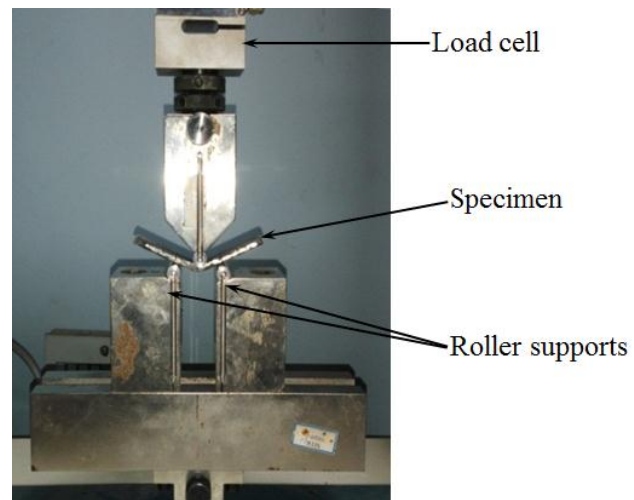


Figure 3.16 Attachment for 3-point bend test



Figure 3.17 Vickers microhardness tester

3.8 METALLURGICAL CHARACTERIZATION OF MICROWAVE WELDED JOINT

The excess material at the sides of welded joints obtained after profile cutting through WEDM was used for metallurgical characterization.

3.8.1 Specimen preparation

The specimens were core mounted using cold setting acrylic resin DPI RR Cold Cure and allowed to set. The core mounted specimens were rough polished on a belt polishing machine to obtain a flat surface. A series of SiC polish papers of grades 500, 600, 800, 1000, 1200, 1500 and 2000 were employed on a disc polishing machine (Make: Ducom) at a rotational speed of 300rpm to attain fine finish on the candidate surface. Final polishing of the specimens was carried out with a velvet cloth using diamond paste along with kerosene as a lubricant to obtain a mirror finish surface. In the next phase, the specimens were chemically etched through Marbels reagent by swabbing for 20 seconds to expose the grain structure. Marbels reagent was prepared using 10g CuSO_4 +50ml HCl+50ml distilled water.

3.8.2 X-Ray Diffraction

XRD analysis of the welded joints was performed on BRUKER D8 Advance instrument with Cu-K α radiation. The scan rate was maintained at 1°/min with scan range from 20° to 100°. The XRD patterns obtained were analyzed with the help of PCPDFWIN software to identify the formation of different phases like carbides, nitrides and intermetallic elements.

3.8.3 Optical Microscope

Figure 3.18 shows the optical microscope used to capture and analyze the microstructures of the welded joints. The equipment consists of an inverted microscope (Make: ARTRAY-130MI) with BIOVIS image analyzer software.

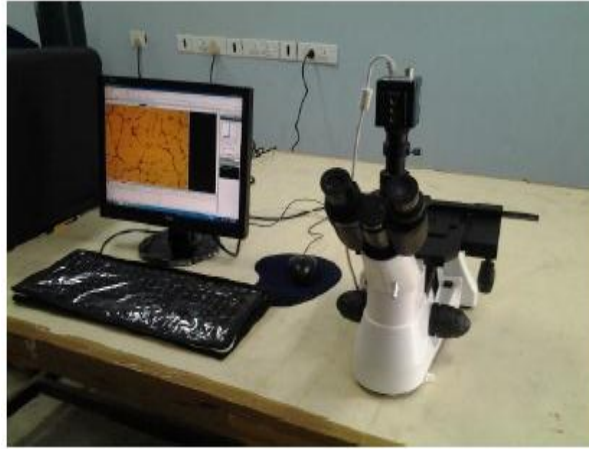


Figure 3.18 Optical Microscope

3.8.4 Scanning Electron Microscope

Joint microstructure was investigated through SEM (JSM-6380 LA; JEOL, Japan) shown in Figure 3.19 equipped with energy dispersive X-ray detector (EDS or EDAX) with a resolution of 3nm at 30kV.



Figure 3.19 Scanning Electron Microscope

EDS analysis was carried out at different locations in the microstructures to determine the elements in the secondary as well as primary phases.

3.9 DESIGN OF EXPERIMENTS

Taguchi method facilitates the designer with a systematic and efficient approach for performing experiments to determine near optimum settings of design parameters in terms of performance and cost. In the present work multiple trial experiments were conducted to determine the levels of the process parameters. In order to determine the influence of process parameters and their interactions on quality characteristics in microwave assisted welding of Inconel-625 alloy, Taguchi design of experiments with one parameter at four levels and two parameters at two levels were considered.

Table 3.4 Control factors and their levels

Code	Parameters	Levels			
		1	2	3	4
A	Separator	Gr	Gwl	GrF	GwlF
B	Susceptor	Coal	SiC	--	--
C	FP APS (μm)	50	75	--	--

FP – Filler powder, Gr – Graphite, Gwl – Glasswool, GrF – Graphite with flux bed, GwlF – Glasswool with flux bed. Flux used – UV420TT

Table 3.4 presents the process parameters and their levels used in the present investigation. The experiments were carried out according to Taguchi L_{16} mixed orthogonal array (Table 3.5) by considering three factors, separator with four levels and susceptor and interface filler powder size with two levels each. The study aims to maximize the ultimate tensile strength (UTS) and flexural strength (FS) of the welded joints developed through MHH. The condition of optimality is recognized by the main effects of each of the parameters. The necessary number of experiments is indicated by the number of rows present in the particular orthogonal array. The number of rows of an orthogonal array must be at least equivalent to the degrees of freedom coupled with the

selected factors i.e. the control variables. The multiple responses selected were ultimate tensile strength and flexural strength of the joints developed at 900W and 600W microwave power levels. The necessary number of experiments is selected based on the degrees of freedom (DF) of individual factors and the addition DF of their interaction factors. The number of rows of an orthogonal array must be at least equivalent or greater than DF coupled with the selected factors i.e. the control variables and their interactions. In general, total DF of each factor and the interactions DF with addition of errors DF is selected for total number of experiments to be conducted.

Table 3.5 L₁₆ orthogonal array

Trial No.	Parameters		
	A	B	C
1	1	1	1
2	1	1	2
3	1	2	1
4	1	2	2
5	2	1	1
6	2	1	2
7	2	2	1
8	2	2	2
9	3	1	1
10	3	1	2
11	3	2	1
12	3	2	2
13	4	1	1
14	4	1	2
15	4	2	1
16	4	2	2

In the present study 13 experiments have to be conducted (Factor A has 4 Levels i.e., DF_A is $4-1=3$, Factor B has 2 levels i.e., DF_B is $2-1=1$, Factor C has 2 levels i.e., DF_C is $2-1=1$, Interactions DF is: $3+1+3=7$ and Errors $DF=1$; Total $DF=13$.) as per total DF however, the nearest OA of design is L_{16} and therefore, L_{16} OA was selected for the experimentation.

3.10 ANALYSIS OF VARIANCE (ANOVA)

Taguchi suggested two different ways to perform the complete analysis. First one is the standard approach, where the results of a single experiment or the mean of repetitive experiments are treated through main effect plot and ANOVA analysis (Raw data analysis) and the second route is to employ signal-to-noise (S/N) ratio for the analysis. The S/N ratio (signal to noise ratio) considers both mean and variability of the experimental results into account. It depends on the quality characteristic of output responses/results and environmental factors. Once the S/N ratio is calculated for all the experimental trials, it converts the entire parameters unit into single standard decibel unit (DB) so that the analysis of data becomes simpler. The main effects show the general tendencies of influence of each control factor. The knowledge of percentage contribution of individual factors is important in determining the type of control to be established on a manufacturing process.

Analysis of variance (ANOVA) is a computational technique used to determine the significance of parameters on the responses and also the significance (as a percentage) of the contribution on the responses (Ross, 1996). ANOVA is a statistical tool used to ascertain the significance of process parameters on the performance measures at 95% confidence level. The general trends of the contributing factors towards the process can be characterized by studying the main effects plot. ANOVA consists of sum of squares, degrees of freedom, mean square, F-ratio and P value. The total SS is the sum of the squared differences between the response value and the sample mean. It represents the total variation in the response values. F-ratio is the test statistic for a test of whether the model differs significantly from a model where all predicted values are the response

mean. The large value of F means the effect of that factor is large and the more important that factor is influencing the process response. The P-value for the test measures the probability of obtaining an F-ratio as large as what is observed, given that all parameters except the intercepts are zero. The percentage contribution of the ANOVA table represents the Adj SS divided by the Total Adj SS. The larger value of the percentage contribution represents the most influential factor in the process.

In the present investigation, the raw data analysis has been performed. The influence of the process parameters on the ultimate tensile strength and flexural strength have been studied through the main effects plots based on raw data. The optimum condition for each of the quality characteristics has been established through the raw data analysis.

3.11 GREY RELATIONAL ANALYSIS (GRA)

Different statistical tools have been used by several researchers to optimize the process parameters. The Taguchi method is one of the most convenient techniques for optimization of single quality characteristic employed for a number of engineering problems. However, in practice most of the engineering components possess multiple quality characteristics to be determined. A single combination of process parameters may be optimum for one response characteristic but the same combination of parameters may not yield best results for the other response characteristic. Therefore, it is necessary to obtain an optimum combination of the control factors so as to produce a component with optimal or near optimal quality characteristics. In the present work, Taguchi method is used to study the effect of each individual parameter on each quality characteristic and multi-response optimization has been carried out through Taguchi-based GRA to obtain an optimum setting of process parameters.

GRA is an appropriate tool for demonstrating the complex interrelationships between multiple parameters and variables. A grey system comprises of unknown data represented by grey variables and grey numbers. In grey system, black denotes a system lacking information, while white represents complete information. Hence, the information that is

either inadequate or uncertain is referred to as grey. The most important benefit of GRA is that it can deal with both inadequate information as well as uncertain problems very accurately (Lin and Lin, 2002). In GRA, the experimental results of UTS and FS are first normalized in the range zero (0) to one (1), which is called generation of grey relation. Subsequently, the grey relational coefficient (GRC) is computed from the normalized experimental results to express the relationship between the actual and desired results. Then, the grey relational grade is calculated by taking the average of the GRC of respective performance characteristic. Highest grey relational grade corresponds to the optimal level of the process parameters. Further, ANOVA study is made to ensure the process parameters that are significant statistically. Finally, a confirmation experiment is carried out to ascertain the combination of optimum process parameters obtained.

3.12 SUMMARY

The current chapter presents the plan of experimentation in detail with emphasizes on selection of materials for experimentation, procedure for welding through MHH, preparation of specimens and subsequent characterization techniques adapted. In addition, particulars of the facilities employed for carrying out tensile test, 3-point bend test, microhardness, XRD, and microstructural studies is also elucidated. Further, the selection of orthogonal array based on Taguchi method and optimization techniques adapted in the present study for multi response optimization have been discussed.

CHAPTER 4

ANALYSIS OF RESULTS AND CHARACTERIZATION

4.1 INTRODUCTION

This chapter presents the characteristics of the Inconel-625 welded joints developed through MHH. Experiments were performed according to Taguchi L₁₆ orthogonal array (OA) and the effects of process parameters on ultimate tensile strength (UTS) and flexural strength (FS) are studied. Taguchi method has been employed to determine the optimal combination of process parameters that yield the best UTS and FS under different processing conditions. The microwave welded joints were characterized in terms of XRD analysis, microstructure study, microhardness, grain size and porosity.

4.2 EXPERIMENTAL RESULTS

Joining of Inconel-625 plates were carried out as per L₁₆ OA to study the effect of process parameters on response characteristics. Ultimate tensile strength (UTS) and flexural strength (FS) were the output responses investigated. The layout of the experiments was designed using Minitab-16 software. The input parameters and their levels used in the present study, as listed in Table 3.4, were selected through literature survey and pilot experimentation. Table 4.1 shows the results of tensile strength and flexural strength of Inconel-625 welded joints developed through MHH at 600W and 900W power levels.

4.3 EFFECT OF PROCESS PARAMETERS ON OUTPUT RESPONSES

The influence of individual process parameters in microwave welding on ultimate tensile strength (UTS) and flexural strength (FS) are discussed in the following section. The mean values of the quality characteristics for each parameter at different levels are computed from experimental results and the main effects of process parameters for raw data are plotted. The effects of process parameters on UTS and FS are investigated using main effects plots. ANOVA study is performed to identify the significant process

parameters and to determine their effects on UTS and FS. The most favorable combination (optimal sets) of process parameters are determined by examining the ANOVA and response tables.

Table 4.1 Experimental results for UTS and FS using L₁₆ orthogonal array

Expt. No.	Separator	Susceptor	FP	Response at 600W power		Response at 900W power	
			APS (μm)	UTS (MPa)	FS (MPa)	UTS (MPa)	FS (MPa)
	A	B	C				
1	1	1	1	347	615	309	562
2	1	1	2	318	516	247	434
3	1	2	1	312	573	345	537
4	1	2	2	236	429	257	476
5	2	1	1	326	651	234	429
6	2	1	2	290	560	228	310
7	2	2	1	304	456	295	526
8	2	2	2	281	393	182	418
9	3	1	1	376	612	304	519
10	3	1	2	298	418	254	464
11	3	2	1	345	559	315	551
12	3	2	2	318	461	280	483
13	4	1	1	353	665	320	427
14	4	1	2	309	485	228	355
15	4	2	1	296	530	290	540
16	4	2	2	249	402	279	414

FP-Filler powder, APS-Average particle size

4.3.1 Effect of separator on UTS and FS

The main effects plots for means of ultimate tensile strength (UTS) and flexural strength (FS) are shown in Figure 4.1. Observed strength values show a clear trend the graphite

(Gr) separator has a positive effect to increase the UTS and FS when used alone or in combination with flux. This is due to the fact that graphite being a carbonaceous material possesses a high dielectric loss factor that readily absorbs microwave energy and provides efficient heating to the joint interface through rapid conduction of heat compared to glasswool (Gwl).

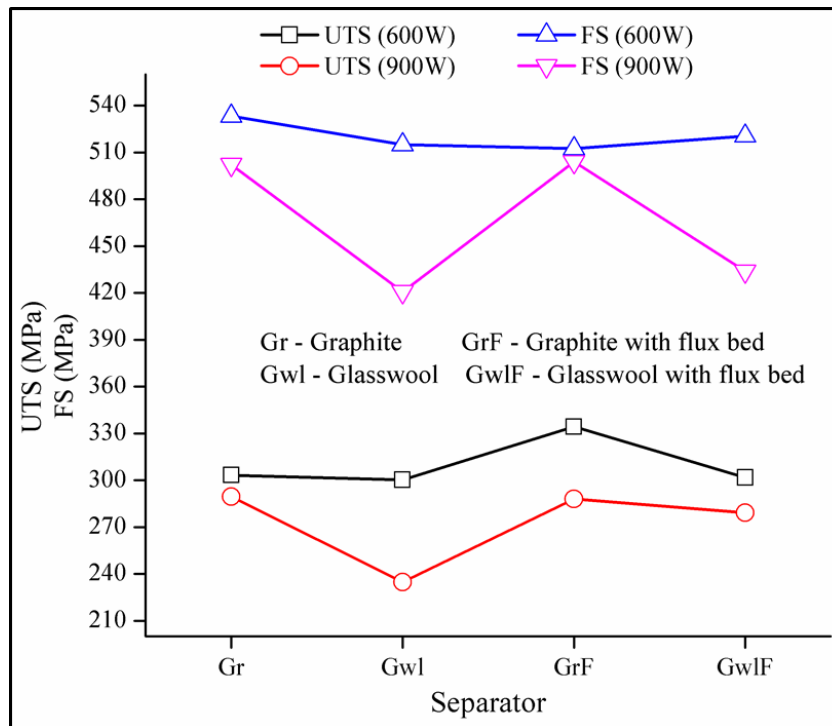


Figure 4.1 Influence of separator on UTS and FS of welded joints processed at 600W and 900W

The use of graphite as a separator largely influences the strength of the welded joint. As evident, a significant decrease in the strength of the joint is observed with glasswool separator. Glasswool separator for both UTS and FS shows lowest response while it is seen to be increased when glasswool is used in combination with flux for all the specimens regardless of power used for processing. This is due to the fact that, the rate of heat transfer from the separator to interface powder is high in case when graphite is used since it has a higher thermal conductivity. However, glasswool has a poor thermal conductivity and is transparent to microwaves (low loss material) at room temperature

with extremely large penetration depth; it allows microwaves to pass through without any significant absorption and at the same time hinders the heat transfer from the susceptor to sample during the initial stage. With the increase in the temperature, glasswool melts ($\sim 750^{\circ}\text{C}$) and there exists a possibility that a small volume of this melt could get included in the filler interface so as to form brittle phases resulting in lower joint strength.

On the other hand when flux is used along with glasswool, the fused flux bed serves as separator and forms a layer of slag on the molten filler interface which prevents oxidation resulting in improved joint strength. This fact has also been observed by Bansal et al. (2015) during joining Inconel-718 alloy through MHH wherein UV420TT flux was used as a separator. However, a marginal improvement in strength of specimens was noticed with combination of graphite and flux. Furthermore, it was noticed that specimens processed at 600W exhibit higher strength when compared to those developed at 900W. This is attributed to the lower heat input associated with 600W which results in rapid cooling of the welded joint thereby reducing the time for segregation. With the application of higher power, a surplus of heat is induced in the surroundings of the joint interface which might result in formation of blow holes and voids, since at elevated temperature metals show increased absorption of gases which later escape out during the solidification consequently resulting in porosity (Dwivedi et al., 2014).

4.3.2 Effect of susceptor on UTS and FS

Another factor to be considered is the heat transfer mechanism through susceptor that affects the quality of the welded joint produced. It is evident from Figure 4.2 that, both UTS and FS have higher values when processed with coal at 600W and conversely exhibit higher values with SiC at 900W power. This is because SiC exhibits better heating characteristics compared to coal when processing at 900W. With 900W comparatively a higher power, coal is burnt at faster rate and converted into ash. This would cause insufficient supply of heat at the joint zone resulting in lower strength of the joint. While with 600W, coal burns for a longer time and ensures continuous supply of

heat. Anklekar et al. (2001) and Gamit (2017) in different works have demonstrated the fact that, carbon based susceptors exhibit a higher heating rates as compared to SiC.

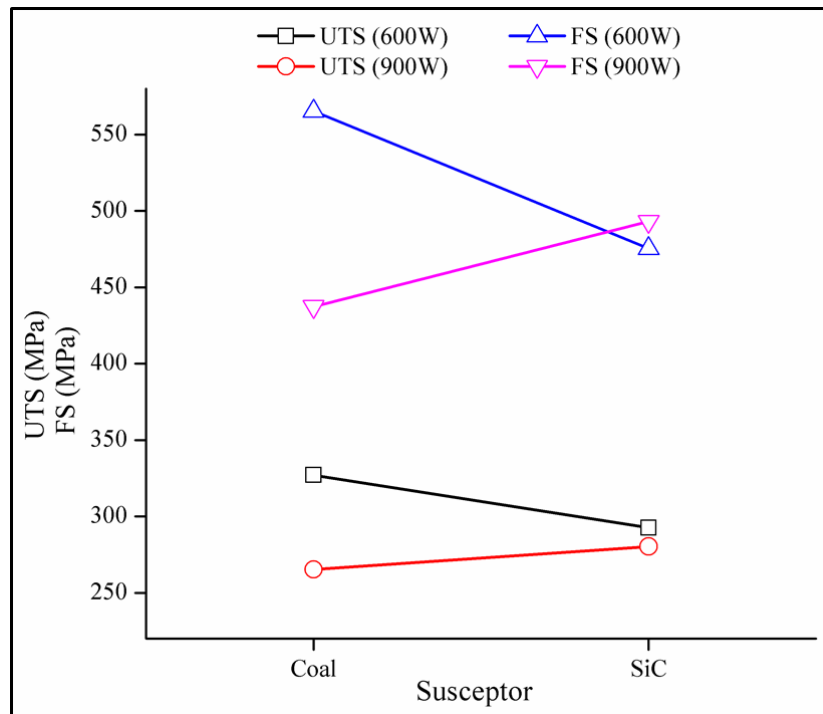


Figure 4.2 Influence of susceptor on UTS and FS of welded joints processed at 600W and 900W

Both SiC and coal are highly lossy materials that rapidly absorb microwaves and convert incident electromagnetic energy into heat. In addition, loss tangent value for SiC is higher than that of coal and therefore higher heating rates can be achieved with SiC. However, it was noticed that, SiC requires a small warm up time to couple with microwaves and thus initial high temperatures were achieved at faster rate with coal as it is a carbonaceous material which contains pure carbon compared to SiC (Rao et al., 1999). Furthermore it can be seen that, the flexural strength of specimens processed at 600W power marginally improved with coal and graphite combination.

4.3.3 Effect of interface powder on UTS and FS

It is witnessed from Figure 4.3 that, filler powder size 50 μm exhibits the best microwave heating characteristics for all the specimens irrespective of power input. This is attributed to the fact that, microwave heating rate is largely affected by the electrical conductivity of the materials which in turn depends on the skin depth. Lower the skin depth, higher will be the conductivity and hence lower heating rate. As the interface powder particle size increases, the neighboring particles come in contact with each other consequently, electrical conductivity of the powder particles increases thereby decreasing the heating rate (Ma et al., 2007).

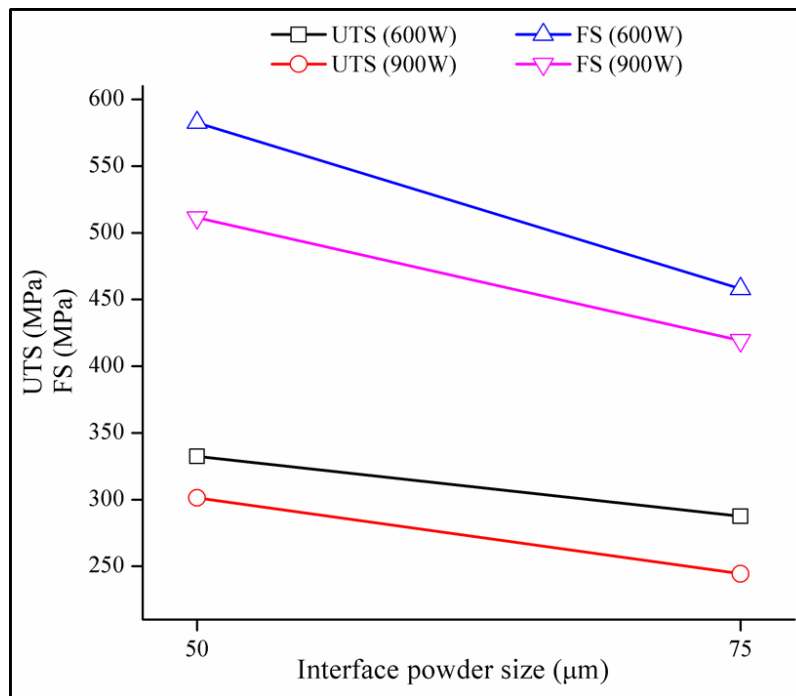


Figure 4.3 Influence of interface powder size on UTS and FS of welded joints processed at 600W and 900W

Mondal et al. (2008) and Yoshikawa et al. (2006) have shown that heating rate is largely affected by the particle size of the metallic powder; the smaller the particle size better is the heating rate. At a particular power level, with increase in particle size heating rate decreases and after certain time it becomes constant. Crane et al. (2014) reported that it is

not only the particle size but also the ratio of particle radius to the skin depth which is more critical in deciding the characteristic of heating rate. However in addition, the combined effect of the type of susceptor and separator along with filler powder size has to be taken into consideration. In a similar work, Bagha et al. (2017) and Soni et al. (2018) observed that with decreasing powder size there was significant increase in the tensile strength of welded joints developed through MHH. However, it was also noticed that, with decreased powder size the HAZ also increased resulting in higher hardness of the joints.

4.4 ESTIMATION OF OPTIMAL RESPONSE CHARACTERISTICS

The response Table 4.2 shows the average of each response characteristic (raw data) for each level of each factor. The tables comprise of ranks based on delta statistics that compare the relative magnitude of effects. The delta statistics is the highest minus the lowest average for each factor. Minitab allocates ranks based on delta values; rank 1 to the highest delta value, rank 2 to the second highest, and so on. The ranks indicate the relative importance of each factor to the response. The ranks and delta values for various parameters indicate that filler powder size has the greatest effect on UTS and FS followed by susceptor and separator in that order when processing with 900W. It can be further seen that the separator has at least significant role while processing with 600W. The optimal combination of process parameters that determine maximum strength of the welded joints can be obtained as presented in Table 4.3.

The optimal combination of process variables for obtaining best ultimate tensile strength values with the specimens processed at 600W and 900W are observed as A3B1C1 (Expt. No. 9) and A1B2C1 (Expt. No. 3) respectively as shown in Table 4.1. Similarly the optimal combination of process parameters for better flexural strength of the Inconel-625 microwave induced welded joints is determined as A1B1C1 (Expt. No. 1) and A3B2C1 (Expt. No. 11) when processed with 600W and 900W power respectively as presented in Table 4.1. Further it is observed that, filler powder APS is the most significant parameter

followed by separator and susceptor. This is much obvious since in a typical microwave heating during the initial stage, interface filler powder requires susceptor assisted heating.

Table 4.2 Response Tables for UTS and FS

	Level	Separator	Susceptor	Filler powder
UTS (600W)	1	303.3	327.1	332.4
	2	300.3	292.6	287.4
	3	334.3	----	----
	4	301.8	----	----
	Delta	34.0	34.5	45.0
	Rank	3	2	1
	UTS (900W)	1	289.5	265.4
2		234.8	280.4	244.4
3		288.3	----	----
4		279.3	----	----
Delta		54.8	14.9	57.1
Rank		2	3	1
FS (600W)		1	533.3	565.3
	2	515.0	475.4	458.0
	3	512.5	----	----
	4	520.5	----	----
	Delta	20.8	89.9	124.6
	Rank	3	2	1
	FS (900W)	1	502.3	437.4
2		420.8	493.1	419.3
3		504.0	----	----
4		434.0	----	----
Delta		83.5	55.6	92.1
Rank		2	3	1

Susceptors that usually couple well with the microwaves are initially used to raise the temperature of the joint interface. Once the critical temperature is reached, thereafter heating primarily occurs due to microwave-metal powder surface interaction.

Table 4.3 Optimum combination of process parameters

Response characteristics	Power (W)	Process Parameter		
		Separator	Susceptor	Filler powder APS (μm)
UTS	600	GrF	Coal	50
UTS	900	Gr	SiC	50
FS	600	Gr	Coal	50
FS	900	GrF	SiC	50

APS-Average particle size

4.5 ANOVA STUDY

In order to study the significance of the process parameters towards UTS and FS, analysis of variance (ANOVA) was performed. It was found that filler powder size is the most significant process parameter for determining the strength of the welded joint. Table 4.4 shows the results of ANOVA for response characteristics. The general trend of contributing factors towards the process can be characterized by studying the main effects plot. ANOVA consists of sum of squares (SS), degrees of freedom (DF), mean square (MS), F-ratio and P value. The total SS represents the total variation in the response values and is the sum of the squared differences between the response value and the sample mean. The error SS is the sum of squared differences between the fitted values and the actual values, remains unexplained by the fitted model. F-ratio is the statistical evaluation in which the test statistics has a F-distribution under the null hypothesis. F-statistics is ratio of mean square of parameter and the error. Highest F value signifies the highest percentage of contribution on the output responses. The P-value for the test

measures the probability of obtaining a F-ratio as large as what is observed, given that all parameters except the intercepts are zero.

Table 4.4 Results of ANOVA for response characteristics

	Source	DF	Seq SS	Adj MS	F-value	P-value	P %	Remarks
UTS (600W)	Separator	3	3186.8	1062.3	2.69	0.103	10	Insignificant
	Susceptor	1	4761	4761	12.04	0.006	21.8	Significant
	FPS	1	8100	8100	20.49	0.001	38.5	Significant
	Error	10	3954	395.4			29.7	
	Total	15	20001.8				100	
UTS (900W)	Separator	3	8027.7	2675.9	4.91	0.024	23.3	Significant
	Susceptor	1	885.1	885.1	1.62	0.231	1.24	Insignificant
	FPS	1	13053.1	13053.1	23.95	0.001	45.62	Significant
	Error	10	5451.1	545.1			29.84	
	Total	15	27416.9				100	
FS (600W)	Separator	3	1027	342	0.14	0.931	-	Insignificant
	Susceptor	1	32310	32310	13.58	0.004	25.09	Significant
	FPS	1	62126	62126	26.11	0.000	50.09	Significant
	Error	10	23797	2380			24.82	
	Total	15	119259				100	
FS (900W)	Separator	3	23387	7796	8.10	0.005	25.8	Significant
	Susceptor	1	12377	12377	12.87	0.005	14.38	Significant
	FPS	1	33948	33948	35.29	0.000	41.58	Significant
	Error	10	9620	962			18.24	
	Total	15	79331				100	

FPS - Filler powder size

From Table 4.4, it is seen that filler powder size, separator type and susceptor type significantly affect the mean variation. The parameters for which the corresponding P-value is less than 0.05 are considered as significant. It is seen that filler powder size is the most significant parameter with the highest contribution in all the cases. This influence is identified from the F-value and corresponding P-values which is less than 0.05 (95% confidence) (Basavarajappa et al., 2009; Jangra et al., 2016). From the ANOVA table it is analyzed that the interaction effect of all the process parameters that is not statistically significant on the output responses can be eliminated from the model and the model can be refitted. Hence, the sum of squares and degrees of freedom corresponding to the eliminated terms are added into the residual sum of squares and degrees of freedom and it is considered as pooled error during calculating ANOVA.

The microwave power also significantly influences the UTS and FS of welded joints since the welded samples at 600W exhibit better characteristics due to the lower heat input associated with the process. Furthermore, it is observed that separator becomes insignificant when processing is carried out at 600W power. This could be due to the fact that in a typical microwave heating when processing is carried out at lower power, susceptor assisted heating continues for a longer time resulting in slow and uniform heating of the joint interface and thus the role of separator is restricted. However, when processing with higher power, there exists a possibility that susceptor burns at faster rate and continued supply of heat to the joint interface is ensured by separator and thus it has significant role.

4.6 CHARACTERIZATION OF THE DEVELOPED JOINTS

In order to investigate the metallurgical and mechanical characteristics of the specimens that exhibited best results under the optimum combinations of process parameters as revealed by Taguchi method has been carried out. From Figures 4.1 to 4.3 and Table 4.3 it is seen that specimen developed from experiment No. 1, 3, 9 and 11 showcase the best results and therefore these specimens were selected for characterization as discussed in following sections.

4.6.1 XRD observations

Figures 4.4 to 4.7 show the XRD patterns obtained for the specimens 1, 3, 9 and 11. The XRD patterns indicate the presence of chromium carbide (Cr_{23}C_6 and CrC at 2-theta values 44.22° and 38.61° respectively) nickel carbide (NiCx) and molybdenum carbide (Mo_2C) corresponding to 2-theta values of 29.40° and 39.41° respectively. The presence of carbon in the base metal strongly influences the formation of carbides. These phases are formed due to the affinity of Ni, Cr and Mo with carbon at elevated temperatures. In addition, as the process is carried out in atmospheric conditions, it leads to the formation of oxides such as nickel oxide (NiO) and titanium molybdenum oxide (TiMoO_5) that are identified corresponding to 2-theta values of 43.27° and 48.52° respectively. Further the intermetallic phases like nickel-chromate $\text{Ni}(\text{Cr}_2\text{O}_4)$, NiCrFe , and CrFe_4 are also observed corresponding to 2-theta values of 35.98° , 44.7° , 47.53° and 65.02° respectively. In addition, small traces of TiN are also encountered (Figure 4.7) at 2-Theta corresponding to 43.26° .

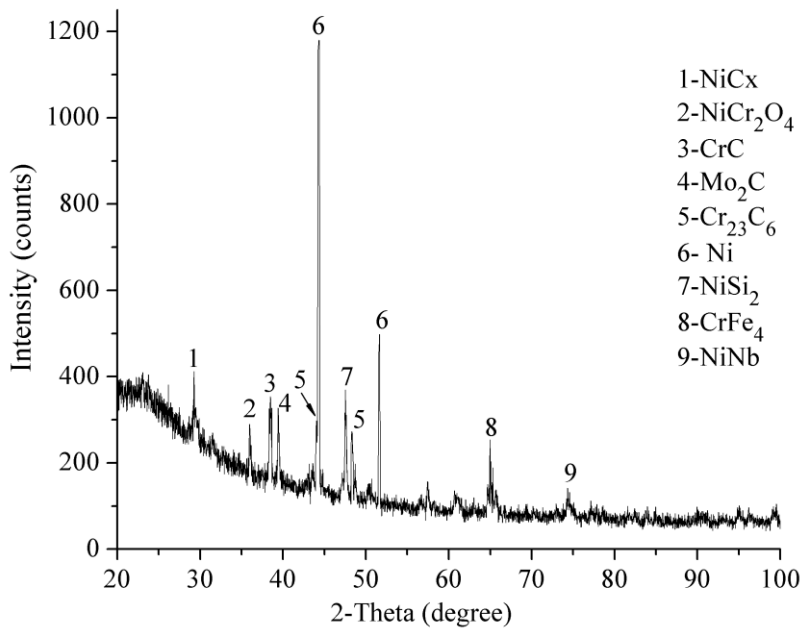


Figure 4.4 XRD pattern of the joint developed in experiment No. 1

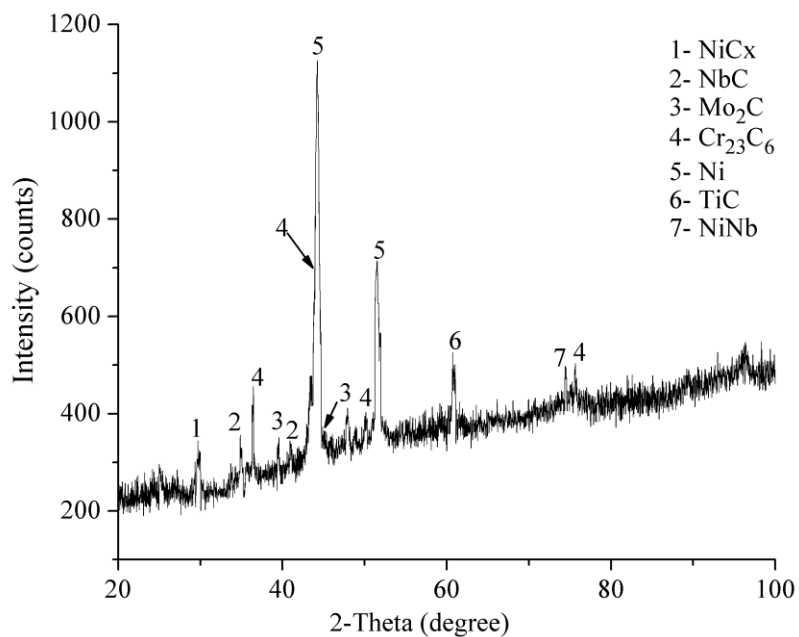


Figure 4.5 XRD pattern of the joint developed in experiment No. 3

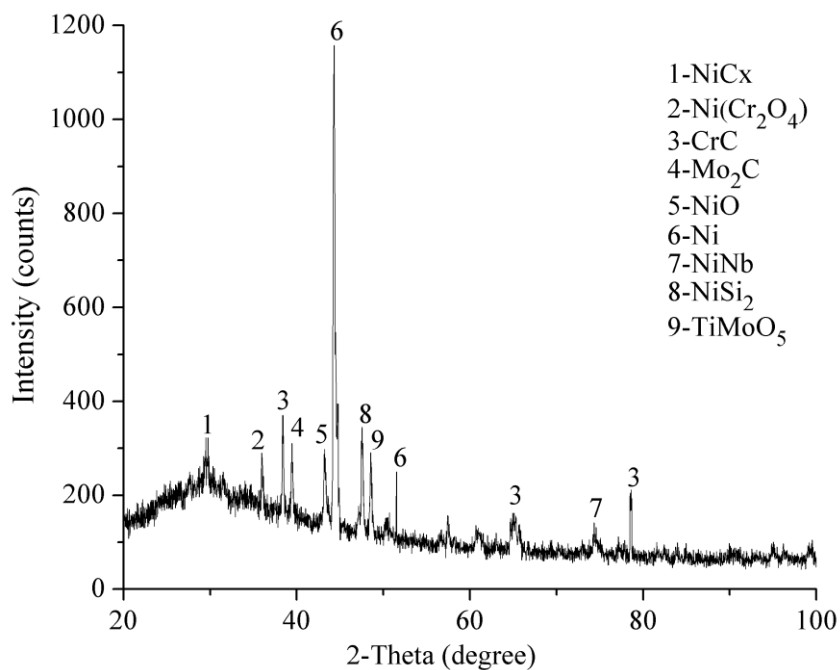


Figure 4.6 XRD pattern of the joint developed in experiment No. 9

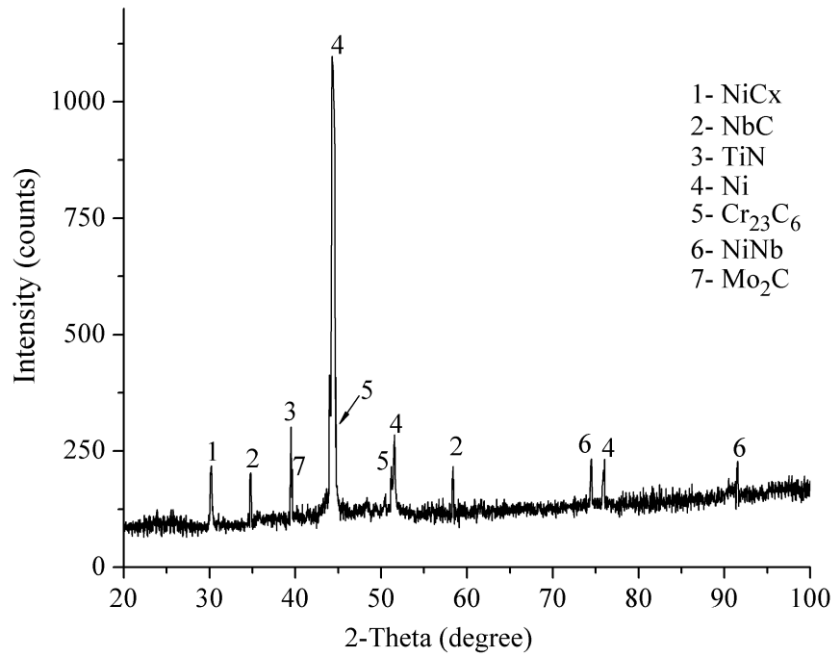


Figure 4.7 XRD pattern of the joint developed in experiment No. 11

Silva et al. (2013) reported that occurrence of TiN in the fused metal supports the formation of niobium carbide. Since the melting point of TiN is much higher than Inconel-625 alloy, it does not dissolve in the molten pool and hence serves as nucleating agent for the formation of NbC. The formation of carbides is attributed to the strong affinity of niobium and chromium with carbon at elevated temperatures. The equilibrium distribution coefficient of niobium in nickel-based alloys is less than unity (0.46); hence, it easily segregates into interdendritic region during solidification and produces niobium carbide (DuPont, 1999). Development of intermetallic compounds is due to the fact that various alloying elements are found in free form in the starting powder; however during heating, these alloying elements react and combine with each other at high temperatures resulting in formation of intermetallic phases.

The formation of intermetallic phases, carbides and oxides all have a significant impact on the dielectric properties of the material and contributes to better coupling of interface material with microwaves to raise the joint temperature (Mahmoud et al., 2015; Bansal et al., 2015; Srinath et al., 2011). Development of these phases could be due to the thermal

cycle in which rapid heating is followed by slow cooling. Microwaves initially travel through the alumina insulation and interact with susceptor. Consequently the susceptor is heated up and transfers heat to the interface powder in the joint zone. As a result, wetting of nickel based powder in the joint region takes place. At this elevated temperature, fusion of the powder in the interface region occurs and continued heating results in formation of molten pool in the joint interface. With the removal of microwave power the rotation of dipoles stops instantaneously and the component cools down to the room temperature. As the dielectric properties are dependent on solid state transformations, the presence of these carbides and oxides promotes the better coupling of microwaves with the interface powder.

4.6.2 Microstructural observations

The optical microstructures of the welded joints shown in Figure 4.8 exhibited a good metallurgical bonding with the base metal and a complete melting of nickel based powder can be seen. A cellular structure with fused weld interface and its vicinity without any visible cracks are clearly realized from the microstructures. Figure 4.9 depicts typical SEM micrographs of the microwave welded joints obtained from experiments 1, 3, 9 and 11. Figures 4.10 to 4.13 show the SEM microstructure of the joint zone of specimen No. 1, 3, 9 and 11 developed through MHH. EDS analysis was carried out at two locations mainly inside the grain and at the interdendritic region.

The elemental composition of some of the major elements in locations 1 and 2 are tabulated in Figures 4.10 to 4.13. Inconel-625 is a complex alloy of Ni-Cr composition since its microstructure exhibits the possibility of formation of variety of phases during processing. Investigation in the interior of the grain at point 2 in Figures 4.10 to 4.13 shows the presence of nickel rich matrix since nickel is the dominating element in starting interface powder. At elevated temperatures chromium from the base metal due to higher affinity with carbon, forms chromium carbide and segregates along the grain boundaries.

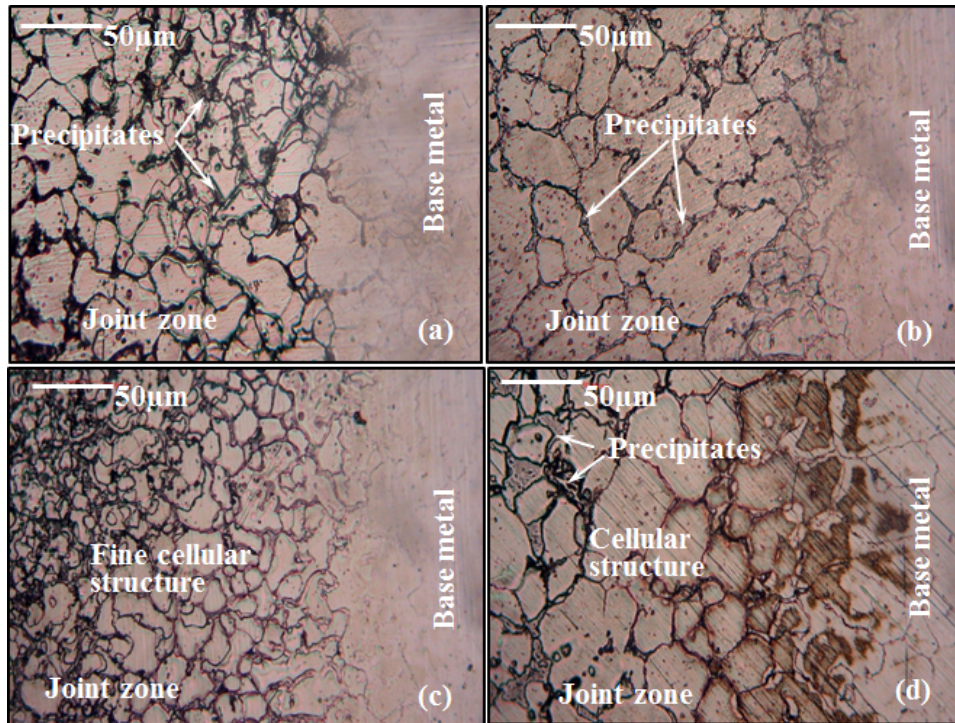


Figure 4.8 Optical microscope images showing the welded joint and base metal obtained from experiment No. (a) 1 (b) 3 (c) 9 and (d) 11.

As dielectric properties depend upon solid state phase transformations (Clark and Sutton, 1996) the formation of chromium carbide influences the process and contributes in better coupling of microwaves with the interface material in the joint. A similar trend was noticed with all the specimens except small variations in elemental composition. Furthermore, the chemical composition analysis indicates depletion of Nb and Mo from the base metal into the interdendritic region.

Figure 4.14 illustrates the SEM microstructure of microwave welded joint showing the segregation of niobium and molybdenum in intergranular region. It is noticed that core interdendritic areas are greatly depleted of niobium compared to the base metal. Similarly titanium and molybdenum also follow the same trend, however, to a lower degree than

niobium. Since niobium, molybdenum, and titanium are elements of higher atomic weight, the amount of segregation associated with these elements is higher than other elements.

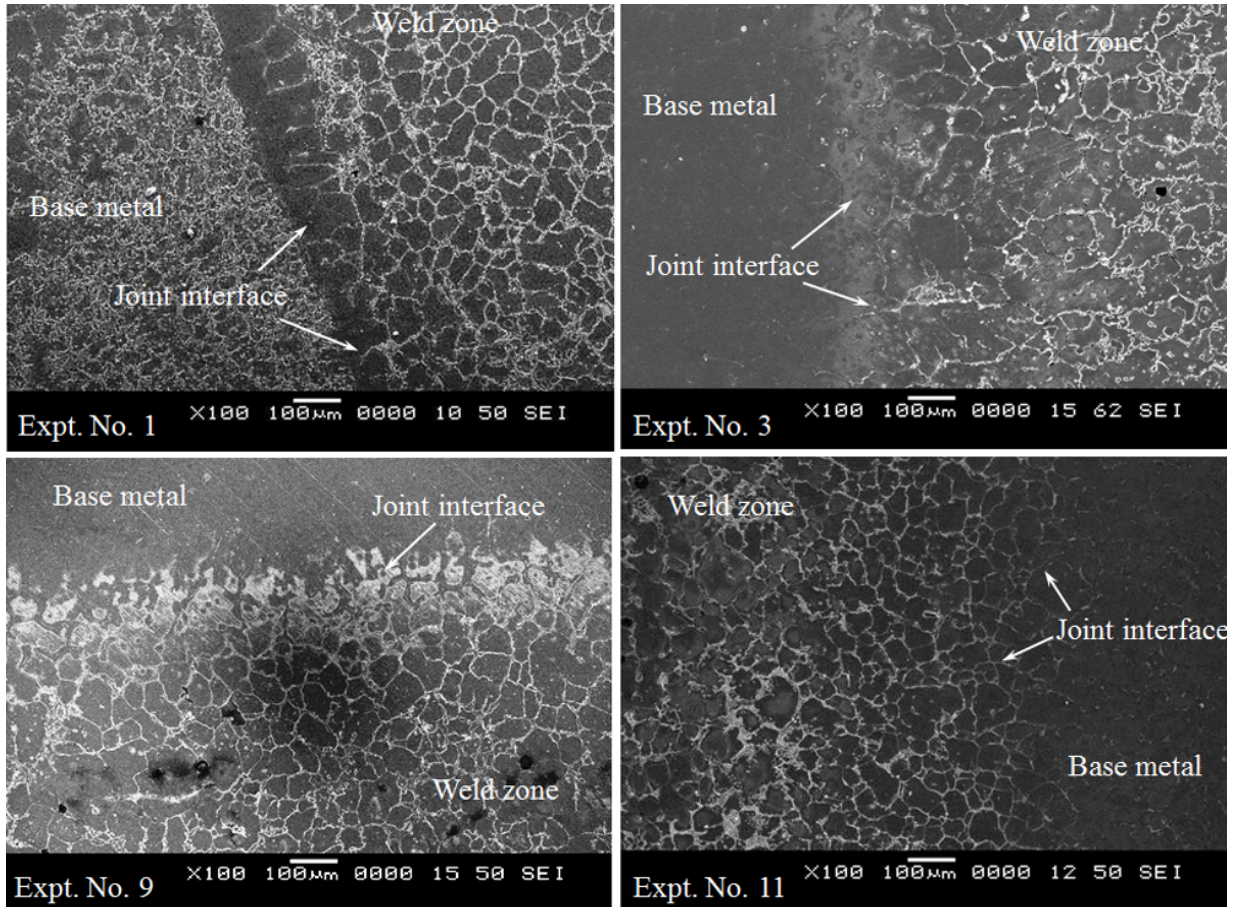


Figure 4.9 Typical SEM micrographs of microwave welded joints

Even though the interdendritic areas are enriched with niobium, molybdenum, and titanium, on the other hand the depletion of nickel, iron, and chromium is observed in these areas. The weld zone exhibits a cast structure which is susceptible to cracking if cooling rate is high. The solidification of Ni based alloys takes place in three steps as (i) primary $L \rightarrow \gamma$ after which the interdendritic liquid becomes rich in Nb and C (ii) Eutectic phase $L \rightarrow (\gamma + NbC)$ through depletion of interdendritic liquid of C and (iii) completion of solidification through formation of another eutectic $L \rightarrow (\gamma + Laves)$. However, the termination reaction depends on the elemental composition of the liquid.

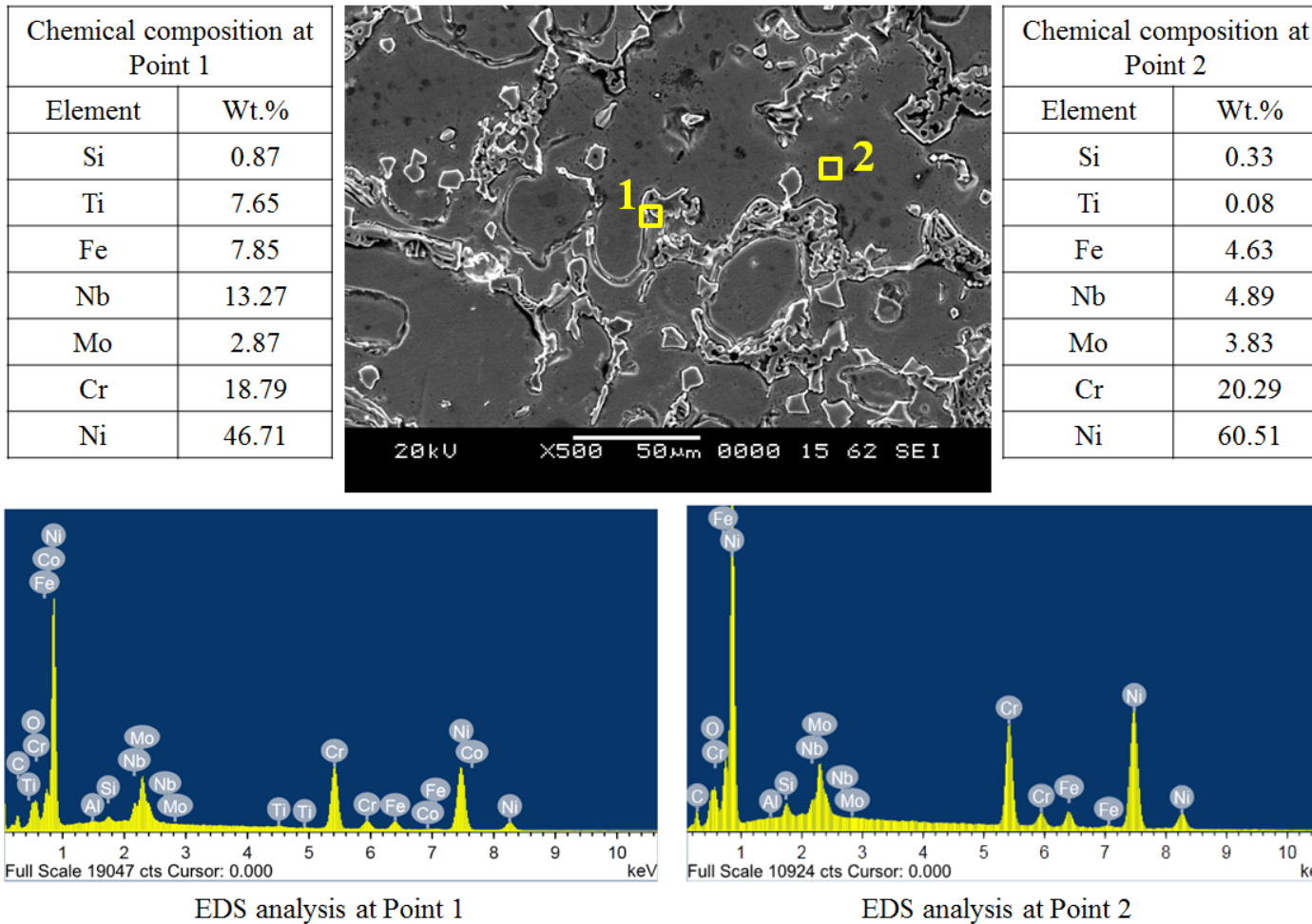
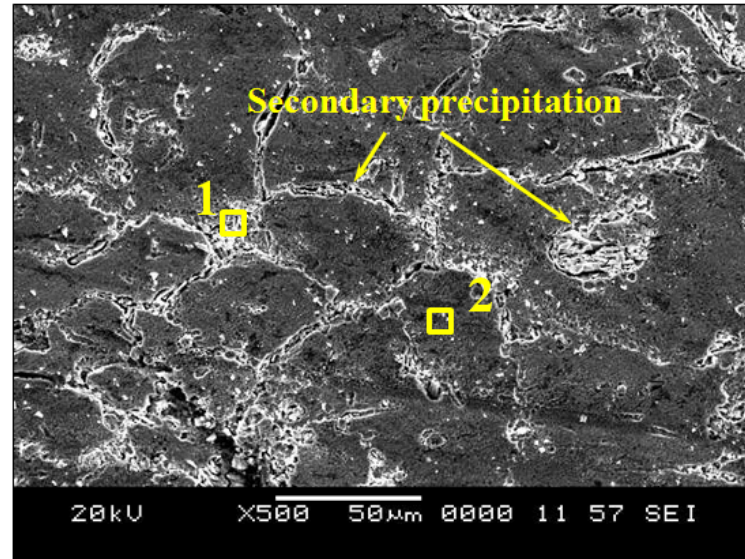
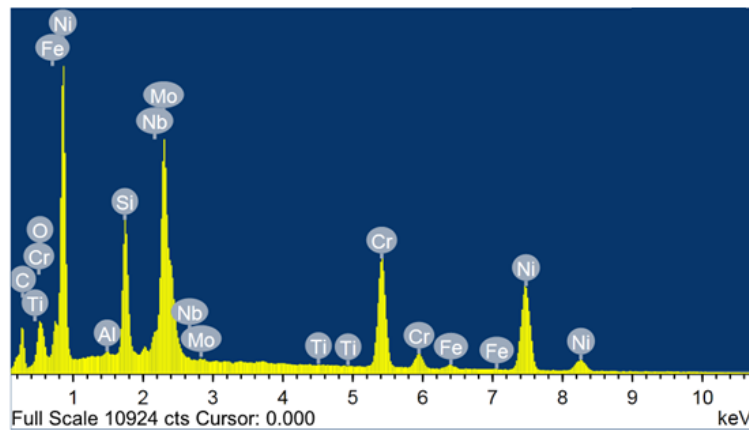


Figure 4.10 SEM microstructure of specimen No.1 and EDS analysis at grain boundary (Point 1) and grain interior (Point 2)

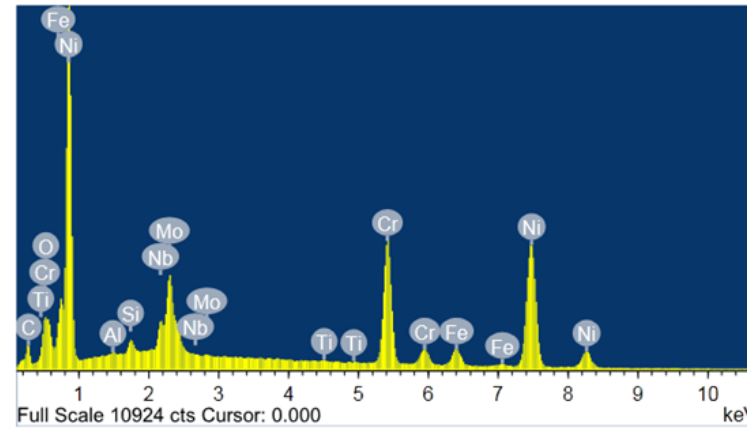
Chemical composition at Point 1	
Element	Wt.%
Si	1.1
Ti	1.21
Fe	8.09
Nb	15.18
Mo	5.41
Cr	19.24
Ni	45.59



Chemical composition at Point 2	
Element	Wt.%
Si	0.56
Ti	0.16
Fe	4.55
Nb	3.40
Mo	4.49
Cr	21.64
Ni	58.95



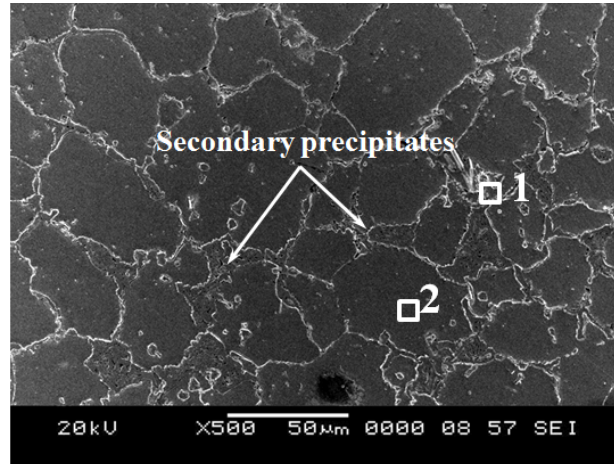
EDS analysis at Point 1



EDS analysis at Point 2

Figure 4.11 SEM microstructure of specimen No.3 and EDS analysis at grain boundary (Point 1) and grain interior (Point 2)

Chemical composition at Point 1	
Element	Wt.%
Si	0.98
Ti	5.36
Fe	8.7
Nb	13.33
Mo	1.82
Cr	18.63
Ni	48.36



Chemical composition at Point 2	
Element	Wt.%
Si	0.43
Ti	0.13
Fe	0.97
Nb	2.46
Mo	3.08
Cr	19.7
Ni	62.45

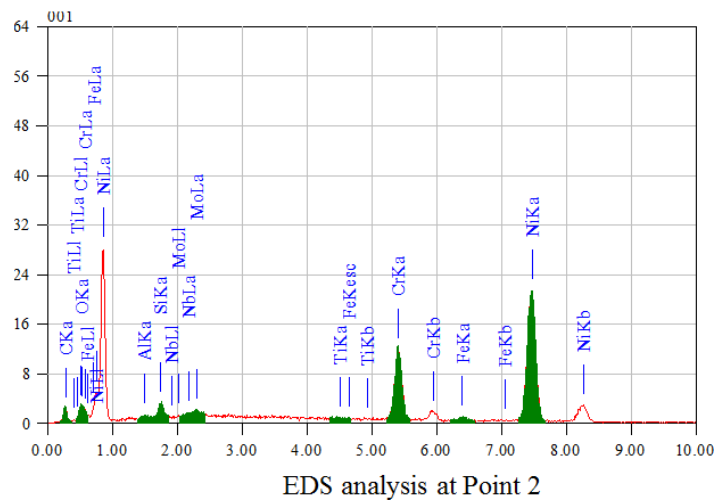
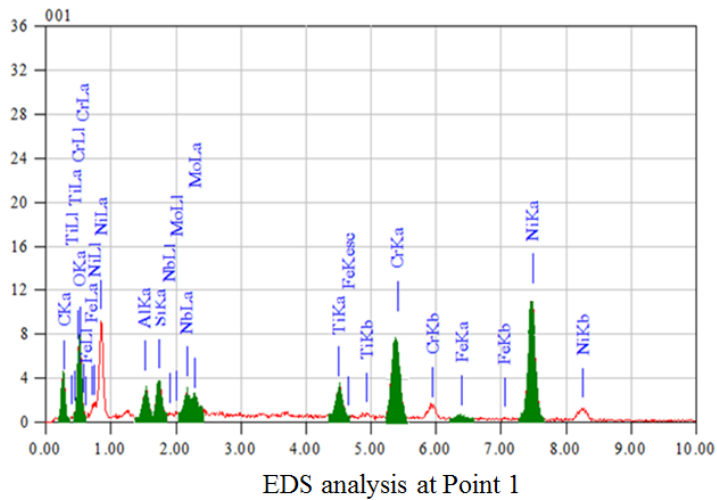
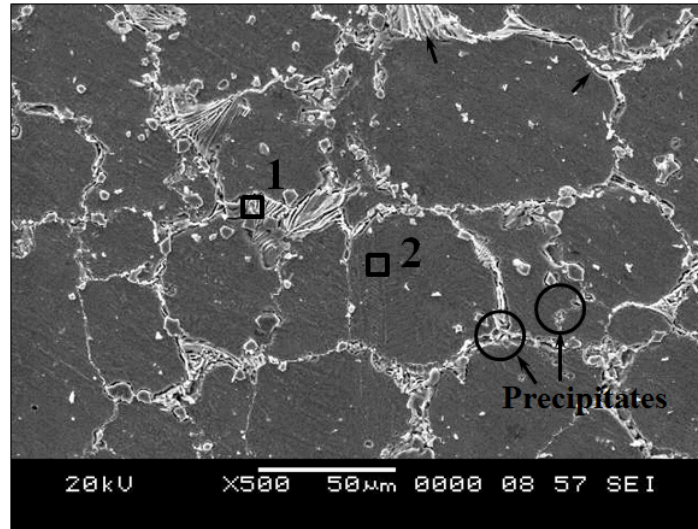


Figure 4.12 SEM microstructure of specimen No.9 and EDS analysis at grain boundary (Point 1) and grain interior (Point 2)

Chemical composition at Point 1	
Element	Wt.%
Si	1.31
Ti	0.48
Fe	7.8
Nb	12.66
Mo	4.50
Cr	16.31
Ni	47.48



Chemical composition at Point 2	
Element	Wt.%
Si	0.46
Ti	0.09
Fe	3.86
Nb	2.16
Mo	3.08
Cr	14.7
Ni	61.24

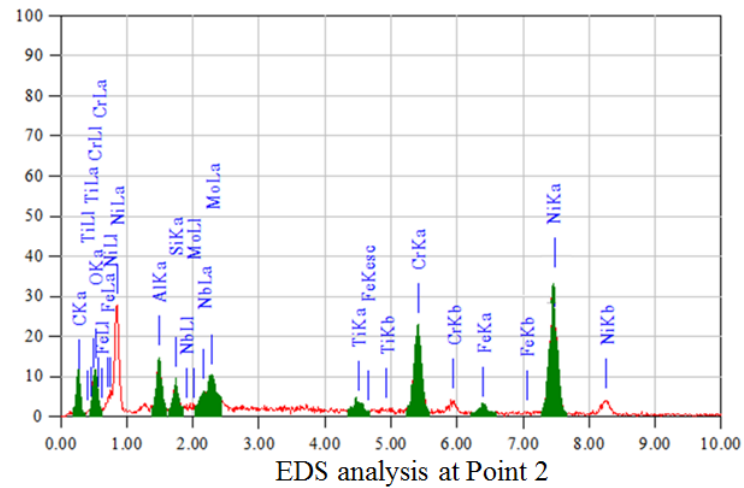
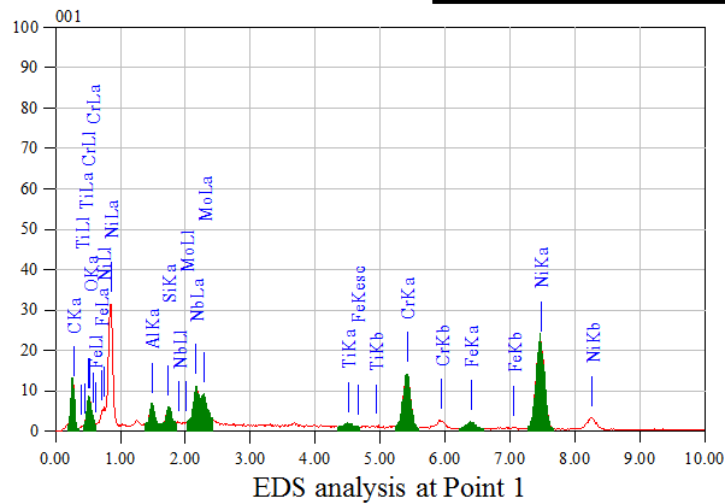


Figure 4.13 SEM microstructure of specimen No.11 and EDS analysis at grain boundary (Point 1) and at grain interior (Point 2)

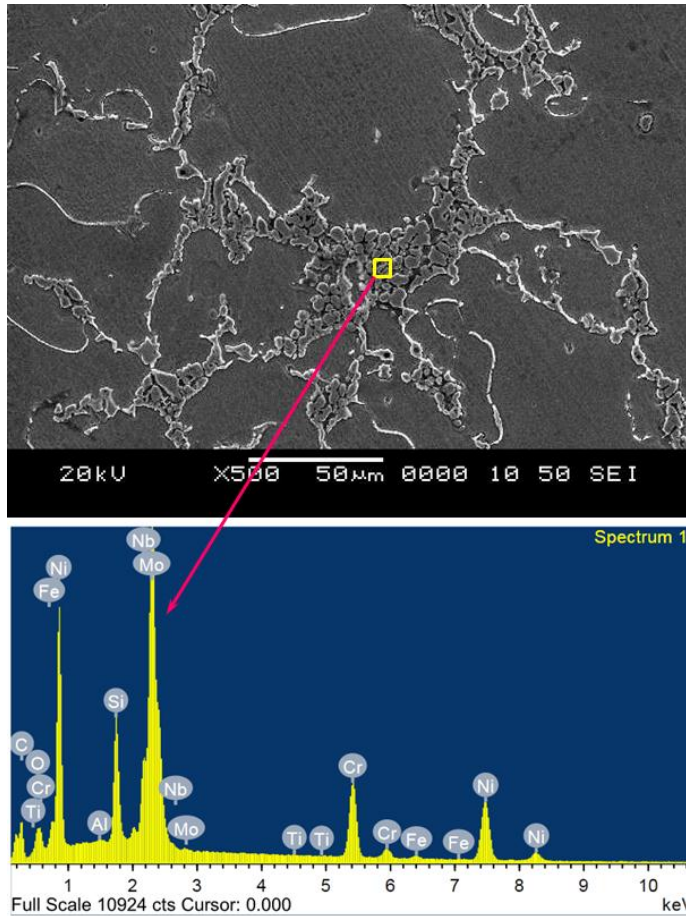


Figure 4.14 SEM microstructure showing the segregation of alloying elements

Inconel-625 alloy with relatively higher carbon percentage ($C > 0.075$ wt%) and lower Nb content (< 2 wt%) terminates the solidification with $L \rightarrow (\gamma + \text{NbC})$ phase and does not exhibit $L \rightarrow (\gamma + \text{Laves})$ reaction. On the other hand, higher Si content results in $L \rightarrow (\gamma + \text{Laves})$ reaction (DuPont, 1998).

During the processing of materials through MHH, volumetric heating of the joint interface takes place followed by slow cooling. Microwave heating occurs due to frictional heat generated through dipolar rotation and with the removal of microwave power the rotation of dipoles stops instantaneously. However, due to slightly lower

cooling rate associated with specimens processed at 900W, a higher amount of segregation is observed in the fusion zone and its vicinity.

The segregation of niobium results in the formation of Laves phases which further depends on weld cooling rate and the amount of heat input. The slow cooling rate mostly results in formation of comparatively large dendritic arm spacing. These dendritic arm spacings are the favorable locations for precipitation of niobium and molybdenum during solidification. Though the flux employed in the present work reduces the oxidation of faying surfaces at elevated temperatures, it considerably decreases the cooling rate of welded joint, which in turn leads to the segregation of alloying elements. The presence of Laves phases is detrimental to the strength of the welded joint, since this consumes the alloying elements significantly that are required for strengthening of the matrix phase. At elevated temperature, the dilution of niobium and molybdenum takes place from the base metal to the fusion zone (these elements are absent in the starting interface powder) that further leads to the formation of Laves phases. To form Laves phase at least 10-12% Nb is required and the amount of Laves phases, its composition and scattering in the weld microstructure are intensely influenced by the solidification condition (Janaki Ram et al., 2004). In the present study, as revealed by EDS analysis the composition of Si is reasonably high which promotes the formation of Laves phase in the interdendritic regions.

The amounts of Nb, Ti, Mo and Si content listed in Tables 4.5 was noticed to be substantially lower in secondary phase of joints developed at 600W as with those produced at 900W power. This is attributed to the lower heat input associated with 600W power followed by rapid cooling which results in lower amount of Nb segregation and less time available for redistribution of solute. This would consequently result in lower amount of Laves volume fraction in the welded joints developed at 600W. Similar observations have been made by Silva et al. (2013), Janaki Ram et al. (2004) and Arulmurugan and Manikandan (2017) during GTAW of various Inconel alloy grades.

Table 4.5 Elemental composition of microwave welded specimens in different experiments

Experiment number	Power used for processing (W)	Element wt.%						
		Ni	Cr	Fe	Nb	Ti	Mo	Si
1	600	51.23	18.36	8.65	13.53	0.79	4.27	0.93
3	600	46.35	19.52	9.34	14.88	0.86	5.28	0.98
9	600	49.38	18.59	7.86	13.64	0.98	2.86	0.87
11	600	48.57	18.24	8.54	13.92	0.86	4.83	0.96
1	900	48.54	17.06	8.58	18.54	1.16	7.53	1.1
3	900	43.46	16.57	10.16	18.75	1.18	7.89	1.13
9	900	47.71	16.73	9.49	16.87	1.09	6.53	1.07
11	900	47.41	16.98	9.82	17.13	1.11	6.48	0.99

Indicated values correspond the average of 3 measurements

4.6.3 Grain size and porosity measurement

Grain size has a significant influence on the mechanical properties of the welded joints. Finer grain size promotes the strength and toughness of the joints while, coarser grain improves the high temperature creep resistance. The grain size measurement of the specimens 1, 3, 9 and 11 was carried out using image analysis. Figure 4.15 and 4.16 show the microstructures of the fusion area of these specimens with varying grain sizes. It can be inferred that the specimens produced with 600W power yielded fine grained microstructures compared to their counterparts produced at 900W which is attributed to the lower heat input followed by rapid cooling phenomenon associated with former case. In addition it is also seen that specimen No. 9 consists of fine grained structure in either case of processing condition. This could be due to the fact that, grain growth depends on atomic diffusion across the grain boundaries. Diffusion rate increases with the increasing temperature which in turn increases the migration of grain boundaries and this promotes the grain growth. In the present study, the heating rate for specimen No.9 is relatively less since it is processed using coal which results in lower diffusion rate leading to

reduced grain growth. This fact is further explained by Arrhenius-type equation as shown below.

$$D=D_0 \times e^{(-Q/RT)} \quad \text{—————Eq. 4.1}$$

where, D is diffusivity; D_0 is the proportionality constant; Q is the activation energy (J/mol); R is the molar gas constant (8.314J/mol/K); and T is the absolute temperature (K) (Min et al., 2016; Lee and Lee, 2008).

Thus from Eq. 4.1 it is seen that the diffusion rate increases exponentially with increasing temperature and thus promotes grain growth. Table 4.6 presents the average grain size for the microstructures shown in Figures 4.15 and 4.16 measured by linear intercept method. It is clear from Table 4.6 that, specimen No. 9 and 1 comprise of smaller size grains compared to other specimens. Owing to this fact, specimen No. 9 and 1 exhibit relatively higher hardness values as revealed by microhardness study. Further, uniaxial tensile test and 3-point bend test results also imply that the specimen No. 9 and 1 experience a higher amount of plastic deformation and exhibits higher strength.

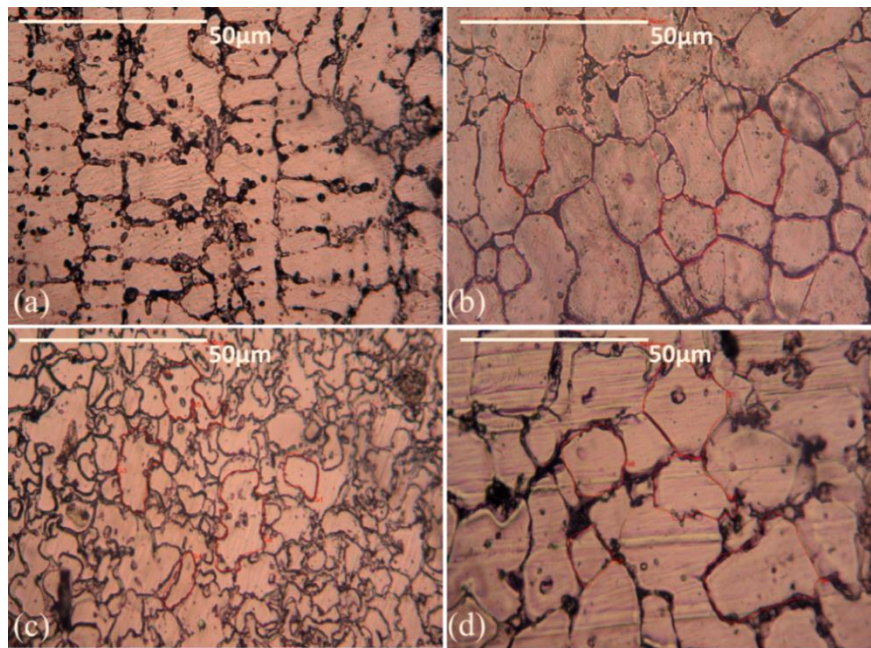


Figure 4.15 Fusion zone microstructures of specimen processed at 600W in expt. No. (a) 1 (b) 3 (c) 9 and (d) 11

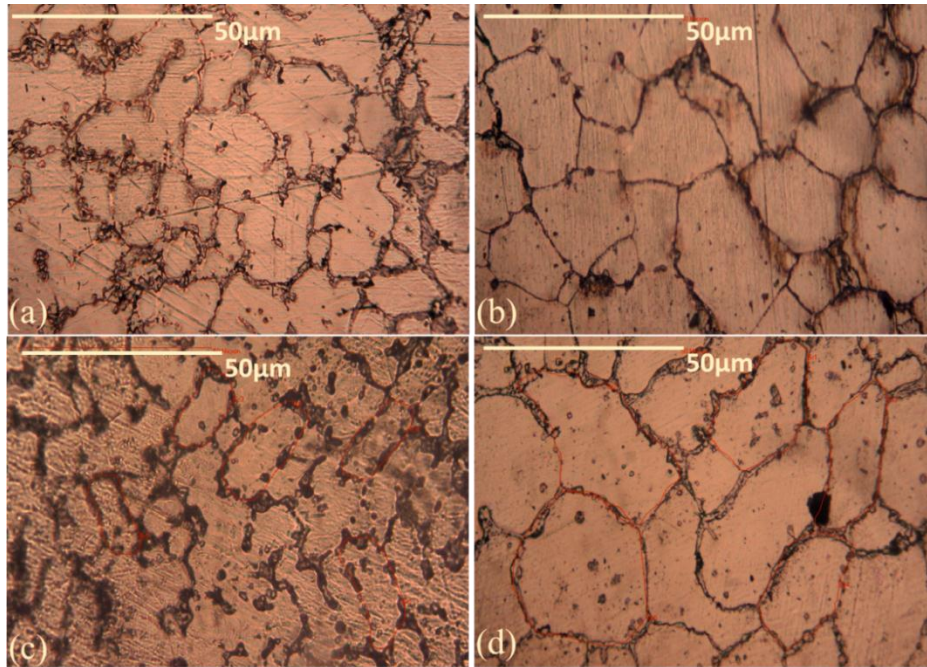


Figure 4.16 Fusion zone microstructures of specimen processed at 900W in expt. No. (a) 1 (b) 3 (c) 9 and (d) 11

Table 4.6 Grain size measurement and porosity

Specimen No.	Power employed (W)	Grain size (μm)	Porosity (%)
1	600	11	1.89
3		12	2.04
9		5	1.58
11		13	2.27
1	900	12	2.69
3		17	3.08
9		10	2.98
11		16	3.03

Porosity of the joint microstructures was measured at three locations using Biovis Material Plus image analyzer software and the average of measured values is presented in Table 4.6. Porosity, to a great extent depends on heating rate employed for processing (Mondal et al. 2008); as the heating rate increases it is accompanied by increase in porosity. From Table 4.6 it is observed that specimens processed at 600W exhibit lower porosity compared to their counterparts.

4.6.4 Observations on microhardness

Microhardness of the microwave induced joints depends on the combined effect of solidification rate and grain size obtained in the final structure. Microhardness indentations in the present study were obtained across the joint by maintaining a distance of 50 μ m between successive indentations. Microhardness of the welded joints was measured in the fusion zone, interface and adjacent base metal regions. At each location, five indentations were obtained and the mean value was considered to plot the variation profile. Figure 4.17 shows a typical SEM micrograph of microhardness indentations obtained in different regions of the microwave induced joint. The variations in the microhardness profile of specimens 1, 3, 9 and 11 are plotted in Figure 4.18 and 4.19.

It is seen that hardness increases from center of the joint towards the interface and is observed to be maximum as it approaches interface region. Further it is witnessed from Figure 4.17(c) that the dimensions and geometry of the indentations are different in the interface (smaller indentation size) and weld zone. This is due to the fact that when the indenter makes contact with the hard carbide phase, there is an obstruction for the plastic flow of material (Gupta and Sharma, 2011; Bansal et al., 2014). This increased hardness in the interface region is attributed to the formation of chromium and molybdenum carbides (Mo_2C , Cr_{23}C_6 and CrC) as identified by XRD analysis in Figures 4.4 to 4.7. Due to the dilution of matrix during microwave heating, the elements from the matrix diffuse into the interface region and react with carbon to form carbides along the joint interface. Furthermore, formation of intermetallic phases also contributes towards increasing the hardness.

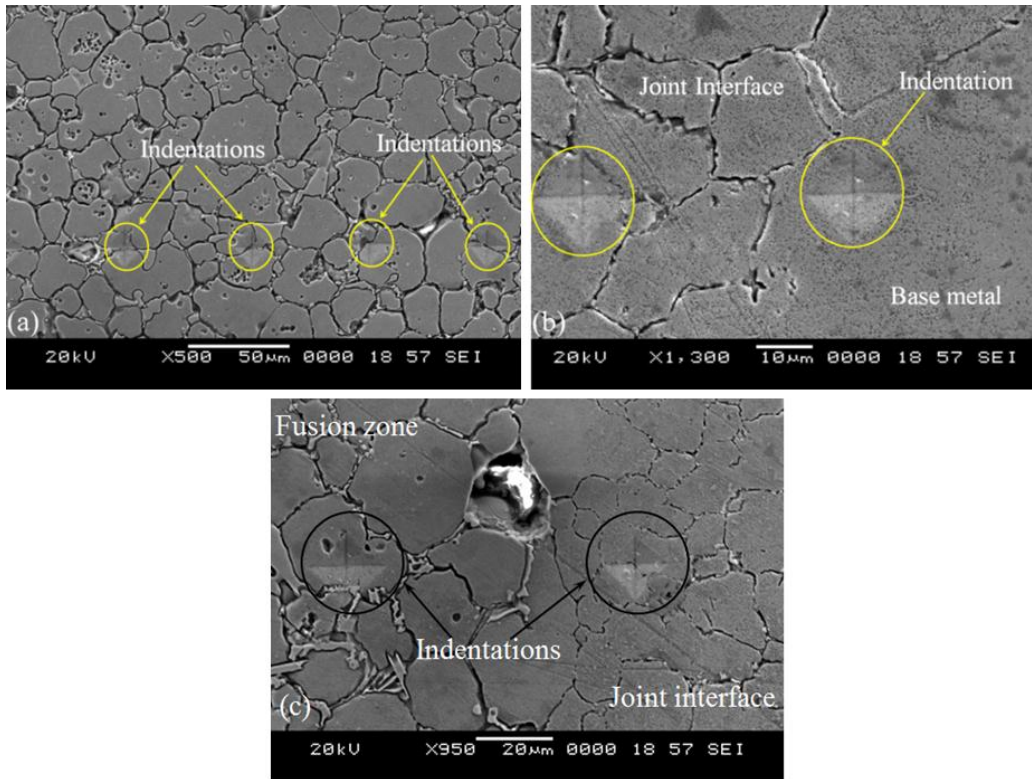


Figure 4.17 Typical SEM micrographs showing microhardness indentations in (a) weld zone (b) base metal and joint interface (c) joint interface and weld zone

As witnessed from Figure 4.18, specimen No. 1 developed at 600W exhibited higher hardness compared to other specimens and a higher standard deviation is also seen in the interface region. Figure 4.19 depicts the variation in the microhardness profile obtained for specimens produced at 900W. Relatively lower hardness values are exhibited by these specimens with respect to those produced at 600W. Specimen No. 1 reveals higher hardness, compared to other specimens. It is also noticed that the hardness values in specimens developed at 900W are deviating to a large extent which is attributed to the segregation of Nb, Ti and Mo in the interdendritic region at elevated temperature to form Laves phase.

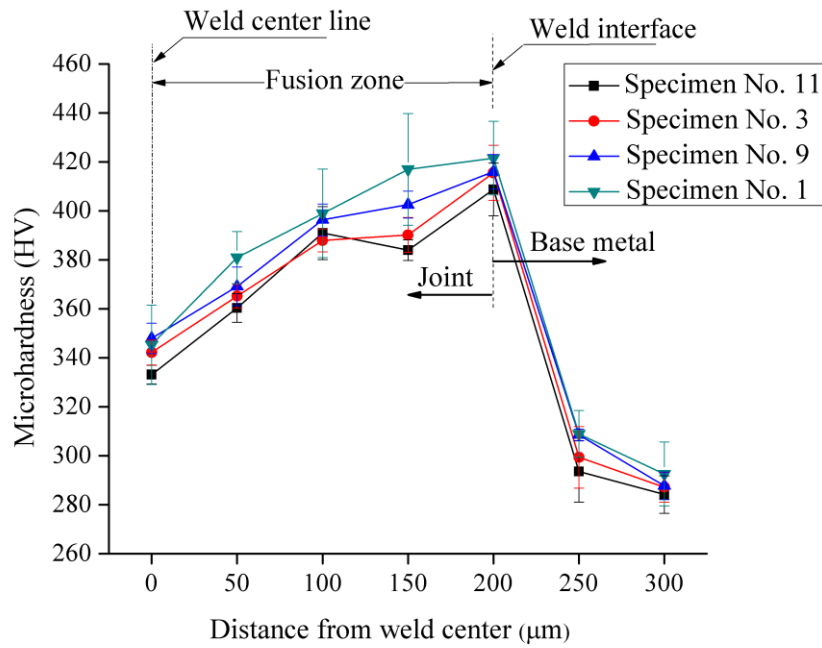


Figure 4.18 Microhardness profile obtained across the joints for the specimens developed at 600W power

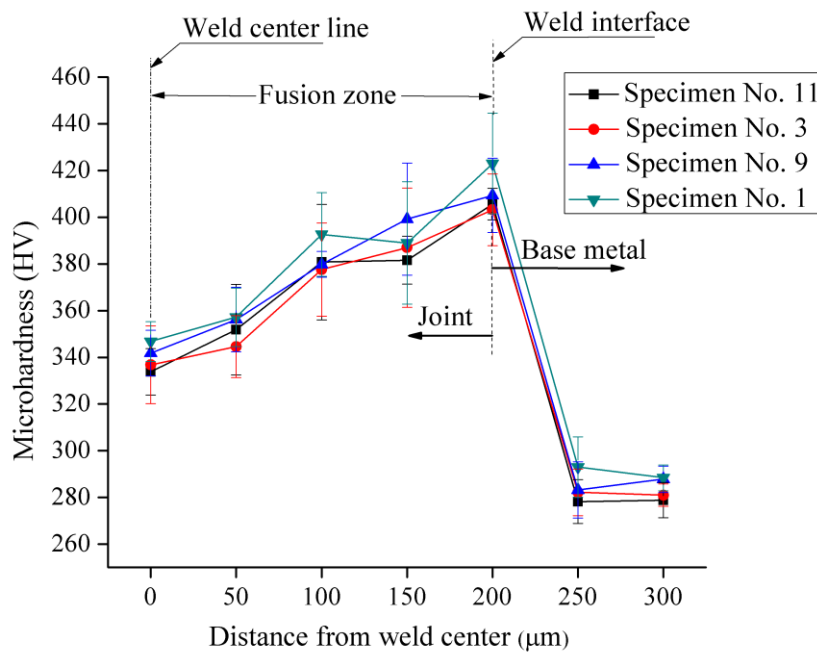


Figure 4.19 Microhardness profile obtained across the joints for the specimens developed at 900W power

Table 4.7 Vickers microhardness values in different regions

Specimen No.	Power used (W)	Average hardness (HV)		
		Fusion zone	WI	Base metal
1	600	386±17	421±15	301±11
3		371±5.5	415±11	293±9
9		379±6.5	416±7	298±4
11		367±6.0	408±11	289±10
1	900	371±16	423±21	291±9
3		361±19	403±15	282±7
9		369±13	409±16	285±9
11		362±11	405±7	279±9

WI - Weld interface

A similar trend in variation of hardness profile was reported by Srinath et al. (2011) and Bansal et al. (2016) in different works. However, it is interesting to note that joint hardness values obtained with microwave-induced welding are similar to the hardness values as that obtained with TIG welded joints (Ramkumar et al., 2017). Table 4.7 highlights the average hardness values of the specimens recorded in different regions. Mathematically, the relationship between hardness and grain size is expressed as,

$$HV = H_0 + \frac{k_H}{\sqrt{d}} \quad \text{————— Eq. 4.2}$$

where, HV is Vickers hardness, d is the grain size and H_0 and k_H are constants. Thus it is concluded that a decrease in grain size, increases the hardness of the fusion zone (Peng et al. 2011).

4.6.5 Observations from tensile test

In order to evaluate the tensile properties of the microwave processed joints the specimens were further subjected to uniaxial tensile test in a UTM facility. Figure 4.20

shows the results of uniaxial tensile test conducted on specimens developed using MHH. All the specimens were machined according to ASTM-E8 standards with an initial gauge length of 25 mm and were loaded with a uniform strain rate 0.008 mm s^{-1} .

Table 4.8 summarizes the characteristic behavior revealed by the specimens during the uniaxial tensile test. The transition between elastic and plastic regions for the stress-strain curves in Figure 4.20 was determined by 0.2% strain offset method. It is noticed from Table 4.1 that specimens processed at 600W exhibit higher yield points when compared to those developed at 900W. This is attributed to the lower heat input associated with 600W which resulted in rapid cooling of the welded joint thereby reducing the time for segregation (Wilson et al., 1991).

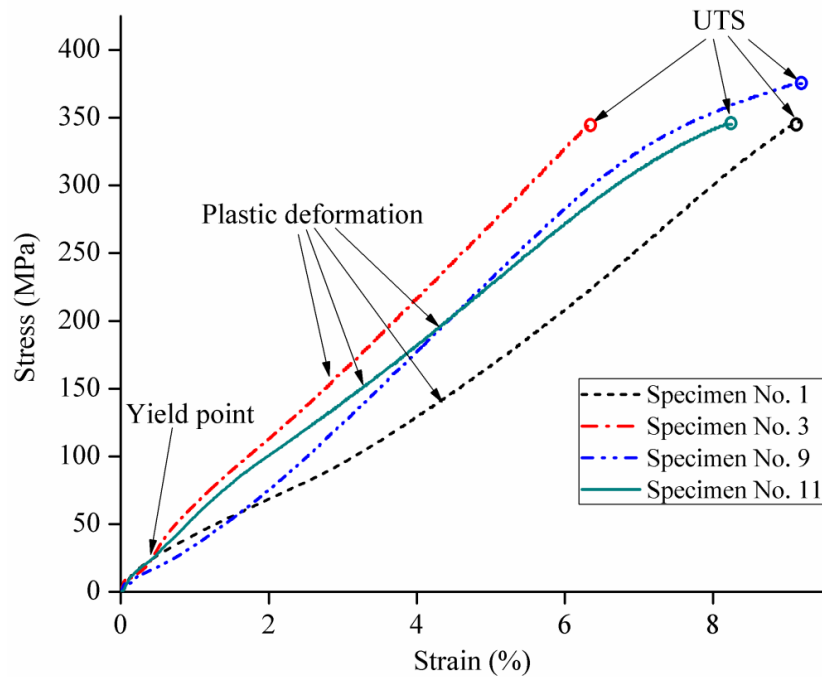


Figure 4.20 Stress-strain curves from uniaxial tensile test

Table 4.8 Tensile properties of MHH processed welded joints

Specimen No.	UTS (MPa)	Percentage elongation (%)
1	347	9.1
3	345	10.8
9	376	9.2
11	345	8.2

Specimen No. 3 exhibited more ductile behavior compared to other specimens (% elongation 10.8). Further this fact is also verified from the microhardness profile in which it is clearly seen that specimen No. 3 exhibits lower hardness values. Specimen No. 9 which was developed using graphite and flux separator exhibits maximum UTS value (376MPa). Graphite being a strong microwave absorbing material used for processing of specimen No.9 sustains elevated temperatures and can provide higher heating rates. Additionally, the use of flux bed further contributes in uniform heating of the joint zone and does not undergo any chemical change without any change in its dielectric properties (Bansal et al., 2015). It is also observed that, specimen No. 9 processed experiences a larger strain hardening effect.

During tensile loading of the microwave-induced joints, the plastic deformation of matrix phase takes place easily however, the hard secondary phase (Laves and carbides) do not get deformed plastically along with the matrix. Moreover, there is no continuity of lattice planes across the matrix and Laves phase interface. As a result, a pile up of moving dislocations takes place along their slip planes at the carbide/matrix interfaces during plastic deformation. As the plastic deformation in the weld zone continues, more and more dislocations are pushed towards the grain boundaries so that piling up of dislocations takes place. During this process the external load is dominated by the resisting force exerted by dislocations which signifies the toughness of the joint. Thus, a shear stress is built up at the head of this pile of dislocations which squeezes them together. When this shear stress at the head of dislocation pile up reaches a critical value, the dislocations are further pushed closer to an extent that they combine with each other

to form microcracks at the brittle grain boundary. The crack growth by plastic deformation continues as long as the dislocation sources force dislocations to pile up (Dieter, 1988).

It has been reported that (Bansal et al., 2015) the shearing stresses are involved only in forcing the dislocations together. Tensile stresses do not influence the microcrack initiation process. However, tensile stresses open microcracks and enhance the propagation of microcracks through hard and brittle phases. With further increase in the load, crack propagation takes place along Laves/matrix due to tensile stress and failure of the specimen takes place.

4.6.6 Observations from 3-point bend test

The 3-point bend test specimens were machined according to ASTM E190-92 guidelines with dimensions $100 \times 20 \times 4 \text{ mm}^3$ and at a strain rate of 0.01 mm s^{-1} to assess the flexural strength of the microwave welded joints. The characteristic behavior of the specimen Nos. 1, 3, 9 and 11 during 3-point bend test is illustrated through stress-strain curves in Figure 4.21(a). It is clearly evident from Table 4.1 that most of the specimens processed at 600W power exhibited higher flexural strength which is attributed to the lower heat input followed by rapid cooling. On the other hand, the specimens produced at 900W were subjected to higher heating rates followed by slow cooling thereby allowing more time for segregation at the grain boundaries.

As seen from Figure 4.21, all the specimens exhibited similar behavior during the deformation since the curves are almost parallel; however specimen No. 9 shows higher flexural strength. The deformation of the specimen during 3-point bend test occurs as depicted in Figure 4.21(b) in three stages; (i) displacement up to the elastic limit (Stage-I), (ii) displacement during plastic deformation (Stage-II) and (iii) displacement till the complete fracture of the specimen (Stage-III). In stage-I, the welded joint exhibits a uniform load-displacement behavior since, the ductile phase in the joint deforms elastically under the action of applied load and layers below the neutral axis get elongated

under tensile stresses. However at the same time, layers above the neutral axis also deform elastically and are subjected to compressive stresses.

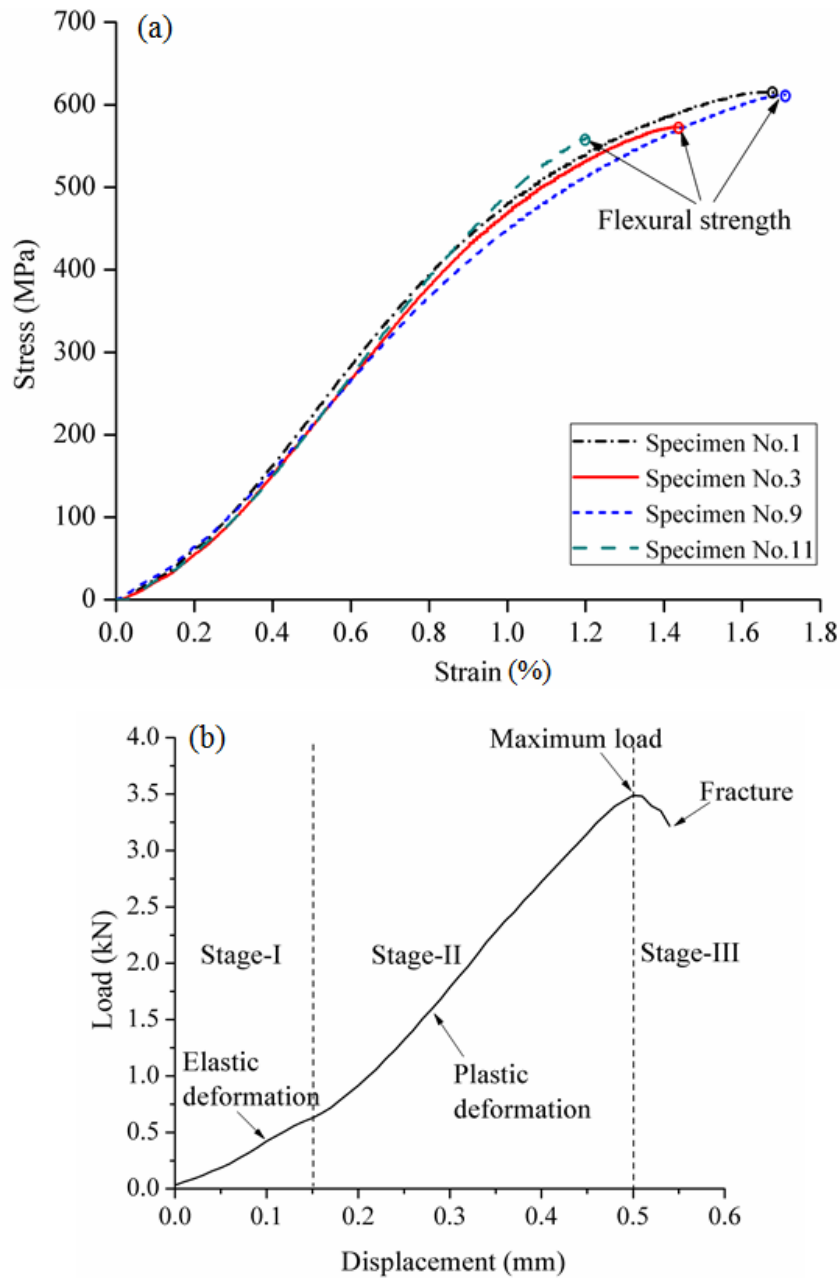


Figure 4.21 (a) Stress-strain curves from 3-point bend test (b) Typical load-displacement characteristics during 3-point bend test

A deviation in the stress-strain curve (Stage-II) is observed when loading is increased beyond the elastic limit which is the initiation of plastic state. The corresponding deformation during this stage becomes plastic and increases with increasing load up to the maximum load experienced by the welded joint. As the load increases the fibers below the neutral axis deform under the tensile stresses and lead to the formation of microcracks (Stage-III). Development of microcracks is also attributed to the presence of brittle phase at grain boundaries which serves as the source for initiation of microcracks (Dieter; 1988). Further loading causes opening of the microcracks under tensile stresses and a sudden drop in the load-elongation characteristics is observed. During this stage, a sharp decrease in the load accompanied by a small increase in the magnitude of displacement can be seen. This is attributed to the growth of microcracks and their rapid propagation through the weld cross section which results in a complete fracture of the specimen (Bansal et al., 2016).

4.6.7 Fractography

Fractured specimens after the tensile test and 3-point bend test were further subjected to fractography study using SEM. Figure 4.22 and 4.23 show the photographs of fractured specimens obtained after uniaxial tensile test of specimens 1, 3, 9 and 11. It can be seen that all the welded specimens fractured in the joint zone. The hardness measurements were found to be in good agreement with the tensile test data. Because of the higher hardness values observed in the interface region due to carbide precipitation the specimens failed in the joint zone. Similar observations have been reported by Bansal et al. (2016) during dissimilar welding of SS-316L and Inconel-718 through MHH.

Tensile stress-strain curves depicted in Figure 4.20 indicated that, specimen No. 9 experienced a relatively larger amount of plastic deformation prior to failure. This is further confirmed through the observation of the failure edge (material torn out from the parent metal in irregular manner) of the specimen in Figure 4.22. Figures 4.24 and 4.25 depict typical SEM micrographs of the tensile fractured surfaces. All the specimens

exhibited a mixed mode type of fracture since the structures in Figures 4.24 and 4.25 show the existence of both dimpled fibrous pattern and shear failure or cleavage pattern.



Figure 4.22 Fractured tensile specimens processed at 600W



Figure 4.23 Fractured tensile specimens processed at 900W

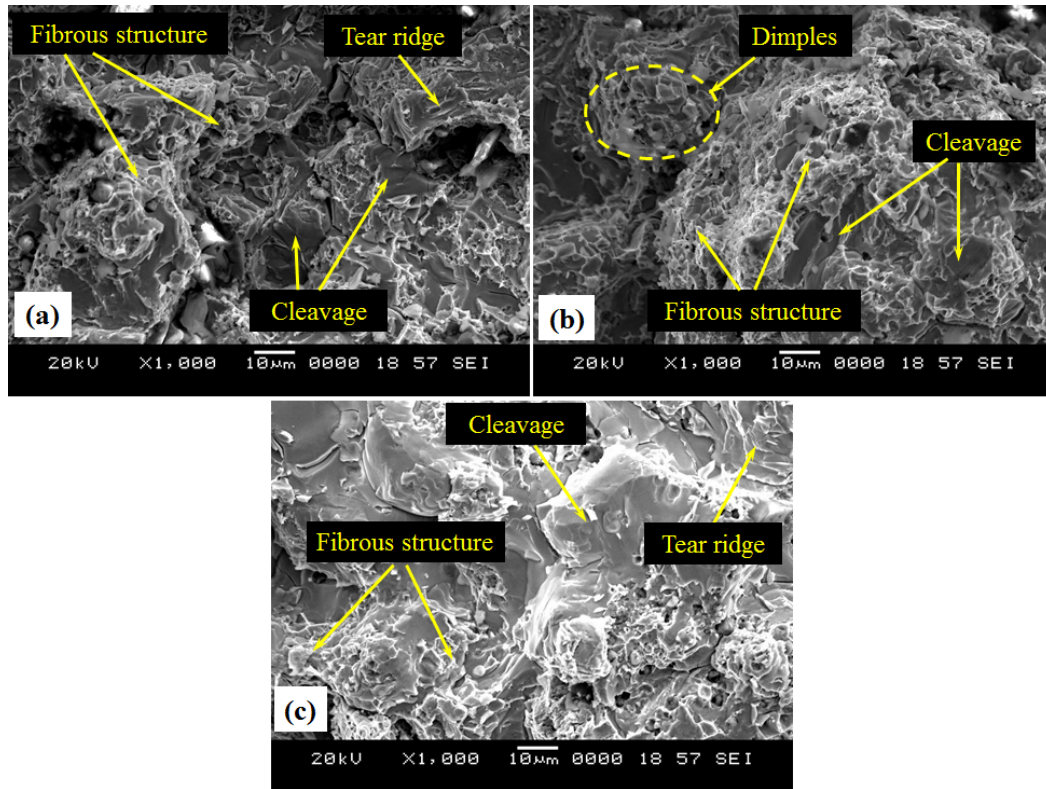


Figure 4.24 SEM micrographs showing tensile fractured surfaces of the specimens developed with 600W power

It may be noted that the strength properties of the specimens produced at 600W power are better than those produced at 900W. Ductile fracture is characterized by fibrous pattern with dimples as it is clearly seen at many locations in Figures 4.24 and 4.25. Typically, failure commences with the formation of minute voids around small inclusions or preexisting discontinuities which then grow and merge leading to the formation of cracks that propagate with the application of load, resulting in fracture of the specimen. However in Figures 4.24 and 4.25, tear ridges as a result of shear failure are also seen which signify a cleavage fracture. The occurrence of cleavage fracture is attributed to the initiation of a crack in the Laves-matrix interface. The presence of carbides and intermetallic phases at the grain boundaries as revealed by XRD (Figure 4.4 to 4.7) and EDS (Figure 4.10 to 4.13) studies also serves as the sources for crack initiation. When a

crack moves through a crystal along number of parallel planes, it results in a series of plateaus and connecting ledges, leading to the formation of river markings (Dieter, 1988; Pineau et al., 2016). Therefore, it is evident from the above discussion that mixed mode type of a fracture takes place. It is also observed that the fracture in the welds took place preferentially along the interdendritic regions in all the specimens and the specimens produced at 600W exhibit more ductile features compared to their counterparts.

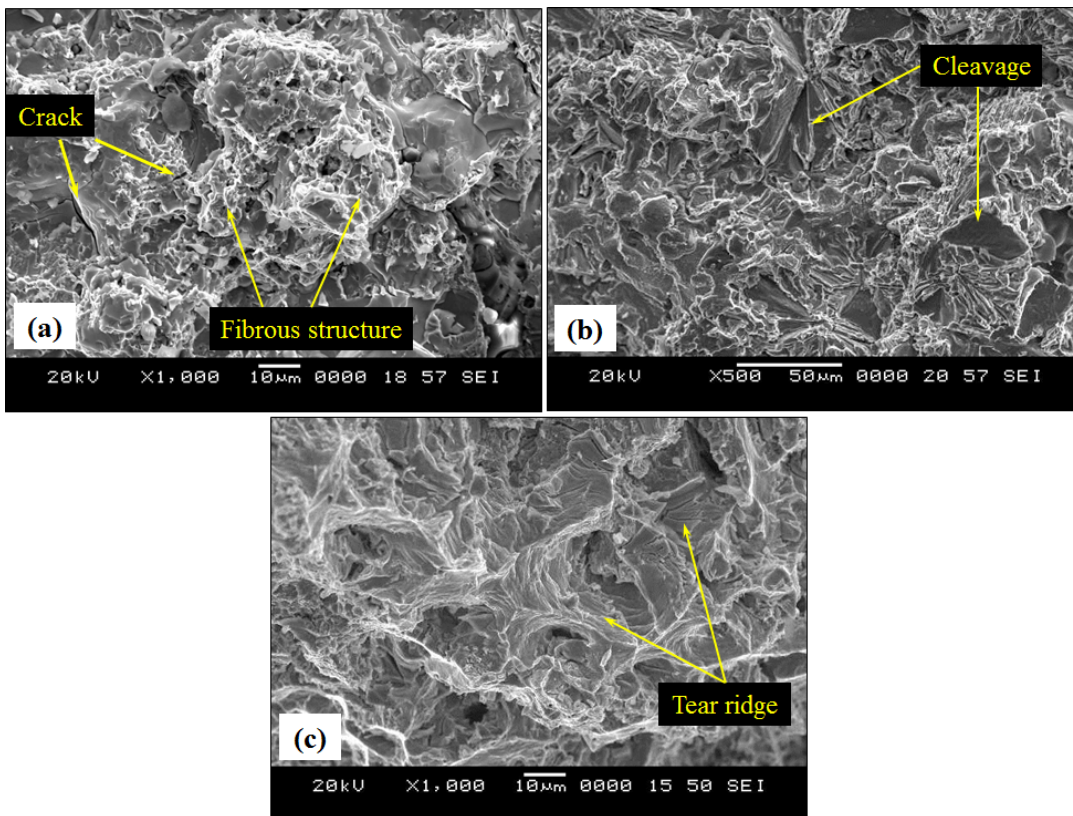


Figure 4.25 SEM micrographs showing tensile fractured surfaces of the specimens developed with 900W power

Figure 4.26 and 4.27 show the photographs of fractured specimens after 3-point bend test. Similar to tensile specimens, all the specimens fractured in the joint zone. Figures 4.28 and 4.29 depict typical SEM micrographs of the fractured surfaces.



Figure 4.26 Fractured 3-point bend test specimens processed at 600W

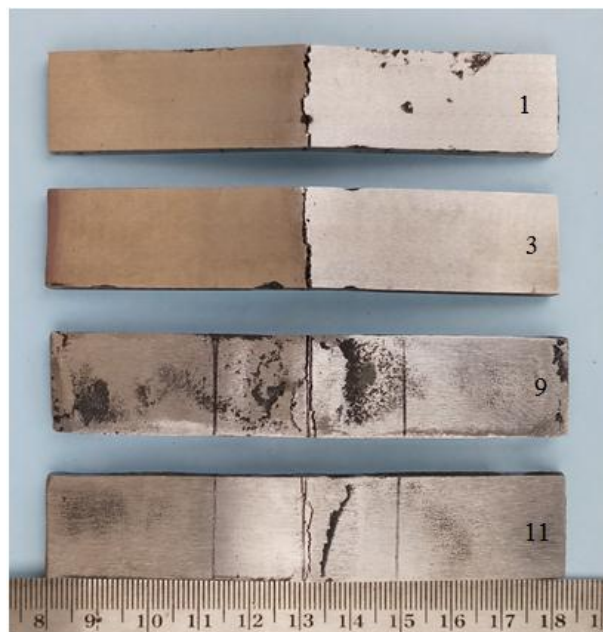


Figure 4.27 Fractured 3-point bend test specimens processed at 900W

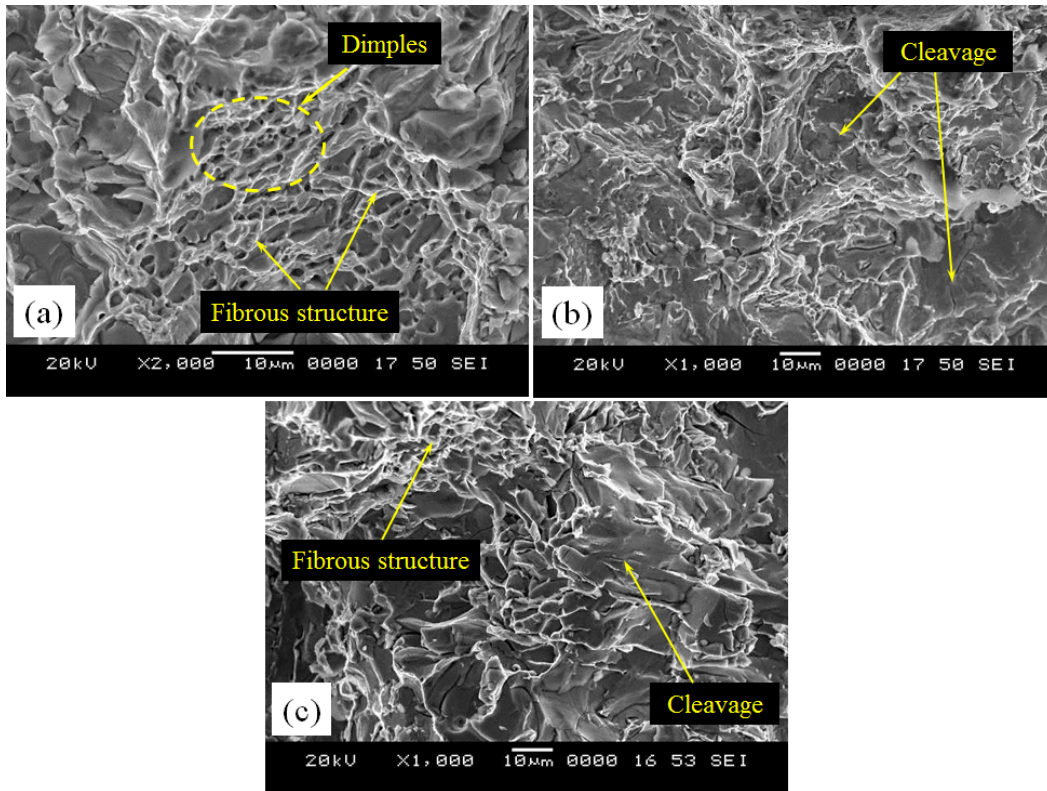


Figure 4.28 SEM micrographs showing fractured surfaces of the specimens developed with 600W power

Specimens processed with 600W power exhibited fibrous structures consisting of dimples along with cleavage facets whereas, those processed with 900W power were observed to consist of multi directional cracks which might have originated from micro voids. Initially, the load is taken up by the nickel-based ductile phase and later with increased loading the welded joint undergoes a severe plastic deformation leading to the development of microcracks. Brittle metallic phases at the grain boundaries act as crack initiation sites. In addition, tensile stress induced in the welded joint also promotes growth and propagation of these cracks. As a result, the cracks grow in multiple directions and propagate through the cross section of the weld. Furthermore, specimens during 3-point bend test experienced a significant amount of deformation prior to fracture and thus lead to a mixed mode fracture. It is also observed from EDS spectra in Figure 4.10 to 4.13 that the hard particles of carbides are mostly concentrated at the grain

boundaries. These hard phases do not allow the material to flow plastically during loading and thus shearing action at the joint zone, leading to sudden failure of the material at the joint area (Dieter, 1988; Pineau et al., 2016). The dominance of brittle failure in joint zone could be in the area where total melting of the powder particles in sandwich layer during microwave irradiation and subsequent re-solidification occurs.

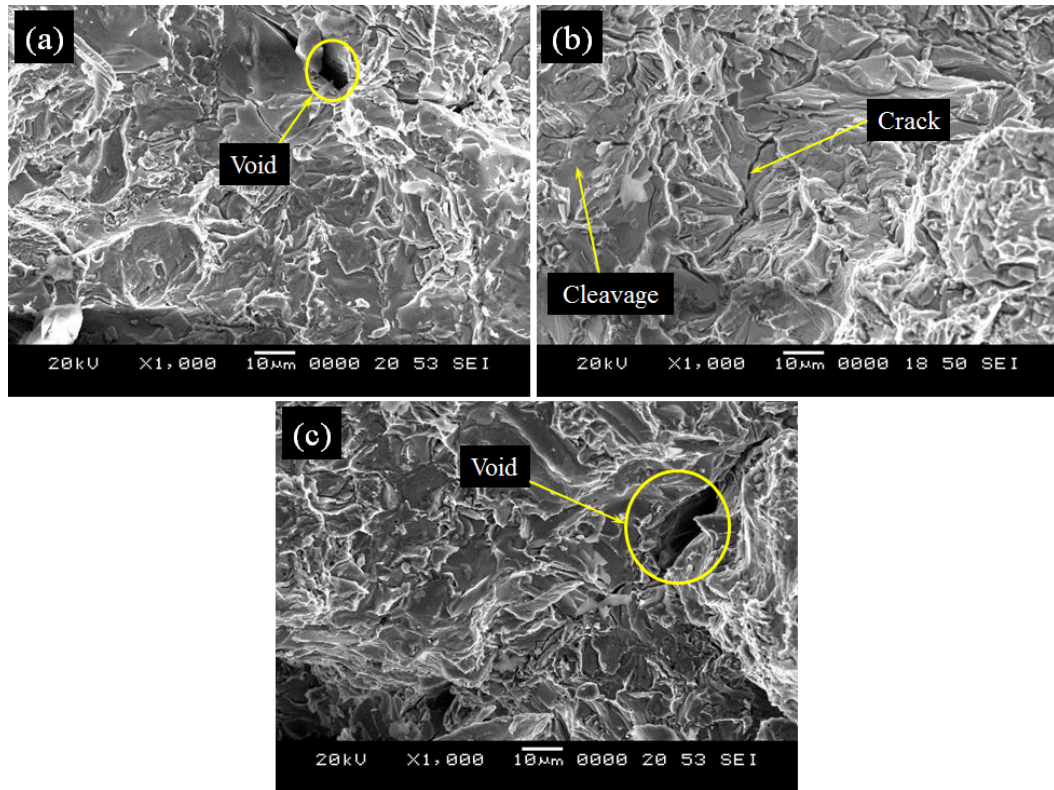


Figure 4.29 SEM micrographs showing fractured surfaces of the specimens developed with 900W power

4.7 SUMMARY

The effect of process parameters on ultimate tensile strength and flexural strength of Inconel-625 welded joints developed through MHH technique have been investigated. The experiments were conducted as per L_{16} orthogonal array to understand the effects of process parameters such as susceptor material, separator material and interface filler powder size. Further, the effect of input power on quality characteristics of the welded

joints has been studied. Based on the experimental results and discussion, the following conclusions were drawn.

1. The most significant parameter was found to be the interface filler powder. Use of finer interface filler powder with an average particle size $50\mu\text{m}$ improves the ultimate tensile strength and flexural strength of the joint.
2. Graphite as a separator material exhibited better heating characteristics and improved mechanical properties of the welded joints. Both ultimate tensile strength and flexural strength reduced when glasswool was used as separator. However, a marginal increase in ultimate tensile strength and flexural strength was observed when glasswool was used in combination with flux for all the specimens regardless of power used for processing. Both SiC and coal are highly lossy materials that rapidly absorb microwaves and convert incident electromagnetic energy into heat. However, it was noticed that, SiC exhibited better heating characteristics compared to coal when processing at 900W.
3. XRD study revealed the formation of chromium carbide Cr_{23}C_6 and CrC in the joint interface which contribute to the increased hardness in this region. In addition to this, presence of oxides such as nickel oxide (NiO) and titanium molybdenum oxide (TiMoO_5) and intermetallic phases like nickel-chromate $\text{Ni}(\text{Cr}_2\text{O}_4)$, NiCrFe, and CrFe_4 is also identified. EDS analysis showed that the amount of Nb, Ti, Mo and Si content was substantially lower in secondary phase of joints developed at 600W which would consequently result in lower amount of Laves volume fraction.
4. The specimens produced with 600W power yielded a fine grained structure (average grain size $5\mu\text{m}$) compared to their counterparts produced at 900W (average grain size $17\mu\text{m}$) which is attributed to the lower heat input followed by rapid cooling phenomenon associated with the former case. Furthermore the specimens processed at 600W exhibited lower porosity (1.58%) which is attributed to the lower heating rate associated.

5. Specimens developed at 600W exhibited higher microhardness values attributed to the fine grain structure. Further, it was also noticed that even though, the hardness values with the specimens developed at 900W are low, a large deviation was observed with the measured hardness values due to the presence of hard phase in the matrix.
6. Fractography studies revealed that the specimens failed due to mixed mode of fracture. However, the specimens processed with 600W power experienced a higher amount of plastic deformation prior to failure.

CHAPTER 5

MULTI OBJECTIVE OPTIMIZATION USING GREY RELATIONAL ANALYSIS

5.1 INTRODUCTION

Most of the engineering systems possess multiple quality characteristics to be determined however; a single combination of process parameters may be optimum for one response characteristic but the same combination of parameters may not yield best results for the other response characteristic. Thus, it becomes necessary to obtain an optimum combination of the control factors to produce a system with optimal or near optimal quality characteristics. In Chapter 4 the Taguchi method was used to determine the combination of process parameters that produce best quality characteristic however; it was noticed that ultimate tensile strength and flexural strength were not correlated mutually and each of the quality characteristics depended differently with control parameters. Therefore, in this Chapter, the Taguchi method of optimization is extended for the complete evaluation of multiple quality characteristics in joining of Inconel-625 alloy using MHH technique through GRA.

5.2 GREY RELATIONAL ANALYSIS

In the first step of GRA pre-processing of data is performed so as to normalize the raw data. Normalization of S/N ratio (larger is better) for multiple quality characteristics is computed using Eq. 5.1 and tabulated in Table 5.1.

$$Z_{ij} = \frac{y_{ij} - \min(y_{ij}, i = 1, 2, \dots, n)}{\max(y_{ij}, i = 1, 2, \dots, n) - \min(y_{ij}, i = 1, 2, \dots, n)} \quad \text{Eq. 5.1}$$

where,

y_{ij} is S/N ratio for the i^{th} performance characteristic considered in the j^{th} experiment.

Z_{ij} is the normalized S/N ratio of i^{th} performance characteristic in the j^{th} experiment.

The grey relational coefficient is calculated to express the relationship between the ideal and actual normalized results. Prior to this, the deviation sequence for reference sequence and comparability sequence are computed using Eq. 5.2 (Dey et al., 2017).

$$\xi_i(k) = \frac{\Delta_{\min} + \zeta\Delta_{\max}}{\Delta_{oi}(k) + \zeta\Delta_{\max}} \quad \text{Eq. 5.2}$$

where, $\Delta_{oi}(k)$ (Eq. 5.3) is the deviation sequence of reference and comparability

Table 5.1 Pre-processing of data by normalizing S/N ratio

Expt. No.	S/N ratio (raw data)				S/N ratio normalized			
	UTS (600W)	UTS (900W)	FS (600W)	FS (900W)	UTS (600W)	UTS (900W)	FS (600W)	FS (900W)
1	50.807	49.799	55.778	54.995	0.828	0.828	0.851	1.000
2	50.049	47.854	54.253	52.750	0.640	0.478	0.518	0.566
3	49.883	50.756	55.163	54.599	0.599	1.001	0.717	0.924
4	47.458	48.199	52.649	53.552	0.000	0.540	0.167	0.721
5	50.264	47.384	56.272	52.649	0.694	0.393	0.960	0.546
6	49.248	47.159	54.964	49.827	0.442	0.353	0.673	0.000
7	49.657	49.396	53.179	54.420	0.544	0.756	0.283	0.889
8	48.974	45.201	51.888	52.424	0.375	0.000	0.000	0.502
9	51.504	49.657	55.735	54.303	1.000	0.803	0.842	0.866
10	49.484	48.097	52.424	53.330	0.501	0.522	0.117	0.678
11	50.756	49.966	54.948	54.823	0.815	0.859	0.670	0.967
12	50.049	48.943	53.274	53.679	0.640	0.674	0.303	0.745
13	50.955	50.103	56.456	52.609	0.864	0.883	1.000	0.538
14	49.799	47.159	53.715	51.005	0.579	0.353	0.400	0.228
15	49.426	49.248	54.486	54.648	0.486	0.729	0.569	0.933
16	47.924	48.912	52.085	52.340	0.115	0.669	0.043	0.486

$$\Delta_{oi}(k) = \|y_0(k) - y_i(k)\| \quad \text{————— Eq. 5.3}$$

$$\Delta_{\min} = \min_{j \in i} \min_{\forall k} \|y_0(k) - y_j(k)\| \quad \text{————— Eq. 5.4}$$

$$\Delta_{\max} = \max_{j \in i} \max_{\forall k} \|y_0(k) - y_j(k)\| \quad \text{————— Eq. 5.5}$$

$y_0(k)$ is the sequence and $y_j(k)$ the comparability sequence. ζ is the distinguishing coefficient.

Table 5.2 Calculated grey relational coefficient, grey relational grade and rank

Expt. No.	Grey relational coefficient				Grey relational grade	Rank
	UTS (600W)	UTS (900W)	FS (600W)	FS (900W)		
1	0.744	0.745	0.771	1.000	0.815	2
2	0.582	0.489	0.509	0.535	0.529	11
3	0.555	1.002	0.638	0.867	0.766	5
4	0.333	0.521	0.375	0.642	0.468	12
5	0.620	0.452	0.925	0.524	0.630	7
6	0.473	0.436	0.605	0.333	0.462	13
7	0.523	0.672	0.411	0.818	0.606	8
8	0.444	0.333	0.333	0.501	0.403	16
9	1.000	0.717	0.760	0.789	0.816	1
10	0.500	0.511	0.362	0.608	0.495	10
11	0.730	0.779	0.602	0.938	0.762	4
12	0.582	0.605	0.418	0.663	0.567	9
13	0.787	0.811	1.000	0.520	0.779	3
14	0.543	0.436	0.454	0.393	0.457	14
15	0.493	0.649	0.537	0.882	0.640	6
16	0.361	0.601	0.343	0.493	0.450	15

The smaller the value of ζ , the more significant is the distinguishing ability. The value of ζ is assumed in the range $0 < \zeta < 1$. In the present study $\zeta = 0.5$ is used. The grey relational grade is computed by taking the average of grey relational coefficients corresponding to each performance characteristic. The overall performance characteristic of the multiple response process depends on the computed grey relational grade. It is calculated using Eq. 5.6. Grey relational coefficient and corresponding grades for each experiment of L_{16} orthogonal array are summarized in Table 5.2.

$$\gamma_i = \frac{1}{n} \sum_{k=1}^n \xi_i(k) \quad \text{----- Eq. 5.6}$$

Where, γ_i is the grey relational grade corresponding to j^{th} experiment and k denotes the number of performance characteristics (Dey et al., 2017).

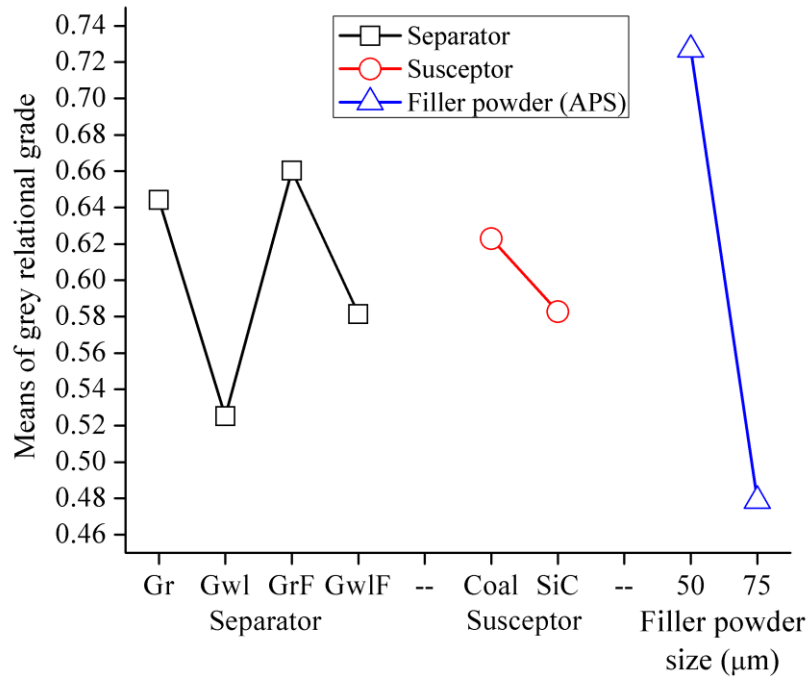
The effect of each process parameter can be separated at different levels on the grey relational grade, since the design of experiments is orthogonal. The means of grey relational grade for each level of the process parameters are highlighted in Table 5.3.

The optimum combination observed from Table 5.3 is A3B1C1 i.e. GrF separator followed by coal susceptor and 50micron (APS) filler powder.

Table 5.3 Response table for grey relational grade

Parameter	Level				Total Mean of GRG	Rank
	1	2	3	4		
A	0.644	0.525	0.660	0.581		2
B	0.623	0.583	----	----	0.603	3
C	0.727	0.479	----	----		1

Influence of control factors is shown in Figure 5.1 through main effects plot of grey relational grade. Use of coal as susceptor and finer filler powder size contribute in increasing the grey relational grade. Experiment No. 9 was found to present the optimum multiple performance characteristics among the sixteen experiments as it has highest grey relational grade.



Gr - Graphite, Gwl - Glasswool, GrF - Graphite with flux bed, GwlF - Glasswool with flux bed

Figure 5.1 Influence of control factors

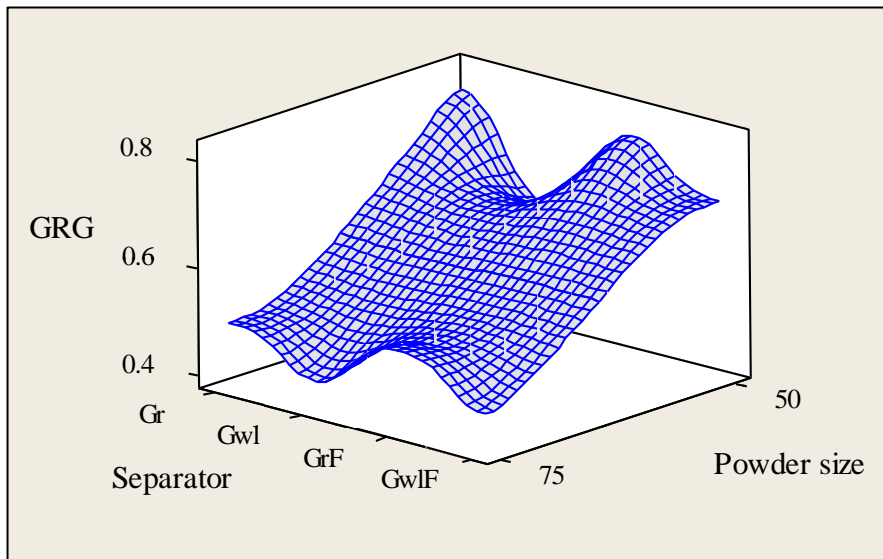


Figure 5.2 Surface plot of GRG versus separator and powder size

Figure 5.2 shows the effect of separator and powder size on GRG. Graphite separator exhibits increased GRG values regardless of the powder size. As evident, a significant decrease in GRG is observed when glasswool is used as separator. Glasswool separator shows a lowest response while a marginal increase in GRG is observed when glasswool is used in combination with flux. This may be due to glasswool has a poor thermal conductivity and is transparent to microwaves (low loss material) at room temperature with extremely large penetration depth, it allows microwaves to pass through without any significant absorption and at the same time obstructs the heat transfer from the susceptor to sample during the initial stage. On the other hand, when flux is used along with glasswool, the fused flux bed serves as separator and forms a layer of slag on the molten filler interface which prevents oxidation resulting in improved joint strength. Furthermore it is also noticed that, for all the combinations of separator 50 μm powder size exhibits higher GRG values compared to that of 75 μm .

Effect of powder size and susceptor on GRG is illustrated in Figure 5.3 It is seen that, coal in combination with 50 μm powder size exhibits maximum GRG, while 75 μm powder size resulted in lower GRG values.

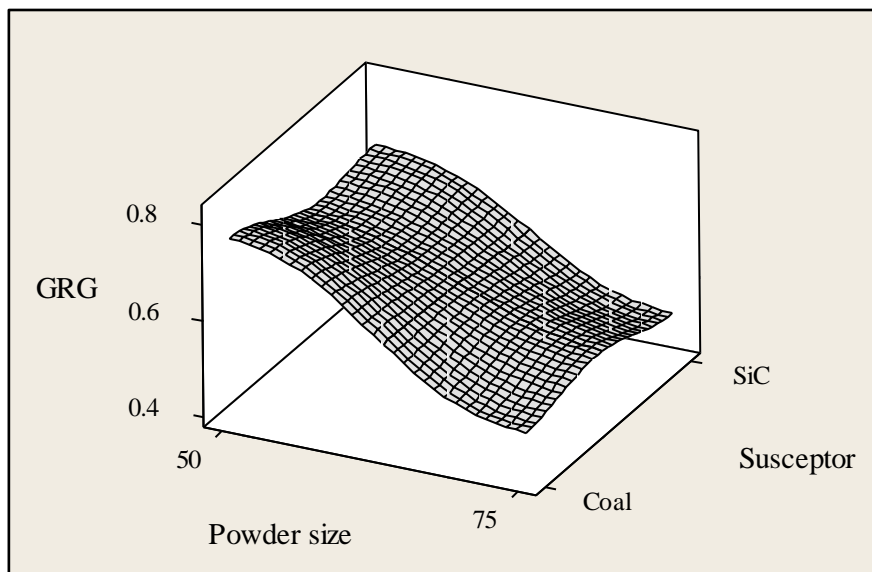


Figure 5.3 Surface plot of GRG versus susceptor and powder size

On the other hand, the SiC susceptor in comparison with coal shows marginally reduced GRG values. This is due to the fact that, SiC requires a small warm up time to couple with microwaves and thus initial high temperatures are achieved at faster rate with coal as it is a carbonaceous material (Rao et al., 1999). Further, from Figures 5.2 and 5.3 it is seen that 50 μ m powder exhibits better GRG values compared to 75 μ m, which is because microwave heating rate largely depends on the electrical conductivity of the materials. Higher the powder size, higher is the electrical conductivity resulting in lower heating rates. As the interface powder particle size increases, the nearby particles establish contact with each other consequently, electrical conductivity of the powder particles increases thereby decreasing the heating rate (Mondal et al., 2009).

Effect of separator and susceptor heating on GRG is shown in Figure 5.4 As stated earlier, the GrF separator yields higher GRG values. In addition it is seen that the combination of GrF and coal results in maximum GRG value since both are carbonaceous materials which yield higher heating rate through rapid coupling with microwaves.

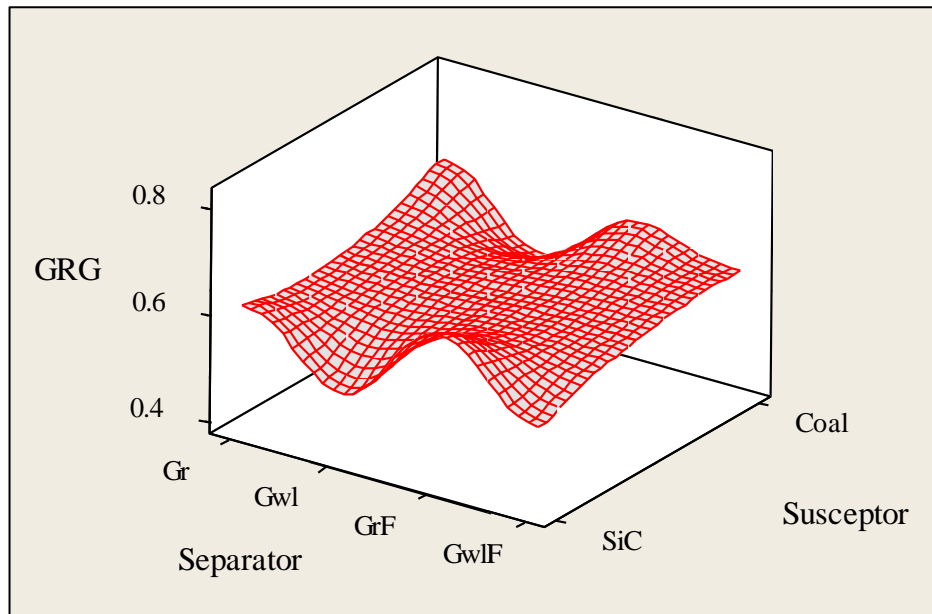


Figure 5.4 Surface plot of GRG versus susceptor and separator

5.3 ANOVA STUDY

In order to study the significance of the process parameters towards UTS and FS, analysis of variance (ANOVA) was performed. It was found that filler powder size is the significant process parameter for determining the strength of the welded joint. ANOVA of grey relational grade is presented in Table 5.4 in which filler powder (APS) and separator are the significant parameters that determine 78% and 13% variability respectively.

Table 5.4 ANOVA of grey relational grade

Source	Degrees of Freedom	Seq SS	Adj MS	Test F	p-value
Separator	3	0.046	0.015	8.36	0.004
Susceptor	1	0.006	0.006	3.53	0.090
Filler powder	1	0.246	0.246	134.26	0.000
Error	10	0.018	0.0018		
Total	15	0.317			

In Table 5.4 F-statistics is the ratio of mean square of parameter and the error. Highest F value signifies the highest percentage of contribution on the output responses. The P-value for the test measures the probability of obtaining a F-ratio as large as what is observed, given that all parameters except the intercepts are zero. The parameters for which the corresponding P-value is less than 0.05 are considered as significant (Basavarajappa et al.; 2009, Jangra et al.; 2015). It is seen that filler powder is the most significant parameter with the highest contribution in all the cases. This influence is identified from the F-value and corresponding P-values which is less than 0.05 (95% confidence level).

5.4 CONFIRMATION TEST

The confirmation test for the optimum process parameters were conducted to verify the quality characteristics of the microwave welded Inconel-625 joints. Table 5.2 presents the highest grey relational grade highlighting the combination of initial process parameters as A3B1C1 (Experiment No. 9) which gives the best multiple performances among the sixteen experiments. Table 5.5 shows the comparison between the experimental results for optimal condition (A3B1C1) and that of predicted results for optimal condition (A3B1C1). Confirmation experiment results shown in Table 5.5 indicate a good agreement between the initial experiment and predicted results. The predicted values were estimated by Eq. 5.7.

$$PR = \text{Avg. (A3)} + \text{Avg. (B1)} + \text{Avg. (C1)} - 2(\text{Mean of response } y_{ij}) \quad \text{————— Eq. 5.7}$$
where, PR is the predicted response and y_{ij} is the value of response.

Table 5.5 Predicted and confirmation test results for optimal condition A3B1C1

Response characteristics	Predicted	Experimental	% error
UTS (600W)	374MPa	382MPa	2.09
UTS (900W)	309MPa	322MPa	4.03
FS (600W)	620MPa	623MPa	0.48
FS (900W)	523MPa	517MPa	1.1

5.5 CHARACTERIZATION OF MICROWAVE WELDED JOINTS

After the confirmation experiment, the microwave welded specimens were subjected to metallurgical characterization through XRD and scanning electron microscopy and microhardness studies.

5.5.1 XRD observations

XRD patterns obtained for the specimens produced at 600W and 900W are shown in Figures 5.5 and 5.6 respectively. Dominant peaks of Nickel along with the formation of various carbides and intermetallic compounds can be clearly seen.

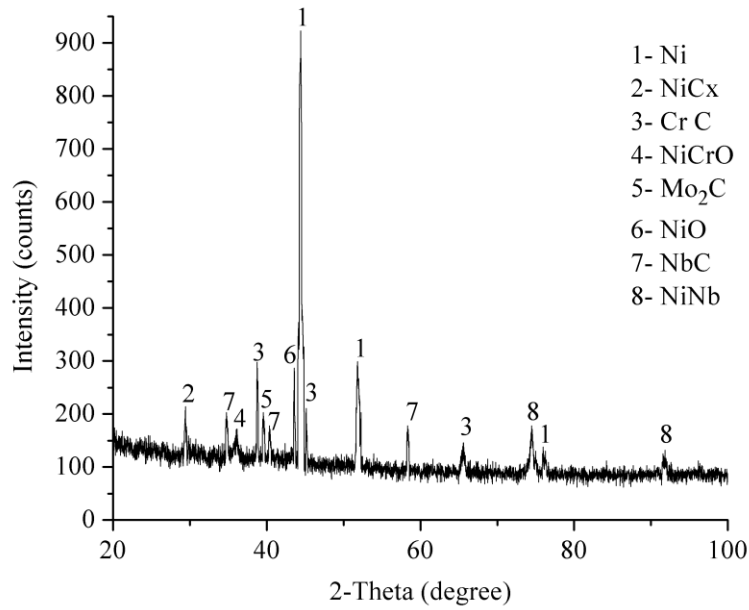


Figure 5.5 XRD pattern of the welded joint developed at 600W

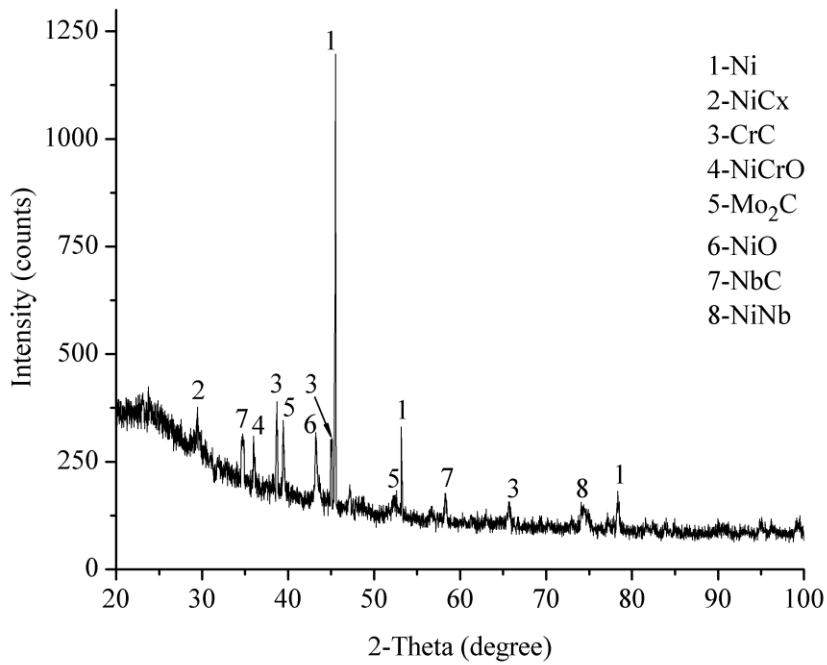


Figure 5.6 XRD pattern of the welded joint developed at 900W

Figures 5.5 and 5.6 show the presence of Chromium carbide (CrC), Niobium carbide (NbC), Molybdenum carbide (Mo₂C), intermetallic compound Nickel Niobium (NiNb),

along with NiO. The formation of carbides is attributed to the strong affinity of niobium and chromium with carbon at elevated temperatures. The equilibrium distribution coefficient of Nb in nickel-based alloys is less than unity (0.46); hence, it easily segregates into interdendritic region during solidification and produces niobium carbide (DuPont 1998). Development of intermetallic compounds is due to the fact that various alloying elements are found in free form in the starting powder; however during heating, these alloying elements react and combine with each other at high temperatures resulting in formation of intermetallic phases. As the dielectric properties are dependent on solid state transformations, the presence of these carbides and oxides promotes the better coupling of microwaves with the interface powder.

The approximate amounts of various phases present in the weld zone were further determined by using the intensity peaks of the respective phases. Table 5.6 and 5.7 present the peak intensity values of the phases existing in the joint zone. Peelamedu et al. (2002) have proposed a method to determine the approximate amount of phase present in any material system through normalized intensity ratio (NIR). Accordingly, Eq. 5.8 was used to determine the NIR of phase 1 (Ni) in the joint zones of the specimens developed using 600W and 900W respectively.

Table 5.6 Relative phase intensities in the joint zone of the specimen processed at 600W

Sl.No.	Phase	I ₁	I ₂	I ₃	I ₄	I ₅	I ₆	I ₇	I ₈	I _{back}	NIR%
1	Ni	923								125	54
2	NiC _x		213							125	5.96
3	CrC			298						125	11.7
4	NiCrO				172					125	3.1
5	Mo ₂ C					203				125	5.2
6	NiO						287			125	10.9
7	NbC							202		125	5.2
8	NiNb								178	125	3.6

Table 5.7 Relative phase intensities in the joint zone of the specimen processed at 900W

Sl.No.	Phase	I ₁	I ₂	I ₃	I ₄	I ₅	I ₆	I ₇	I ₈	I _{back}	NIR%
1	Ni	1198								125	44.5
2	NiCx		377							125	10.45
3	CrC			390						125	11.0
4	NiCrO				310					125	7.6
5	Mo ₂ C					347				125	9.2
6	NiO						318			125	8.0
7	NbC							315		125	7.8
8	NiNb								156	125	1.28

Similarly, the NIR of the other phases can be ascertained using these equations.

$$\text{NIR}_1 = \frac{I_1 - I_{\text{back}}}{I_1 + I_2 + I_3 + I_4 + I_5 + I_6 + I_7 + I_8 - 8(I_{\text{back}})} \quad \text{Eq. 5.8}$$

I₁, I₂, I₃, I₄, I₅, I₆, I₇ and I₈ are the corresponding phase intensities of phases 1 to 8 as seen from figures 5.5 and 5.6 and I_{back} is the background intensity. In case of multiple peaks of the same element/phase, highest peak corresponding to that particular phase is considered for determination of NIR. The NIR values indicated in Tables 5.6 and 5.7 may not give the exact amount of phases; however a relative approximation of amount of phases could be certainly predicted. From Tables 5.6 and 5.7 it is clearly seen that, during joining of Inconel-625 through microwave hybrid heating at 600W and 900W approximately 45.66% and 55.33% respectively of the starting EWAC powder was converted into various carbides and intermetallic phases.

5.5.2 SEM observations

Figures 5.7 (a) and (b) show the SEM micrographs of Inconel-625 alloy welded using MHH at 600W and 900W power respectively. Complete metallurgical bonding of the powder particles can be observed clearly which has resulted in a cellular structure in both the cases. However, lower amount of precipitation in the interdendritic region is observed

with specimen processed at 600W compared to that produced at 900W. This is attributed to more uniform heating characteristics observed while heating at 600W power. Lower heat input associated with 600W power followed by rapid cooling resulted in less segregation due to less time available for redistribution of solute as seen from Figure 5.7 (a). Wilson et al. (1991) reported that, amount of secondary phase developed depends upon the process employed for welding as well as the amount of heat input supplied to the process. Several researchers (Ramkumar et al., 2014; Kumar et al., 2015; Ramkumar et al., 2017) successfully demonstrated this fact by varying the heat input during GTAW process. Lower amount of the secondary phases were noticed for the welded joints developed using low heat input process that in turn resulted in better mechanical properties.

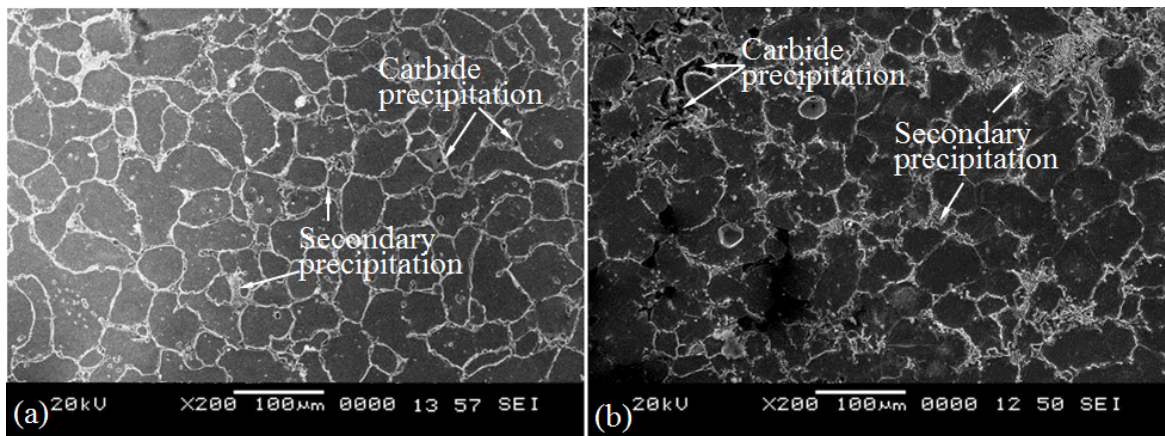


Figure 5.7 SEM micrographs of Inconel-625 welded joints obtained after confirmation experiment processed at (a) 600W (b) 900W power levels

In order to determine the elemental composition, EDS analysis was carried out at interior of the grain and at the grain boundaries as illustrated in Figures 5.8 and 5.9. The elemental composition in the interior of grain in Figure 5.8 consists of nickel rich soft phase compared to the elemental composition at grain boundaries where secondary precipitation is observed. Figure 5.9 shows the EDS analysis for the specimen welded at 600W power wherein clear grain boundaries in the fusion zone can be identified which is attributed to uniform heating when compared to specimen processed at 900W.

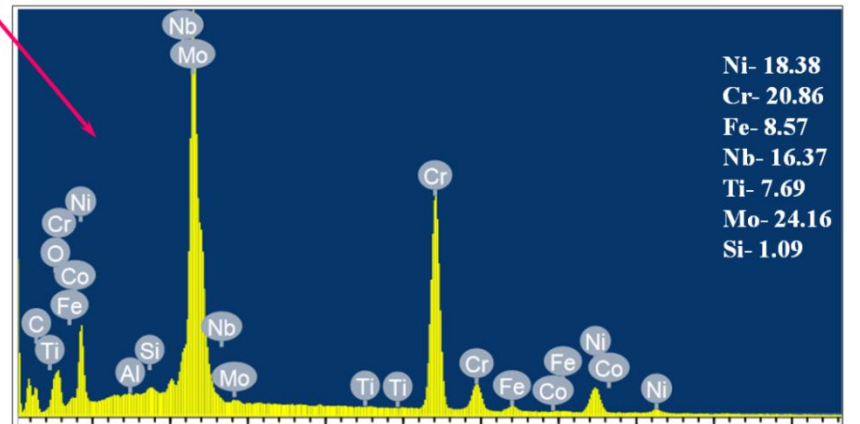
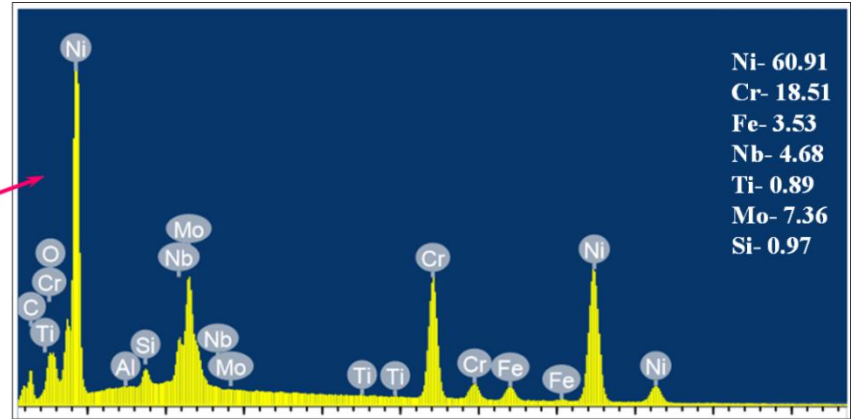
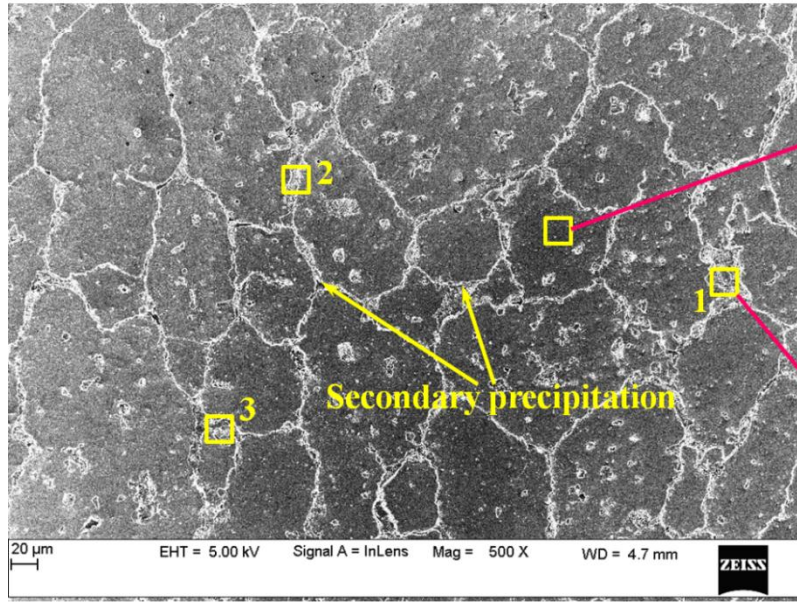


Figure 5.8 SEM micrograph and EDS analysis of Inconel-625 specimen welded at 900W

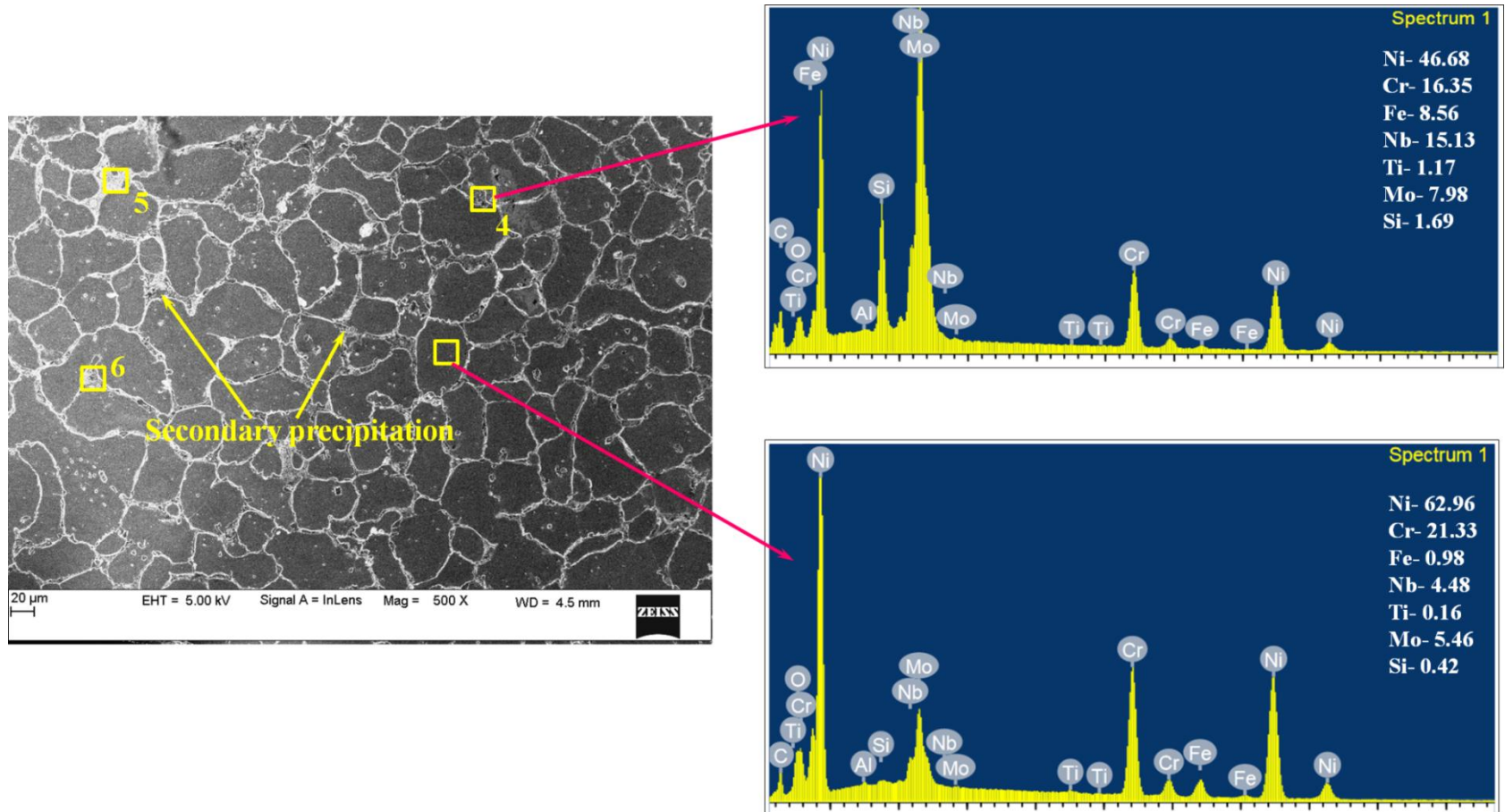


Figure 5.9 SEM micrograph and EDS analysis of Inconel-625 specimen welded at 600W

Table 5.8 Elemental composition in the secondary phase

Power used for processing (W)	Element wt.%						
	Ni	Cr	Fe	Nb	Ti	Mo	Si
600	49.38	18.59	7.86	13.64	0.98	2.86	0.87
900	47.71	16.73	9.49	16.87	1.09	6.53	1.07

The elemental composition at the interior of the grain in Figure 5.9 is almost the same as that observed in Figure 5.8. However, at the grain boundaries relatively less amount of segregation is witnessed in Figure 5.9 than that observed in Figure 5.8. Consequently, smaller amount of hard carbide phase is noticed at the grain boundaries with the specimen processed with 600W as shown in Figure 5.7(a). As a contrast, increased carbide formation can be seen at the grain boundaries in Figure 5.7(b). Similar observations were made by Srinath et al. (2011) during joining of SS-316 through MHH using EWAC powder.

Table 5.8 highlights the average elemental composition in the secondary phase determined at points 1, 2 and 3 in Figure 5.8 and at points 4, 5 and 6 in Figure 5.9. It was observed that the amount of Nb, Ti, Mo and Si content were substantially lower in the welded joints developed at 600W compared to those produced at 900W power levels. This is attributed to the lower heat input associated with 600W power followed by rapid cooling which results in lower amount of Nb segregation and less time available for redistribution of solute.

5.5.3 Observations on microhardness

Microhardness indentations of the specimens produced at 600W and 900W were obtained across the joint by maintaining a distance of 50 μ m between successive indentations. Microhardness of the welded joints was measured in the fusion zone, interface and adjacent base metal regions.

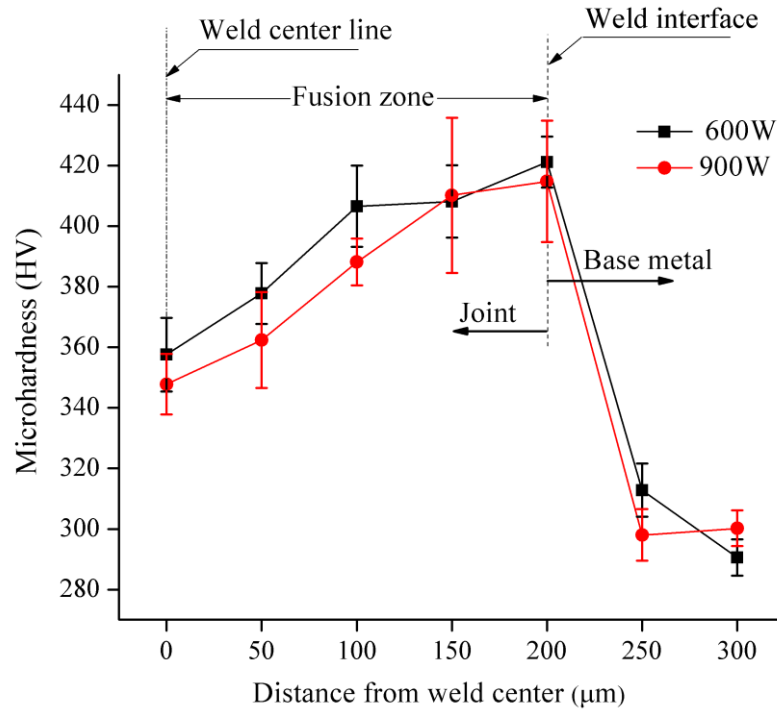


Figure 5.10 Variation in hardness profile of specimens processed at 600W and 900W

At each location, five indentations were obtained and the mean value was considered to plot the variation profile. Figure 5.10 shows the variation in microhardness profile across the joints. Hardness increases from center of the joint towards the interface and is observed to be maximum as it approaches interface region. This increased hardness in the interface region is attributed to the formation of chromium and molybdenum carbides as revealed by EDS analysis.

Due to the dilution of matrix during microwave heating, the elements from the matrix diffuse into the interface region and react with carbon to form carbides along the joint interface. Furthermore, formation of intermetallic phases also contributes towards increasing the hardness. As witnessed from Figure 5.10, specimen developed at 600W exhibits relatively higher hardness and a higher standard deviation is seen in the interface region. This is due to fine grain structure of the joints developed at lower heat input as can be seen from Figure 5.11. Comparatively lower hardness values were exhibited by

the specimen developed at 900W with respect to that produced at 600W. It is also noticed that the hardness values are deviating to a large extent which is attributed to the segregation of Nb, Ti and Mo in the interdendritic region at elevated temperature to form metallic carbide/Laves phase as revealed by EDS analysis in Figure 5.8. Further, the presence of chromium carbide (CrC) is also confirmed through XRD analysis (Figure 5.5 and Table 5.6) in the fusion zone which contributes to the increased hardness of the joints developed at 600W.

Table 5.9 highlights the maximum hardness values observed for the three specimens in different regions.

Table 5.9 Vickers microhardness values in different regions

Specimen type	Maximum hardness (HV)		
	FZ	WI	BM
Processed at 600W	421	428	328
Processed at 900W	438	433	310

FZ-Fusion zone, WI-Weld interface, BM-Base metal

5.5.4 Grain size and porosity

Figure 5.11(a) and (b) show the fusion zone microstructures of the microwave welded joints developed at 600W and 900W. Specimen produced with 600W power exhibited fine grained microstructures compared to their counterparts produced at 900W which is attributed to the lower heat input followed by rapid cooling phenomenon associated with former case. The average grain size observed were 5.8 μ m and 9 μ m respectively for the specimens developed with 600W and 900W. As the grain growth depends on atomic diffusion across the grain boundaries, diffusion rate increases with the increasing temperature which in turn increases the migration of grain boundaries resulting in enhancement of grain growth (Min et al., 2016).

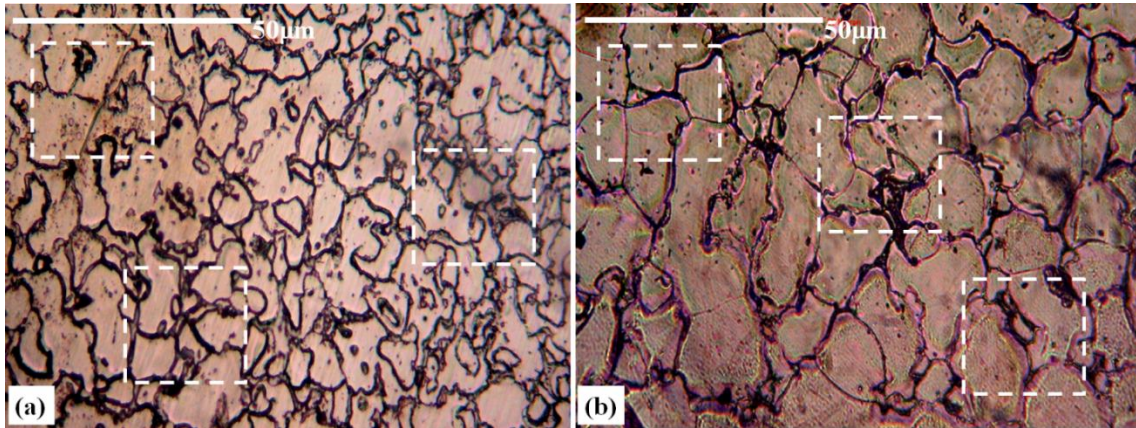


Figure 5.11 Fusion zone optical microstructures of welded joints developed at (a) 600W (b) 900W

Porosity, depends largely on the heating rate employed for processing; as it increases it is accompanied by increased porosity. Porosity of the weld joint microstructures was measured at three locations shown by dotted area in Figure 5.11 using Biovis Material Plus image analyzer software and the indicated porosity represent the average values. Specimen processed at 600W exhibited 1.71% and that processed at 900W exhibited 3.14% porosities. In a similar study Dwivedi et al. (2014) observed that processing with decreased microwave power levels resulted in reduced porosity of the welded joints. This is due to the fact that when higher power is used for processing, a large amount of heat is introduced in the joint zone which in turn leads to the formation of gases. These gases escape out to the environment consequently resulting in increased porosity thereby weakening the joint.

5.5.5 Fractography

In order to assess the mode of failure, fractured specimens were subjected to fractography analysis using SEM. Figures 5.12 (a) and (b) present the SEM micrographs of fractured surfaces of the specimens that were processed at 600W and 900W respectively. In both the cases mixed mode type of fracture is observed. The specimen processed at 600W exhibited the formation of dimples in the fusion zone (Figure 5.12 (a)) which shows that the specimen has experienced a large amount of plastic deformation prior to failure. On the other hand in Figure 5.12 (b) development of cracks and void is observed which is

attributed to the presence of hard carbide phases at the grain boundaries that act as location for crack initiation as the specimen deforms.

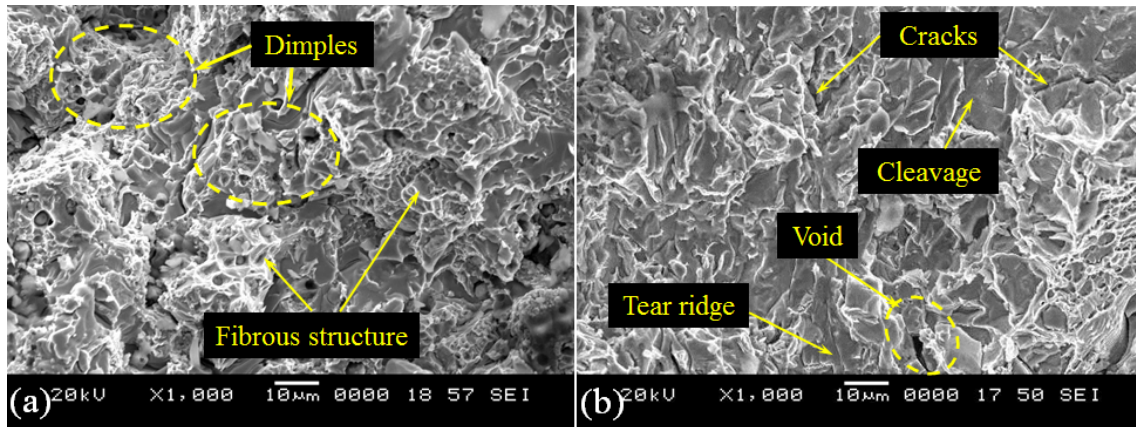


Figure 5.12 SEM micrographs of fractured specimens processed at (a) 600W (b) 900W

Therefore, it is concluded that specimens processed at 600W power exhibit better mechanical properties as well as metallurgical characteristics compared to those processed at 900W power. In addition, it is also observed that the combined effect of process parameters also plays an important role in deciding the quality of the joint produced. Further, during the experimentation it was observed that a slight variation in the thickness of the separator, size of the susceptor and location of specimen inside the cavity also affect the heating characteristics of the process which in turn influence the strength of the joint produced. However, it requires a further investigation in this direction so as to overcome the uncertainties associated with the microwave effects.

5.6 SUMMARY

Grey relational analysis was adopted to solve the problem of multiple quality characteristics since it was observed that, ultimate tensile strength and flexural strength were not correlated mutually and each of the quality characteristics depended differently with control parameters. Therefore, Taguchi method of optimization was extended for the complete evaluation of multiple quality characteristics in joining of Inconl-625 alloy using MHH technique through GRA. Following are the conclusions drawn:

1. Experiment No. 9 yielded optimum combination of process parameters obtained through GRA which was observed to be separator with combination of graphite and flux followed by coal susceptor and 50 μ m (APS) filler powder.
2. ANOVA results of grey relational grade indicate that, interface filler powder is the most significant parameter followed by separator and susceptor. Further, the confirmation experiment results were found to be in agreement with that of predicted results.
3. Normalized intensity ratio analysis indicated that, during joining of Inconel-625 through microwave hybrid heating at 600W and 900W approximately 45.66% and 55.33% of the starting EWAC powder transformed into various carbides and intermetallic phases.
4. As revealed by SEM and EDS analysis, specimens processed with 600W power exhibit better microstructural characteristics and superior strength (UTS 382MPa and FS 623MPa) compared to those processed with 900W (UTS 322MPa and FS 517MPa). This is attributed to the lower amount of segregation observed with welded joints processed with 600W power which further validates the results obtained through optimization process.
5. Specimen developed at 600W power exhibited a higher hardness with finer grain size and reduced porosity values compared to its counterpart produced at 900W.

CHAPTER 6

CONCLUSIONS AND SCOPE FOR FUTURE WORK

6.1 CONCLUSIONS

In the present work Inconel-625 plates were joined successfully through microwave hybrid heating using nickel based powder as interface filler material. The effects of process parameters like (separator type, susceptor type and fineness of interface powder) on UTS and FS of the microwave induced joints have been investigated. The experiments were designed according to Taguchi L_{16} orthogonal array. Influence of process parameters on quality characteristics is investigated using Taguchi method and set of process parameters that yield the optimal UTS and FS of the welded joints were determined. ANOVA was used to analyze the most significant process parameter and percentage contribution of the parameters. Further, the optimization of multi performance characteristics of welding process is carried out through grey relational analysis. Based on the experimental and predicted results the following conclusions were drawn.

1. Phase analysis of the joints revealed the formation of carbides of molybdenum, niobium and chromium which is attributed to higher chemical affinity of these elements with carbon at elevated temperature. In addition, various intermetallics were also observed in the joint zone which were absent in the starting interface powder. Intermetallic phases, carbides and oxides have a significant impact on the dielectric properties of the material and contribute to improved coupling of interface material with microwaves so as to raise the joint temperature more rapidly manner. Furthermore, this results in volumetric heating and facilitates the diffusion of various elements across the joint zone. Consequently local melting of the joint zone takes place leading to metallurgical bonding of faying surfaces.
2. SEM and EDS analysis showed the segregation of Nb, and Mo which resulted in the formation of metallic carbides in the interdendritic region. However, substantially reduced segregation was observed with the joints developed at 600W

which is attributed to the lower heat input followed by rapid cooling. Consequently, the joints developed at 600W exhibited superior mechanical properties.

3. Average microhardness of the microwave induced joints developed at 600W power was observed to be $395 \pm 10\text{HV}$ (1.5 times higher than base metal hardness). On the other hand, microwave induced joints developed at 900W exhibited an average hardness of $385 \pm 16\text{HV}$ in the joint zone (1.4 times higher than base metal hardness). Maximum tensile strength and flexural strength of the joints were recorded as 382MPa and 623MPa which correspond to 40.5% and 35% respectively of the base metal strength.
4. Increased tensile strength and flexural strength of the welded joints were obtained when smaller size powder was used as an interface filler material. The welded joints produced at 600W exhibited smaller grain size ($5.8\mu\text{m}$) and lower porosity (1.71%) which signifies the improved mechanical properties of the joint. Examination of fractured surfaces revealed a mixed mode fracture in all the specimens; however the specimens processed at 600W exhibited more ductile features compared to their counterparts developed at 900W.
5. Glasswool separator showed a lowest mean response (UTS 234.8MPa and FS 420.8MPa) while a marginal increase in mean response was observed when glasswool was used in combination with flux. Joints processed with graphite separator exhibited higher grey relational grade (GRG) values regardless of the powder size. A significant decrease in GRG was observed when glasswool was used as separator. Combination of GrF (graphite+flux) separator and coal susceptor resulted in maximum GRG value (0.816) since both (graphite and coal) are carbonaceous materials which produce higher heating rate through rapid coupling with microwaves.
6. The optimum combination of process parameters obtained through GRA was separator GrF, coal susceptor and $50\mu\text{m}$ filler powder size (A3B1C1).

7. Based on ANOVA results of GRG it was also seen that interface filler powder fineness is the most significant parameter followed by separator type and susceptor type. Percentage contributions of filler powder and separator were found to be 78% and 13% respectively. The application of GRA technique transformed the complex multi-objective problem into a single grey relational grade response and thus simplified the optimization procedure.

6.2 SCOPE FOR FUTURE WORK

Joining of metals through microwave hybrid heating is a recently developed process and has revealed its potential to produce welded joints with appreciable strength. However the process being in the development stage, several challenges are being encountered by the researchers and still there is a scope for further investigation. Some of the future work and suggestions are highlighted for further research.

1. Development of welded joints with different configurations for butt joints (such as V, J, etc.) can be considered and further detailed characterization of these joints may be carried out.
2. Most of the recent works related to microwave joining have been focusing on joining of bulk metals while; very limited works have been reported on microwave joining of metal matrix composites. Thus the possibility of joining various metal matrix composites using MHH can be explored.
3. The published works on joining of bulk metals through MHH are limited to investigation of joint characteristics through metallurgical (microstructural studies, phase analysis, porosity etc.) and mechanical (microhardness, uniaxial tensile test and 3-point bend test) characterization. However, it is pointed out that no works have been reported on estimation of residual stresses induced in the microwave welded joints. Hence, there is a scope to evaluate the residual stresses developed in the microwave welded joints.

4. The microwave welding process needs to be integrated with real-time temperature measurement of the joint zone so as to ensure repeatability of results and to achieve better control over the process.
5. Influence other possible process parameters such as temperature, time, and processing atmosphere, interface gap between faying surfaces etc., on the quality of the microwave induced joints may be investigated and advanced optimization techniques can be used to investigate the influence of these parameters on the joint strength.
6. Simulation of the MHH joining process can be carried out to understand the physical interpretation of microwave-material interaction and temperature distribution pattern across the joint.

6.3 CHALLENGES IN MICROWAVE PROCESSING OF MATERIALS

For decades microwave energy has been effectively utilized to process many engineering materials. However, microwave processing of materials offers many challenges that have to be overcome by continued research.

1. The non-uniform heating behavior associated with the process calls for the use of special fixtures.
2. As the dielectric properties of materials are temperature dependent, real-time measurement of these material properties is difficult.
3. Due to inadequate experimental data about material-microwave behavior, modeling and simulation of the process has narrow scope.
4. Microwave processing involves the interaction of electromagnetic waves with the atoms which necessitates the researchers to realize absorption of microwaves at atomic level so as to understand change in material properties and physics behind the heating.
5. Another fact observed during microwave processing is poor repeatability of results and hence absence of adequate data for newly developed processes such as

cladding and joining which further restricts the use of microwave processing in the industries.

6. Further, the size of component that can be processed using microwave radiation depends upon the size of the applicators. However, microwave applicators are being customized for selective heating which require huge investments.

REFERENCES

Anklekar, R.M., Agrawal, D.K. and Roy, R. (2001). "Microwave sintering and mechanical properties of PM copper steel." *Powder Metall.*, 44(4), 355-362.

Anklekar, R.M., Bauer, K., Agrawal, D.K. and Roy, R. (2005). "Improved mechanical properties and microstructural development of microwave sintered copper and nickel steel PM parts." *Powder Metall.*, 48(1), 39-46.

Annamalai, R., Upadhyaya, A. and Agrawal, D. (2013). "An investigation on microwave sintering of Fe, Fe-Cu and Fe-Cu-C alloys." *Bull. Mater. Sci.*, 36(3), 447-456.

Aravindan, S. and Krishnamurthy, R. (1999). "Joining of ceramic composites by microwave heating." *Mater. Lett.*, 38(4), 245-249.

Arulmurugan, B. and Manikandan, M. (2017). "Development of welding technology for improving the metallurgical and mechanical properties of 21st century nickel based superalloy 686." *Mat. Sci. Eng. A-Struct.*, 691, 126-140.

ASTM International Standard E190-92 (reapproved 2003). "Standard test method for guided bend test for ductility of welds." *ASTM book of standards*.

ASTM. (2011). E8/E8M-11, "Standard test methods for tension testing of metallic materials." *ASTM book of standards*.

Bagha, L., Sehgal, S., Thakur, A. and Kumar, H. (2017). "Effects of powder size of interface material on selective hybrid carbon microwave joining of SS304-SS304." *J. Manuf. Process.*, 25, 290-295.

Bansal, A., Sharma, A.K. and Das, S. (2013). "Metallurgical and mechanical characterization of mild steel-mild steel joint formed by microwave hybrid heating process." *Sadhana*, 38(4), 679-686.

Bansal, A., Sharma, A.K., Das, S. and Kumar, P. (2016). "On microstructure and strength properties of microwave welded Inconel 718/stainless steel (SS-316L)." *Proc. Inst. Mech. Eng., Part L*, 230(5), 939-948.

Bansal, A., Sharma, A.K., Kumar, P. and Das, S. (2014). "Characterization of bulk stainless steel joints developed through microwave hybrid heating." *Mater. Charact.*, 91, 34-41.

Bansal, A., Sharma, A.K., Kumar, P. and Das, S. (2015). "Structure-property correlations in microwave joining of Inconel 718." *JOM*, 67(9), 2087-2098.

Bansal, A., Sharma, A.K., Kumar, P. and Das, S. (2016). "Investigation on microstructure and mechanical properties of the dissimilar weld between mild steel and stainless steel-316 formed using microwave energy." *Proc. Inst. Mech. Eng., Part B*, 230(3), 439-448.

Bansal, A., Zafar, S. and Sharma, A.K. (2015). "Microstructure and abrasive wear performance of Ni-WC composite microwave clad." *J. Mater. Eng. Perform.*, 24(10), 3708-3716.

Barmatz, M., Jackson, H.W. and Radtke, R.P. (2000). *U.S. Patent No. 6,054,693*. Washington, DC: U.S. Patent and Trademark Office.

Basavarajappa, S., Arun, K.V. and Davim, J.P. (2009). "Effect of filler materials on dry sliding wear behavior of polymer matrix composites-a Taguchi approach." *J. Miner. Mater. Charact. Eng.*, 8(5), 379.

Bhattacharya, M. and Basak, T. (2016). "A review on the susceptor assisted microwave processing of materials." *Energy*, 97, 306-338.

Borrell, A. and Salvador, M.D. (2018). "Advanced Ceramic Materials Sintered by Microwave Technology." In *Sintering Technology-Method and Application*. IntechOpen.

Brosnan, K.H., Messing, G.L. and Agrawal, D.K. (2003). "Microwave sintering of alumina at 2.45 GHz." *J. Am. Ceram. Soc.*, 86(8), 1307-1312.

Budinger, D.E. (2008). *U.S. Patent No. 7,775,416*. Washington, DC: U.S. Patent and Trademark Office.

Caiazzo, F., Alfieri, V., Cardaropoli, F. and Sergi, V. (2017). "Investigation on edge joints of Inconel 625 sheets processed with laser welding." *Opt. Laser Technol.*, 93, 180-186.

Chandrasekaran, S., Basak, T. and Ramanathan, S. (2011). "Experimental and theoretical investigation on microwave melting of metals." *J. Mater. Process. Technol.*, 211(3), 482-487.

Chandrasekaran, S., Ramanathan, S. and Basak, T. (2012). "Microwave material processing-a review." *AIChE J.*, 58(2), 330-363.

Charmond, S., Carry, C.P. and Bouvard, D. (2010). "Densification and microstructure evolution of Y-Tetragonal Zirconia Polycrystal powder during direct and hybrid microwave sintering in a single-mode cavity." *J. Eur. Ceram. Soc.*, 30(6), 1211-1221.

Clark, D.E. and Sutton, W.H. (1996). "Microwave processing of materials." *Annu. Rev. Mater. Sci.*, 26(1), 299-331.

Clark, D.E., Folz, D.C., Folgar, C.E. and Mahmoud, M.M. (2005). "What is microwave processing." *Microwave solutions for ceramic engineer. Ohio: John Wiley & Sons.*

Crane, C.A., Pantoya, M.L., Weeks, B.L. and Saed, M. (2014). "The effects of particle size on microwave heating of metal and metal oxide powders." *Powder Technol.*, 256, 113-117.

Dey, A., Debnath, S. and Pandey, K.M. (2017). "Optimization of electrical discharge machining process parameters for Al6061/cenosphere composite using grey-based hybrid approach." *Trans. Nonferrous Met. Soc. China*, 27(5), 998-1010.

Dieter, G.E. (1988). "Mechanical metallurgy," SI Metric edn., McGraw-Hill Book Company Ltd.

Duan, M., Wang, Y., Ran, H., Ma, R. and Wei, L. (2014). "Study on Inconel 625 hollow structure manufactured by explosive welding." *Mater. Manuf. Processes*, 29(8), 1011-1016.

DuPont, J.N., Lippold, J.C. and Kiser, S.D. (2009). "Welding Metallurgy and Weldability of Nickel-Base Alloys." John Wiley & Sons, Inc.: USA.

DuPont, J.N., Notis, M.R., Marder, A.R., Robino, C.V. and Michael, J. R. (1998). "Solidification of Nb-bearing superalloys: Part I. Reaction sequences." *Metall. Mater. Trans. A*, 29(11), 2785-2796.

DuPont, J.N., Robino, C.V. and Marder, A. R. (1999). "Modelling mushy zones in welds of multicomponent alloys: implications for solidification cracking." *Sci. Technol. Weld. Joining*, 4(1), 1-14.

Dwivedi, S.P. and Sharma, S. (2014). "Effect of process parameters on tensile strength of 1018 mild steel joints fabricated by microwave welding." *Metallogr., Microstruct., Anal.*, 3(1), 58-69.

Ertugrul, O., Park, H.S., Onel, K. and Willert-Porada, M. (2014). "Effect of particle size and heating rate in microwave sintering of 316L stainless steel." *Powder Technol.*, 253, 703-709.

Gamit, D.N. (2017) "Effect of Susceptor Heating on Joining of Metallic Pipes Using Microwave Energy." *Int. J. Emerging Technol. Eng. Res.*, 5(9), 49-52.

Gamit, D., Mishra, R.R. and Sharma, A.K. (2017). "Joining of mild steel pipes using microwave hybrid heating at 2.45 GHz and joint characterization." *J. Manuf. Process*, 27, 158-168.

Ganpat Industrial corporation. (2016). <https://www.ganpatind.com/inconel-625-flanges>.

Goldstein, A., Giefman, L. and Ziv, S.B. (1998). "Susceptor assisted microwave sintering of MgAl₂O₄ powder at 2.45 GHz." *J. Mater. Sci. Lett.*, 17(12), 977-979.

Gupta, D. and Sharma, A.K. (2011). "Investigation on sliding wear performance of WC₁₀Co₂Ni cladding developed through microwave irradiation." *Wear*, 271(9-10), 1642-1650.

Gupta, D. and Sharma, A. K. (2011). "Development and microstructural characterization of microwave cladding on austenitic stainless steel." *Surf. Coat. Technol.*, 205(21-22), 5147-5155.

Gupta, D., Bhovi, P.M., Sharma, A.K. and Dutta, S. (2012). "Development and characterization of microwave composite cladding." *J. Manuf. Process.*, 14(3), 243-249.

Gupta, M., and Leong, E.W.W. (2008). "Microwaves and metals." John Wiley & Sons (Asia).

Gupta, M. and Wong, W.L.E. (2005). "Enhancing overall mechanical performance of metallic materials using two-directional microwave assisted rapid sintering." *Scr. Mater.*, 52(6), 479-483.

Gupta, P. and Kumar, S. (2014). "Investigation of stainless steel joint fabricated through microwave energy." *Mater. Manuf. Processes*, 29(8), 910-915.

Haynes international. (2015). "Industrial gas turbines." <https://www.haynesintl.com/markets/power-generation>

Hebbale, A.M. and Srinath, M.S. (2016). "Microstructural investigation of Ni based cladding developed on austenitic SS-304 through microwave irradiation." *J. Mater. Res. Technol.*, 5(4), 293-301.

Henderson, M.B., Arrell, D., Larsson, R., Heobel, M. and Marchant, G. (2004). "Nickel based superalloy welding practices for industrial gas turbine applications." *Sci. Technol. Weld. Joining*, 9(1), 13-21.

Hosseini, H.S., Shamanian, M. and Kermanpur, A. (2011). "Characterization of microstructures and mechanical properties of Inconel 617/310 stainless steel dissimilar welds." *Mater. Charact.*, 62(4), 425-431.

Janaki Ram, G.D., Venugopal Reddy, A., Prasad Rao, K. and Madhusudhan Reddy, G. (2004). "Control of Laves phase in Inconel 718 GTA welds with current pulsing." *Sci. Technol. Weld. Joining*, 9(5), 390-398.

Jangra, K.K., Sharma, N., Khanna, R. and Matta, D. (2016). "An experimental investigation and optimization of friction stir welding process for AA6082 T6 (cryogenic treated and untreated) using an integrated approach of Taguchi, grey relational analysis and entropy method." *Proc. Inst. Mech. Eng., Part L*, 230(2), 454-469.

Kaushal, S., Singh, B., Gupta, D., Bhowmick, H. and Jain, V. (2018). "An approach for developing nickel–alumina powder-based metal matrix composite cladding on SS-304 substrate through microwave heating." *J. Compos. Mater.*, 52(16), 2131-2138.

Kaushal, S., Sirohi, V., Gupta, D., Bhowmick, H. and Singh, S. (2018). "Processing and characterization of composite cladding through microwave heating on martensitic steel." *Proc. Inst. Mech. Eng., Part L*, 232(1), 80-86.

Korrapati, P.K., Avasarala, V.K., Bhushan, M., Ramkumar, K.D., Arivazhagan, N.N. and Narayanan, S. (2014). "Assessment of Mechanical properties of PCGTA weldments of Inconel 625." *Procedia Eng.*, 75, 9-13.

Kumar, C.S. (2010). "Optimization of process parameters in microwave joining of metallic materials in a multimode microwave applicator" M.Tech Thesis, Indian Institute of Technology Roorkee., Uttarakhand, India.

Kumar, K.G., Ramkumar, K.D. and Arivazhagan, N. (2015). "Characterization of metallurgical and mechanical properties on the multi-pass welding of Inconel 625 and AISI 316L." *J. Mech. Sci. Technol.*, 29(3), 1039-1047.

Kutty, M.G. and Bhaduri, S.B. (2004). "Gradient surface porosity in titanium dental implants: relation between processing parameters and microstructure." *J. Mater. Sci.: Mater. Med.*, 15(2), 145-150.

Lakshminarayanan, A.K. and Balasubramanian, V. (2010). "An assessment of microstructure, hardness, tensile and impact strength of friction stir welded ferritic stainless steel joints." *Mater. Des.*, 31(10), 4592-4600.

Lee, H.T., Jeng, S.L., Yen, C.H. and Kuo, T.Y. (2004). "Dissimilar welding of nickel-based Alloy 690 to SUS 304L with Ti addition." *J. Nucl. Mater.*, 335(1), 59-69.

Lee, S.J. and Lee, Y.K. (2008). "Prediction of austenite grain growth during austenitization of low alloy steels." *Mater. Des.*, 29(9), 1840-1844.

Lewis, D., Rayne, R.J., Bender, B.A., Kurihara, L.K., Chow, G.M., Fliflet, A., Kincaid, A and Bruce, R. (1997). "Conventional and high frequency microwave processing of nanophase ceramic materials." *Nanostruct. Mater.*, 9(1-8), 97-100.

Li, G., Huang, J. and Wu, Y. (2015). "An investigation on microstructure and properties of dissimilar welded Inconel 625 and SUS 304 using high-power CO₂ laser." *Int. J. Adv. Manuf. Technol.*, 76(5-8), 1203-1214.

Lin, H.L. (2013). "Optimization of Inconel 718 alloy welds in an activated GTA welding via Taguchi method, gray relational analysis, and a neural network." *Int. J. Adv. Manuf. Technol.*, 67(1-4), 939-950.

Lin, J.L. and Lin, C.L. (2002). "The use of the orthogonal array with grey relational analysis to optimize the electrical discharge machining process with multiple performance characteristics." *Int. J. Mach. Tool. Manu.*, 42(2), 237-244.

Luo, S.D., Yan, M., Schaffer, G.B. and Qian, M. (2011). "Sintering of titanium in vacuum by microwave radiation." *Metall. Mater. Trans. A*, 42(8), 2466.

Ma, J., Diehl, J.F., Johnson, E.J., Martin, K.R., Miskovsky, N.M., Smith, C.T., Weisel, G.J., Weiss, B.L. and Zimmerman, D.T. (2007). "Systematic study of microwave absorption, heating, and microstructure evolution of porous copper powder metal compacts." *J. Appl. Phys.*, 101(7), 074906.

Mahmoud, M.M., Link, G. and Thumm, M. (2015). "The role of the native oxide shell on the microwave sintering of copper metal powder compacts." *J. Alloys Compd*, 627, 231-237.

Menezes, R.R. and Kiminami, R.H.G.A. (2008). "Microwave sintering of alumina-zirconia nanocomposites." *J. Mater. Process. Technol.*, 203(1-3), 513-517.

Meredith, R. J. (1998). *Engineers' handbook of industrial microwave heating* (No. 25). Iet.

Min, L.I.U., Zheng, W.J., Xiang, J.Z., Song, Z.G., Pu, E.X. and Han, F.E.N.G. (2016). "Grain growth behavior of inconel 625 superalloy." *J. Iron Steel. Res. Int.*, 23(10), 1111-1118.

Mishra, R.R. and Sharma, A.K. (2017). "Effect of susceptor and mold material on microstructure of in-situ microwave casts of Al-Zn-Mg alloy." *Mater. Des.*, 131, 428-440.

Mondal, A., Agrawal, D. and Upadhyaya, A. (2008). "Microwave heating of pure copper powder with varying particle size and porosity." *J. Microwave Power*, 43(1), 5-10.

Mondal, A., Agrawal, D. and Upadhyaya, A. (2010). "Microwave sintering of refractory metals/alloys: W, Mo, Re, W-Cu, W-Ni-Cu and W-Ni-Fe alloys." *J. Microwave Power*, 44(1), 28-44.

Mondal, A., Upadhyaya, A. and Agrawal, D. (2011). "Effect of heating mode and sintering temperature on the consolidation of 90W-7Ni-3Fe alloys." *J. Alloys Compd*, 509(2), 301-310.

Montgomery, D.C. (2013). "Design and analysis of experiments." eighth ed., John Wiley & Sons, New York, USA.

Moran, J., Granada, E., Míguez, J.L. and Porteiro, J. (2006). "Use of grey relational analysis to assess and optimize small biomass boilers." *Fuel Process. Technol.*, 87(2), 123-127.

Naffakh, H., Shamanian, M. and Ashrafizadeh, F. (2009). "Dissimilar welding of AISI 310 austenitic stainless steel to nickel-based alloy Inconel 657." *J. Mater. Process. Technol.*, 209(7), 3628-3639.

Oghbaei, M. and Mirzaee, O. (2010). "Microwave versus conventional sintering: a review of fundamentals, advantages and applications." *J. Alloys Compd*, 494(1-2), 175-189.

- Osepchuk, J.M. (2002). "Microwave power applications." *IEEE Transactions on Microwave Theory and Techniques*, 50(3), 975-985.
- Padmanaban, G. and Balasubramanian, V. (2011). "Optimization of pulsed current gas tungsten arc welding process parameters to attain maximum tensile strength in AZ31B magnesium alloy." *Trans. Nonferrous Met. Soc. China*, 21(3), 467-476.
- Padmavathi, C., Upadhyaya, A. and Agrawal, D. (2012). "Microwave assisted sintering of Al-Cu-Mg-Si-Sn alloy." *J. Microwave Power*, 46(3), 115-127.
- Pathania, A., Singh, S., Gupta, D., and Jain, V. (2015). "Development and analysis of tribological behavior of microwave processed EWAC+ 20% WC10Co2Ni composite cladding on mild steel substrate." *J. Manuf. Process*, 20, 79-87.
- Patterson, R. and Milewski, J.O. (1985). "GTA Weld Cracking-Alloy 625 to 304." *Weld. J.*, 64(8), 227.
- Peelamedu, R.D., Roy, R. and Agrawal, D.K. (2002). "Microwave-induced reaction sintering of NiAl₂O₄." *Mater. Lett.*, 55(4), 234-240.
- Peng, J. and Binner, J. (2002). "Microwave ignited combustion synthesis of aluminium nitride." *J. Mater. Sci. Lett.*, 21(3), 247-250.
- Pineau, A., Benzerga, A. A. and Pardoën, T. (2016). "Failure of metals I: Brittle and ductile fracture." *Acta Mater.*, 107, 424-483.
- Prabhu, G., Chakraborty, A. and Sarma, B. (2009). "Microwave sintering of tungsten." *Int. J. Refract. Met. Hard Mater.*, 27(3), 545-548.

Prasad, K.S., Chalamalasetti, S.R., & Damera, N.R. (2015). "Application of grey relational analysis for optimizing weld bead geometry parameters of pulsed current micro plasma arc welded inconel 625 sheets." *Int. J. Adv. Manuf. Technol.*, 78(1-4), 625-632.

Prasad, K.S., Rao, C.S. and Rao, D.N. (2016). "Optimization of fusion zone grain size, hardness, and ultimate tensile strength of pulsed current micro plasma arc welded Inconel 625 sheets using genetic algorithm." *Int. J. Adv. Manuf. Technol.*, 85(9-12), 2287-2295.

Precision sport industries (2019). "Eisenmann Inconel Alloy 625 Performance Exhaust for E92/3 M3", <http://www.precisionsport.com>

Rai, S.K., Kumar, A., Shankar, V., Jayakumar, T., Rao, K.B.S. and Raj, B. (2004). "Characterization of microstructures in Inconel 625 using X-ray diffraction peak broadening and lattice parameter measurements." *Scr. Mater.*, 51(1), 59-63.

Rajani, H.Z. and Mousavi, S.A. (2012). "The effect of explosive welding parameters on metallurgical and mechanical interfacial features of Inconel 625/plain carbon steel bimetal plate." *Mat. Sci. Eng. A-Struct.*, 556, 454-464.

Rajkumar, K. and Aravindan, S. (2009). "Microwave sintering of copper-graphite composites." *J. Mater. Process. Technol.*, 209(15-16), 5601-5605.

Ramesh, P.D., Brandon, D. and Schächter, L. (1999). "Use of partially oxidized SiC particle bed for microwave sintering of low loss ceramics." *Mat. Sci. Eng. A-Struct.*, 266(1-2), 211-220.

Ramezani, H., Akbari Mousavi, S.A.A. and Ebrahimzadeh, H. (2014). "The effect of process parameters on pulsed Nd: YAG laser welding of Inconel 625." *Adv. Mater. Res.*, 829, 36-40.

Ramkumar, K.D., Abraham, W.S., Viyash, V., Arivazhagan, N. and Rabel, A.M. (2017). "Investigations on the microstructure, tensile strength and high temperature corrosion behaviour of Inconel 625 and Inconel 718 dissimilar joints." *J. Manuf. Process.*, 25, 306-322.

Ramkumar, K.D., Mithilesh, P., Varun, D., Reddy, A.R.G., Arivazhagan, N., Narayanan, S. and Kumar, K.G. (2014). "Characterization of microstructure and mechanical properties of Inconel 625 and AISI 304 dissimilar weldments." *ISIJ Int.*, 54(4), 900-908.

Ramkumar, K.D., Sridhar, R., Periwai, S., Oza, S., Saxena, V., Hidad, P. and Arivazhagan, N. (2015). "Investigations on the structure-Property relationships of electron beam welded Inconel 625 and UNS 32205." *Mater. Des.*, 68, 158-166.

Rao, K. J., Vaidhyanathan, B., Ganguli, M. and Ramakrishnan, P. A. (1999). "Synthesis of inorganic solids using microwaves." *Chem. Mater.*, 11(4), 882-895.

RoEdiger, K., Dreyer, K., Gerdes, T. and Willert-Porada, M. (1998). "Microwave sintering of hardmetals." *Int. J. Refract. Met. Hard Mater*, 16(4-6), 409-416.

Ross PJ. Taguchi Techniques for Quality Engineering. McGraw-Hill: New York.1996.

Roy, R. K. (2001). Design of experiments using the Taguchi approach: 16 steps to product and process improvement. John Wiley & Sons.

Roy, R., Agrawal, D., Cheng, J. and Gedeveanishvili, S. (1999). "Full sintering of powdered-metal bodies in a microwave field." *Nature*, 399(6737), 668.

Sabol, G. P. and Stickler, R. (1969). "Microstructure of Nickel-Based Superalloys." *Phys. Status Solidi*, 35(1), 11-52.

Sahu, P. K. and Pal, S. (2015). "Multi-response optimization of process parameters in friction stir welded AM20 magnesium alloy by Taguchi grey relational analysis." *J. Magnesium Alloys*, 3(1), 36-46.

Saitou, K. (2006). "Microwave sintering of iron, cobalt, nickel, copper and stainless steel powders." *Scr. Mater.*, 54(5), 875-879.

Saxena, S., Bansal, S., Deo, R. and Khan, S. (2014). "Joining of Bulk Metallic Pipes by Microwave Hybrid Heating Process under Parametrical Regulations." *IOSR J. Mech. Civ. Eng*, 11(6), 62-69.

Shakil, M., Ahmad, M., Tariq, N.H., Hasan, B.A., Akhter, J.I., Ahmed, E., Mehmood, M., Choudhry, M.A. and Iqbal, M. (2014). "Microstructure and hardness studies of electron beam welded Inconel 625 and stainless steel 304L." *Vacuum*, 110, 121-126.

Shankar, V., Rao, K.B.S. and Mannan, S.L. (2001). "Microstructure and mechanical properties of Inconel 625 superalloy." *J. Nucl. Mater.*, 288(2-3), 222-232.

Shanmugarajan, B., Shrivastava, R., Sathiya, P. and Buvanashakaran, G. (2016). "Optimisation of laser welding parameters for welding of P92 material using Taguchi based grey relational analysis." *Def. Technol.*, 12(4), 343-350.

Sharma, A.K. and Gupta, D. (2012). "On microstructure and flexural strength of metal–ceramic composite cladding developed through microwave heating." *Appl. Surf. Sci.*, 258(15), 5583-5592.

Sharma, A.K. and Krishnamurthy, R. (2002). "Microwave processing of sprayed alumina composite for enhanced performance." *J. Eur. Ceram. Soc.*, 22(16), 2849-2860.

Sharma, A.K. and Mishra, R.R. (2017). "Role of particle size in microwave processing of metallic material systems." *Mater. Sci. Tech.*, 34(2), 123-137.

Sharma, A.K., Aravindhan, S. and Krishnamurthy, R. (2001). "Microwave glazing of alumina-titania ceramic composite coatings." *Mater. Lett.*, 50(5-6), 295-301.

Shoemaker, L.E. (2005). "Alloys 625 and 725: trends in properties and applications." *Superalloys 718, 625, 706 and Derivatives. TMS*, 409-418.

Silva, C.C., De Miranda, H.C., Motta, M.F., Farias, J.P., Afonso, C.R.M. and Ramirez, A. J. (2013). "New insight on the solidification path of an alloy 625 weld overlay." *J. Mater. Res. Technol.*, 2(3), 228-237.

Singh, S., Singh, P., Gupta, D., Jain, V., Kumar, R. and Kaushal, S. (2018). Development and characterization of microwave processed cast iron joint. *Eng. Sci. Technol. Int. J.*, doi: 10.1016/j.jestch.2018.10.012.

Singh, S., Suri, N.M. and Belokar, R.M. (2015). "Characterization of joint developed by fusion of aluminum metal powder through microwave hybrid heating." *Mater. Today: Proc.*, 2(4-5), 1340-1346.

Siores, E. and Do Rego, D. (1995). "Microwave applications in materials joining." *J. Mater. Process. Technol.*, 48(1-4), 619-625.

Smith, G.D., Tillack, D.J., Patel, S.J. and Loria, E. A. (2001). "Superalloys 718, 625, 706 and Various Derivatives." *TMS, Warrendale, PA*, 35-46.

Song, K.H. and Nakata, K. (2009). "Mechanical properties of friction-stir-welded Inconel 625 alloy." *Mater. Trans.*, 50(10), 2498-2501.

Song, K.H. and Nakata, K. (2010). "Effect of precipitation on post-heat-treated Inconel 625 alloy after friction stir welding." *Mater. Des.*, 31(6), 2942-2947.

Song, K.H., Kim, W.Y. and Nakata, K. (2012). "Evaluation of microstructures and mechanical properties of friction stir welded lap joints of Inconel 600/SS 400." *Mater. Des.*, 35, 126-132.

Soni, P., Sehgal, S., Kumar, H. and Singh, A.P. (2018). "Joining of SS316-SS316 through microwave hybrid heating by using Nickel nano-powder." *Int. J. Appl. Eng. Res.*, 13(8), 6446-6449.

Sridhar, R., Ramkumar, K.D. and Arivazhagan, N. (2014). "Characterization of microstructure, strength, and toughness of dissimilar weldments of Inconel 625 and duplex stainless steel SAF 2205." *Acta Metall. Sin. (Engl. Lett.)*, 27(6), 1018-1030.

Srinath, M.S., Sharma, A.K. and Kumar, P. (2011). "A novel route for joining of austenitic stainless steel (SS-316) using microwave energy." *Proc. Inst. Mech. Eng., Part B*, 225(7), 1083-1091.

Srinath, M.S., Sharma, A.K. and Kumar, P. (2011). "A new approach to joining of bulk copper using microwave energy." *Mater. Des.*, 32(5), 2685-2694.

Srinath, M.S., Sharma, A.K. and Kumar, P. (2011). "Investigation on microstructural and mechanical properties of microwave processed dissimilar joints." *J. Manuf. Process.*, 13(2), 141-146.

Srirangan, A.K. and Paulraj, S. (2016). "Multi-response optimization of process parameters for TIG welding of Incoloy 800HT by Taguchi grey relational analysis." *Eng. Sci. Technol. Int. J.*, 19(2), 811-817.

Sun, Z. and Karppi, R. (1996). "The application of electron beam welding for the joining of dissimilar metals: an overview." *J. Mater. Process. Technol.*, 59(3), 257-267.

Sunil, B.R., Sivaprahasam, D. and Subasri, R. (2010). "Microwave sintering of nanocrystalline WC-12Co: Challenges and perspectives." *Int. J. Refract. Met. Hard Mater*, 28(2), 180-186.

Tang, C.Y., Wong, C.T., Zhang, L.N., Choy, M.T., Chow, T.W., Chan, K.C., Yue, T.M and Chen, Q. (2013). "In situ formation of Ti alloy/TiC porous composites by rapid microwave sintering of Ti6Al4V/MWCNTs powder." *J. Alloys Compd*, 557, 67-72.

Thostenson, E.T. and Chou, T. W. (1999). "Microwave processing: fundamentals and applications." *Composites, Part A*, 30(9), 1055-1071.

Upadhyaya, A., Tiwari, S.K. and Mishra, P. (2007). "Microwave sintering of W-Ni-Fe alloy." *Scr. Mater.*, 56(1), 5-8.

Vaidhyathan, B. and Rao, K.J. (1997). "Microwave assisted synthesis of technologically important transition metal silicides." *J. Mater. Res.*, 12(12), 3225-3229.

Wilson, I.L.W., Gourley, R.G., Walkosak, R.M. and Bruck, G.J. (1991). "The effect of heat input on microstructure and cracking in alloy 625 weld overlays." *Proceedings of the International Symposium on the Metallurgy and Applications of Superalloys*, 718(625), 735-747.

Xu, J.L., Bao, L.Z., Liu, A.H., Jin, X.F., Luo, J.M., Zhong, Z.C. and Zheng, Y.F. (2015). "Effect of pore sizes on the microstructure and properties of the biomedical porous NiTi alloys prepared by microwave sintering." *J. Alloys Compd.*, 645, 137-142.

Yoshikawa, N., Ishizuka, E. and Taniguchi, S. (2006). "Heating of metal particles in a single-mode microwave applicator". *Mater. Trans.*, 47(3), 898-902.

Zafar, S. and Sharma, A.K. (2014). "Development and characterisations of WC-12Co microwave clad." *Mater. Charact.*, 96, 241-248.

Zafar, S. and Sharma, A.K. (2015). "Dry sliding wear performance of nanostructured WC-12Co deposited through microwave cladding." *Tribol. Int.*, 91, 14-22.

Zapirain, F., Zubiri, F., Garciandia, F., Tolosa, I., Chueca, S. and Goiria, A. (2011). "Development of Laser Welding of Ni based Superalloys for Aeronautic Engine Applications (Experimental Process and Obtained Properties)." *Phys. Procedia.*, 12, 105-112.

NATIONAL INSTITUTE OF TECHNOLOGY KARNATAKA, SURATHKAL

LIST OF PUBLICATIONS BASED ON PH.D RESEARCH WORK

Sl. No.	Title of the paper	Authors	Name of the Journal/ Conference/ Symposium, Vol., No., Pages	Month & Year of Publication	*Category
1	Joining of Inconel-625 alloy through microwave hybrid heating and its characterization.	<u>Ravindra Ishwar Badiger</u> Narendranath S Srinath MS	Journal of Manufacturing Processes, 18, 117-123	Feb. 2015	1
2	Microstructure and mechanical properties of Inconel-625 welded joint developed through microwave hybrid heating.	Ravindra Ishwar Badiger Narendranath S Srinath MS	Institution of Mechanical Engineers, Part B Journal of Engineering Manufacture 232(14), 2462-2477	Jan. 2017	1
3	Optimization of parameters influencing tensile strength of inconel-625 welded joints developed through microwave hybrid heating.	<u>Ravindra Ishwar Badiger</u> Narendranath S Srinath MS	Materials Today: Proceedings, 5,7659-7667	2018	3
4	Optimization of process parameters by Taguchi grey relational analysis in joining Inconel-625 through microwave hybrid heating	<u>Ravindra Ishwar Badiger</u> Narendranath S Srinath MS	Metallography, Microstructure and Analysis 8(1), 92-108.	Dec. 2018	1

5	Effect of power input on metallurgical and mechanical characteristics of Inconel-625 welded joints processed through microwave hybrid heating.	<u>Ravindra Ishwar Badiger</u>	Transactions of the Indian Institute of Metals. 72(3), 811-824	Jan. 2019	1
		Narendranath S Srinath MS Ajit M Hebbale			

* Category: 1: Journal paper, full paper reviewed 2: Journal paper, Abstract reviewed 3: Conference/Symposium paper, full paper reviewed 4: Conference/Symposium paper, abstract reviewed 5: others (including papers in Workshops, NITK Research Bulletins, Short notes etc.)



RAVINDRA ISHWAR BADIGER

Name and Signature of Research scholar



Dr. NARENDRANATH. S

Name and Signature of Guide

BIO-DATA



Name : Ravindra. I. Badiger.
Date of Birth : 6th September, 1974.
Phone : 9731150603
E- Mail : rbadiger74@gmail.com

Educational Qualification

- (i) **Ph.D** NITK Surathkal, **May 2019**.
- (ii) **M.Tech** (Design Engg.) from KLECET Belagavi affiliated to VTU, Belagavi **Dec. 2000** with 72% aggregate marks.
- (iii) **B.E** (Industrial and Production Engg.) from KLECET Belagavi affiliated to Karnataka University Dharwad in the year **1996** with 72% aggregate marks.

Professional Experience

Organization	Post Held	Duration
Vaibhavi Engineering, Udyambag , Belgaum.	Worked as a Production Engineer.	July 1996 to April 1997.
Atlas Gears Ltd., Devarwadi Village, Po: Shinoli, Tq: Chandgad, Dist: Kolhapur.	Jr. Engineer in Gear cutting section.	May 1997 to Oct.1998.

Academic Experience

Institute	Post Held	Duration
Bahubali College of Engg., Shravanabelagola.	Lecturer, Dept. of Indl. & Prodn. Engg.	October 2000 to June 2002
Dr.J.J.Magdum College of Engg., Jaysingpur, Maharashtra.	Lecturer, Dept. of Production Engg.	July 2002 to Aug 2007
SDM Institute of Technology Ujire	Sr. Lecturer Dept. of Mechanical Engg.	Sept.2007 to June 2008
Srinivas Institute of Technology, Mangalore.	Asst. Prof. Dept. of Mechanical Engg.	July 2008 to June 2011
Sharad Institute of Technology, Ichalkaranji	Asst. Prof. Dept. of Mechanical Engg.	June 2011 to July 2017
Alva's Institute of Engg. and Technology, Mijar, Moodbidri	Sr. Asst. Prof. Dept. of Mechanical Engg.	August 2017-August 2018
Yenepoya Institute of Technology, Moodbidri	Associate. Prof. Dept. of Mechanical Engg.	Since April 2019

Permanent Address : 531, Mahalaxmi, Mahaveer Nagar,
Behind Sukh Shanti Bhavan
Peeranawadi, Belagavi -590 008.

Ravindra I Badiger